OMNIPHOBIC SURFACES AS ANTIMICROBIAL AND BIOSENSING INTERFACES

HIERARCHICAL OMNIPHOBIC SURFACES FOR PATHOGEN REPELLENCY AND BIOSENSING

By SARA MOETAKEF IMANI B. Eng, M.Sc.

A Thesis Submitted to the School of Graduate Studies in Partial Fulfilment of the Requirements for the Degree Doctor of Philosophy

Doctor of Philosophy (2022), School of Biomedical Engineering, McMaster University Hamilton, Ontario

TITLE: Hierarchical Omniphobic Surfaces for Pathogen Repellency and Biosensing

AUTHOR: Sara Moetakef Imani, B. Eng, M.Sc. (McMaster University)

SUPERVISOR: Dr. Tohid Didar, Dr. Leyla Soleymani

NUMBER OF PAGES: xxvi, 248

Lay Abstract

Repellent surfaces have a variety of applications in healthcare, for coating medical devices (*e.g.* indwelling implants, stethoscopes, and other external devices.), coating hospital surfaces for blood and pathogen repellency, and for developing anti-fouling diagnostic devices. Furthermore, they can be applied in the food sector for limiting contaminations, and in public areas on high-touch surfaces to eliminate the spread of infection. Therefore, there is a need for repellent surface which can be easily applied to surfaces with various form factors while having an easy fabrication method. Featuring hierarchical structures on a heat-shrinkable material, a repellent wrap was designed to be integrated on existing surfaces and repel pathogens and suppress the spread of infection as an intermediate surface. Similar concept was used for designing blood repellent surfaces which were patterned with hydrophilic regions for a rapid dip-based biosensing platform. Finally, surface textures on conductive materials with liquid infused repellent coatings were investigated for electrochemical biosensing in complex biological liquids.

Abstract

Development of repellent surfaces which can supress bacteria adhesion, blood contamination and thrombosis, and non-specific adhesion on diagnostic devices has been a topic of intense research as these characteristics are in high demand. This thesis focused on design and development of omniphobic surfaces based on hierarchical structures and their application for preventing pathogenic contamination and biosensing. First, a flexible hierarchical heat-shrinkable wrap featuring micro and nanostructures, was developed with straightforward scalable methods which can be applied to existing surfaces. These surfaces reduced biofilm formation of World Health Organization-designated priority pathogens as well as minimized risk of spreading contamination from intermediate surfaces. This is due to the broad liquid repellency and the presence of reduced anchor points for bacterial adhesion on the hierarchical surfaces. Next, the developed surfaces were applied to minimize blood contamination and clot formation as well as facile integration of hydrophilic patterns. This led to droplet compartmentalization and was utilized for detection of Interleukin 6 in a rapid dip-based assay. Furthermore, in a review article the need for anti-viral or virus repellent surfaces and future perspectives were discussed as the global COVID-19 pandemic surged and attracted interest toward innovative technologies for suppressing the spread of pathogens. To address the pressing issue of non-specific adhesion in diagnostics devices, an omniphobic liquid infused electrochemical biosensor was developed. This was achieved by electroplating gold nanostructures on fluorosilanized gold electrodes. These electrodes demonstrated rapid and specific detection of *Escherichia coli* within an hour in complex biological liquids (blood, urine, *etc.*) without dilutions or

amplification steps from clinical patient samples which are major bottle necks when rapid detection systems are sought for at the point of care.

Acknowledgment

I would like to express my sincerest gratitude and appreciation to my supervisors Dr. Tohid Didar and Dr. Leyla Soleymani for their continued guidance, support, and encouragement throughout my graduate studies at their labs. I would like to thank my supervisory committee member Dr. Carlos Filipe for his advice and positive energy throughout my research work.

I would like to express my regards to the members of Didar Lab and Soleymani Lab. I have had the privilege to work along side many of them and become friends with many inspiring researchers.

Many thanks to my dearest friends, Sahand, Sara, Yasamin, Amid, Saeede, Sanaz, Ata, Zahra, Hanieh, and Elaheh, for their encouragement and support. You have been an important part of this journey.

Finally, I would like to extend my deepest gratitude to my lovely parents, Farzaneh and Behnam. Thank you for always and unconditionally supporting me through my life. You have empowered me and been my rock through out this journey, thank you for always believing in me.

Table of contents

Contents

Lists of Figures

Lists of Tables

List of all Abbreviations and Symbols

(3-Aminopropyl)triethoxysilane (APTES)

1-ethyl-3-(-3-dimethylaminopropyl) carbodiimide (EDC)

6-mercaptohexanol (MCH)

Apparent contact angle (θ*)

Area under the curve (AUC)

Bovine serum albumin (BSA)

Colony forming unit (CFU)

Contact angle (CA)

Crude intracellular matrix (CIM)

Extracellular polymeric substance (EPS)

Fluorosilane (FS)

Healthcare acquired infections (HAI).

Interleukin 6 (IL-6)

Methicillin-resistant Staphylococcus aureus (MRSA)

Nanoparticle-induced microscale wrinkling (NMW)

N-hydroxysuccinimide (NHS)

Oligo (ethylene glycol) (OEG)

Phosphate buffered saline (PBS)

Poly- (ethylene glycol) (PEG)

Polydimethylsiloxane (PDMS)

Polyolefin (PO)

Polystyrene (PS)

Prostate specific antigen (PSA)

Reactive oxygen species (ROS)

Receiver operating characteristic (ROC)

Scanning electron microscopy (SEM)

Self-assembled monolayers (SAMs)

Silica nanoparticles (SiNPs)

Sliding Angle (SA)

Solid–liquid interface (f_{SL})

Surface tension (γ)

The area fraction of the liquid–air interface underneath the liquid droplet (f_{LV})

the local texture angle (ψ),

Transmission electron microscope (TEM)

Ultraviolet-Ozone (UVO)

Urinary tact infection (UTI)

X-ray Photoelectron Spectroscopy (XPS)

Young's contact angle (θ).

Declaration of Academic Achievement

This dissertation was written to fulfill the requirements of the doctoral degree in the department of Biomedical Engineering at McMaster University. The work described was undertaken in the period spanning January 2018 to August 2022.

Chapter 1: “Introduction”, was drafted by Sara Moetakef Imani and reviewed to the final version by Dr. Tohid Didar and Dr. Leyla Soleymani.

Chapter 2: “Antimicrobial Nanomaterials and Coatings – a Closer Look at Current Antiviral Mechanisms and Future Perspectives to Control the Spread of Viruses Including SARS-CoV-2”, Sara Moetakef Imani and Liane Ladouceur contributed equally towards the writing of the manuscript. Dr. Tohid Didar and Dr. Leyla Soleymani conceived the idea for writing this review paper with Sara Moetakef Imani. The manuscript was reviewed to the final version by Dr. Tohid Didar and Dr. Leyla Soleymani.

Chapter 3: “Flexible Hierarchical Wraps Repel Drug Resistant Gram Negative and Positive Bacteria”, Sara Moetakef Imani performed the experiments, data validation, data visualization, and analysis with help from other authors. Sara Moetakef Imani wrote the manuscript with inputs from Dr. Tohid Didar and Dr. Leyla Soleymani.

Chapter 4: “Hierarchical structures, with submillimeter patterns, micrometer wrinkles, and nanoscale decorations, suppress biofouling and enable rapid droplet digitization” Sara Moetakef Imani performed the experiments, data validation, data visualization, and analysis with help from Roderick Maclachlan, specifically he helped with the surface

repellency measurements on Figure 4.2. Roderick Maclachlan contributed equally to the authorship of the manuscript with inputs from Dr. Tohid Didar and Dr. Leyla Soleymani.

Chapter 5: “Liquid Nano Electrodes enable One-pot Electrochemical Detection of Bacteria in Complex Matrices” Sara Moetakef Imani performed the experiments, data validation, data visualization, and analysis with help from other authors. Sara Moetakef Imani wrote the manuscript with inputs from Dr. Tohid Didar and Dr. Leyla Soleymani.

Chapter 6: “Conclusions and Future Direction”, was drafted by Sara Moetakef Imani and reviewed to the final version by Dr. Tohid Didar and Dr. Leyla Soleymani.

1 Chapter 1: Introduction

Preface

This chapter presents an introduction on bioinspired structured repellent surfaces and discusses principles of hydrophobic surfaces and importance of hierarchical texturing. Fabrication methods are then discussed with applications of such structured interfaces in bacteria and blood repellency. Furthermore, liquid infused coating as a universally repellent coating is introduced and its applications are discussed. Importance of repellency and blocking methods in biosensors and then discussed. Finally, this chapter will conclude with the objectives and the thesis outline.

1.1 Literature Review

1.1.1 Repellent surfaces and their principles

Repellent surface being hydrophobic, oleophobic, or omniphobic (universally repellent to high and low surface tension liquids) have found a range of applications in many fields. [1,2] Some examples of these applications are anti-corrosion, anti-bacterial, anti-fungal, self-cleaning, anti-icing, anti-fogging, anti-wetting, and anti-fouling surfaces. [1–10] These types of surfaces or more specifically, superhydrophobic surfaces (contact angle >150º), have a growing market value with a prediction of more than 50 million USD market value by year 2030. [11] The emergence of the global COVID-19 pandemic, raised awareness towards

surface contaminations and means for reducing pathogen presence on common surfaces. Therefore, the awareness and need for such repellent or antimicrobial coatings, have led to an estimated market value being more than 5.5 billion USD by 2030. [12] Another class of self-cleaning surfaces are superhydrophilic surfaces which lock down water on their interface (contact angle <10º) and have applications in oil-water separations, anti-fogging surfaces, and *etc.* [13] In this section, water repellent surfaces are discussed.

Biomimicry from nature and understanding the natural superhydrophobic and self-cleaning properties of the lotus plant leaves, has attracted many researchers to inspire from these phenomena in nature (Figure 1.1). [1,3,5,9,14–18] The superhydrophobic properties of lotus plants are due to their inherent micro and nanostructures, and this observation has led to developing surfaces with repellent properties with multiple scales of structures. [1,3,5,14,15,19] The multiscale roughness of micro and nanostructures, also referred to as hierarchical structuring, is key to a stable repellency, as it increases the liquid-air infaces and limits the solid-liquid interface resulting in higher contact angle measurements (Figure 1.1). [1,3,5,14,20–24]

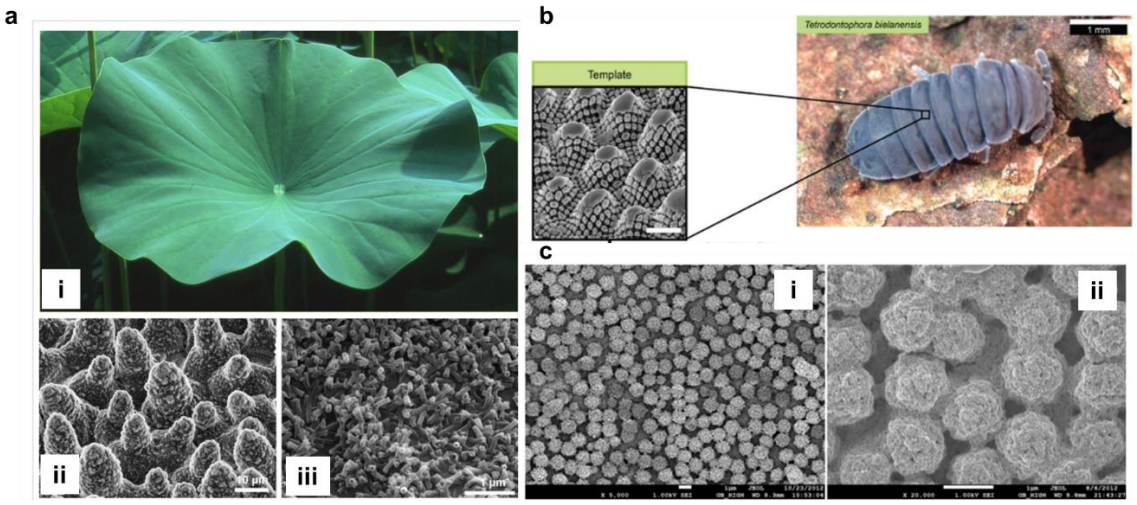

Figure 1.1 Bioinspired surfaces. *(a) i showing a lotus leaf, ii and iii showing scanning electron microscopy images of the hierarchical structure on the leaf.* [18] *(b) Springtail cuticle's hierarchical structure as a blueprint for developing omniphobic surfaces.* [25] *(c) An example from literature showing hierarchical structures of silica.* [26]

Contact angle is the angle at the edge of the droplet with solid surface and is a measure for demonstrating to what extent a surface is hydrophobic or hydrophilic (Figure 1.2). [1,22,27] Young's contact angle was introduced to understand a droplet's contact angle on smoosh surfaces:

$$\cos\theta = \frac{\gamma_{SV} - \gamma_{SL}}{\gamma_{LV}} \qquad \textit{Equation 1.1}$$

Young's theory did not explain the role of added roughness and the enhanced hydrophobicity on the same material into account. Wenzel and the Cassie-Baxter models are mainly considered when studying textured surfaces. [1,28,29] In Wenzel state (Figure 1.2 a.ii), the droplet completely permeates the surface roughness, and the contact angle is determined by this relation where r is the surface roughness (the ratio of the actual surface area to the projected surface area): [1,17,29]

$$\cos\theta^* = r\cos\theta \qquad \textit{Equation 1.2}$$

As r is larger than unity, the wetting ($\theta<90^o$) or non-wetting ($\theta>90^o$) amplifies. In the Cassie-Baxter state (Figure 1.2 a.iii), the liquid does not completely penetrate the surface texture and air pockets remain underneath the droplet. [28] The droplet penetrated till the local texture angle (ψ), becomes equal to the equilibrium Young's contact angle (θ). [1,30] The contact angles can be determined using the Cassie–Baxter relation:

$$\cos\theta^* = f_{SL}\cos\theta - f_{LV} \qquad \textit{Equation 1.3}$$

In this equation, f_{SL} is the area fraction of the solid–liquid interface, f_{LV} is the area fraction of the liquid–air interface underneath the liquid droplet on a surface with uniform roughness. [1,30] In Cassie-Baxter state, apparent contact angle of $\theta^*>>90^o$ can be realized $\theta<90$ and for low surface tension liquids where f_{SL} is low and the f_{LV} is sufficiently high. This is in contrast with the Wenzel state which results in further reduction in the contact angle when introducing roughness for low surface tension liquids. Therefore, Cassie–Baxter state is essential for having an omniphobic surface. [1,30]

The texture's angle (ψ) is also important for having an omniphobic surface for low surface tension liquids with Young's contact angle $\theta<<90^o$ (Figure 1.2 b). [1,30] The liquid contacting the texture in Cassie-Baxter state, holds a contact angle equal to the Young's contact angle θ. The texture can be concave with texture angle $\psi>90^o$ or convex with texture angle $\psi<90^o$. In order to have a stable Cassie-Baxter state, θ should be equal to or bigger than ψ, otherwise the net traction on the liquid–vapor interface would be downward, resulting in the liquid to wick in the solid and demonstrating a Wenzel state. [1,30] Therefore, for low

surface tension liquid (θ<90º) to show a robust Cassie–Baxter state, the texture angle should be ψ<90º (re-entrant texture).[14,31]

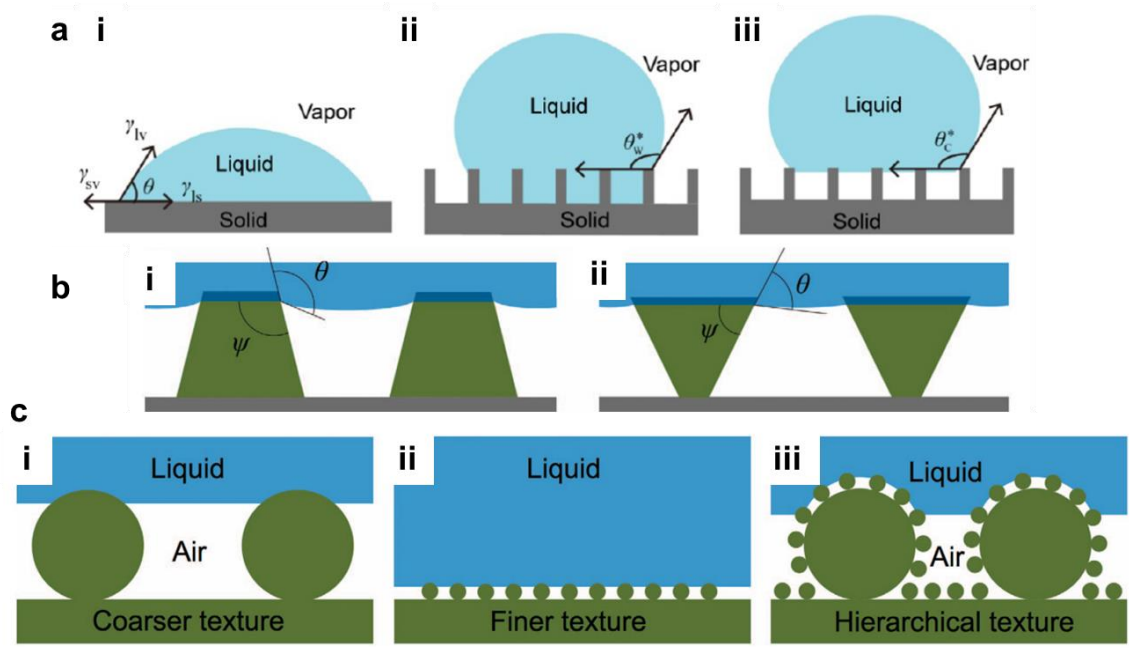

Figure 1.2 Schematic of droplets in different states. *(a) i Young's contact angle (θ), ii liquid droplet in the Wenzel state, iii liquid droplet in the Cassie–Baxter state.* [15] *(b) i a concave texture with texture angle ψ>90º, showing a liquid droplet with θ>90º in the Cassie–Baxter state. ii a convex texture (re-entrant texture) with texture angle ψ<90º, showing a lower surface tension liquid with θ<<90º in the Cassie–Baxter state.* [1] *(c) Schematics of a liquid droplet in the Cassie–Baxter state on a i microstructured surface, ii a nanostructured surface, and iii a hierarchically textured surface.* [1]

Significance of hierarchical structured surfaces shows itself when looking into nature and speculating naturally repellent surfaces such as lotus leaves or springtail cuticle (Figure 1.1). [1,25] When Cassie-Baster state is dominant on the surface of hierarchical structures for all their length scales, liquid droplets would display higher apparent contact angles compared to a single scale textured surface. [1,25] This is due to multiple scales of trapped air for hierarchically structured surfaces while this is happening for only one length scale on

single scale surfaces. By recursively writing the Cassie–Baxter relation, contact angles on hierarchically structured surfaces can be concluded as:

$$\cos\theta_n^* = \left(1 - f_{LV,\,n}\right)\cos\theta_{n-1}^* - f_{LV,\,n} \qquad \textit{Equation 1.4}$$

where n=1, 2, 3, 4, …, is the number of length scales of texture; $f_{LV,n}$ is the area fraction of the liquid-air interface for each scale of texture (n^{th}); θ^*_n and θ^*_{n-1} are the apparent contact angles on hierarchically structured surfaces with n and n-1 scales of texture, respectively. This Equation shows that θ^*_n increases as the number of scales of texture (n) increases. [1] Furthermore, increasing in the number of hierarchical levels, enlarges the energy difference between the Cassie-Baxter and Wenzel states and therefore stabilize the Cassie state. [1] In terms of contact angle hysteresis, for hierarchical surfaces it is lower compared to surfaces with a single scale of texture. Contact angle hysteresis relies on the energy barriers that a liquid droplet encounters as it moves along the surface, therefore it characterizes the resistance to the droplet movement. [1,30] Lesser pinning points as a result of lower solid–liquid contact area in hierarchical surfaces, leads to lower resistance of droplet movement and lower contact angle hysteresis. [1,32] Therefore, the conclusion is that in order to have a stable repellent surface, scales of texture along with a proper angle of texture is required (Figure 1.2 c). [1,30] These finding and the continued research in the field developing omniphobic surfaces, has led to developing many smart materials with multi-functionality. In following subsections, examples and application from literature are discussed.

A recently developed class of omniphobic surfaces which uses another technology to integrate repellency into interfaces is liquid infused surfaces. [33–35] This concept was first

introduced by Wong *et al.* and was inspired by pitcher plants as they have microstructures on their surface and trap a layer water, making their surface slippery such that insects would fall in the plant. [33] This class of surfaces have found many applications in anticorrosion techniques, [36–39] , anti icing [40–44] , droplet manipulation [45–48], biomedical engineering (*e.g.* anti-thrombogenic coatings for medical devices, and anti biofouling). [44,49–5152–54] The main design principles for such surfaces are that the (i) lubricating layer should wet and spread in the solid, and (ii) as for maintaining a proper functionality and repellency, the lubricating layer and test liquids should be immiscible, and (iii) the surface should have a higher affinity towards the lubricant than the other liquids which come in contact with the system. [33,55,56] Some of the drawbacks when comparing to the hierarchical lubricant-free surfaces, are that there is a chance that the liquid layer evaporates in open air setups. Also, it cannot be used in high-touch contact areas, as this coating is wet and does not have a proper design to be touched by human hand. However, liquid infused coatings can be a great candidate for indwelling medical devices or biosensors.

1.1.2 Fabrication of scales of structures and repellent coatings and their applications

In the following paragraphs, some of the recent advancements in fabricating surfaces with scales of structures, and liquid infused platforms are introduced. Furthermore, some studies on the interaction of bacteria and blood with structured repellent surfaces are discussed.

1.1.2.1 Structured surfaces

A variety of methods have been developed to create microstructures, nanostructures, or hierarchical structures to add repellency to existing surfaces or to engineer new materials with repellent properties. Fabrication of microstructures, nanostructures, or hierarchical of then rely on the following techniques: photolithography, [14] casting, [57,58], chemical vapour-phase deposition, [59] emulsion templating, [60] electrospinning, [14,59,61] reactive ion etching, [62–64] electrochemical etching/anodizing, [65] three-dimensional printing, *etc*. [66] Many studies used chemical modifications with fluorine-based chemicals as well to improve repellency. [9]

One of the most common techniques in developing repellent surfaces is lithography methods which creates well defined features and patterns and is mainly used to investigate theories of wetting. [2] Pillar shaped structures have been investigated in many studies, Darmanin *et al*. showed electrodepositing conductive polymers (polypyrrole) on array of pillars on conductive materials, Kota *et al*. investigated spraying FluoroPOSS (Fluorinated Polyhedral Oligomeric SilSesquioxanes) on PDMS pillars. [1,8] Studies also focused on having re-entrant features, Tuteja *et al*. showed Micro-hoodoo (mushroom-like arrays) were fabricated by lithography, etching, and silanization. [14] The surface demonstrated low contact angle hysteresis of high and low surface tension liquids and superhydrophobicity. [14] Mushroom-like re-entrant structures were fabricated by digital light processing, a three-dimensional printing, volumetric shrinkage, and deformation, showing above 150º contact

angle without any sliding angles. [66] Double-ring mushroom was recently developed by reactive ion etching and lithography, showing above 150º for both oil and water. [67]

Wrinkled structures have also been used for adding repellency to surfaces. Scarratt *et al.*, spin coated Teflon, a fluoropolymer, on a shrinkable polymer to create wrinkled structures post heat shrinkage. [4] This method resulted in large contact angle hysteresis and hydrophobicity. Using oxygen reactive ion etch and controllable strain recovery on polystyrene, Sarwate *et al.* created microwrinkles and nanowires resulting in contact angles of above 150º. [68] Using acid etching and sand-blasting, a micro/nano patterned supper hydrophobic titanium surface was fabricated showing wavy and pitted structure, demonstrating more than 150º contact angle for the fluorinated version. [69]

Many of the introduced repellent surfaces in literature, lack the applicability in real-life scenarios, as fabrication methods are too complicated and expensive to scale up, or they are material-specific with limited applications. The introduced repellent surfaces in this thesis mitigated such complications.

1.1.2.1.1 Structured surfaces – bacteria attachment

A topic which has been researched a lot yet limited strong answers to fundamental questions were found, is the antibacterial or bacterial repellency on structured surfaces, to find their relation with the scales of structure in order to facilitate design of such repellent surfaces. [70] These surfaces can be valuable in reducing contamination of biomedical products with pathogens as this is one of the main causes of healthcare acquired infections (HAI). [71] Initial research had focused on use of active biocidal agent, which can contribute

to antibiotic resistance of bacteria or toxicity concerns. [72] However, the focus of this thesis and many other research is to look into the antifouling activity caused by the bacteria-surface interaction and the geometry of the surface. [70–72]

The attachment response of bacteria was studied on wrinkled gold surfaces having either micro or nano structures, showing reduced attachment when having roughness on the surface with elevated contact angles of above 120º. [73] Further studies into marine antifouling showed decreased fouling on uniaxially wrinkled and fluorosilanized PDMS surfaces. [74] Freschauf *et al.* showed a pattern transfer of wrinkled metallic surfaces into plastics and demonstrated lower bacteria recovered from bacteria drops on the textured surfaces compared to flat. [75] Laser-treated titanium superhydrophobic titanium surface with a contact angle of above 160º, was investigated for *Staphylococcus aureus* and *Pseudomonas aeruginosa* attachment, showing suppression of *P. aeruginosa's* attachment while *S. aureus* was colonizing on the surface even more than that of the flat polished surface (Figure 1.3 a). [76] Variola *et al.* investigated oxidative nanopatterning on titanium and showed reduced adhesion of *S. aureus* and *E. coli* due to the structure. [77] Another study showed the number of viable *S. aureus* is reduced on nanostructured gold electrodes (nano-pillar, nano-ring, *etc.*), however no further surface characterizations were reported. [78] By interpenetrating polymer network of polyurethane was sprayed with fluoro functionalized silica and zeolitic imidazolate frameworks (ZIF-8) mixed with fluorosilane, Ashok *et al.* showed a dual action surface that is superhydrophobic and has active agents (Figure 1.3 b). [79]

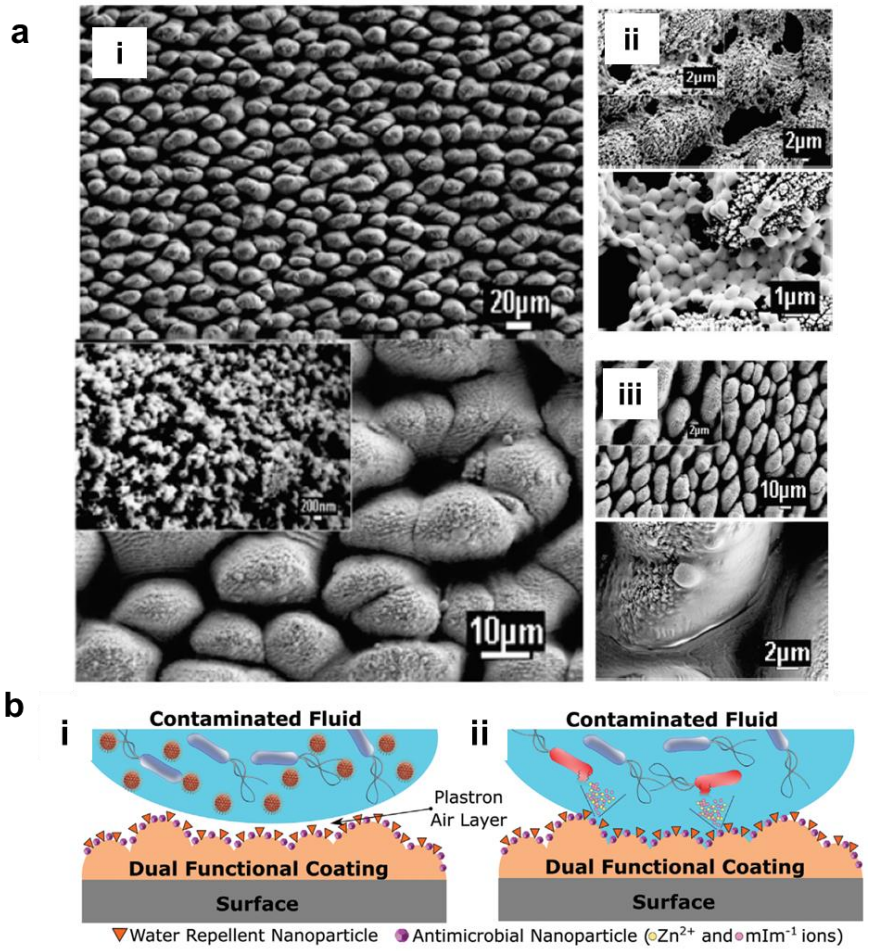

Figure 1.3 Bacteria attachment on structured surfaces. *(a) i SEM images of structured titanium surface. ii S. aureus colonized on the surface while iii P. aeruginosa is repelled.* [76] *(b) Dual functional coating for shielding surfaces from bacteria and viruses. i the air pockets preventing surface contamination, ii Localized loss of superhydrophobicity and the subsequent antimicrobial effect of active nanoparticles.* [79]

In the following chapters of the thesis, novel and straightforward methods are introduced and experimented to create hierarchically structured repellent surfaces and test their antifouling properties with detailed bacterial studies with a vision for real-life applications and scaling up capacities which not only can be applied to existing surfaces, but also can be used as novel repellent material as its own.

1.1.2.1.2 Structured surface – blood attachment

Due to the significant reduction in the blood-surface contact area, textured repellent surfaces have been investigated for their hemocompatibility, as they can be utilized in blood contacting medical devices and diagnostics in whole blood. [30,80,81] The area available for protein adsorption and blood cell or platelet adhesion is reduced, leading to minimizing thrombosis, contaminations, and other complications. [30]

Hou *et al.* developed superhydrophobic polypropylene surfaces with contact angles of above 150º and contacted them by platelet-rich plasma and fresh human whole blood, demonstrating suppression of platelet and blood cell attachment. [82] Rough needle-like ZnO nanofilms fabricated by electrochemical deposition showed superhydrophobic and anticoagulant properties. [83] Under flow conditions, microstructures of PDMS significantly reduced platelet adhesion compared to unstructured surface. [84] Poly(carbonate urethane) with fluorinated alkyl side chains was casted on densely packed multiwall carbon nanotubes, making the surface supper hydrophobic with contact angle of above 160º (Figure 1.4 a). [85] These surfaces were investigated for platelet adhesion demonstrating little adhesion of the platelets compared to non-structured surface. [85] However, they did not perform anti-thrombogenic studies on these surfaces. Bartlet *et al.* fabricated titania nanotube surfaces *via* electrochemical anodization followed by surface modification with fluorocarbons and demonstrated superhydrophobicity, reduced adsorption of human serum albumin and human fibrinogen protein. [86] Paven *et al.* coated stainless steel meshes with fluorinated silica particles and showed human blood protein adsorption was inhibited by more than 95%) (Figure 1.4 b). [87] A porous fluoropolymer membrane was sprayed with

fluorine-based nanoparticles of (poly(vinylidenefluorideco-hexafluoropropylene) followed by fluorocarbons treatment fand used blood membrane oxygenation. [88] Polyurethane sponge were coated with nanoparticles and fluorocarbons which enhanced the nanoscale roughness resulting n reduction in fibrinogen and platelet adhesion without toxic effects. [89] Hierarchically structured superhydrophobic silica surfaces modified with fluorocarbon were investigated by Zhao *et al.* and they showed reduction in the number of adhered platelets compared to an unmodified glass surface. [26]

A point lacking in many studies in the field is that they characterize the repellent behaviours of water rather than blood even though blood surface tension ($\gamma \approx 56$ mN m^{-1}) is lower compared to water surface tension ($\gamma \approx 72$ mN m^{-1}). [30] Many studies have also focused on proteins such as BSA and claimed potential for blood repellency, they lacked using whole blood or design studies carefully for blood interactions. Furthermore, most studies, have characterized the interaction with blood under static conditions without a flow. [30,80] These are points that I tired to address in this thesis by developing straightforward fabrication methods to develop hierarchically structure blood repellent surfaces with detailed studies on blood repellency and coagulations in static and dynamic conditions.

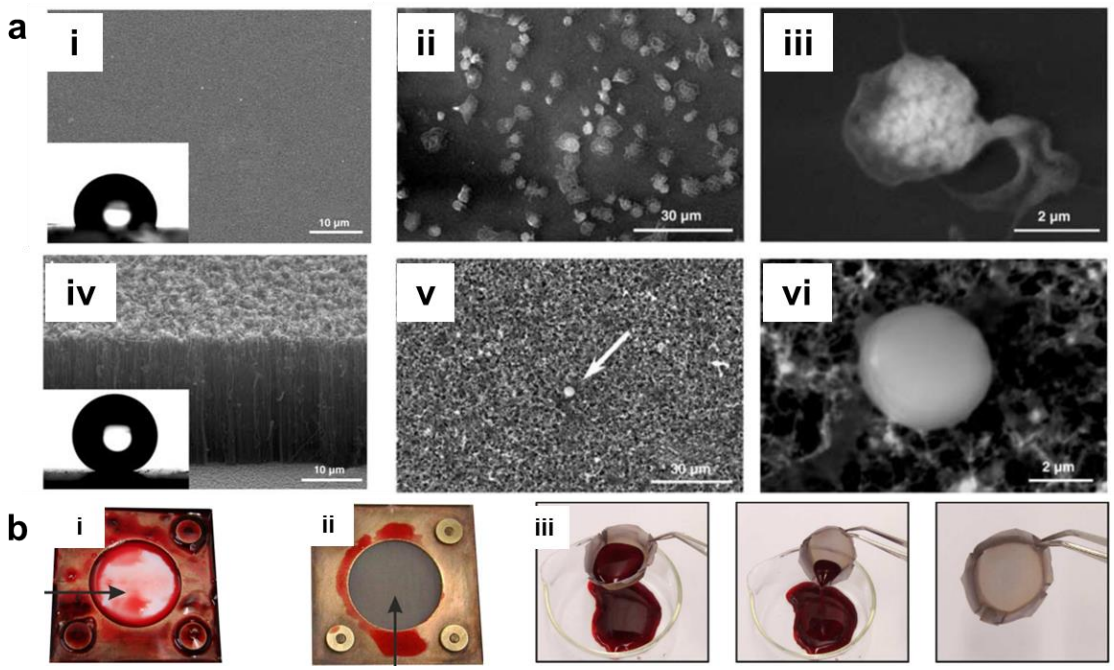

Figure 1.4 blood attachment on structured surfaces. *(a) i smooth polymer film, ii platelet adhesion on the smooth polymer film (iii zoomed in) iv Nanostructured superhydrophobic polymer films, v after platelet adhesion remains clean, vi one detected platelet.* [85] *(b) i uncoated Teflon membrane, ii coated stainless steel meshes with fluorinated silica particles after whole human blood was pumped through a flow cell through them. iii whole human blood rinsed out of fluorinated silica particle coated membrane.* [87]

1.1.2.2 Liquid infused surfaces

Another class of repellent surfaces, introduced in section 1.1.1 is liquid fused surfaces firstly introduced by Wong *et al.* where Teflon nanofibrous membranes were perfused with Fluorinert FC70, and a slippery interface was characterized. [33] *Leslie et al.* fluorosilane-treated variety of medical surfaces by liquid phase chemical modification techniques and showed suppression in bacteria biofilm formation (Figrue 1.5 a,b). [51] This class of coating has been integrated into many metallic materials, such as titanium, [90] stainless steel, [91] cupper, [36] gold, [35] and aluminum [40,92], and non-metallic surfaces such as glass, [46,53] silicon,

[45,49,93] PDMS, [94–96] polystyrene (PS), [97] and poly(methyl methacrylate). [51] Liquid phase deposition and chemical vapor deposition are the two main approaches to induce low-energy chemical coatings to build the liquid infused surface when lubricant properties does not match the surface. Chemical vapor deposition method creates a more homogeneous coating with lesser chemical being used than the Liquid phase deposition method. [53,98]

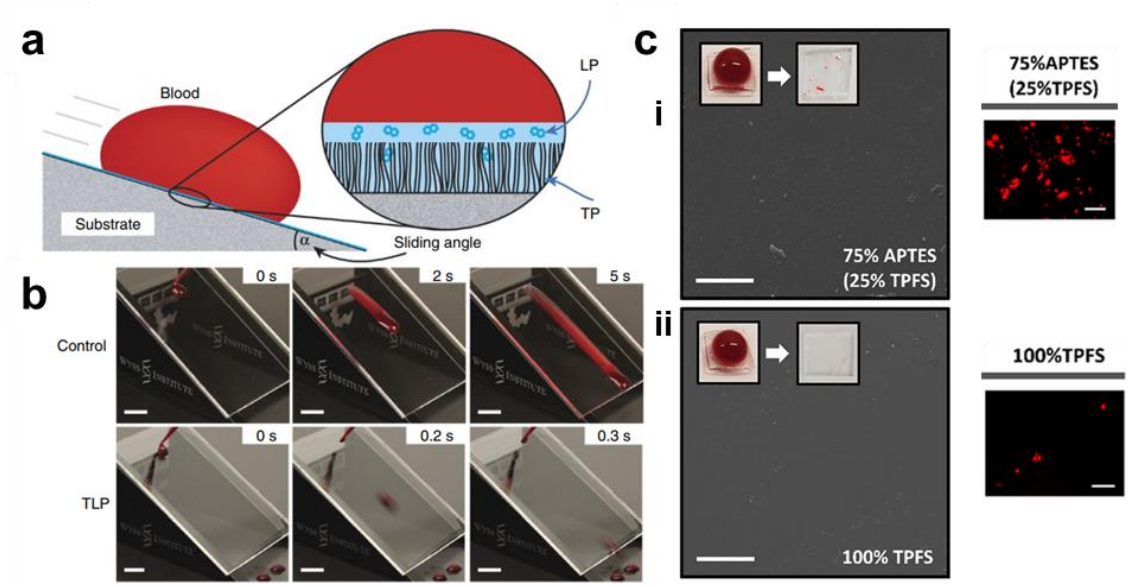

Figure 1.5 Liquid infused surfaces. *(a) schematic of a blood droplet on a liquid infused surface and its components.*[51] *(b) Depositing blood droplets on untreated and treated surfaces, showing blood drops sliding off.* [51] *(c) Dual functionality of liquid infused surfaces, i they repel blood (undesired species), ii but promote selective adhesion of endothelial cell (desired targets, red fluorescent).* [53]

Many studies showed that having scales of texture and roughness on liquid infused surfaces benefits adhesion and the retention of the infiltrated lubricating liquid. [33,40,49,55,99] Electrodeposition of highly textured polypyrrole on Aluminum, [40] or boehmitization of Aluminum surfaces followed by addition of fluorocarbon and lubricating layer showing a low contact angle hysteresis. [55] Kim *et al.* investigated liquid infused flat, microscale,

nanoscale, and hierarchically textured surfaces post lubricant infusion for lubricant retention and omniphobic properties, demonstrating textured surfaces have superior performance with the nanostructures one showing the best performance. [55]

Other studies showed dual functionality of this class of surfaces, meaning that not only they are repellent towards undesired species, but also promote selective adhesion of desired targets. [52–54,100,101] Glass substrates modified with a mixture of fluorosilanes and aminosilanes, followed by biorecognition element immobilization on aminosilane molecules and lubricant infusion, were able to promote cell growth while inhibiting blood clot formation (Figure 1.5 c). [53,101] Other studies, showed the similar concept for immunofluorescence detection with patterns of biofunctional sites microcontact printed on a substrate, followed by addition of fluorosilane and liquid infusion. [101,102]

In the following chapters of the thesis, a textured, conductive, repellent, and liquid infused surface was fabricated to assess biosensing properties in an electrochemical biosensor for *E. coli* detection.

1.1.3 Role of repellency in biosensors for reducing non-specific absorption

An important application for repellent surfaces is reducing non-specific adhesion in biosensors and biofunctional surfaces which has attracted many researchers. The aim and motivation for examining non-specific adsorption techniques are achieving maximum sensitivity, specificity, and selectivity for a particular biosensing application. [103–105]

Electrochemical biosensors in particular, have gained a lot attention due to the potential to be implemented in clinical setups as they are easy processing, low cost and accurate. [106,107]

Electrochemical biosensors contain biorecognition elements that are immobilized on transducers (conductive electrodes). [106] Target analytes then selectively bind to the biorecognition elements, generating an electrical signal dependant on the concentration of the target of interest in the detection solution. [106,108] Proper blocking techniques are imperative to implement in electrochemical biosensors to reduce or eliminate undesired species to interfere with the target capture and recognition on the surface of the electrodes. [107] Non-specific absorptions of the foulant molecules, specially in cases that detection in complex liquids (blood, urine, sewage, *etc*.) is essential, often decrease sensor's performance, result in high background signals, result in false-positive or false-negative responses, and affect reproducibility of the data, making the sensor unreliable. [106,108–119] Biofouling happens *via* several mechanisms where clinical sample matrixes, other analytes, and potentially side products of electrochemical reactions, through hydrophobic or electrostatic forces tend to form a passivating layer on the electrode resulting in blockage of recognition elements and electrodes. [106,108,109,112,119]

There are several techniques for reducing non-specific adhesion, and they can be categorized into physical or chemical modifications. [106,112] Physical surface blockers are often governed by van der Waals forces, hydrophobic interactions, and electrostatic interactions. One of the widely used strategies is blocking with bovine serum albumin (BSA). [106] However, BSA has several drawbacks, having steric hinderance affecting small molecules interaction with the transduction layer, forming a nonuniform layer. [53,106]

Forming polymer films with spin-coating, dip coating and spray coating is another avenue for physical modification strategies for making antifouling electrodes. [106]

Chemical methods often provide stronger immobilization techniques. Self-assembled monolayers (SAMs) of various molecules could be formed such as Poly- (ethylene glycol) (PEG), oligo (ethylene glycol) (OEG), zwitter- ionic, 6-mercaptohexanol (MCH) and 11-mercaptoundecanol, and peptide-based molecules. [49,53,106,112] In a study by Wu *et al.* zwitterionic polymer was used to passivate a glucose sensor, showed promising sensing in human blood plasma, however, they did not show rapid detection in whole blood. [118] Another study showed protease detection in a detection liquid containing BSA as a fouling molecule and a PEG as the blocking agent on the electrode, they did not perform studied in whole biological liquids. [117] Polyaniline (PANI) modifications are another strategy to add antibiofouling properties. [100,102,108,112] By incorporation PANI, studies showed COVID-19 N-gene from 10% fetal bovine serum (FBS), [116] another study showed target detection in human serum by PEGylated PANI nanofibers as the blocking agent. [116] Thiol-terminated sulfo-betaine was used for prostate specific antigen (PSA) in human serum albumin (HSA) for mimicking human whole blood. [113]

One of the most widely used blocking agent is MCH which has negatively charged –OH head group. Therefore, MCH repels the negatively charged phosphate backbone of ssDNA, prevents its adsorption to the electrode surface, and helps the probe DNA to stand perpendicularly to the electrode surface so it would be capable of hybridizing with target DNA, even though the negatively charged MCH backfill exists. [107] However, practical and clinical use of such systems were not possible due to poorly reproducible results. [107]

The recently emerging blocking method, liquid infused coatings, [33] have shown promising results for repelling undesired species in a variety of applications. Inspired by pitcher plant, [6,33,51,55,56] liquid infused surfaces were initially developed to be used for indwelling medical devices to attenuate blood clot formation. [51] However, a dual functionality was then introduced to promote targeted binding on the surface while repelling unwanted species. [52,53,100–102] This lubricant-infused biofunctional coating, found applications in implant integrations, cell patterning, patterned fluorescent based biosensors. [52,53,100–102] These studies showed enhanced performance when comparing to other blocking methods such as BSA or PEG. [49,53]

In Chapter 5, a rapid electrochemical biosensor was introduced which integrates for the first time, a liquid infused coating as a blocking agent, along with nanostructures of gold as sites for probe immobilization to then enable detecting from complex biological liquids. Most of the developed biosensors so far, have either diluted clinical samples, used artificial complex liquids, or have further used amplification steps for the signal processing. This electrochemical biosensor and the integrated blocking method can be useful for a developing a reliable rapid sensor in blood, urine, and other complex liquids, without dilution or complicated amplification steps.

1.2 Objectives

The overall objective of this thesis was to develop novel technologies for fabrication of repellent hydrophobic (or omniphobic) surfaces and exploring their application for supressing biofilm formation, bacterial repellency, blood repellency, anti-thrombogenic behaviour, droplet digitization, and biosensing in complex biological liquids and clinical setups.

Objective A. Enhancing the scalability of hierarchical surface fabrication and exploring the importance of hierarchical structuring on bacteria repellency

Development of repellent surfaces is often relied on complicated steps without an insight on scale-up or universal use. Additionally, the role and importance of hierarchical structuring in repellency and its comparison with other structured surfaces, is an area which is not explored extensively, specially for bacteria repellency. Here, we explore an all solution-based, scalable fabrication method for creating hierarchically structures, and the capability of the designed surface for flexibility in conforming into various shapes as a heat-shrinkable wrap. We further evaluate the importance of hierarchical structuring by comparing it by carefully designed experiments with other scales of texture. We explore whether the engineered hierarchical surface, significantly reduces bacteria biofilm formation and bacteria attachment, and compare its performance with other textured surfaces to understand whether hierarchical structuring is important or not.

Objective B. Developing all solution-based processes for developing patterned hierarchical surfaces for blood repellency and biosensing

Patterning hydrophilic regions within highly repellent surfaces in a straightforward way is beneficial for biosensing and droplet digitization purposes. Furthermore, extensive and systematic studies on blood repellency for textured surfaces, evaluating surfaces with whole human blood, mimicking real-life applications, and contacting blood in dynamic conditions with repellent surfaces, are points missing in many studies in literature. Here, we design an all solution-based hierarchical surface and compare its performance in blood repellency with other scales of texture to explore whether hierarchical structuring significantly reduces clot formation and blood adhesion or not, both in static and dynamic conditions. By integrating hydrophilic patterning, we investigate implementing the patterned surface for high throughput biosensing to examine whether biosensing is possible or not.

Objective C. Developing liquid infused electrodes for rapid and specific electrochemical detection of pathogens and minimizing non-specific absorption

Non-specific absorption has been a challenge when designing electrochemical biosensors, specifically, for detecting from complex biological liquids, imposing an adverse effect on biosensor's performance. Additionally, rapid diagnosis within an hour and eliminating sample dilutions are challenges in detection systems. Here, we investigate integrating a highly repellent liquid infused coating into an electrochemical biosensor to see whether the coating improves the biosensor's performance in terms of minimizing non-specific binding,

detection of pathogens and specificity, and compare it with electrodes without the designed blockings system. Furthermore, the potential of a rapid one-pot pathogen detection system for clinical setups was investigated to minimize detection time and sample processing with no sample dilution.

1.3 Thesis outline

The content of each chapter is briefly discussed in the following paragraphs:

Chapter 2: "Antimicrobial Nanomaterials and Coatings – a Closer Look at Current Antiviral Mechanisms and Future Perspectives to Control the Spread of Viruses Including SARS-CoV-2" This review thoroughly discusses the antiviral materials and coatings that could be implemented for limiting the spread of viruses including SARS-CoV-2 *via* contaminated surfaces. We also present future perspectives with regards to emerging antimicrobial technologies such as omniphobic surfaces. *This review article has been published in ACS Nano.*

Chapter 3: "Flexible Hierarchical Wraps Repel Drug Resistant Gram Negative and Positive Bacteria" This chapter introduces a flexible plastic wrap that combines a hierarchical wrinkled structure and nanoparticles with chemical functionalization. These engineered wraps demonstrate a broad liquid repellency and therefore, reduce bacterial adhesion, biofilm formation, and the transfer of bacteria through an intermediate surface. These wraps

can be applied to already existing high-risk surfaces *via* heat shrinking and can conform into multiple form factors. *This chapter has been published in ACS Nano.*

Chapter 4: "Hierarchical structures, with submillimeter patterns, micrometer wrinkles, and nanoscale decorations, suppress biofouling and enable rapid droplet digitization" This chapter introduces an all solution-based, scalable method for producing liquid repellant flexible films. These surfaces were fabricated through nanoparticle deposition and heat-induced wrinkling. They suppressed blood adhesion, and clot formation, furthermore, hydrophilic patterns were created on them providing a platform for droplet digitization and was further used for Interleukin 6 detection. *This chapter has been published in Small.*

Chapter 5: "Liquid Nano Electrodes enable One-pot Electrochemical Detection of Bacteria in Complex Matrices" This chapter introduces a repellent coating integrated within a conductive nanostructured gold electrode which promotes target binding and repels unwanted species. These electrodes were tested against conventional nanostructured electrodes for *Escherichia coli* detection and showed prominent performance. Furthermore, a panel of clinical patient urine samples and patient blood culture samples were tested on the developed electrodes and showed identification of *E. coli*. *This chapter will be submitted to Advanced Functional Materials.*

Chapter 6: "Conclusion and Future Directions" In this chapter, some general conclusions are mentioned, and future directions are discussed.

1.4 References

(1) Kota, A. K.; Kwon, G.; Tuteja, A. The Design and Applications of Superomniphobic Surfaces. *NPG Asia Mater.* **2014**, *6* (6), e109-16. https://doi.org/10.1038/am.2014.34.

(2) Sahoo, B. N.; Kandasubramanian, B. Recent Progress in Fabrication and Characterisation of Hierarchical Biomimetic Superhydrophobic Structures. *Rsc Adv.* **2014**, *4* (42), 22053–22093.

(3) Tuteja, A.; Choi, W.; McKinley, G. H.; Cohen, R. E.; Rubner, M. F. Design Parameters for Superhydrophobicity and Superoleophobicity. *MRS Bull.* **2008**, *33* (8), 752–758.

(4) Scarratt, L. R. J.; Hoatson, B. S.; Wood, E. S.; Hawkett, B. S.; Neto, C. Durable Superhydrophobic Surfaces via Spontaneous Wrinkling of Teflon AF. *ACS Appl. Mater. Interfaces* **2016**, *8* (10), 6743–6750. https://doi.org/10.1021/acsami.5b12165.

(5) Bhushan, B.; Jung, Y. C.; Koch, K. Micro-, Nano-and Hierarchical Structures for Superhydrophobicity, Self-Cleaning and Low Adhesion. *Philos. Trans. R. Soc. A Math. Phys. Eng. Sci.* **2009**, *367* (1894), 1631–1672.

(6) Yamaguchi, M. Microfabrication of Re-Entrant Surface with Hydrophobicity/Oleophobicity for Liquid Foods. *Sci. Rep.* **2020**, *10* (1), 1–7.

(7) Nguyen-Tri, P.; Tran, H. N.; Plamondon, C. O.; Tuduri, L.; Vo, D.-V. N.; Nanda, S.; Mishra, A.; Chao, H.-P.; Bajpai, A. K. Recent Progress in the Preparation, Properties and Applications of Superhydrophobic Nano-Based Coatings and Surfaces: A Review. *Prog. Org. coatings* **2019**, *132*, 235–256.

(8) Darmanin, T.; Guittard, F.; Amigoni, S.; de Givenchy, E. T.; Noblin, X.; Kofman, R.; Celestini, F. Superoleophobic Behavior of Fluorinated Conductive Polymer Films Combining Electropolymerization and Lithography. *Soft Matter* **2011**, *7* (3), 1053–1057.

(9) Das, S.; Kumar, S.; Samal, S. K.; Mohanty, S.; Nayak, S. K. A Review on Superhydrophobic Polymer Nanocoatings: Recent Development and Applications. *Ind. Eng. Chem. Res.* **2018**, *57* (8), 2727–2745.

(10) Wang, W.; Lockwood, K.; Boyd, L. M.; Davidson, M. D.; Movafaghi, S.; Vahabi, H.; Khetani, S. R.; Kota, A. K. Superhydrophobic Coatings with Edible Materials. *ACS Appl. Mater. Interfaces* **2016**, *8* (29), 18664–18668. https://doi.org/10.1021/acsami.6b06958.

(11) Superhydrophobic Coating Market: Information by Raw Material (Carbon Nanotubes, Silica Nanoparticles), Property (Anti-Microbial, Anti-Corrosion), End-

Use Industry (Electricals & Electronics, Textiles & Leather), Region—Forecast till 2030 https://www.marketresearchfuture.com/reports/superhydrophobic-coating-market-6308.

(12) Anti-Microbial Coating Market By Product (Antimicrobial Powder Coatings, Surface Modifications and Coatings), By Application (Indoor Air Quality, Antimicrobial Textiles, Mold Remediation, Construction, Food, Healthcare) and By Region (North America, Europ https://www.marketresearchfuture.com/reports/anti-microbial-coating-market-9636.

(13) Sethi, S. K.; Manik, G. Recent Progress in Super Hydrophobic/Hydrophilic Self-Cleaning Surfaces for Various Industrial Applications: A Review. *Polym. Plast. Technol. Eng.* **2018**, *57* (18), 1932–1952.

(14) Tuteja, A.; Choi, W.; Mabry, J. M.; McKinley, G. H.; Cohen, R. E. Robust Omniphobic Surfaces. *Proc. Natl. Acad. Sci. U. S. A.* **2008**, *105* (47), 18200–18205. https://doi.org/10.1073/pnas.0804872105.

(15) Yu, F.; Wang, D.; Yang, J.; Zhang, W.; Deng, X. Durable Super-Repellent Surfaces: From Solid–Liquid Interaction to Applications. *Accounts Mater. Res.* **2021**, *2* (10), 920–932.

(16) NEINHUIS, C.; BARTHLOTT, W. Characterization and Distribution of Water-Repellent, Self-Cleaning Plant Surfaces. *Ann. Bot.* **1997**, *79* (6), 667–677. https://doi.org/https://doi.org/10.1006/anbo.1997.0400.

(17) Liu, K.; Tian, Y.; Jiang, L. Bio-Inspired Superoleophobic and Smart Materials: Design, Fabrication, and Application. *Prog. Mater. Sci.* **2013**, *58* (4), 503–564. https://doi.org/https://doi.org/10.1016/j.pmatsci.2012.11.001.

(18) Ensikat, H. J.; Ditsche-Kuru, P.; Neinhuis, C.; Barthlott, W. Superhydrophobicity in Perfection: The Outstanding Properties of the Lotus Leaf. *Beilstein J. Nanotechnol.* **2011**, *2*, 152–161. https://doi.org/10.3762/bjnano.2.19.

(19) Koch, K.; Bohn, H. F.; Barthlott, W. Hierarchically Sculptured Plant Surfaces and Superhydrophobicity. *Langmuir* **2009**, *25* (24), 14116–14120. https://doi.org/10.1021/la9017322.

(20) Shirtcliffe, N. J.; McHale, G.; Newton, M. I.; Chabrol, G.; Perry, C. C. Dual-Scale Roughness Produces Unusually Water-Repellent Surfaces. *Adv. Mater.* **2004**, *16* (21), 1929–1932. https://doi.org/10.1002/adma.200400315.

(21) Nosonovsky, M. Multiscale Roughness and Stability of Superhydrophobic Biomimetic Interfaces. *Langmuir* **2007**, *23* (6), 3157–3161. https://doi.org/10.1021/la062301d.

(22) Lafuma, A.; Quéré, D. Superhydrophobic States. *Nat. Mater.* **2003**, *2* (7), 457–460. https://doi.org/10.1038/nmat924.

(23) Marmur, A. Wetting on Hydrophobic Rough Surfaces: To Be Heterogeneous or Not To Be? *Langmuir* **2003**, *19* (20), 8343–8348. https://doi.org/10.1021/la0344682.

(24) Herminghaus, S. Roughness-Induced Non-Wetting. *Europhys. Lett.* **2000**, *52* (2), 165–170. https://doi.org/10.1209/epl/i2000-00418-8.

(25) Hensel, R.; Neinhuis, C.; Werner, C. The Springtail Cuticle as a Blueprint for Omniphobic Surfaces. *Chem. Soc. Rev.* **2016**, *45* (2), 323–341. https://doi.org/10.1039/c5cs00438a.

(26) Zhao, J.; Song, L.; Yin, J.; Ming, W. Anti-Bioadhesion on Hierarchically Structured, Superhydrophobic Surfaces. *Chem. Commun.* **2013**, *49* (80), 9191–9193. https://doi.org/10.1039/C3CC44971H.

(27) Genzer, J.; Efimenko, K. Recent Developments in Superhydrophobic Surfaces and Their Relevance to Marine Fouling: A Review. *Biofouling* **2006**, *22* (5), 339–360. https://doi.org/10.1080/08927010600980223.

(28) Cassie, A. B. D.; Baxter, S. Wettability of Porous Surfaces. *Trans. Faraday Soc.* **1944**, *40*, 546. https://doi.org/10.1039/tf9444000546.

(29) Wenzel, R. N. Surface Roughness and Contact Angle. *J. Phys. Chem.* **1949**, *53* (9), 1466–1467.

(30) Movafaghi, S.; Wang, W.; Bark, D. L.; Dasi, L. P.; Popat, K. C.; Kota, A. K. Hemocompatibility of Super-Repellent Surfaces: Current and Future. *Mater. Horizons* **2019**, *6* (8), 1596–1610. https://doi.org/10.1039/C9MH00051H.

(31) Anish, T.; Wonjae, C.; Minglin, M.; M., M. J.; A., M. S.; C., R. G.; H., M. G.; E., C. R. Designing Superoleophobic Surfaces. *Science (80-.).* **2007**, *318* (5856), 1618–1622. https://doi.org/10.1126/science.1148326.

(32) Kota, A. K.; Li, Y.; Mabry, J. M.; Tuteja, A. Hierarchically Structured Superoleophobic Surfaces with Ultralow Contact Angle Hysteresis. *Adv. Mater.* **2012**, *24* (43), 5838–5843.

(33) Wong, T.-S.; Kang, S. H.; Tang, S. K. Y.; Smythe, E. J.; Hatton, B. D.; Grinthal, A.; Aizenberg, J. Bioinspired Self-Repairing Slippery Surfaces with Pressure-Stable Omniphobicity. *Nature* **2011**, *477* (7365), 443–447. https://doi.org/10.1038/nature10447.

(34) Yong, J.; Chen, F.; Yang, Q.; Fang, Y.; Huo, J.; Zhang, J.; Hou, X. Nepenthes Inspired Design of Self-Repairing Omniphobic Slippery Liquid Infused Porous Surface (SLIPS) by Femtosecond Laser Direct Writing. *Adv. Mater. Interfaces* **2017**, *4* (20), 1700552. https://doi.org/https://doi.org/10.1002/admi.201700552.

(35) Hosseini, A.; Villegas, M.; Yang, J.; Badv, M.; Weitz, J. I.; Soleymani, L.; Didar, T. F. Conductive Electrochemically Active Lubricant-Infused Nanostructured

Surfaces Attenuate Coagulation and Enable Friction-Less Droplet Manipulation. *Adv. Mater. Interfaces* **2018**, *5* (18), 1800617.

(36) Shi, Z.; Xiao, Y.; Qiu, R.; Niu, S.; Wang, P. A Facile and Mild Route for Fabricating Slippery Liquid-Infused Porous Surface (SLIPS) on CuZn with Corrosion Resistance and Self-Healing Properties. *Surf. Coatings Technol.* **2017**, *330*, 102–112. https://doi.org/https://doi.org/10.1016/j.surfcoat.2017.09.053.

(37) Tuo, Y.; Zhang, H.; Chen, W.; Liu, X. Corrosion Protection Application of Slippery Liquid-Infused Porous Surface Based on Aluminum Foil. *Appl. Surf. Sci.* **2017**, *423*, 365–374. https://doi.org/https://doi.org/10.1016/j.apsusc.2017.06.170.

(38) Han, K.; Heng, L.; Jiang, L. Multiphase Media Antiadhesive Coatings: Hierarchical Self-Assembled Porous Materials Generated Using Breath Figure Patterns. *ACS Nano* **2016**, *10* (12), 11087–11095. https://doi.org/10.1021/acsnano.6b05961.

(39) Qiu, R.; Zhang, Q.; Wang, P.; Jiang, L.; Hou, J.; Guo, W.; Zhang, H. Fabrication of Slippery Liquid-Infused Porous Surface Based on Carbon Fiber with Enhanced Corrosion Inhibition Property. *Colloids Surfaces A Physicochem. Eng. Asp.* **2014**, *453*, 132–141. https://doi.org/https://doi.org/10.1016/j.colsurfa.2014.04.035.

(40) Kim, P.; Wong, T.-S.; Alvarenga, J.; Kreder, M. J.; Adorno-Martinez, W. E.; Aizenberg, J. Liquid-Infused Nanostructured Surfaces with Extreme Anti-Ice and Anti-Frost Performance. *ACS Nano* **2012**, *6* (8), 6569–6577.

(41) Liu, B.; Zhang, K.; Tao, C.; Zhao, Y.; Li, X.; Zhu, K.; Yuan, X. Strategies for Anti-Icing: Low Surface Energy or Liquid-Infused? *RSC Adv.* **2016**, *6* (74), 70251–70260. https://doi.org/10.1039/C6RA11383D.

(42) Chen, J.; Dou, R.; Cui, D.; Zhang, Q.; Zhang, Y.; Xu, F.; Zhou, X.; Wang, J.; Song, Y.; Jiang, L. Robust Prototypical Anti-Icing Coatings with a Self-Lubricating Liquid Water Layer between Ice and Substrate. *ACS Appl. Mater. Interfaces* **2013**, *5* (10), 4026–4030. https://doi.org/10.1021/am401004t.

(43) Elsharkawy, M.; Tortorella, D.; Kapatral, S.; Megaridis, C. M. Combating Frosting with Joule-Heated Liquid-Infused Superhydrophobic Coatings. *Langmuir* **2016**, *32* (17), 4278–4288. https://doi.org/10.1021/acs.langmuir.6b00064.

(44) Juuti, P.; Haapanen, J.; Stenroos, C.; Niemelä-Anttonen, H.; Harra, J.; Koivuluoto, H.; Teisala, H.; Lahti, J.; Tuominen, M.; Kuusipalo, J.; et al. Achieving a Slippery, Liquid-Infused Porous Surface with Anti-Icing Properties by Direct Deposition of Flame Synthesized Aerosol Nanoparticles on a Thermally Fragile Substrate. *Appl. Phys. Lett.* **2017**, *110* (16), 161603. https://doi.org/10.1063/1.4981905.

(45) Luo, J. T.; Geraldi, N. R.; Guan, J. H.; McHale, G.; Wells, G. G.; Fu, Y. Q. Slippery Liquid-Infused Porous Surfaces and Droplet Transportation by Surface

Acoustic Waves. *Phys. Rev. Appl.* **2017**, *7* (1), 14017. https://doi.org/10.1103/PhysRevApplied.7.014017.

(46) Schellenberger, F.; Xie, J.; Encinas, N.; Hardy, A.; Klapper, M.; Papadopoulos, P.; Butt, H.-J.; Vollmer, D. Direct Observation of Drops on Slippery Lubricant-Infused Surfaces. *Soft Matter* **2015**, *11* (38), 7617–7626. https://doi.org/10.1039/C5SM01809A.

(47) Brabcova, Z.; McHale, G.; Wells, G. G.; Brown, C. V; Newton, M. I. Electric Field Induced Reversible Spreading of Droplets into Films on Lubricant Impregnated Surfaces. *Appl. Phys. Lett.* **2017**, *110* (12), 121603. https://doi.org/10.1063/1.4978859.

(48) Guo, T.; Che, P.; Heng, L.; Fan, L.; Jiang, L. Anisotropic Slippery Surfaces: Electric-Driven Smart Control of a Drop's Slide. *Adv. Mater.* **2016**, *28* (32), 6999–7007. https://doi.org/https://doi.org/10.1002/adma.201601239.

(49) Epstein, A. K.; Wong, T.-S.; Belisle, R. a; Boggs, E. M.; Aizenberg, J. Liquid-Infused Structured Surfaces with Exceptional Anti-Biofouling Performance. *Proc. Natl. Acad. Sci. U. S. A.* **2012**, *109* (33), 13182–13187. https://doi.org/10.1073/pnas.1201973109.

(50) Chen, J.; Howell, C.; Haller, C. A.; Patel, M. S.; Ayala, P.; Moravec, K. A.; Dai, E.; Liu, L.; Sotiri, I.; Aizenberg, M.; et al. An Immobilized Liquid Interface Prevents Device Associated Bacterial Infection in Vivo. *Biomaterials* **2017**, *113*, 80–92. https://doi.org/10.1016/j.biomaterials.2016.09.028.

(51) Leslie, D. C.; Waterhouse, A.; Berthet, J. B.; Valentin, T. M.; Watters, A. L.; Jain, A.; Kim, P.; Hatton, B. D.; Nedder, A.; Donovan, K.; et al. A Bioinspired Omniphobic Surface Coating on Medical Devices Prevents Thrombosis and Biofouling. *Nat. Biotechnol.* **2014**, *32* (11), 1134–1140. https://doi.org/10.1038/nbt.3020.

(52) Badv, M.; Weitz, J. I.; Didar, T. F. Lubricant-Infused PET Grafts with Built-In Biofunctional Nanoprobes Attenuate Thrombin Generation and Promote Targeted Binding of Cells. *Small* **2019**, *15* (51), 1905562. https://doi.org/10.1002/smll.201905562.

(53) Badv, M.; Imani, S. M.; Weitz, J. I.; Didar, T. F. Lubricant-Infused Surfaces with Built-in Functional Biomolecules Exhibit Simultaneous Repellency and Tunable Cell Adhesion. *ACS Nano* **2018**, *12* (11), 10890–10902.

(54) Villegas, M.; Zhang, Y.; Badv, M.; Alonso-Cantu, C.; Wilson, D.; Hosseinidoust, Z.; Didar, T. F. Enhancing Osseointegration and Mitigating Bacterial Biofilms on Medical-Grade Titanium with Chitosan-Conjugated Liquid-Infused Coatings. *Sci. Rep.* **2022**, *12* (1), 1–11.

(55) Kim, P.; Kreder, M. J.; Alvarenga, J.; Aizenberg, J. Hierarchical or Not? Effect of

the Length Scale and Hierarchy of the Surface Roughness on Omniphobicity of Lubricant-Infused Substrates. *Nano Lett.* **2013**, *13* (4), 1793–1799. https://doi.org/10.1021/nl4003969.

(56) Villegas, M.; Zhang, Y.; Abu Jarad, N.; Soleymani, L.; Didar, T. F. Liquid-Infused Surfaces: A Review of Theory, Design, and Applications. *ACS Nano* **2019**, *13* (8), 8517–8536.

(57) Xie, Q.; Xu, J.; Feng, L.; Jiang, L.; Tang, W.; Luo, X.; Han, C. C. Facile Creation of a Super-Amphiphobic Coating Surface with Bionic Microstructure. *Adv. Mater.* **2004**, *16* (4), 302–305. https://doi.org/https://doi.org/10.1002/adma.200306281.

(58) Wang, X.; Hu, H.; Ye, Q.; Gao, T.; Zhou, F.; Xue, Q. Superamphiphobic Coatings with Coralline-like Structure Enabled by One-Step Spray of Polyurethane/Carbon Nanotube Composites. *J. Mater. Chem.* **2012**, *22* (19), 9624–9631. https://doi.org/10.1039/C2JM30744H.

(59) Coulson, S. R.; Woodward, I.; Badyal, J. P. S.; Brewer, S. A.; Willis, C. Super-Repellent Composite Fluoropolymer Surfaces. *J. Phys. Chem. B* **2000**, *104* (37), 8836–8840. https://doi.org/10.1021/jp0000174.

(60) Zhu, P.; Kong, T.; Tang, X.; Wang, L. Well-Defined Porous Membranes for Robust Omniphobic Surfaces via Microfluidic Emulsion Templating. *Nat. Commun.* **2017**, *8* (May). https://doi.org/10.1038/ncomms15823.

(61) Han, D.; Steckl, A. J. Superhydrophobic and Oleophobic Fibers by Coaxial Electrospinning. *Langmuir* **2009**, *25* (16), 9454–9462. https://doi.org/10.1021/la900660v.

(62) Cao, L.; Price, T. P.; Weiss, M.; Gao, D. Super Water- and Oil-Repellent Surfaces on Intrinsically Hydrophilic and Oleophilic Porous Silicon Films. *Langmuir* **2008**, *24* (5), 1640–1643. https://doi.org/10.1021/la703401f.

(63) Ahuja, A.; Taylor, J. A.; Lifton, V.; Sidorenko, A. A.; Salamon, T. R.; Lobaton, E. J.; Kolodner, P.; Krupenkin, T. N. Nanonails: A Simple Geometrical Approach to Electrically Tunable Superlyophobic Surfaces. *Langmuir* **2008**, *24* (1), 9–14. https://doi.org/10.1021/la702327z.

(64) Mazumder, P.; Jiang, Y.; Baker, D.; Carrilero, A.; Tulli, D.; Infante, D.; Hunt, A. T.; Pruneri, V. Superomniphobic, Transparent, and Antireflection Surfaces Based on Hierarchical Nanostructures. *Nano Lett.* **2014**, *14* (8), 4677–4681.

(65) Wu, W.; Wang, X.; Wang, D.; Chen, M.; Zhou, F.; Liu, W.; Xue, Q. Alumina Nanowire Forests via Unconventional Anodization and Super-Repellency plus Low Adhesion to Diverse Liquids. *Chem. Commun.* **2009**, No. 9, 1043–1045.

(66) Kim, D. H.; Kim, S.; Park, S. R.; Fang, N. X.; Cho, Y. T. Shape-Deformed Mushroom-like Reentrant Structures for Robust Liquid-Repellent Surfaces. *ACS Appl. Mater. Interfaces* **2021**, *13* (28), 33618–33626.

(67) Kim, H.; Kim, H. N.; Kang, S. M. Robust Fabrication of Double-Ring Mushroom Structure for Reliable Omniphobic Surfaces. *Surfaces and Interfaces* **2022**, *29*, 101778.

(68) Sarwate, P.; Chakraborty, A.; Garg, V.; Luo, C. Controllable Strain Recovery of Shape Memory Polystyrene to Achieve Superhydrophobicity with Tunable Adhesion. *J. Micromechanics Microengineering* **2014**, *24* (11). https://doi.org/10.1088/0960-1317/24/11/115006.

(69) Wang, Z.; Ren, B. Preparation of Superhydrophobic Titanium Surface via the Combined Modification of Hierarchical Micro/Nanopatterning and Fluorination. *J. Coatings Technol. Res.* **2022**. https://doi.org/10.1007/s11998-021-00576-9.

(70) Elbourne, A.; Crawford, R. J.; Ivanova, E. P. Nano-Structured Antimicrobial Surfaces: From Nature to Synthetic Analogues. *J. Colloid Interface Sci.* **2017**, *508*, 603–616. https://doi.org/https://doi.org/10.1016/j.jcis.2017.07.021.

(71) Sheridan, M.; Winters, C.; Zamboni, F.; Collins, M. N. Biomaterials: Antimicrobial Surfaces in Biomedical Engineering and Healthcare. *Curr. Opin. Biomed. Eng.* **2022**, *22*, 100373. https://doi.org/https://doi.org/10.1016/j.cobme.2022.100373.

(72) Elbourne, A.; Chapman, J.; Gelmi, A.; Cozzolino, D.; Crawford, R. J.; Truong, V. K. Bacterial-Nanostructure Interactions: The Role of Cell Elasticity and Adhesion Forces. *J. Colloid Interface Sci.* **2019**, *546*, 192–210. https://doi.org/https://doi.org/10.1016/j.jcis.2019.03.050.

(73) Nguyen, D. H. K.; Pham, V. T. H.; Truong, V. K.; Sbarski, I.; Wang, J.; Balčytis, A.; Juodkazis, S.; Mainwaring, D. E.; Crawford, R. J.; Ivanova, E. P. Role of Topological Scale in the Differential Fouling of: Pseudomonas Aeruginosa and Staphylococcus Aureus Bacterial Cells on Wrinkled Gold-Coated Polystyrene Surfaces. *Nanoscale* **2018**, *10* (11), 5089–5096. https://doi.org/10.1039/c7nr08178b.

(74) Efimenko, K.; Finlay, J.; Callow, M. E.; Callow, J. A.; Genzer, J. Development and Testing of Hierarchically Wrinkled Coatings for Marine Antifouling. *ACS Appl. Mater. Interfaces* **2009**, *1* (5), 1031–1040. https://doi.org/10.1021/am9000562.

(75) Freschauf, L. R.; McLane, J.; Sharma, H.; Khine, M. Shrink-Induced Superhydrophobic and Antibacterial Surfaces in Consumer Plastics. **2012**.

(76) Fadeeva, E.; Truong, V. K.; Stiesch, M.; Chichkov, B. N.; Crawford, R. J.; Wang, J.; Ivanova, E. P. Bacterial Retention on Superhydrophobic Titanium Surfaces Fabricated by Femtosecond Laser Ablation. *Langmuir* **2011**, *27* (6), 3012–3019. https://doi.org/10.1021/la104607g.

(77) Variola, F.; Zalzal, S. F.; Leduc, A.; Barbeau, J.; Nanci, A. Oxidative

Nanopatterning of Titanium Generates Mesoporous Surfaces with Antimicrobial Properties. *Int. J. Nanomedicine* **2014**, *9*, 2319–2325. https://doi.org/10.2147/IJN.S61333.

(78) Wu, S.; Zuber, F.; Brugger, J.; Maniura-Weber, K.; Ren, Q. Antibacterial Au Nanostructured Surfaces. *Nanoscale* **2016**, *8* (5), 2620–2625. https://doi.org/10.1039/C5NR06157A.

(79) Ashok, D.; Taheri, M.; Garg, P.; Webb, D.; Parajuli, P.; Wang, Y.; Funnell, B.; Taylor, B.; Tscharke, D. C.; Tsuzuki, T. Shielding Surfaces from Viruses and Bacteria with a Multiscale Coating. *Adv. Sci.* **2022**, 2201415.

(80) Jokinen, V.; Kankuri, E.; Hoshian, S.; Franssila, S.; Ras, R. *Superhydrophobic Blood-Repellent Surfaces*; 2018; Vol. 30. https://doi.org/10.1002/adma.201705104.

(81) Wu, X. H.; Liew, Y. K.; Mai, C.-W.; Then, Y. Y. Potential of Superhydrophobic Surface for Blood-Contacting Medical Devices. *International Journal of Molecular Sciences* . 2021. https://doi.org/10.3390/ijms22073341.

(82) Hou, X.; Wang, X.; Zhu, Q.; Bao, J.; Mao, C.; Jiang, L.; Shen, J. Preparation of Polypropylene Superhydrophobic Surface and Its Blood Compatibility. *Colloids Surfaces B Biointerfaces* **2010**, *80* (2), 247–250. https://doi.org/https://doi.org/10.1016/j.colsurfb.2010.06.013.

(83) Hong, Z.; Yu, X.; Jiang, H.; Xue, M.; Peng, S.; Luo, Y.; Yin, Z.; Xie, C. Influence of Surface Morphology and Surface Free Energy on the Anticoagulant Properties of Nanocone-shaped ZnO Films. *J. Appl. Polym. Sci.* **2022**, *139* (17), 52005.

(84) Pham, T. T.; Wiedemeier, S.; Maenz, S.; Gastrock, G.; Settmacher, U.; Jandt, K. D.; Zanow, J.; Lüdecke, C.; Bossert, J. Hemodynamic Aspects of Reduced Platelet Adhesion on Bioinspired Microstructured Surfaces. *Colloids Surfaces B Biointerfaces* **2016**, *145*, 502–509. https://doi.org/https://doi.org/10.1016/j.colsurfb.2016.05.022.

(85) Sun, T.; Tan, H.; Han, D.; Fu, Q.; Jiang, L. No Platelet Can Adhere—Largely Improved Blood Compatibility on Nanostructured Superhydrophobic Surfaces. *Small* **2005**, *1* (10), 959–963. https://doi.org/https://doi.org/10.1002/smll.200500095.

(86) Bartlet, K.; Movafaghi, S.; Kota, A.; Popat, K. C. Superhemophobic Titania Nanotube Array Surfaces for Blood Contacting Medical Devices. *RSC Adv.* **2017**, *7* (56), 35466–35476. https://doi.org/10.1039/C7RA03373G.

(87) Paven, M.; Papadopoulos, P.; Schöttler, S.; Deng, X.; Mailänder, V.; Vollmer, D.; Butt, H.-J. Super Liquid-Repellent Gas Membranes for Carbon Dioxide Capture and Heart–Lung Machines. *Nat. Commun.* **2013**, *4* (1). https://doi.org/10.1038/ncomms3512.

(88) Yi, E.; Kang, H. S.; Lim, S. M.; Heo, H. J.; Han, D.; Kim, J. F.; Park, A.; Choi, D.

H.; Park, Y.-I.; Park, H.; et al. Superamphiphobic Blood-Repellent Surface Modification of Porous Fluoropolymer Membranes for Blood Oxygenation Applications. *J. Memb. Sci.* **2022**, *648*, 120363. https://doi.org/https://doi.org/10.1016/j.memsci.2022.120363.

(89) Ozkan, E.; Mondal, A.; Singha, P.; Douglass, M.; Hopkins, S. P.; Devine, R.; Garren, M.; Manuel, J.; Warnock, J.; Handa, H. Fabrication of Bacteria- and Blood-Repellent Superhydrophobic Polyurethane Sponge Materials. *ACS Appl. Mater. Interfaces* **2020**, *12* (46), 51160–51173. https://doi.org/10.1021/acsami.0c13098.

(90) Doll, K.; Fadeeva, E.; Schaeske, J.; Ehmke, T.; Winkel, A.; Heisterkamp, A.; Chichkov, B. N.; Stiesch, M.; Stumpp, N. S. Development of Laser-Structured Liquid-Infused Titanium with Strong Biofilm-Repellent Properties. *ACS Appl. Mater. Interfaces* **2017**, *9* (11), 9359–9368. https://doi.org/10.1021/acsami.6b16159.

(91) Zouaghi, S.; Six, T.; Bellayer, S.; Moradi, S.; Hatzikiriakos, S. G.; Dargent, T.; Thomy, V.; Coffinier, Y.; André, C.; Delaplace, G.; et al. Antifouling Biomimetic Liquid-Infused Stainless Steel: Application to Dairy Industrial Processing. *ACS Appl. Mater. Interfaces* **2017**, *9* (31), 26565–26573. https://doi.org/10.1021/acsami.7b06709.

(92) Wang, P.; Lu, Z.; Zhang, D. Slippery Liquid-Infused Porous Surfaces Fabricated on Aluminum as a Barrier to Corrosion Induced by Sulfate Reducing Bacteria. *Corros. Sci.* **2015**, *93*, 159–166. https://doi.org/https://doi.org/10.1016/j.corsci.2015.01.015.

(93) Wu, Y.; Zhou, S.; You, B.; Wu, L. Bioinspired Design of Three-Dimensional Ordered Tribrachia-Post Arrays with Re-Entrant Geometry for Omniphobic and Slippery Surfaces. *ACS Nano* **2017**, *11* (8), 8265–8272. https://doi.org/10.1021/acsnano.7b03433.

(94) Villegas, M.; Cetinic, Z.; Shakeri, A.; Didar, T. F. Fabricating Smooth PDMS Microfluidic Channels from Low-Resolution 3D Printed Molds Using an Omniphobic Lubricant-Infused Coating. *Anal. Chim. Acta* **2018**, *1000*, 248–255. https://doi.org/10.1016/j.aca.2017.11.063.

(95) Howell, C.; Vu, T. L.; Lin, J. J.; Kolle, S.; Juthani, N.; Watson, E.; Weaver, J. C.; Alvarenga, J.; Aizenberg, J. Self-Replenishing Vascularized Fouling-Release Surfaces. *ACS Appl. Mater. Interfaces* **2014**, *6* (15), 13299–13307. https://doi.org/10.1021/am503150y.

(96) Yeong, Y. H.; Wang, C.; Wynne, K. J.; Gupta, M. C. Oil-Infused Superhydrophobic Silicone Material for Low Ice Adhesion with Long-Term Infusion Stability. *ACS Appl. Mater. Interfaces* **2016**, *8* (46), 32050–32059. https://doi.org/10.1021/acsami.6b11184.

(97) Yuan, S.; Luan, S.; Yan, S.; Shi, H.; Yin, J. Facile Fabrication of Lubricant-Infused Wrinkling Surface for Preventing Thrombus Formation and Infection. *ACS Appl. Mater. Interfaces* **2015**, *7* (34), 19466–19473. https://doi.org/10.1021/acsami.5b05865.

(98) Badv, M.; Jaffer, I. H.; Weitz, J. I.; Didar, T. F. An Omniphobic Lubricant-Infused Coating Produced by Chemical Vapor Deposition of Hydrophobic Organosilanes Attenuates Clotting on Catheter Surfaces. *Sci. Rep.* **2017**, *7* (1), 11639. https://doi.org/10.1038/s41598-017-12149-1.

(99) Tesler, A. B.; Kim, P.; Kolle, S.; Howell, C.; Ahanotu, O.; Aizenberg, J. Extremely Durable Biofouling-Resistant Metallic Surfaces Based on Electrodeposited Nanoporous Tungstite Films on Steel. *Nat. Commun.* **2015**, *6*, 8649.

(100) Badv, M.; Bayat, F.; Weitz, J. I.; Didar, T. F. Single and Multi-Functional Coating Strategies for Enhancing the Biocompatibility and Tissue Integration of Blood-Contacting Medical Implants. *Biomaterials* **2020**, *258*, 120291.

(101) Imani, S. M.; Badv, M.; Shakeri, A.; Yousefi, H.; Yip, D.; Fine, C.; Didar, T. F. Micropatterned Biofunctional Lubricant-Infused Surfaces Promote Selective Localized Cell Adhesion and Patterning. *Lab Chip* **2019**, *19* (19), 3228–3237. https://doi.org/10.1039/c9lc00608g.

(102) Shakeri, A.; Jarad, N. A.; Terryberry, J.; Khan, S.; Leung, A.; Chen, S.; Didar, T. F. Antibody Micropatterned Lubricant-Infused Biosensors Enable Sub-Picogram Immunofluorescence Detection of Interleukin 6 in Human Whole Plasma. *Small* **2020**, *16* (45), 2003844.

(103) Contreras-Naranjo, J. E.; Aguilar, O. Suppressing Non-Specific Binding of Proteins onto Electrode Surfaces in the Development of Electrochemical Immunosensors. *Biosensors* **2019**, *9* (1), 15.

(104) Lichtenberg, J. Y.; Ling, Y.; Kim, S. Non-Specific Adsorption Reduction Methods in Biosensing. *Sensors* **2019**, *19* (11), 2488.

(105) Lichtenberg, J. Y.; Ling, Y.; Kim, S. Non-Specific Adsorption Reduction Methods in Biosensing. *Sensors* . 2019. https://doi.org/10.3390/s19112488.

(106) Lin, P.-H.; Li, B.-R. Antifouling Strategies in Advanced Electrochemical Sensors and Biosensors. *Analyst* **2020**, *145* (4), 1110–1120.

(107) Szymczyk, A.; Soliwodzka, K.; Moskal, M.; Różanowski, K.; Ziółkowski, R. Further Insight into the Possible Influence of Electrode Blocking Agents on the Stem-Loop Based Electrochemical DNA Sensor Parameters. *Sensors Actuators B Chem.* **2022**, *354*, 131086. https://doi.org/https://doi.org/10.1016/j.snb.2021.131086.

(108) Liu, N.; Xu, Z.; Morrin, A.; Luo, X. Low Fouling Strategies for Electrochemical Biosensors Targeting Disease Biomarkers. *Anal. Methods* **2019**, *11* (6), 702–711.

(109) Bertok, T.; Klukova, L.; Sediva, A.; Kasak, P.; Semak, V.; Micusik, M.; Omastova, M.; Chovanová, L.; Vlček, M.; Imrich, R. Ultrasensitive Impedimetric Lectin Biosensors with Efficient Antifouling Properties Applied in Glycoprofiling of Human Serum Samples. *Anal. Chem.* **2013**, *85* (15), 7324–7332.

(110) Marchlewicz, K.; Ostrowska, I.; Oszwałdowski, S.; Zasada, A.; Ziółkowski, R.; Malinowska, E. Molecular Diagnostic of Toxigenic Corynebacterium Diphtheriae Strain by DNA Sensor Potentially Suitable for Electrochemical Point-of-Care Diagnostic. *Talanta* **2021**, *227*, 122161. https://doi.org/https://doi.org/10.1016/j.talanta.2021.122161.

(111) Ziółkowski, R.; Kaczmarek, A.; Kośnik, I.; Malinowska, E. Reduced Nonspecific Protein Adsorption by Application of Diethyldithiocarbamate in Receptor Layer of Diphtheria Toxoid Electrochemical Immunosensor. *Bioelectrochemistry* **2020**, *132*, 107415. https://doi.org/https://doi.org/10.1016/j.bioelechem.2019.107415.

(112) Campuzano, S.; Pedrero, M.; Yáñez-Sedeño, P.; Pingarrón, J. M. Antifouling (Bio) Materials for Electrochemical (Bio) Sensing. *Int. J. Mol. Sci.* **2019**, *20* (2), 423.

(113) Jolly, P.; Formisano, N.; Tkáč, J.; Kasák, P.; Frost, C. G.; Estrela, P. Label-Free Impedimetric Aptasensor with Antifouling Surface Chemistry: A Prostate Specific Antigen Case Study. *Sensors Actuators B Chem.* **2015**, *209*, 306–312. https://doi.org/https://doi.org/10.1016/j.snb.2014.11.083.

(114) Hui, N.; Sun, X.; Niu, S.; Luo, X. PEGylated Polyaniline Nanofibers: Antifouling and Conducting Biomaterial for Electrochemical DNA Sensing. *ACS Appl. Mater. Interfaces* **2017**, *9* (3), 2914–2923. https://doi.org/10.1021/acsami.6b11682.

(115) Song, Z.; Ma, Y.; Chen, M.; Ambrosi, A.; Ding, C.; Luo, X. Electrochemical Biosensor with Enhanced Antifouling Capability for COVID-19 Nucleic Acid Detection in Complex Biological Media. *Anal. Chem.* **2021**, *93* (14), 5963–5971. https://doi.org/10.1021/acs.analchem.1c00724.

(116) Russo, M. J.; Han, M.; Desroches, P. E.; Manasa, C. S.; Dennaoui, J.; Quigley, A. F.; Kapsa, R. M. I.; Moulton, S. E.; Guijt, R. M.; Greene, G. W. Antifouling Strategies for Electrochemical Biosensing: Mechanisms and Performance toward Point of Care Based Diagnostic Applications. *ACS sensors* **2021**, *6* (4), 1482–1507.

(117) González-Fernández, E.; Staderini, M.; Avlonitis, N.; Murray, A. F.; Mount, A. R.; Bradley, M. Effect of Spacer Length on the Performance of Peptide-Based Electrochemical Biosensors for Protease Detection. *Sensors Actuators B Chem.* **2018**, *255*, 3040–3046.

(118) Wu, H.; Lee, C.-J.; Wang, H.; Hu, Y.; Young, M.; Han, Y.; Xu, F.-J.; Cong, H.; Cheng, G. Highly Sensitive and Stable Zwitterionic Poly (Sulfobetaine-3, 4-Ethylenedioxythiophene)(PSBEDOT) Glucose Biosensor. *Chem. Sci.* **2018**, *9* (9), 2540–2546.

(119) Hasanzadeh, M.; Shadjou, N. Electrochemical Nanobiosensing in Whole Blood: Recent Advances. *TrAC Trends Anal. Chem.* **2016**, *80*, 167–176.

2 Chapter 2: Antimicrobial Nanomaterials and Coatings – a Closer Look at Current Antiviral Mechanisms and Future Perspectives to Control the Spread of Viruses Including SARS-CoV-2

Sara M. Imani, Liane Ladouceur, Terrel Marshall, Roderick Maclachlan, Leyla Soleymani*, Tohid F. Didar*

ACS Nano 2020, 14, 10, 12341–12369, doi: 10.1021/acsnano.0c05937

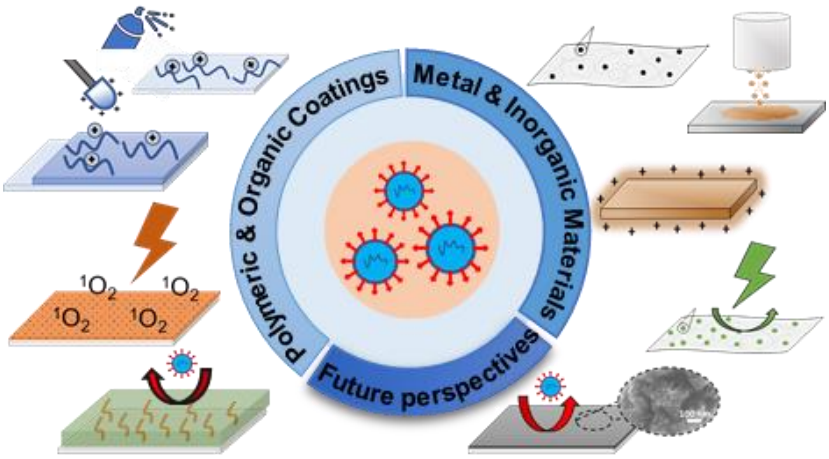

Preface

This chapter presents and extensive literature review on antiviral materials and coatings with the potential to be implemented for suppressing the spread of SARS-CoV-2. Various classes and mechanisms of action of the antiviral properties are discussed along with environmental and toxicity concerns which are comparable with existing means of antibacterial action. Finally, future perspectives with regards to emerging antimicrobial technologies for potential use in mitigating viral contaminations are discussed, specifically

we speculate use of virus repellent surfaces, following the extensive research done as discussed in chapter 3 on bacteria repellent surfaces.

2.1 Abstract

The global COVID-19 pandemic has attracted considerable attention toward innovative methods and technologies for suppressing the spread of viruses. Transmission *via* contaminated surfaces has been recognized as an important route for spreading SARS-CoV-2. While significant efforts have been made to develop antibacterial surface coatings, the literature remains scarce for a systematic study on broad-range antiviral coatings. Here, we aim to provide a comprehensive overview of the antiviral materials and coatings that could be implemented for suppressing the spread of SARS-CoV-2 *via* contaminated surfaces. We discuss the mechanism of operation and effectivity of several types of inorganic and organic materials, in the bulk and nanomaterial form, and assess the possibility of implementing these as antiviral coatings. Toxicity and environmental concerns are also discussed for the presented approaches. Finally, we present future perspectives with regards to emerging antimicrobial technologies such as omniphobic surfaces and assess their potential in suppressing surface-mediated virus transfer. Although some of these emerging technologies have not yet been tested directly as antiviral coatings, they hold great potential for designing the next generation of antiviral surfaces.

Keywords: antiviral surfaces, antimicrobial coatings, pathogen-repellent surfaces, nanocoatings, photoactive materials, engineered surfaces, COVID-19, virus inactivation, virus repellent

2.2 Introduction

The COVID-19 pandemic has intensified the world's attention toward the spread of contamination facilitated by *high touch* surfaces. In response, surfaces and coatings capable of minimizing the presence of active viral pathogens are being explored for application in a variety of settings such as healthcare centres, long-term care facilities, public transport, schools, and various businesses, to reduce human exposure and mitigate the spread of infectious pathogens.

One area of particular significance in the transmission of infectious diseases is the ability of microbes to survive on surfaces, both in healthcare settings and on common surfaces. Considerable research has been conducted to investigate solutions that prevent bacterial transmission and biofilm formation by killing and/or reducing attachment of microbes. These have been realized through surface-bound active antimicrobials and biocidal coatings [1] or passive pathogen-repellent surfaces [2] developed using nanomaterials, chemical modifications, and micro- and nanostructuring.[2–5]

Many of the previously-reported antimicrobial coatings have focused on antibacterial capabilities; however, there has been much less focus on antiviral surfaces and coatings. Persistence of active viruses on surfaces varies dramatically based on the type of the surface

and the virus.[6] For example, the viability of coronaviruses on surfaces ranges from 2 hours to 9 days.[6] Lack of host cells, immediate inactivation of some viruses on surfaces (*e.g.* Rinderpest virus),[7] and incapability of some viruses to spread outside the body (*e.g.* Human Immunodeficiency Virus-HIV),[8] have attracted less attention to the transmission of viruses *via* surfaces. However, infectious viruses such as SARS-CoV-2 that remain viable on surfaces pose a great risk for transmission *via* the surface route, highlighting the urgent need for effective solutions that prevent the survival of viruses on surfaces.[6,9] In order to highlight antimicrobial research which has definitively demonstrated antiviral capabilities, throughout this review we will use the term antiviral to refer to nanomaterials and coatings which have proven antiviral capabilities, whereas the term antimicrobial will be used as a more general term to characterize nanomaterials and coatings that demonstrate effectiveness against other microorganisms, such as bacteria, but to date have no proven antiviral capability.

A challenge encountered in reviewing the antiviral surface literature is related to the wide range of viruses used in testing. It is common to find tests conducted using bacteriophages, influenza, or HIV, however, there is often no systematic study that allows for the precise understanding of virucidal behaviour. Viruses have a multitude of architectures – enveloped or non-enveloped, RNA-based or DNA-based – and can be further classified as positive- or negative-sense, or single- or double-stranded, respectively. This is only the high-level variation witnessed in viruses, which illustrates the clear need for more robust testing when claiming antiviral capabilities.

Despite these caveats related to the lack of standardized evaluation methods, this review aims to provide a comprehensive summary of the current state of research toward antiviral materials and surfaces (Figure 2.1), using antimicrobial research as a starting point, whereas other review papers regarding reducing the spread of COVID-19 have focused on therapeutics and tools that inactivate SARS-CoV-2.[10,11] First, we present a comprehensive review of metal and inorganic materials, with a focus on nanomaterials, with antiviral properties namely, copper, silver, zinc, and titanium dioxide. We then discuss polymeric and organic surface coatings such as polyelectrolytes and photosensitizer materials that inactivate viruses (Figure 2.1). The toxicity and environmental concerns considered for each of these approaches will also be discussed. We finally present and propose emerging technologies that have not yet been used for antiviral purposes but hold great promise and potential for the future engineering of antiviral surfaces as they have been tested for their antimicrobial properties.

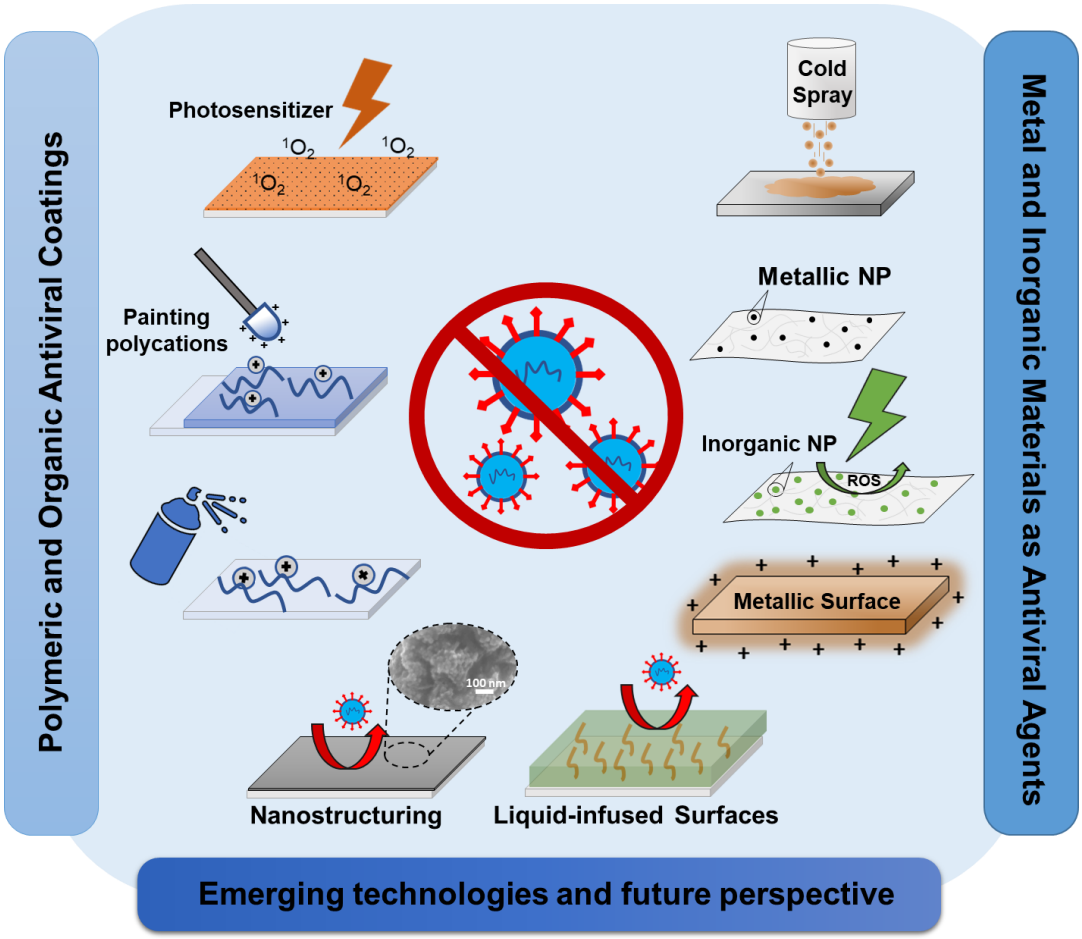

Figure 2.1 Schematic diagram of the current research and emerging antiviral coatings and surfaces, including metal and inorganic nanomaterials, polymeric and organic coatings and emerging technologies such as omniphobic pathogen-repellent coatings.

2.3 Metal and Inorganic Materials as Antiviral Agents

2.3.1 Copper

Copper is perhaps the most widely-recognized and well-characterized antimicrobial metal used to date.[12] Use of copper in medicine, as an antiseptic and anti-inflammatory agent, dates back millennia.[13] Through bacterial investigations, modern research has identified multiple antimicrobial mechanisms for copper such as: (1) plasma membrane permeabilization, (2) membrane lipid peroxidation, (3) alteration of proteins, (4) inhibition

of protein assembly and activity, or (5) denaturation of nucleic acids.[14] Membrane disruption can occur due to the electrostatic forces exerted by copper ions on the outer plasma membrane of cells.[15] Damage to proteins occurs *via* the displacement of essential metals from their native binding sites on proteins or direct interactions with the proteins.[16] Copper-binding sites on nucleic acids also enable protein denaturation.[17] Additionally, cyclic redox reactions between Cu^{+} and Cu^{2+} are known to produce highly reactive hydroxyl radicals. Reactive oxygen species (ROS) are either responsible for or contribute to cell death by interaction with the cell membrane.[18]

While some hypotheses have been made into the virucidal action of copper, the majority of antimicrobial copper research is focused on its antibacterial properties.[12] Research has demonstrated that copper targets the viral genome, particularly encoding genes that are essential for viral infectivity (Figure 2.2a).[19] It has been demonstrated that the primary effectors of inactivation for viruses such as murine norovirus are Cu(II) and Cu(I).[20] Additionally, many researchers have postulated that the same ROS mechanism found in antibacterial activity can act on the viral envelope or capsid.[12] Notably, viruses are susceptible to the damage induced by copper since they do not possess the repair mechanisms found in bacteria or fungi.[14]

Mechanisms that result in the immediate deactivation of microbes upon contact are commonly referred to as "contact killing".[21] Researchers have taken advantage of this functionality to create copper-based antiviral surfaces (Table 2.1). Inactivation of influenza A was demonstrated to be significantly higher on planar copper in comparison to stainless steel, leaving only 500 infectious virus particles after 6 hours from the 2×10^6 virus particles

inoculated, while stainless steel retained 500,000 infectious virus particles after 24 hours.[22] Influenza A and *Escherichia* bacteriophage (Qβ) were also tested on solid-state copper compounds and compared to solid-state silver compounds, with efficient inactivation achieved using cuprous oxide in solid-state but not cupric oxide or silver sulfide solid-states.[23] This difference between cuprous oxide solid-state copper and cupric compounds was in line with work by Sunada *et al.* using bacteriophage Qβ, which revealed a 6-log reduction for cuprous oxide (Cu_2O) in 30 minutes but a less than 1-log reduction on cupric oxide (CuO) in the same duration.[18] In tests on copper coupons, a copper-mediated inactivation was illustrated for a range of bacteriophages by Li and Dennehy.[24] This study included a range of double-stranded DNA, single-stranded DNA, and single-stranded RNA bacteriophages, with lipid-containing bacteriophages demonstrating the most susceptibility to copper in solution, such as *Pseudomonas* bacteriophage (bacteriophage Φ6) showing a 2-log reduction in the first hour.[24] Studies using copper have also demonstrated significant reduction to orthopoxviruses, with monkeypox virus and vaccinia virus being inactivated within three minutes of contact with copper surfaces.[21] Warnes and Keevil have highlighted the effectiveness of copper alloys, with 60% or higher copper component, in completely inactivating dry touch murine norovirus as fast as 5 minutes and showing significant reductions to wet fomite infectivity, up to complete inactivation within 60 minutes.[20] Of particular interest for the current COVID-19 pandemic, in 2015 Warnes *et al.* investigated the use of copper alloys for the inactivation of human coronavirus 229E and showed that complete inactivation of 10^3 PFU applied to a 1 cm^2 coupon occurred in less than 60

minutes on a range of alloys, with Cu/Zn brasses being very effective at 70% or higher copper concentrations.[25]

Researchers have also investigated the incorporation of copper ions into other materials to invoke antiviral capabilities. The research in this area was pioneered by Karlstrom and Levine in 1991 when the inhibition of proteases, proteins essential for viral replication, from human immunodeficiency virus 1 (HIV-1) was investigated under the influence of copper and mercury ions, Cu^{2+} and Hg^{2+}.[16] This study demonstrated that oxygen was not required for the inactivation of the protease and that approximately stoichiometric concentrations of copper and mercury ions caused rapid and irreversible inactivation. While this research notes that a clear cation binding site exists on aspartic proteases, tests have also shown that copper does not directly inactivate these proteases. Instead, it is postulated that copper acts on the substrates for proteases, though this has not been clearly demonstrated.[16]

Copper ions and particles have also been used in antimicrobial and antiviral textiles, filters, and polymeric materials such as latex.[26–29] Early examples of this include the work by Borkow and Gabbay, which created latex gloves impregnated with copper for testing against HIV-1 and copper filters tested with both HIV-1 and West-Nile virus (WNV).[26] Antiviral effectiveness of latex samples in this study was based on the amount of copper incorporated in a dose-dependent manner, while the filters demonstrated a roughly 5-log reduction for both HIV-1 and WNV. Filters constructed from a layer of nonwoven polypropylene fibers on top of nonwoven carbon fibers were doped with copper-oxide and investigated in a study by Borkow *et al.* that demonstrated reduction in various viruses,

starting at a maximum of 2-log reduction of rhinovirus-2, and decreasing reductions were seen with yellow fever, influenza A, measles, respiratory syncytial, parainfluenza 3, Punta Toro, Pichinde, HIV-1, adenovirus type 1, and cytomegalovirus, with vaccinia virus demonstrating the lowest reduction of just 0.47 log (see Table 2.1).[27] Interestingly, copper oxide was incorporated into face masks, which resulted in the elimination of the human influenza A virus within 30 minutes, compared to 4.67 ± 1.35 $\log_{10}$ $TCID_{50}$ (Median Tissue Culture Infectious Dose) recovered from control masks (Figure 2.3a) by aerosolized challenge with 5.66 ± 0.51 $\log_{10}$ $TCID_{50}$ of the virus.[28] It has also been demonstrated that by using a cotton textile on which zeolite A was chemically synthesized, the structural component Na^+ can be replaced with Cu^{2+} ions to then allow the textile to inactivate both highly pathogenic H5N1 and less pathogenic H5N3 influenza viruses.[29]

Copper nanoparticles (CuNPs) present great promise for use in antimicrobial and antiviral surfaces due to their smaller size and high surface to volume ratio. This facilitates interaction with microbes and allows broad-spectrum antimicrobial and antiviral activity.[30] Li *et al.* used CuNPs as part of a layered system, by combining the antimicrobial and antiviral properties of copper and chlorine dioxide (ClO_2).[31] This work investigated the use of a polymeric micelle preparation, coated on glass, for the slow release of ClO_2 over a 15-day span. In order to increase the contact killing efficiency of this material, CuNP were covalently clustered on the micelle surface.[31] Testing of this coating demonstrated a broad spectrum of activity that killed a range of microbes including viruses (H1N1), bacteria, and spores. Transmission electron microscope (TEM) images demonstrated significant degradation in virus structure upon contact with this coating (Figure 2.3b). The complete

inactivation of the influenza virus was demonstrated *via* plaque assay with this coating within one minute.[31]

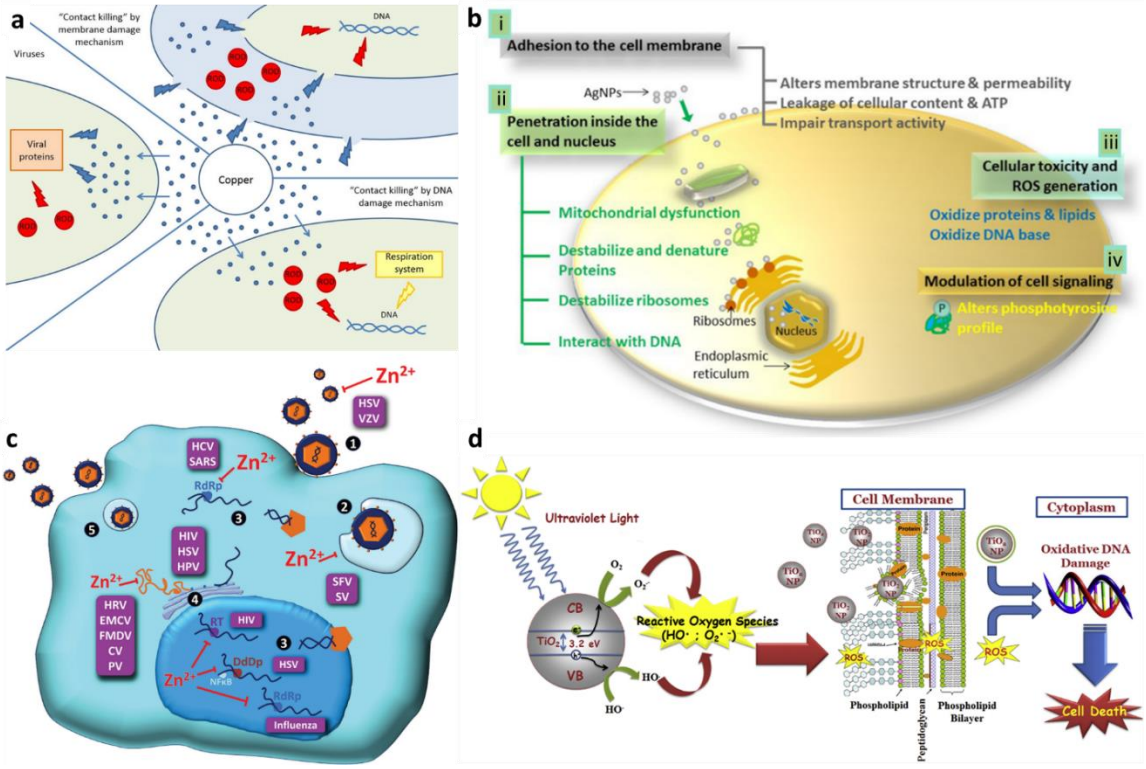

Figure 2.2 Antiviral mechanisms of inorganic materials. *(a) Antimicrobial contact killing mechanisms for copper, include membrane degradation, genotoxicity and potentially ROS. Reproduced with permission from [12] (b) Four prominent routes of antimicrobial action for silver include adhesions to cell membrane (i), penetration into cell and nucleus (ii), cellular toxicity and ROS generation (iii) and modulation of cell signaling (iv). Reproduced with permission from [32] (c) The actions of zinc throughout the cell and proposed mechanisms for antiviral properties include free virus inactivation (1), inhibition of viral uncoating (2), viral genome transcription (3), and viral protein translation and polyprotein processing (4) Reproduced with permission from [33] (d) The photocatalytic process by which TiO_2 nanoparticles and TiO_2 compounds produce reactive oxygen species (ROS) to cause disturbance of lipid membranes and damage to genetic information, ultimately resulting in bacterial cell death or viral inactivation. Reproduced with permission from [34]*

Finally, work published by Champagne *et al.* has demonstrated different methods of applying copper powder on surfaces.[35] Specifically, they tested spray coating methods with

copper powder to convey antimicrobial and antiviral effects. They also discovered that using a cold-coating approach, coating at a velocity of 500-1000 m/s and a temperature of 150-400°C, similar to many commercial approaches that exist to apply metal coatings, was most effective against influenza A, with 100% inhibition after just 10 minutes of exposure to a 100 µL aliquot of virus.[35]

2.3.2 Silver

Silver is another antiviral material that deactivates viruses by interaction with the viral envelope and viral surface proteins, blocking of viral penetration into cells, blocking cellular pathways, interaction with the viral genome, and interaction with viral replication factors (Figure 2.2b).[36] A significant portion of antiviral research for silver remains in solution.[32] Nevertheless, previous studies have specifically investigated the use of silver in the form of ions, nanoparticles, and hybrid coatings to develop antiviral surfaces (Table 2.1). Work by Lara *et al.* aimed at elucidating the mechanism of viral deactivation for silver using HIV-1, suggesting that silver nanoparticles (AgNPs) function as early-stage antivirals that disrupt viral replication.[37] They hypothesized these to inhibit viral entry by binding or fusion to cells, though AgNPs also demonstrated inhibition at later stages in viral replication for which the mechanism was not confirmed.[37] It is also evident that silver interacts differently with different families of viruses.[38] Unlike copper, solid-state silver compounds do not appear to have strong antiviral capabilities. In a comparative study conducted by Minoshima *et al.*, it was found that while solid-state cuprous oxide effectively inactivated influenza A virus and bacteriophage Qβ, solid-state silver sulfide showed little antiviral activity.[23] Silver as an antimicrobial and antiviral has an affinity toward sulfur and

phosphate groups,[39] which can disrupt the cell membrane due to the interaction with phospholipid tails and proteins containing cysteine or methionine. Additionally, Ag^+ produces reactive oxygen species (ROS) within cells, leading to an antimicrobial and antiviral ability.[40] In bacterial studies, AgNPs are thought to disrupt the mitochondrial respiratory chain leading to the production of ROS.[41] More specific to antiviral activities, AgNPs are thought to inhibit the entry of the virus to cells due to binding of envelope proteins, such as glycoprotein gp120, which prevent CD4-dependent virion binding, fusion and infectivity.[37]

The use of metal ions within coatings is a common approach found in literature. A study conducted by Hodek *et al.* investigated the use of silver, as well as copper and zinc, as part of a sol-gel, hybrid coating.[42] Antiviral tests used HIV-1, dengue virus, herpes simplex virus (HSV), influenza virus, and coxsackievirus to provide comprehensive analysis on enveloped and non-enveloped, as well as DNA- and RNA-based viruses. Results were most favourable with HIV-1, with one method of coating showing a 99.8% reduction in virus titer.[42] Log-scale reductions were significant for all types of viruses (Table 2.1), though this coating was less effective against influenza and coxsackievirus, which is thought to be due to the nature of each virus as negative-sense RNA based or non-enveloped, respectively.[42] Castro-Mayorga *et al.* demonstrated the effectiveness of both silver nitrate and AgNPs in reducing recovered titer levels of norovirus surrogates for up to 150 days.[38] Using feline calicivirus (FCV) and murine norovirus (MNV), statistically significant reductions in surface recovery of both viruses were seen in the presence of the ions and AgNPs (see Table 2.1). Notably, AgNP activity as an antiviral increased or remained constant up to 150 days

if the concentration was higher than 2.1 mg/L, however, silver nitrate was most effective over only the first 75 days, likely due to the reduction and aggregation of ions.[38] Here, silver nitrate was more effective against FCV, while AgNPs maintained higher and more prolonged effectiveness against MNV. This study further tested a AgNP film, produced by electrospinning a coating of poly(3-hydroxybutyrate-co-3-hydroxyvalerate) (PHBV)/AgNP fiber mats, which were tested at both 25°C and 37°C.[38] Reductions of 1.42- and 0.14-log were demonstrated for FCV and MNV, respectively at 25°C, which were not shown to be statistically significant compared to control PHBV films exposed to the virus.[38] At 37°C, the reduction of FCV was greater than 2.26-log, while the reduction in MNV was less successful, at only 0.86-log. It is here hypothesized that the release of silver ions from the immobilized AgNPs are responsible for the viral inactivation observed here; however, further testing and research is required to confirm this mechanism.[38]

Similar to the work of Castro-Mayorga *et al.*, AgNPs are combined with many different materials to lend antiviral capabilities. For example, chitin-nanofiber sheets (CNFS) have been combined with AgNPs to form antimicrobial and antiviral biomaterials including a 2-log decrease in influenza A.[43] Integration of AgNPs into sheets was also the approach taken by Chen *et al.*, with their research on the antiviral activity of graphene-oxide sheets with silver particles (GO-Ag).[44] Using both an enveloped and non-enveloped virus, researchers found that inhibition of viruses depended on the concentration of GO-Ag.[44] The minimum concentration of GO-Ag required to inhibit infectious bursa virus (IBDV) inoculated at 9 x 10^2 $TCID_{50}$/mL was 0.125 mg/mL, while a higher inoculation of the virus, 9 x 10^3 $TCID_{50}$/mL IBDV, required 1 mg/mL of GO-Ag for inhibition. For inoculation of 4.7 x 10^4

$TCID_{50}$/mL of feline coronavirus (FCoV), 0.1 mg/mL concentration of GO-Ag caused 24.8% inhibition.[44] For this study, silver doubled the capability of graphene oxide sheets against enveloped viruses, while it was the sole source of inhibition against the non-enveloped virus.

Integration of nanoparticles into membranes and filters is another common theme throughout the literature. Similar to copper, AgNPs can be incorporated into textiles and membranes in order to confer antiviral capabilities. Zodrow *et al*. investigated the use of AgNPs with polysulfone membranes, which exhibit promising antiviral properties, although a significant loss of silver from the membrane resulted in short-lived antibacterial and antiviral activity.[45] While the exact mechanism for antiviral capabilities was not confirmed, the possibility of change in membrane permeability, depth of filtration, electrostatic adsorption or inactivation by Ag^+ ions allowed for influent concentrations of up to $5\pm0.2 \times 10^5$ PFU/mL to be completely removed, while membranes without silver retained 10^2 PFU/mL.[45] Similarly, work by De Gusseme *et al.* produced biogenic silver, which is associated with the bacterial cell surface of *Lactobacillus fermentum*, immobilized onto polyvinylidene fluoride (PVDF) membranes.[46] This work tested antiviral properties using bacteriophage UZ1 and based on the slow release of Ag^+, at least a 3.4-log decrease in virus load was achieved. Integration of silver into polylactide (PLA) films functions in the same manner as biogenic silver on PVDF, with the slow migration of silver from the film as demonstrated by Martinez-Abad *et al.* when tested against FCV.[47] Similar to this approach with membranes, silver can be integrated into filters in order to trap airborne virus particles. In research conducted by Joe *et al.*, AgNPs were coated onto a medium air filter,

which showed increased filter efficacy over 15 minutes of testing, with a density of 1.5 x 10^9 particles/cm^2 demonstrating roughly 70% antiviral efficiency without the presence of dust.[48] Importantly, efficiency increased with silver density but decreased as dust buildup accumulated.

Research to date has demonstrated that the size of AgNPs influences their effectiveness as antiviral agents, with 25 nm as their upper size limit.[49] Interestingly, Rogers *et al.* discovered that larger AgNPs – at diameters of 25 nm, 55 nm, and 80 nm – increase the number of plaque-forming units compared to controls, promoting virus survival.[50] A proposed explanation for this is that when the AgNPs are too large to establish a strong physical interaction with the glycoprotein present on viruses, they are unable to inhibit viral binding to cell surfaces and instead, these nanoparticles may agglomerate facilitating interaction of the virus with the host cells.[50]

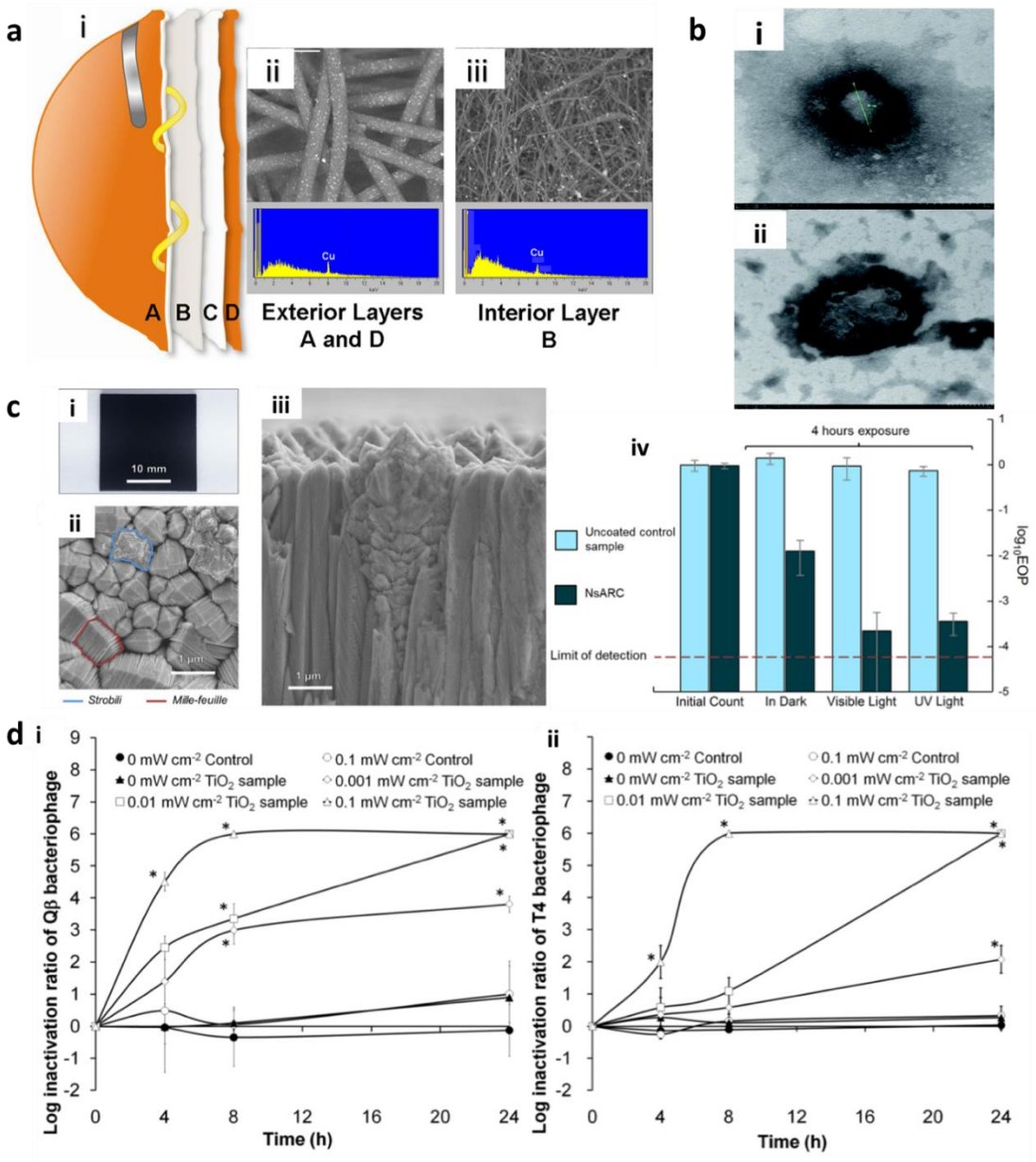

Figure 2.3 Examples of inorganic antiviral coatings. *(a) Copper impregnation on face mask. Reproduced with permission from* [28] *(b) Demonstration of virucidal capabilities conferred through a multi-functional antimicrobial and antiviral coating consisting micelles containing copper nanoparticles. (i) TEM image of influenza H1N1; (ii) TEM image of H1N1 virus after contact with coating. Reproduced with permission from* [31] *(c) i. Surface of composite nanostructured anatase-rutile-carbon (NsARC) coating on stainless steel. ii. SEM of NsARC coating surface morphology. iii. SEM of NsARC coating cross section. The nanoscale features resembling anatase sheets (mille-feuille) and rutile cones (strobili) increase the coating's surface area, promoting efficient charge separation to elicit the photocatalytic effect. iv. Reduction in the number of E. coli live cells after 4 h*

exposure to UV light, visible light, and dark conditions on uncoated stainless steel and NsARC-coated stainless steel. Reproduced with permission from [51] (d) Antiviral performance of a TiO_2 solid coating on glass with UVA irradiation intensities of 0, 0.001, 0.01, and 0.1 mW/cm^2 against (i) Bacteriophage Qβ and (ii) Bacteriophage T4. Reproduced with permission from [52]

2.3.3 Zinc

Zinc has also been demonstrated as an antiviral agent since the publication of a study in 1974 by Korant *et al.* demonstrating its effectiveness against the human rhinovirus (HRV).[53] Their use of 0.1 mM zinc chloride provided a 99.99% reduction in the number of plaques formed for HRV. It was also demonstrated in this work that the most dramatic effect of zinc as an antiviral was in inhibiting proteolytic cleavage, thereby halting the synthesis of viral polypeptides.[53] As with most metals, the mechanism for antiviral applications varies between viruses. Studies have shown mechanisms that interfere with viral replication, including free virus inactivation and inhibition of viral uncoating, viral genome transcription, and viral protein translation and polyprotein processing (Figure 2.2c).[33] For example, the effects of zinc on HSV-1 and -2 have been studied for over 40 years and research has suggested antiviral functionality in all aspects of the virus life cycle including polymerase function, protein production and processing, and free virus inactivation.[54–56] It is worth noting that many viruses rely on a zinc-finger architecture for their replication by host cells, demonstrating the relevance of zinc as an antiviral agent. Zinc-fingers are protein motifs that contain one or more amino acid sequence that allows the coordination of one of more zinc ions.[57] Williams *et al.* illustrated that subtle changes in the zinc-finger structure of the nucleocapsid protein in HIV-1 reduced the effectiveness

of chaperone activity that destabilizes nucleic acids during the reverse transcription process of viral replication.[57]

For antiviral surface applications, zinc is typically combined with other metals, whether as part of an alloy [19] or as an ion within a coating.[42] Researchers have investigated the use of solid surfaces containing zinc combined with copper to create an antiviral alloy. Surfaces showed synergistic capabilities between zinc and copper with up to 40% zinc showing some efficacy to inactivate murine norovirus (MNV) and alloys containing up to 30% zinc completely inactivating 5 x 10^5 PFU/cm^2 within 2 hours.[19] Notably, this study found a 1-log reduction in the infectivity of MNV using pure zinc, which conveys its capability as an antiviral on its own.

Zinc oxide (ZnO) has also been used to create structures that act as viricidal agents. Mishra *et al.* generated zinc oxide micro-nano structures (ZnO-MNSs), which mimicked the naturally-occurring filopodia-like structures observed on the surface of HSV-1. These structures are thought to compete with the virus to bind heparan sulfate on the cell surface and also efficiently trap virions outside cells due to partial negatively charged oxygen vacancies.[58] Pre-incubation of ZnO-MNSs with HSV-1 for 90 minutes significantly blocked viral entry. Monitoring the enzymatic activity of infected cells measured using optical density showed that at a ZnO-MNSs concentration of 100 µg/mL, below 20% of HSV-1 entered the cell, which increased to just below 30% entry when the ZnO-MNSs concentration is at 0.1 µg/mL, while the PBS control showed roughly 70% HSV-1 entry into cells.[58] This reduction of virus cell entry was increased by the use of ultraviolet (UV) light to create oxygen vacancies in the structure of ZnO-MNSs.

Zinc ionophores, substances responsible for transporting zinc ions across lipid membranes, are another intriguing use of the metal for antiviral capabilities. In research conducted by Qiu *et al.*, the use of pyrithione (PT), which is a zinc ionophore, proved effective in inhibiting HSV-1 and HSV-2 replication.[59] Here, PT facilitated the inhibition of HSV late gene expression and the production of viral progeny, which is presumed to be due to its role in the transport of Zn^{2+}, as inactivation was dependent on ion presence.

2.3.4 Titanium Dioxide (TiO_2)

TiO_2 has attracted much attention for its photocatalytic properties and its resultant applications to the inactivation of bacteria and viruses. The mechanism of pathogenic inactivation in TiO_2 is related to light absorption, electron/hole generation, and the oxidation of organic material by ROS, such as superoxide anions and hydroxyl radicals, generated *via* valence band holes and conduction band electrons (Figure 2.2d).[34,60–63] As with other compounds, research into the antimicrobial properties of TiO_2 has largely focused on antibacterial applications, leaving studies into its virucidal activity relatively scarce.

Early studies investigated the mechanisms of TiO_2 photoinactivation of microbes in solution. Akhtar *et al.* developed TiO_2 colloidal nanoparticles by a sonochemical method and demonstrated antibacterial and antiviral activity.[64] The authors note that gram-negative bacteria were more resistant to TiO_2, citing enzymatic and DNA damage as probable mechanisms alongside membrane disruption. They qualitatively demonstrated antiviral activity by inoculating chick allantoises with Newcastle disease virus (NDV) and a sample

of nano-colloids (see Table 2.1). The presence of active virus was characterized by hemagglutination of the allantois; virucidal behaviour was demonstrated at concentrations above 6.25 μg/mL.[64]

Planar surface coatings of TiO_2 have been effective antibacterial agents. Nakano *et al.* tested the antibacterial activity of TiO_2-coated glass slides on a range of bacteria, finding that all tested strains were photocatalytically inactivated on TiO_2-coated glass under UVA exposure. They also demonstrated that gram-negative bacteria were significantly more resistant to TiO_2 catalysis, further implicating the lipid membrane as a locus of ROS activity.[65] Krumdieck *et al.* report growing a nanostructured, solid, composite surface coating of anatase and rutile formations of TiO_2 with carbon on stainless steel by a scalable vapour deposition method.[51] The co-deposition of amorphous carbon enhances the photocatalytic activity of the coating by broadening the range of excitation wavelengths. They reported sizeable reductions of bacterial activity under UV and visible light irradiation and under totally dark conditions (Figure 2.3c).[51] Several studies have identified alterations to cell membrane potential, increasing permeability to damaging agents, as a possible "dark" mechanism of TiO_2 antimicrobial action.[51,66,61] These techniques are likely to be effective in antiviral applications, particularly against enveloped viruses in which the outer lipid membrane is susceptible to the same disruption mechanisms as the bacterial plasma membrane.

With the antibacterial nature of TiO_2 nanoparticles and coatings well-established, some recent studies have focused on the direct application of TiO_2 compounds to the development of antimicrobial – and, in growing numbers, antiviral – surfaces for use in

areas with high rates of infection, such as hospitals (Table 2.1). Nakano *et al.* demonstrated virucidal photocatalytic activity in TiO_2 coatings using the enveloped influenza virus and non-enveloped FCV.[65] They report a 3.6-log reduction in influenza virus activation after 4 h of UVA exposure on the TiO_2-coated glass and 1.7-log inactivation of FCV after 8 h. Inactivation of the viruses past the lower detection limit of their experiment occurred at 8 h and 16 h for influenza virus and FCV, respectively.[65] Similarly to the bacterial case, they ascribe this stark difference to the absence of a phospholipid bilayer in non-enveloped viruses like FCV.[65] Ishiguro *et al.* demonstrated antiviral activity of TiO_2 spin-coated on glass plates against bacteriophages Qβ and T4 upon exposure to 0.1, 0.01, and 0.001 mW/cm^2 intensity UVA light (351 nm) (Figure 2.3d).[52] The lowest intensities they tested are representative of the typical UVA irradiation encountered indoors. At the lowest intensity, they showed 5-log and 2-log reductions in viral activity after 24 h of irradiation for bacteriophages Qβ and T4, respectively.[52] More rapid inactivation was observed at 0.1 and 0.01 mW/cm^2 for both viral species. They also hypothesized that the probable target of ROS released by photocatalysis is the protein capsid of the bacteriophage after performing tests with bovine serum albumin in solution as a competitor,[52] which resulted in lower bacteriophage activation. The results of Nakano *et al.* discussed above indicate that this surface coating may perform better against enveloped viruses, in which the outer lipid envelope would be more effectively targeted than a protein capsid.[65]

The effect of modifications to TiO_2 surface coatings with fluorine compounds to increase the efficiency of ROS production is also an active area of research. Park *et al.* investigated the virucidal activity of fluorinated TiO_2 surface coatings on bacteriophage MS2, FCV, and

MNV.[60] Their goal was to adapt the high-energy photon requirements of normal TiO_2 photocatalytic activity through fluorination, which would allow the phenomenon to occur with only the intensity of UVA irradiation encountered in a typical office with fluorescent lighting (3.5 $\mu W/cm^2$ of UVA at a wavelength of ~365 nm).[60] They suspended TiO_2 nanoparticles in a PEG solution before spreading, drying, and calcifying the mixture onto glass slides, followed by immersion in a NaF solution to achieve fluorination.[60] They obtained 90% inactivation of bacteriophage MS2 under 3.5 $\mu W/cm^2$ of UVA (~365 nm) intensity after 42 mins on glass with an F-TiO_2 surface coating. In a realistic office setting, residual UVA exposure from fluorescent lighting is typically around 2.4 $\mu W/cm^2$. Infectivity of MS2 on their coating fell below detection levels after 12 h under these conditions, validating the potential for F-TiO_2 coatings to prevent viral transmission in indoor environments.[60]

In addition, creating coatings that combine TiO_2 with other metals demonstrates higher viral inactivation (*e.g.* bacteriophage MS2) compared to coatings that contain only TiO_2. As demonstrated by Rao *et al.*, loading TiO_2 nanowire membranes with silver and copper increased the disinfection of drinking water in comparison to TiO_2 alone, or in combination with just one metal.[67] Testing with bacteriophage MS2 demonstrated a 4.02-log reduction for Cu-Ag-TiO_2 in the UV light irradiation condition compared to less than 3-log reduction for TiO_2 alone, a difference that was attributed directly to the co-loading of Ag and Cu.[67] Furthermore, Moongraksathum *et al.* demonstrated the antiviral capability of a silver-doped TiO_2 coating prepared using a sol-gel method and deposited on a glass substrate.[62] They achieved photocatalytic activity under both UVA and visible light irradiation, demonstrated

by the degradation of a methylene blue solution, and observed that a 1 wt% concentration of Ag in the TiO_2 sol-gel produced the most photoactive coatings.[62] They tested the antiviral capability of their coating against influenza A and enterovirus and achieved a >99.99% (>4.17-log) reduction in viral activity after irradiation with a 15 W UVA lamp for 20 mins. They also confirmed that the Ag-TiO_2 composite outperformed a simple TiO_2 coating in terms of percent antibacterial effectiveness by more than six times.[62]

2.3.5 Other inorganic antiviral materials

Although copper, silver, zinc, and TiO_2 are the most widely studied inorganic materials, other inorganic materials and nanoparticles (*e.g.* gold, magnesium, transition metals, silica, and perovskites) have also been investigated in the antiviral research literature (Table 2.1). Gold nanoparticles (AuNPs) have historically been used for drug delivery alone or in combinations with other, more viricidal, metals such as copper.[68] Different surface modifications, such as increased porosity or sulfate-ended ligands, as well as combination with other bioactive metals, such as copper or iron, have been used to achieve antiviral and, more often, antibacterial functionality.[68–70] Broglie *et al.* investigated a gold/copper sulfide core/shell nanoparticle which was able to rapidly inactivate norovirus GI.1 (Norwalk) virus-like particles, that replicate the activity of human norovirus in solution.[68] This work provided evidence that capsid protein degradation and capsid damage appeared to be the mechanism associated with viral inactivation, showing a direct reliance on nanoparticle concentration as well as treatment time. Reports as far back as 2010 from Di Gianvincenzo *et al.* hold promise for the use of capped gold nanoparticles as functional units that could be applied to surfaces to convey antiviral capabilities.[70] These AuNPs were

coated with multiple copies of an amphiphilic sulfate-ended ligand that is able to bind to HIV and inhibit the infection *in vitro*. More recent work by Cagno *et al.* seems to suggest a similar possibility for surface coating, this time implementing gold nanoparticles as well as iron oxide.[71] Using long and flexible linkers that mimic heparan sulfate proteoglycans (HSPG), tests with HSV-2, vesicular stomatitis virus pseudo-typed lentivirus (LS-VSV-G), human papillomavirus (HPV) and respiratory syncytial virus (RSV) illustrated the effectiveness as an antiviral agent.[71]

Use of transition metals, including iron, magnesium, and manganese, has also proven effective in combination with TiO_2 due to their higher sensitivity to visible light for the creation of radicals. Choi and Cho created a visible-light-induced photocatalyst coating using a sol-gel method, which eradicated more than 99% of influenza virus H1N1 within 30 minutes.[72] Here, the proposed mechanism of action is through the hydroxyl radicals that are generated in photocatalytic reactions, similar to the mechanisms discussed for TiO_2 itself.[72]

A silica nanoparticle-based antimicrobial and antiviral coating was developed by Botequim *et al.* by incorporating quaternary ammonium cationic surfactant, didodecyldimethylammonium bromide (DDAB) on the surface of nanoparticles.[73] They showed complete inactivation of influenza A/PR/8/34 (H1N1) virus on glass coated with DDAB treated nanoparticles with 0% virus survival. Notably, the antiviral mechanism does not require leaching of DDAB from the particle's surface and is predicted to be similar to polycations with quaternary ammonium monomeric unity where they attract the viruses through favorable surface charges.[73]

Use of perovskites for antimicrobial capability is another growing area of research. Perovskites, referring to all compounds with the same crystal structure as calcium titanate, have been the subject of recent energy research, with perovskite-based solar cells reported in 2009.[74] The application of these materials for antimicrobial and antiviral use has gained traction due to their superb oxidative ability, as reported by Weng *et al.*.[75] Using nonstoichiometric perovskite-type La_xMnO_3, research has demonstrated the oxidation of amino acid residues within the viral envelope which neutralized the infectivity of influenza A virus. The best disinfection was achieved using $La_{0.9}MnO_3$ drop-coated onto glass coverslips, which neutralized 76% of influenza A within 15 minutes.[75] Additional research has remained focused on antibacterial capabilities of materials such as perovskite lanthanum aluminate (PLA) and $La_{0.8}Ag_{0.15}MnO_3$ (LAMO) magnetic nanoparticles (MNPs), which are thought to function through the interaction of positively charged NPs with the negatively charged cell wall of bacteria such as *S. aureus*, *Bacillus subtilis*, *E. coli*, and *Pseudomonas aeruginosa*.[76,77]

Table 2.1 *Metal and inorganic antiviral materials*

Material Form	Virus			Virucidal Activity	Deactivation time	Proposed applications	Ref.
	Name	Envelope	Genetic Material				
Copper							
Solid state	Influenza A	Enveloped	Negative sense ssRNA	2×10^6 reduced to 500 infectious virus particles	6 hours	Replacement of steel fittings; Copper surfaces in schools and healthcare facilities	22
Solid (coupons)	Bacteriophage Φ6	Enveloped	dsRNA	2-log decline	1 hour	Noted copper	24

Material Form	Virus			Virucidal Activity	Deactivation time	Proposed applications	Ref.
	Name	Envelope	Genetic Material				
						usage in sanitary and medical contexts	
Solid state (coupons)	Monkeypox	Enveloped	dsDNA	Complete viral inactivation uponcontact	3 minutes	Positioned as useful in hospital trials	21
	Vaccinia virus	Enveloped	dsDNA	Complete viral inactivation upon of contact	3 minutes		
Copper alloys	Murine norovirus	Non-enveloped	Positive sense ssRNA	**Dependent on alloy composition** *Dry touch*: Complete inactivation *Wet fomite:* Range from complete inactivation to a 2-4 log reduction	*Dry touch*: 5 to 120 minutes *Wet fomite:* Within 2 hours	Suggest use of copper alloys as dry surfaces in health care and community environments to prevent spread of pathogens, in combination with regular and efficient cleaning and decontamination regimes	20
Copper/Zinc alloy	Human coronavirus 229E	Enveloped	Positive sense ssRNA	Inactivation for dry fingertip method 10^3 PFU in wet-droplet contamination (20 µl per cm^2) inactivated	*Dry fingertip*: 5 mintues *Wet Droplet*: <60 minutes	Incorporation of copper alloy surfaces along with effective cleaning regimens and good clinical practice.	25
Solid state oxide (Cuprous oxide)	Influenza A	Enveloped	Negative sense RNA	3.7-log reduction after exposure to 2.1 µmol on glass slide	30 minutes	Tackle novel forms of the virus and potential resistance to drugs to reduce transmission. Treatment of both public and living spaces to	23

Material Form	Virus			Virucidal Activity	Deactivation time	Proposed applications	Ref.
	Name	Envelope	Genetic Material				
						help limit or prevent future pandemics	
Solid state oxide (Cuprous oxide)	Bacteriophage Qβ	Non-enveloped	Positive sense ssRNA	6-log reduction	30 minutes	Demonstrated potential for public and private living environments to reduce the risk of infections from pathogens	18
Copper-oxide within filters	Rhinovirus-2	Non-enveloped	Positive sense, ssRNA	2 ± 1.7 log reduction	2 minutes	Represent an inexpensive way to quickly deactivate viruses in contaminated liquids.	27
	Yellow fever virus	Enveloped	Positive sense ssRNA	1.1 ± 0.5 log reduction	2 minutes		
	Influenza A	Enveloped	Negative sense RNA	1.77 ± 0.87 log reduction	2 minutes		
	Measles virus	Enveloped	Negative sense ssRNA	≥3.67 log reduction	2 minutes		
	Respiratory syncytial	Enveloped	Negative sense ssRNA	1.5 ± 0.5 log reduction	2 minutes		
	Parainfluenza virus 3	Enveloped	Negative sense ssRNA	1.11 ± 0.5 log reduction	2 minutes		
	Punta Toro virus	Enveloped	Negative sense ssRNA	1.73 ± 1.55 log reduction	2 minutes		
	Pichinde virus	Enveloped	Negative sense ssRNA	1.7 ± 1.47 log reduction	2 minutes		
	HIV-1	Enveloped	Positive sense ssRNA	4.6 ± 0.6 log reduction	2 minutes		
	Adenovirus	Non-Enveloped	dsDNA	2.2 ± 0.36 log reduction	2 minutes		
	Cytomegalovirus	Enveloped	dsDNA	4.3 ± 0.26 log reduction	2 minutes		
	Vaccinia virus	Enveloped	dsDNA	0.47 ± 0.45 log reduction	2 minutes		
Copper oxide impregnated face masks	Influenza A	Enveloped	Negative sense RNA	No infectious titers recovered from surface	30 minutes	Reduction of contamination risk	28

Material Form	Virus			Virucidal Activity	Deactivation time	Proposed applications	Ref.
	Name	Envelope	Genetic Material				
						during use or removal of masks	
Ionic impregnation of latex and filters	HIV-1	Enveloped	Positive sense ssRNA	*Latex:* Dose dependent withincubation on glove surface *Filter:* 5-log reduction	*Latex:* 20 minutes *Filter:* 5 mL/min	Example of reduction of nosocomial infections in hospitals using copper in fabrics, paper, latex, *etc.*	26
	West Nile Virus	Enveloped	Positive sense ssRNA	5-log reduction	5 mL/min		
Zeolite textiles, Cu^{2+}	H5N1 avian influenza	Enveloped	Negative sense ssRNA	*Ck/Yamaguchi/7/04:* > 5.0 log reduction *Who.s/Hokkaido/1/08:* 2.3-log reduction	*Ck/Yamaguchi/7/04:* 30 seconds *Who.s/Hokkaido/1/08:* 1 minute	CuZeo-textile has wide applications as a microbicidal agent or in environmental healthcare goods. Can be applied as a comprehensive healthcare item such as in protective wear (clothes, masks and gloves), sheets covering beds or pillows in hospitals, and air or water purifiers in facilities such as hospitals or farms, *etc.*	29
	H5N3 avian influenza	Enveloped	Negative sense ssRNA	> 5.0 log reductionfor Whi.s/Shimane/499/83	10 minutes		

Material Form	Virus			Virucidal Activity	Deactivation time	Proposed applications	Ref.
	Name	Envelope	Genetic Material				
Nanoparticles within coating	Influenza H1N1	Enveloped	Negative sense ssRNA	Complete inactivation	1 minute	Authors propose that this anti-pathogen coating can provide an additional measure of protection against the spread of diseases in natural and manmade disasters, and during outbreaks of disease in either human or animal populations.	31
Copper powder within spray	Influenza A	Enveloped	Negative sense RNA	100% inhibition	10 minutes	Demonstration of spray coating that is effective as an antimicrobial, which can be used on surfaces within healthcare facilities.	35
Silver							
Hybrid coating (ionic)	HIV-1	Enveloped	Positive sense ssRNA	99.8% reduction	20 minutes	A broad-spectrum antimicrobial surface coating would have great impact on the battle against hospital-acquired	42
	Dengue virus	Enveloped	Positive sense ssRNA	1.1log $TCID_{50}$ reduction	4 hours		
	HSV	Enveloped	dsDNA	Complete inactivation	4 hours		
	Influenza	Enveloped	Negative sense ssRNA	0.7-log $TCID_{50}$ reduction	4 hours		

Material Form	Virus			Virucidal Activity	Deactivation time	Proposed applications	Ref.
	Name	Envelope	Genetic Material				
	Coxsackie	Non-enveloped	Positive sense ssRNA	0.2-log $TCID_{50}$ reduction	4 hours	infections. Potential to provide antimicrobial protection on surfaces and materials in hospital settings.	
Silver Nitrate in solution	Feline calicivirus	Non-enveloped	Positive sense ssRNA	3-log reduction in recovery in 2.1mg/L concentration	75 days	Technology proposed here would allow for custom design of active, adaptive packaging and contact surfaces.	38
	Murine norovirus	Non-enveloped	Positive sense ssRNA	1 log reduction after 75 days with 2.1mg/L concentration	75 days		
Nanoparticle in solution or film	Feline calicivirus	Non-enveloped	Positive sense ssRNA	*In solution*: 4-log reduction in recovery of virus if concentration was higher than 10.5mg/L *As film:* 1.42 log reduction of FCV at 25°C Complete inactivation of FCV at 37°C	*In solution:* Maintained over 150 days *As film:* Overnight incubation		
	Murine norovirus	Non-enveloped	Positive sense ssRNA	*In solution*: Initial 3-log reduction in recovery of virus, increased to complete inactivation over 150 days if concentration was higher than 10.5mg/L *As film:* 0.14 log reduction of MNV at 25°C 0.86 log reduction of MNV at 37°C	*In solution:* 1 day, increased over 150 days *As film:* Overnight incubation		
Nanoparticle impregnation	Influenza A (A/PR/8/34 (H1N1))	Enveloped	Negative-sense RNA	2-log decrease at concentration of	1 hour	Chitin-nanofiber sheets with	43

Material Form	Virus			Virucidal Activity	Deactivation time	Proposed applications	Ref.
	Name	Envelope	Genetic Material				
of nanofiber sheets				AgNPs at 8.5 µl/cm^2		potential to act as wound dressings	
Nanoparticle within Graphene Oxide	Infectious bursa virus	Non-enveloped	dsRNA	0.125mg/mL led to complete inhibition of 9 x 10^2 $TCID_{50}$/mL; 1 mg/mL against the infection of 9 x 10^3 $TCID_{50}$/mL	1 hour	Further application of GO and GO-Ag can be considered for personal protection equipment to decrease the transmission of viruses	44
	Feline coronavirus (FCoV)	Enveloped	Positive sense, ssRNA	0.1mg/mL caused 24.8% inhibition for 4.7 x 10^4 $TCID_{50}$/mL	1 hour		
Nanoparticle within membrane	Bacteriophage MS2	Non-enveloped	Positive sense ssRNA	5 ± 0.2 x 10^5 PFU/mL completely removed	Flow rate not reported	Membranes used for water treatment	45
Nanoparticle within membrane	Bacteriophage UZ1	-	-	3.4-log decrease in virus load	Flux of 3.1 L m^{-2} h^{-1}	Development of an innovative strategy for preventing outbreaks of waterborne diseases	46
Nanoparticle within film	Feline Calicivirus (FCV)	Non-enveloped	Positive sense ssRNA	> 4.4 log $TCID_{50}$/mL reduction after contact with films	24 hours	Excellent potential for PLA-silver films for food contact applications as well as in active packaging technologies for food safety and quality.	47
Nanoparticle within filter	Bacteriophage MS2 virus	Non-enveloped	Positive sense ssRNA	Density of 1.5 x 10^9 particles/cm^2 demonstrates roughly 70% antiviral efficiency without the presence of dust	15 minutes	Use as air filters within all types of public facilities.	48
Zinc							

Material Form	Virus			Virucidal Activity	Deactivation time	Proposed applications	Ref.
	Name	Envelope	Genetic Material				
Solid state	Murine norovirus	Non-enveloped	ssRNA	1-log reduction for pure zinc	2 hours	Suggests the incorporation of copper alloy surfaces to help prevent infection spread, such as within hospitals	19
Zinc Oxide filopodia-like structures	Herpes simplex virus type 1	Enveloped	dsDNA	Dose dependent reduction of viral entry; incubation with 100ug/mL ZnO-MNSs led to below 20% entry	90 minutes	Suggests development of these micro-nanostructures as a topical agent for prevention of HSV-1 infection.	58
Ionic solution	Human rhinovirus	Non-enveloped	Positive sense, ssRNA	99% reduction in number plaques using zinc chloride after virus exposure	1 hour	Investigation focused on the mechanism of action.	53
TiO_2							
Colloidal nanoparticles	Newcastle disease virus	Enveloped	Negative sense ssRNA	Qualitative; chick allantoises did not hemagglutinate after incubation with nano-colloids	96 hours	Starting point for the development of antiviral drugs	64
Solid state coating	Influenza virus	Enveloped	Negative sense ssRNA	3.6-log reduction (UVA intensity 0.1 mW/cm^2)	4 hours	Integration into surfaces in high-risk environments to reduce the spread of infection, such as at hospitals and daycare centers	65
	Feline calicivirus	Non-enveloped	Positive sense ssRNA	1.7-log reduction (UVA intensity 0.1 mW/cm^2)	8 hours		
Solid-state anatase coating	Bacteriophage Qβ	Non-enveloped	Positive sense ssRNA	4.5-log reduction (UVA intensity 0.1 mW/cm^2)	4 hours	Prevention of viral transmission	52

Material Form	Virus			Virucidal Activity	Deactivation time	Proposed applications	Ref.
	Name	Envelope	Genetic Material				
	Bacteriophage T4	Non-enveloped	dsDNA	2-log reduction (UVA intensity 0.1 mW/cm^2)	4 hours	in indoor and outdoor living spaces	
Fluorinated nanoparticles	Bacteriophage MS2	Non-enveloped	Positive sense ssRNA	2.6-log reduction (UVA intensity 0.01 mW/cm^2)	60 minutes	Prevention of viral transmission in indoor commercial spaces with fluorescent lighting	60
	Feline calicivirus	Non-enveloped	Positive sense ssRNA	2.0-log reduction (UVA intensity 0.01 mW/cm^2)	60 minutes		
	Murine norovirus	Non-enveloped	Positive sense ssRNA	2.6-log reduction (UVA intensity 0.01 mW/cm^2)	6 minutes		
Ag- and Cu-doped nanowire membranes	Bacteriophage MS2	Non-enveloped	Positive sense ssRNA	4.02-log reduction after filtration	30 minutes	Filtration and disinfection of drinking water	67
Ag-doped solid-state coating	Influenza A	Enveloped	Negative sense ssRNA	≥4.17-log reduction 15 W UVA light from 35 cm)	20 minutes	Disinfection of publicly-used surfaces and breakdown of organic pollutants	62
	Enterovirus	Non-enveloped	Positive sense ssRNA	≥4.17-log reduction (15 W UVA light from 35 cm)	20 minutes		
Other inorganic antiviral materials							
Modified Gold Nanoparticle in solution	Virus-like particles (VLPs), replicating human norovirus, GI.1 VLPs	Replicates Non-enveloped	Replicates RNA	Complete inactivation of VLPs at a concentration of 0.37 µg/mL using 0.083 µM Au/CuS NPs	1 hour	Proposed as an antiviral	68

Material Form	Virus			Virucidal Activity	Deactivation time	Proposed applications	Ref.
	Name	Envelope	Genetic Material				
Multivalent gold nanoparticles with sulfate ligands	HIV	Enveloped	Positive sense ssRNA	<20% infection rate of T-cells after incubation with sulfonated gold nanoparticles	30 minutes	Development of a multifunctional therapeutic anti-HIV system	[70]
Gold nanoparticles with undecanesulfonic acid(MUS)-containing ligands	HSV-1	Enveloped	dsDNA	Irreversible loss of infectivity (0 PFU) after pre-incubation of virus with gold NPs	1 hour	Production of virucidal drugs to fight viral infections	[71]
	HSV-2	Enveloped	dsDNA	Irreversible loss of infectivity (0 PFU) after pre-incubation of virus with gold NPs	1 hour		
	Human papillomavirus type 16 (HPV-16)	Non-Enveloped	dsDNA	Irreversible loss of infectivity (0 FFU) after pre-incubation of virus with gold NPs	1 hour		
	RSV	Enveloped	Negative sense ssRNA	Irreversible loss of infectivity (0 PFU) after pre-incubation of virus with gold NPs	1 hour		
	Vesicular stomatitis virus pseudo-typed lentivirus (LV-VSV-G)	Enveloped	Negative sense ssRNA	Irreversible loss of infectivity (0 transduction units) after pre-incubation of virus with gold NPs	1 hour		
	Adenovirus-5(AD5)	Non-Enveloped	dsDNA	No inhibition (virus is not	1 hour		

Material Form	Virus			Virucidal Activity	Deactivation time	Proposed applications	Ref.
	Name	Envelope	Genetic Material				
				HSPG-dependent)			
Ion doping of coating with Transition Metals (*i.e.* iron, magnesium, manganese)	Influenza H1N1	Enveloped	Negative-sense RNA	99% eradication with a fluorescent lamp	30 minutes	Suggest use for inactivation of virus inside buildings with fluorescent light.	72
Silica Nanoparticle in coating	Influenza A/PR/8/34 (H1N1)	Enveloped	Negative-sense RNA	Complete inactivation after incubation of virus suspension on surface	30 minutes	Use as a microbicidal coating	73
Nonstoichiometric perovskite-type LaxMnO3	Influenza A	Enveloped	Negative-sense RNA	Neutralized 76% of influenza A	15 minutes	Proposed as a sterilizing method to minimize transmission of virus *via* multiple routes, including aerosol and contaminated fluids	75

2.4 Polymeric and Organic Antiviral Coatings

2.4.1 Polyelectrolyte-coated Surfaces

It has been shown that the positive charge of polycations in polymers such as polyethylenimine attracts viruses having an inherent negative charge, interferes with their genomic content or structural units, and causes complete viral disintegration (Figure 2.4a).[78,79] It has been claimed that this class of coating, typically applied through "painting", can permanently convey antiviral and antibacterial properties even after being subjected to

multiple washes.[80] Herein, the literature involving polycations, mainly polyethylenimines, is discussed and is summarized in Table 2.2.

Immobilizing polycations on various surfaces has been shown to convey antiviral properties for both enveloped and non-enveloped viruses.[81,82] Immobilized hydrophobic polyethylenimine-based and dendrimer-based polycations have reduced the titer of viruses. A study on bacteriophage PRD1 interaction with polyethylenimine coated glass slides demonstrated that positive charges and hydrophobicity (conferred by 4-bromobutyrylated polyethylenimine treated glass with N,Ndimethylhexadecylamine) result in a significant decrease in the virus titer compared to uncoated glass.[82] Overall, having only polycations (minimal hydrophobicity) also showed a reduction in the virus titer, however, the combination of hydrophobicity with acetylated surfaces and positive charges of polyethylenimine was more effective.[82] The antiviral activity was also proportional to the surface area of the treated glass. This was also confirmed by exposing treated glass powders to the virus solution, demonstrating higher titer reduction compared to treated surfaces.[82] Moreover, N-alkylated polyethylenimines, namely linear N,N-dodecyl,methyl polyethylenimines, have also demonstrated antiviral properties for non-enveloped viruses when "painted" on polyethylene.[81] Using this method, Larson *et al.* showed slightly elevated antiviral activity as incubation time was increased and nearly 100% virucidal activity after 15 minutes of

incubation.[81] Furthermore, they tested another N-alkylated polyethylenimine, branched N,N-hexyl,methyl *via* covalent attachment to glass slides, and similarly demonstrated complete elimination of the rotavirus after 30 minutes of incubation.[81] Their studies showed

effective antiviral behaviour of the polycation coating not only on enveloped viruses such as influenza but also on non-enveloped viruses such as poliovirus and rotavirus.[81] To elucidate the role of the polyethylenimines, Haldar *et al.* demonstrated that their molecular weight is important for the virucidal characteristics, as they must be large enough to penetrate the viruses.[83] They tested 750 kDa, 25 kDa, and 2 kDa sizes of polyethylenimines, with only the 750 kDa polyethylenimine showing complete inactivation of the influenza virus. Moreover, the polycation (polyethylenimines) was compared to a polyanion and a neutral coating.[83] It was shown that the polyanion has partial virucidal activity, while the neutral coating was not virucidal. The fact that both polycations and polyanions showed antiviral characteristics was hypothesized to be due to availability of both positively and negatively charged domains on the virus (*i.e.* influenza virus), with the negatively charged domains being dominant, which explains the superiority of polycations in antiviral activity (polycation and polyanion having 100% and 66% viricidal activity respectively).[83] Similarly, a study by Dang *et al.* showed positively- and negatively-charged polyelectrolyte multilayers (PEMs) deposited on a quartz crystal microbalance (QCM).[84] They claimed that with various designs for the PEMs it is possible to manipulate the adhesive properties of the surfaces towards viruses. Negatively charged surfaces (*e.g.* poly(styrene-4-sulfonate) terminated) showed relatively lower amounts of bacteriophage MS2 due to the unfavorable electrostatic interaction between the bacteriophage and the anionic surface.[84] On the other hand, positively charged PEMs showed higher amounts of MS2 deposition, which is in line with the findings by Haldar *et al.* From the molecular perspective, polycations with both branched and linear polyethylenimines (*e.g.* N,N-dodecyl,methyl-polyethylenimine) were

lethal towards influenza virus A,[85–87] even to strains which were resistant towards commercial drugs.[87] PEMs can be easily applied to surfaces using methods such as spray coating, dip coating, and painting, for the development of scalable antiviral coatings.

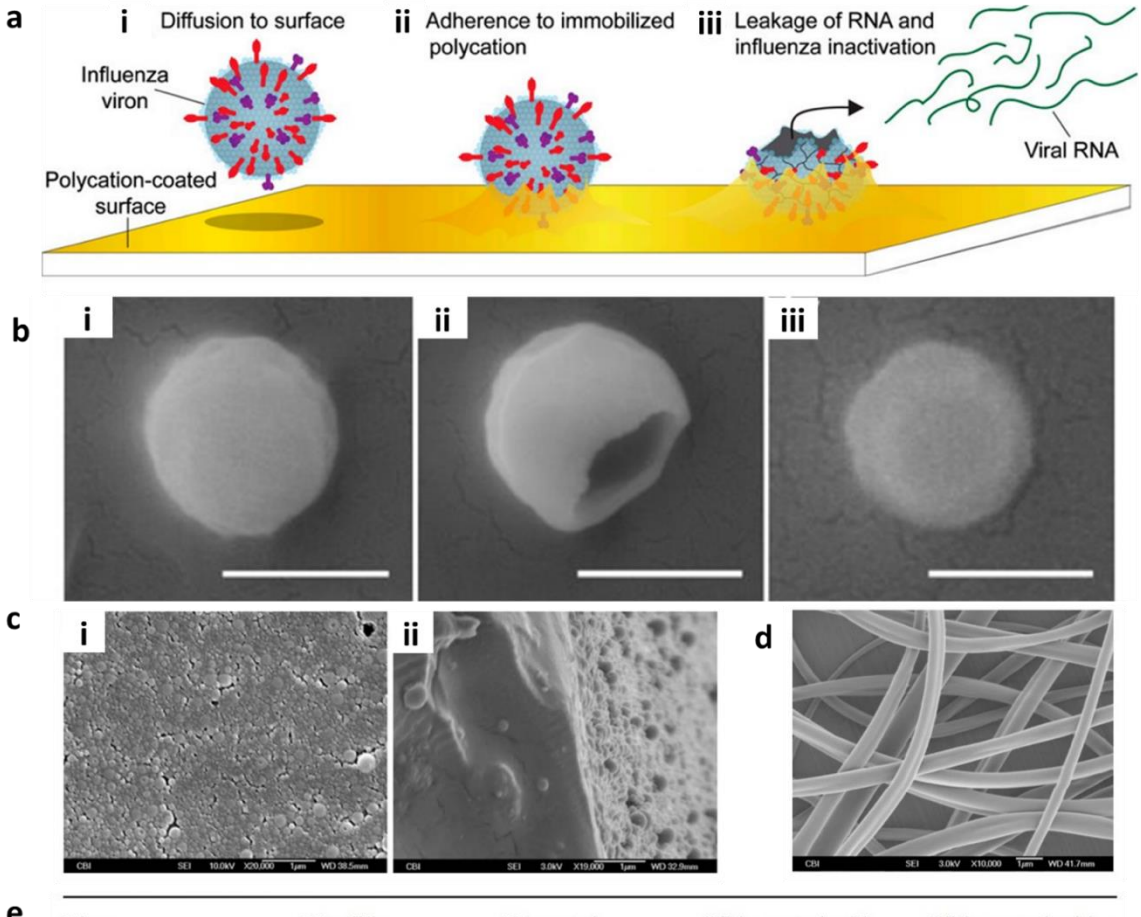

e

Virus	No slide	Uncoated slide	Slide coated with a solution	Slide coated with a nanosuspension
Influenza (pfu/ml)	$(5.9\pm1.7)\times10^4$	$(2.2\pm0.3)\times10^4$	0	0
Poliovirus (pfu/ml)	$(3.8\pm1.0)\times10^5$	$(1.7\pm0.4)\times10^5$	$(1.6\pm0.4)\times10^5$	$(1.4\pm0.5)\times10^5$

Figure 2.4 Polycation coatings. *(a) Mechanism of enveloped virus inactivation by polycation coating. (i) diffusion of the virus particle to the surface from solution (ii) adhesion on polycation surface (iii) the genomic material leaks out and the virus gets inactivated. Reproduced with permission from [79] (b) SEM images of influenza virus after exposure to uncoated (i) and N;N-dodecyl,methyl-PEI-coated (ii and iii) silicon wafers. Reproduced with permission from [79] (c) SEM images of a polyethylene surface coated with Quat-12-PU nanoparticles. (i) Top view (ii) cross-section Reproduced with permission from [88] (d) The SEM of Quat-12-PU electrospun nanofibers. Reproduced with permission*

from [88] (e) Antiviral activities of uncoated and Quat-12-PU coated polyethylene slides solution-based or nanosuspension deposition. Reproduced with permission from [88].

Further studies by Hsu *et al.* investigated the role of the underlying substrate on the antiviral properties.[79] Polyethylene and polypropylene were used as alternatives to glass. It was discovered that all three types of substrates used for coating demonstrated complete disinfection of the virus, proving that the polycation painting is the key to the antiviral activity of the materials.[79] In order to better understand the mechanism and fate of viruses when coming in contact with the polycation coating, the viral nucleoprotein was assayed using colorimetric ELISA as a marker indicating viral rupture.[79] The assay demonstrated the disappearance of the viral particles from the solution exposed to the polycation, indicating that the viruses attach to the hydrophobic polycationic coatings (Figure 2.4a). Furthermore, real-time reverse-transcriptase PCR (qRT–PCR) was used to evaluate the detectable viral RNA in solution where its presence would indicate loss of infectivity of the virus due to the viral genomic material being exposed.[79] It was shown that a significant amount of viral RNA was detectable, therefore the polycation layer is not only attracting the virus but also inactivating the virus.[79] This was also validated with scanning electron microscopy (SEM) (Figure 2.4b) of the influenza virus, showing that the integrity of the influenza virus was compromised for 54% of the 132 surveyed viruses.[79] The monomer of the polycation N;N-dodecyl,methyl-polyethylenimine, dodecyltrimethylammonium bromide (DTAB), was also capable of inactivating the influenza virus in test solutions. This hinted towards the antiviral activity being related to the hydrophobic quaternary ammonium

salt moiety, that is maintained within the polymeric and surface-immobilized form of the polycation.

In another approach for coating the polycations, a study by Liu *et al.* demonstrated use of N,N-hexyl,methyl-polyethylenimine with an aerosol-assisted plasma deposition technique on glass surfaces.[89] This allows for the covalent immobilization of N,N-hexyl,methyl-polyethylenimine through a one-step method and has been shown to be thermally stable (up to 150 ºC) and durable upon exposure to vigorous washes and exposure to detergents. This study demonstrated a greater than 4-log reduction in the influenza H1N1 virus for N,N-hexyl,methyl-polyethylenimine treated surfaces.[89]

Another class of polyelectrolytes used as antiviral coatings is polyurethane-based materials, such as N,N-dodecyl,methyl-polyurethane (Quat-12-PU), which are versatile, abrasion-resistant, and robust for long periods of time.[88] Quat-12-PU can be coated onto surfaces through three different methods: (1) spray coating on polyethylene or glass slides, (2) synthesizing Quat-12-PU nanoparticles by dissolving Quat-12-PU in Tetrahydrofuran (THF) and subsequently spraying the nanoparticle solution on glass slides (SEM image shown in Figure 2.4c i and ii) or, (3) by electrospinning Quat-12-PU nanofibers onto glass slides (scanning electron microscopy image shown in Figure 2.4d).[88] The study by Park *et al.* demonstrated antiviral properties with complete inactivation of influenza virus (enveloped, with 0 PFU/ml of virus detected) but not poliovirus (non-enveloped) by subjecting the solution-treated or nanoparticle-treated surfaces to the respective virus solutions and comparing each to uncoated substrates (Figure 2.4e).[88] The antiviral properties were attributed to the Quat-12-PU interfering with the lipid envelope of the virus

protecting its RNA. Comparing the Quat-12-PU to the N,N-dodecyl,methyl-polyethylenimine coated surfaces, it was previously shown that the latter disinfects poliovirus.[81] Park *et al* showed that the polioviruses adhere to N,N-dodecyl,methyl-polyethylenimine surfaces but not to Quat-12-PU coated ones by subjecting N,N-dodecyl,methyl-polyethylenimine surfaces to detergent washes and assessing the extent of the recovered viruses. This can be attributed to the different chemistries on these surfaces.[88]

A polyelectrolyte-based method was used to develop filtration membranes for reducing the amount of virus in drinking water.[78] Through a covalent layer-by-layer deposition method, multiple layers of polyethyleneimine were created with use of terephthalaldehyde as the cross-linking agent. It was found that there was a 4-log reduction in the virus titer from the solution.[78] Furthermore, silver and copper nanoparticles were incorporated within the polyethyleneimine layer and tested for antiviral properties, indicating 4.5- to 5-log reduction in PFU.[78] They also ran qRT-PCR on the permeates of the membrane, which confirmed the hypothesis that the polycationic coating actually inactivates the virus and exposes the genomic content.[78] Their overall findings suggested that this polyelectrolyte coating can be integrated on a planar surface (*e.g.* glass), as well as on irregular surfaces (*e.g.* porous membranes).[78]

In another study, quaternary ammonium compounds (QACs) were coated onto glass and plastic surfaces in order to add antiviral properties. The QAC polymer was dissolved in acetone and a thin layer was added to either glass or well plates and subsequently dried, making a positively charged layer.[90] Enveloped influenza A (H1N1) virus and non-enveloped poliovirus Sabin 1 were tested for virucidal activity on the surfaces. Influenza A

showed reduction in the virus infectivity after 2 minutes; on the other hand, poliovirus did not show reduction even after longer incubation times.[90]

2.4.2 Photosensitizer materials

A number of recent studies have integrated photosensitive compounds other than TiO_2, such as rose bengal and C_{60}, onto surfaces to exploit the ROS-dependent antimicrobial and antiviral pathways.[91] Photosensitizers, light-activated molecules, are also used for antimicrobial photodynamic therapy as an alternative for antibiotic chemotherapies.[92] Antimicrobial photodynamic inactivation operates on the principle that a photosensitizer gets excited *via* visible light absorption and subsequently reacts with oxygen.[92] There are two pathways (type I and type II), shown in Figure 2.5a, through which active products are generated that induce damage to viruses, bacteria, or other organic species. In the type I pathway, the photosensitizer reacts with bio-organic molecules and produces ROS (*e.g.* superoxide, hydroxyl radicals, and hydrogen peroxide). The type II pathway occurs as the excited photosensitizer transfers energy to molecular oxygen and generates singlet oxygen ($^1O_2$), which induces oxidative damages to biological species.[92,93] More specifically, saturated lipids are the target for free radicals and singlet oxygen attacks. This leads to lipid peroxidation and the alteration of surrounding proteins, nucleic acids (mainly guanine) and other molecules. Therefore, it is hypothesized that the generation of ROS damages the viral envelope and causes viral inactivation.[93] This makes enveloped viruses more susceptible to photodynamic inactivation than non-enveloped ones. However, non-enveloped viruses have also shown photodynamic inactivation of their viral proteins.[93] The advantages of

such antimicrobial pathways over antiviral and antimicrobial drugs include non-specific damage leading to an inability to develop resistance, $^1O_2$ being environmentally benign, and the non-toxicity of photosensitizers.[92,93]

Si *et al*. reported on developing a fine membrane of electrospun poly(vinyl alcohol-co-ethylene) nanofibers functionalized with benzophenone tetracarboxylic dianhydride and chlorogenic acid.[94] They recognized the limitations of UV-dependent photoactivity exhibited by most photoactive materials and sought to develop an antibacterial and antiviral surface excitable in daylight conditions by ambient visible and UVA light. They achieved a 5-log reduction in viral activity of bacteriophage T7 in daylight conditions, with similar results for antibacterial action against *E. coli* and *L. innocua*.[94] As mentioned previously, non-enveloped bacteriophages such as T7 generally show increased resistance to most ROS- or contact-killing-based antiviral mechanisms, and the authors predicted that enveloped viruses would be targeted even more effectively due to the presence of a lipid membrane.[94] The nanofiber membrane is also notable for its filtration capabilities, which effectively impedes the penetration of small particles and microorganisms. It also possesses the ability to "store" photoactivity by achieving a metastable electronic structure in the event that hydrogen abstraction is not completely reversed by ROS production.[94] This allows it to maintain its antimicrobial characteristics in the dark. Si *et al.* tested their nanofiber membrane on personal protective equipment such as lab coats and N100 masks and demonstrated that it provided a nearly 6-log reduction in T7 phage plaque-forming units compared to the unmodified materials.[94]

Cellulose has been researched with the aim to reduce nosocomial infections in hospital textiles.[95] In order to introduce antimicrobial and antiviral characteristics to cellulose, Alvarado *et al.* developed photosensitizer-linked nanofibrillated cellulose (PS-NFC) through utilizing triazine linking and covalently bonding a porphyrin-based photosensitizer to nanofibrillated cellulose (NFC).[95] The antiviral behaviour of this technology relies on the production of reactive singlet oxygen ($^1O_2$) and other ROS upon illumination of the photosensitizer and the extremely high surface area of NFC is a contributing factor. Free-base, [5-(4-aminophenyl)-10,15,20-tris-(4-N-methylpyridinium)porphyrin (A^3B^{3+})], and metallated, [5-(4-aminophenyl)-10,15,20-tris- (4-N-methylpyridinium) porphyrinato] zinc(II) (Zn-A_3B^{3+}), photosensitizers were applied to NFC (A^3B^{3+}-NFC and Zn-A_3B^{3+}-NFC) (Figure 2.5b and c) in order to integrate photoactive behaviour to NFC.[95] Vesicular stomatitis virus (VSV) and dengue-1, both enveloped viruses, were used to assess the antiviral behaviour of the modified NFC. After illumination, both treated NFC materials showed complete inactivation of the viruses (Figure d and e).[95] A study by Carpenter *et al.* conjugated cationic, anionic, and neutral porphyrins to cellulose fibers to add antimicrobial properties to the surface against enveloped (dengue-1 and influenza A) and non-enveloped viruses (human adenovirus-5 (Had-5)).[96] The anionic and neutral porphyrins did not show promising results in a reduction in CFU/mL in their bacteria studies, which they attributed to electrostatic repulsion and/or hydrophobicity of those surfaces not allowing interaction of the porphyrins with the bacteria.[96] For the virus studies, they implemented porphyrin-positive treated cellulose, due to its better performance with bacteria. Dengue-1 and influenza A showed >99.995% and ~99.5% reduction in FFU/mL, however, the non-

enveloped viruses (HAd-5) were harder to inactivate and showed ~99% reduction in FFU/mL using immunofoci staining. The reductions in FFU were attributed to the protein-based capsid and the lipid-bilayers, which in the case of enveloped viruses, were found less resistant towards photosensitization.[96] In another study, wipes with polypropylene fibers were coated with the photosensitizer rose bengal, which is immobilized on the fibers through multiple amide bonds and produces singlet oxygen during exposure to visible light.[97] Wipes were spiked with various viruses including the human norovirus GI.4 and GII.4, murine norovirus 1 (MNV-1), human adenovirus type 5 (hAdV-5), and influenza virus H1N1. The non-enveloped viruses did not exhibit prompt inactivation, with the time needed for the first 1-log reduction being more than 7 hours, while enveloped viruses showed immediate and complete inactivation (more than 4-log).[97] Furthermore, the transfer and persistence of viruses from a steel surface were tested after being wiped with the treated and untreated wipes, and the proportion of viruses recovered from the wiped surface to the unwiped one through viral genome quantification was reported. For MNV-1 and influenza virus, no viruses were discovered after wiping the contaminated steel surfaces. However, residual amounts (0.2%-0.6% residual virus proportions) of norovirus were found on the steel surfaces.[97] Notably, in this case, no difference was found between the treated and untreated wipes. They further tested the already used wipes (used on steel surfaces) on a secondary steel surface to investigate cross contamination and revealed that non-enveloped viruses demonstrated cross-contamination.[97] The development of wipes that remain clean is an avenue for reducing cross-contamination and halting the spread of infection *via* surfaces.

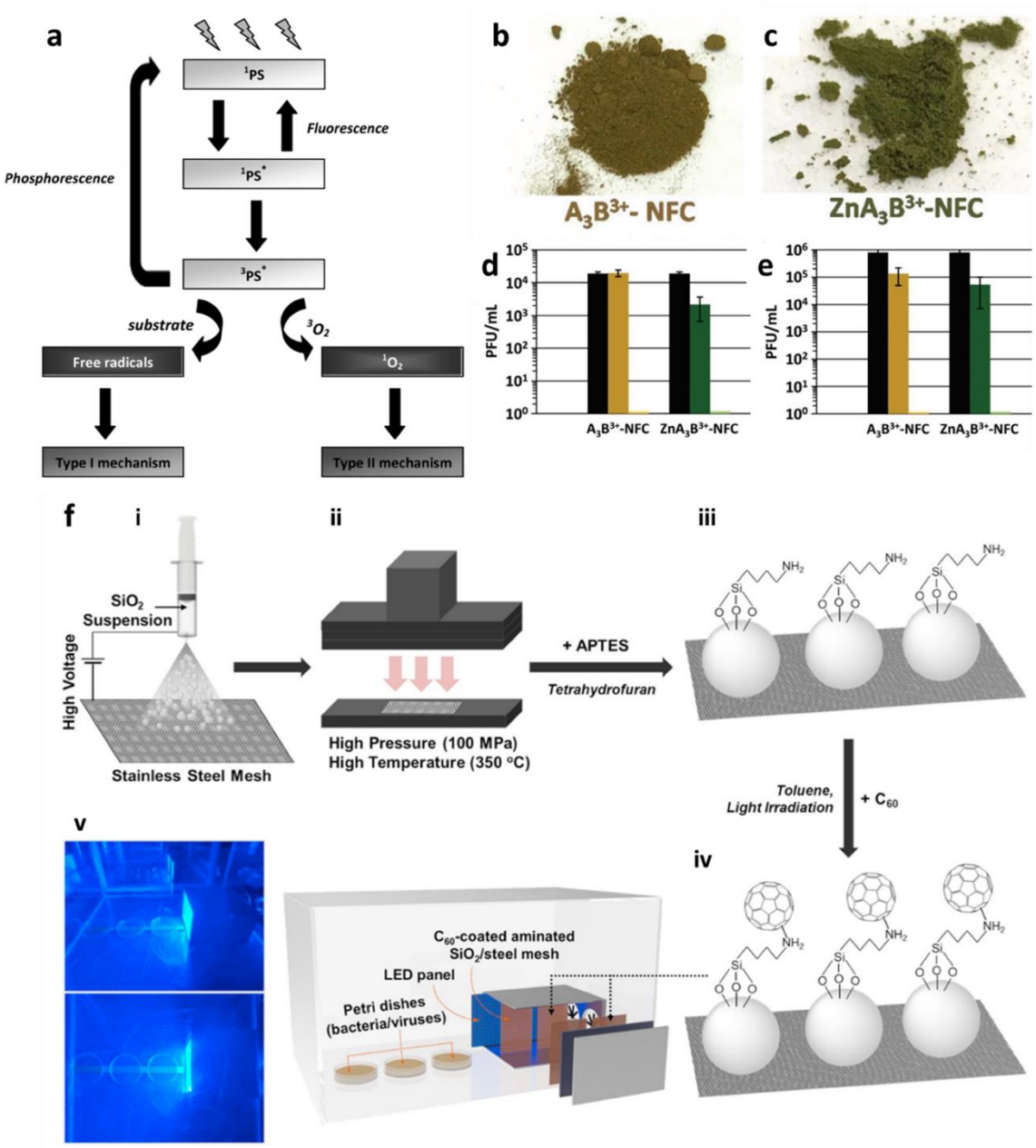

Figure 2.5 Photosensitizer–cellulose conjugate materials. *(a) Schematic representation of the photosensitization process. Reproduced with permission from [93] (b) A3B3+-NFC and (c) Zn-A3B3+-NFC. Photodynamic inactivation studies of the (d) dengue-1 and (e) vesicular stomatitis virus (VSV). Dark yellow and dark green bars are dark controls. Light yellow and light green bars are illuminated. Black bar is the initial virus concentration. Slight decrease in the virus infectivity was observed in dark environments, which, due to observed strong virucidal behaviour in illumination conditions, was attributed to the accidental light exposure while running the assays. Reproduced with permission from [95] (f) Fabrication process of C_{60} coated stainless-steel mesh and virus assay setup. (i)*

Electrospraying silica particles on stainless-steel mesh; (ii) hot pressing (iii) APTES treating silica (iv) covalent C_{60} attachment (v) visible-light-sensitized remote singlet oxygenation and virus inactivation setup. Reproduced with permission from [98].

A C_{60}-based sensitizer was developed to evaluate virus inactivation in air due to its high yield of singlet oxygen production. Briefly, SiO_2 was electrosprayed on a stainless-steel mesh to serve as a support for a layer of (3-aminopropyl)triethoxysilane (APTES).[98] This allowed for the SiO_2 to attach to the double bonds of C_{60}. To assess antiviral activity in air, inactivation rates of bacteriophage MS2 were evaluated at various distances from the singlet oxygen source (C_{60} coated mesh).[98] The schematic of the production process and virus assay setup are shown in Figure 2.5f. It was found that bacteriophage MS2 was deactivated ((N0-N)/N0, the quantity of the residual bacteriophage MS2 remaining relative to the initial quantity in PFU/mL) by 55.8%, 37.7%, and 24.3% respectively when the C_{60} coated mesh was used at 5, 15, 30 cm distances after 3 hours.[98]

Within the field of photosensitized material and their virucidal activity, there are some studies that produce polycaprolactone, polyurethane, and polyacrylonitrile nanofibers, and dope them with photosensitizers such as 5,10,5,20-tetraphenylporphyrin, polyacrylonitrile, and porphyrin positive mixtures while electrospinning the fibers.[99,100] These have been shown to inactivate non-enveloped viruses such as polyomaviruses (30 minutes, quantification was not elaborated) and adenovirus 5 (30 minutes, ~99.8% reduction in PFU/mL), as well as enveloped viruses such as baculoviruses and VSV.[99,100]

2.4.3 Other coatings

To introduce antiviral properties to textiles, Iyigundogdu *et al.* immersed cotton fabrics into a solution containing sodium pentaborate pentahydrate and triclosan.[101] They tested adenovirus type 5 and poliovirus type 1, demonstrating that the amount of decline for the virus titer is 3-log on the sodium pentaborate pentahydrate and triclosan solution-treated textiles, whereas the non-treated textiles do not show any decrease.[101] This was confirmed by observing the cell deaths as a result of contact with the virus solution passed through the fabrics.

Table 2.2 *Polymeric and organic antiviral coatings*

Material			**Virus**			**Virucidal Activity**	**Deactivation time**	**Proposed applications**	**Ref.**
Coating	**Method**	**Backbone Material**	**Name**	**Envelope**	**Genetic Material**				
Polycations									
4-bromobutyrylated N,Ndimethylhexadecylamine	Covalent bonding	Glass, glass powder	Bacteriophages PRD1	Non-enveloped	dsDNA	77± 3% titer reduction	24 hours	Removing viruses from water by adsorption	82
N,N-hexyl,methyl polyethylenimines (750 kDa)	Covalent bonding	Glass	poliovirus	Non-enveloped	Positive sense ssRNA	100% virucidal activity (PFU/mL)	30 minutes	disinfect aqueous solutions	81
N,N-dodecyl,methyl-polyethylenimines (217 kDa)	Physical absorption (painting)	Polyethylene	poliovirus	Non-enveloped	Positive sense ssRNA	~100% virucidal activity (PFU/mL)	30 minutes	disinfect aqueous solutions	81
	Physical absorption (painting)	Polyethylene	rotavirus	Non-enveloped	dsRNA	100% virucidal activity (PFU/mL)	15 and 30 minutes	disinfect aqueous solutions	81

Material			Virus			Virucidal Activity	Deactivation time	Proposed applications	Ref.
Coating	Method	Backbone Material	Name	Envelope	Genetic Material				
	Physical absorption (painting)	Glass, Polypropylene, Polyethylene	WSN influenza strain WSN/33 (H1N1), PR/8/34 (H1N1), turkey/MN/833/80 (H4N2	Non-enveloped	Negative sense dsRNA	Final viral titer (PFU/ml) = 0 100% virucidal activity (PFU/mL) viral nucleoprotein by ELISA =< 0.1 (pfu/ml) qRT–PCR RNA leakage detection <50% viral RNA in solution Scanning electron microscopy survey for damaged viruses, 54% showed structural damage	5 minuutes	Not specified Antimicrobial surfaces	79

Material			Virus			Virucidal Activity	Deactivation time	Proposed applications	Ref.
Coating	Method	Backbone Material	Name	Envelope	Genetic Material				
N,N-hexyl,methyl-polyethylenimine (Mw non specified)	Covalent aerosol-assisted plasma deposition	Glass	Influenza A/PR/8/34 (H1N1)	Non-enveloped	Negative sense dsRNA	>4 log reduction in viral titer	10 minutes	Not specified Antimicrobial surfaces	89
N,N-dodecyl,methyl-polyethylenimines (750 kDa)	Physical absorption (painting)	Glass	influenza virus A/WSN/33 (H1N1)	enveloped	Negative sense ssRNA	100% virucidal activity (PFU/mL)	30 minutes	Preventing the spread of infection	83
	Physical absorption (painting)		influenza A Wuhan (H3N2), avian influenza A turkey (H4N2) virus, drug-resistant strains of a human influenza A Wuhan (H3N2) and an avian influenza A turkey (H4N2)	enveloped	Negative sense ssRNA	Final viral titer (PFU/ml) = 0	30 minutes	preventing the spread of influenza	87
N,N-dodecyl,methyl-polyurethane (Quat-12-PU)	solution treated or nanoparticle treated by spray coating (physical absorption)	Glass	Influenza virus	enveloped	Negative sense ssRNA	Final viral titer (PFU/ml) = 0	15 minutes	Not specified Antimicrobial surfaces	88
Polyethyleneimine (25 kDa)	chemical-crosslinking (covalent)	Glass, micro-filtration membranes	Bacteriophage MS2	Non-enveloped	Positive sense ssRNA	4-log of reduction in the	30 minutes	filtration membranes for drinking water	78

Material			Virus			Viruci dal Activit y	Deacti vation time	Propos ed applica tions	R ef .
Coating	Method	Backbo ne Materi al	Name	Enve lope	Gen etic Mat erial				
						virus titer 3–3.5-log of reducti on in the virus titer qRT-PCR for quantifi cation of genom e copies ~2-log reducti on			
Polyethyleneimine (25 kDa)+ AgNP and/or CuNP	chemica l-crosslin king (covalen t)	Glass, micro-filtratio n membra nes	Bacteriop hage MS2	Non-envel oped	Posit ive sens e ssR NA	4.5- to 5-log reducti on in the virus titer qRT-PCR for quantifi cation of genom e copies >2-log reducti on	30 minute s	filtratio n membr anes for drinkin g water	78
Quaternary ammonium compounds (QACs)	Physical absorpti on by thin layer depositi on	Glass, Plastic	influenza A (H1N1)	envel oped	Neg ative sens e ssR NA	Compl ete inactiv ation,	1 hour	Not specifie d Antimi crobial	90

Material			Virus			Viruci dal Activit y	Deacti vation time	Propos ed applica tions	R ef .
Coating	Method	Backbo ne Materi al	Name	Enve lope	Gen etic Mat erial				
			poliovirus Sabin 1	non-envel oped	Posit ive sens e ssR NA	No inactiv ation observe d	1 hour	surface s	
Photosensitizer materials									
poly(vinyl alcohol-co-ethylene) nanofibers functionalized with benzophenone tetracarboxylic dianhydride and chloro- genic acid	Electros pinning followed by grafting	N/A (standal one membra ne)	Bacteriop hage T7	Non-envel oped	dsD NA	5-log PFU/m L reducti on	5 mins dayligh t exposu re	Protecti on of high-risk surface s and persona l protecti ve equipm ent (*e.g.* protecti ve suit)	94
free-base 5-(4-aminophenyl)-10,15,20-tris-(4-N-methylpyridinium)porphyrin (A^3B^{3+})	Covalen t bonding	nanofibr illated cellulos e	Vesicular stomatitis virus (VSV)	envel oped	Neg ative sens e ssR NA	Final viral titer (PFU/ ml) = 0	30-minute illumin ation	Integrat ion in textiles for the prevent ion of nosoco mial infectio ns	95
			Dengue-1	envel oped	Posit ive sens e ssR NA	Final viral titer (PFU/ ml) = 0	30-minute illumin ation		
metallated [5-(4-aminophenyl)-10,15,20-tris-(4-N-methylpyridinium)porphyrinato]zinc(II) (Zn-A^3B^{3+})	Covalen t bonding	nanofibr illated cellulos e	Vesicular stomatitis virus (VSV)	envel oped	Neg ative sens e ssR NA	Final viral titer (PFU/ ml) = 0	30-minute illumin ation	Integrat ion in textiles for the prevent ion of nosoco mial infectio ns	95
			Dengue-1	envel oped	Posit ive sens e ssR NA	Final viral titer (PFU/ ml) = 0	30-minute illumin ation		
cationic porphyrin	Covalen t bonding	cellulos e fiber (paper)	dengue-1	Envel oped	Posit ive sens e	>99.99 5% reducti on in	30-minute illumin ation	autono mously sterilize materia	96

Material			Virus			Viruci dal Activit y	Deacti vation time	Propos ed applica tions	R ef .
Coating	Method	Backbo ne Materi al	Name	Enve lope	Gen etic Mat erial				
					ssR NA	FFU/m L		ls for hospital s and healthc are-related industri es, prevent ing the spread of infectio n	
			Influenza A	Envel oped	Neg ative sens e ssR NA	~99.5 % reducti on in FFU/m L	30-minute illumin ation		
			human adenoviru s-5 (HAd-5)	non-envel oped	dsD NA	~99% reducti on in FFU/m L	30-minute illumin ation		
rose Bengal	Covalen t bonding	wipes with polypro pylene fibers	murine norovirus 1 (MNV-1),	non-envel oped	Posit ive sens e ssR NA	8.7 hours first 1-log reducti on	8.7 hours	one-step proced ure for cleanin g and disinfec ting influen za virus-contam inated surface s	97
			human adenoviru s type 5 (hAdV-5),	non-envel oped	dsD NA	7 hours first 1-log reducti on	7 hours		
			influenza virus H1N1	envel oped	Neg ative sens e ssR NA	Immedi ate and comple te inactiv ation (more than 4-log)	0 minute s		

Material			Virus			Viruci dal Activit y	Deacti vation time	Propos ed applica tions	R ef .
Coating	**Method**	**Backbo ne Materi al**	**Name**	**Enve lope**	**Gen etic Mat erial**				
C_{60}	Covalen t bonding	SiO_2 electros prayed on a stainless -steel mesh	Bacteriop hage MS2	Non-envel oped	Posit ive sens e ssR NA	inactiv ation levels at 5 cm distanc e = 55.8%	3-hour illumin ation	remote disinfec tion	98
Other									
Sodium pentaborate pentahydrate and triclosan	Physical absorpti on by immersi on	Fabric	adenoviru s type 5	non-envel oped	dsD NA	3-log decline in virus titer based on micros copic observa tion of the infecte d cells	Not Given	antivira l textile finishes for medical applicat ions, daily use, and technic al textiles	10 1
			poliovirus type 1	non-envel oped	Posit ive sens e ssR NA	3-log decline in virus titer based on micros copic observa tion of the infecte d cells	Not Given		
			poliovirus Sabin 1	non-envel oped	Posit ive sens e ssR NA	No inactiv ation observe d	Not applica ble		

2.5 Toxicity and environmental considerations

The use of metals and inorganic materials can present health and environmental risks. Bowkow and Gabbay conducted animal studies with antimicrobial and antiviral fabrics impregnated with copper to determine the fabric's skin-sensitizing potential in both guinea pigs and rabbits.[26] In studies that looked at exposure to these fabrics, no skin irritation was demonstrated over a 14 day period.[26] Furthermore, Gerhard *et al.* reviewed the effects of TiO_2 on the skin and found that there was little evidence to suggest that the use of TiO_2 nanoparticles in cosmetics pose a risk to human health.[102] However, Scokaj *et al.* reported in a similar review that the evidence for the safety of TiO_2 in humans is still under debate, especially for its nanoparticulate forms.[103] For example, Qiang *et al.* demonstrated that a culture of HFL1 cells treated with a 0.50 mg/mL suspension of TiO_2 nanoparticles and incubated for 48 h experienced a 40% reduction in viability relative to control cultures using an MTT assay (for cell metabolic assessment).[104]

Research conducted by Hodek *et al.* performed cytotoxicity tests of their hybrid coating containing silver, copper, and zinc on Vero and HeLa cells, demonstrating viability values above 90% for both cell lines after 4 hours.[42] Similarly, the graphene-oxide-silver nanocomposite created by Chen *et al.* successfully immobilized AgNPs to prevent toxicological effects and reduce potential downstream environmental impacts caused by free AgNPs.[44] Additionally, some research has suggested that AgNP exposure induces metabolic arrest rather than cell death and that human cells have greater resistance than other organisms, providing some justification for their use for healthcare.[105,106]

Polyethyleneimine compounds have shown minimal cytotoxicity in mammalian cells.[78] A study by Shi *et al.* evaluated the cytotoxicity of polyethyleneimines through an MTT assay on 3T3 mouse fibroblasts, showing no statistically significant difference between the polyethyleneimine treated surfaces, untreated surfaces, and growth culture medium.[107] Furthermore, photosensitizer materials such as rose bengal, which have been implemented in wipes, have also shown no toxic effect on mammalian cells.[97]

Impact of metal nanoparticles on the environment has been a concern since their popularity increased due to antimicrobial activity without the possibility for resistance.[36] The mechanism of toxicity for nanoparticles is through association with the cell surface, dissolution of material by releasing toxic ions which impair enzyme function or DNA, or generation of ROS leading to oxidative stress.[108] Recent studies have considered the environmental toxicity of the fabrication of these nanoparticles. In the study conducted by Li *et al.*, copper nanoparticles were generated *via* a biosynthesis method, which incorporates L-vitamin C to avoid the toxicity of ROS created when CuNPs are exposed to air.[31,109] Additionally, strategies have been considered which will reduce the environmental impact of nanoparticles, such as negative surfaces on nanomaterials to reduce cell surface interactions,[110] capping of nanoparticles to reduce dissolution *via* toxic ions,[111] and tethering of antioxidant molecules to nanoparticle surfaces to reduce ROS impact.[112]

2.6 Emerging technologies and future perspective

In the previous sections, we introduced antiviral agents and coatings that have shown antiviral effects. Although these technologies have been effective in inactivating viruses on

various surfaces, they still suffer from several shortcomings that inhibit their practical application for use in daily life. Most of these methods are not universal and their effectiveness depends on the type of the virus. In addition, they might require long incubation times with the attached viruses that could contribute to the interim transmission of the virus. Challenges with mass production and material cost are other drawbacks to many of these technologies, including polyethyleneimine-based antiviral coatings and nanoparticle-based antiviral solutions. In this section, we introduce potential emerging technologies that could be used stand-alone or in combination with the currently-available antiviral technologies to provide synergistic effects for creating antiviral surfaces (Table 2.3).

Pathogen-repellent surfaces, rather than surfaces impregnated with microbicides, have shown great promise for preventing bacterial adhesion and biofilm formation;[2] however, there is limited information on the applicability of these surfaces in repelling viruses. These repellent surfaces are mostly inspired by natural systems and involve combining nanostructures, microstructures, and chemical functionality. Bioinspired hierarchical micro and nanostructures have been shown to demonstrate antimicrobial effects, while also preventing the binding and attachment of pathogenic organisms to the surface in the first place.[2] Due to the unique wetting properties/states of hierarchical structures, many biological contaminants have been shown to have poor adhesion to these surfaces.[2] This has been most commonly seen with complex fluids such as blood,[113] as well as with solutions containing bacteria, showing low surface contamination and bacterial growth.[114] Nanostructuring of surfaces is a bioinspired technique that researchers regularly employ to

obtain self-cleaning characteristics and varying levels of repellency. Similar to the lotus leaf and pitcher plant providing inspiration for self-cleaning surfaces,[115] insect wings have inspired a nanostructured approach for antimicrobial capability.[116] In addition to this, combining the chemical modifications, micro and/or nanostructures with an infused liquid layer, mimics the effect of the pitcher plant,[117,118] thus creating a class of surfaces called lubricant-infused surfaces. These surfaces have displayed superior performance in suppressing blood contamination and clotting,[119–124] while also preventing the growth and attachment of bacteria and their biofilms.[5,125–127] Figure 2.6a shows the growth of planktonic bacteria biofilm after 21 days of incubation on dissolved oxygen-permeable membranes with and without a lubricant-infused coating. Although lubricant-infused surfaces show superior properties for pathogen repellency compared to other technologies, the stability of the lubricant layer, especially on surfaces open to air, is a current drawback of these coatings that could be addressed by choosing more stable lubricants.

Recently, nanostructured surfaces were tested by Hasan *et al.* for the purpose of antiviral capabilities (Figure 2.6b). Studying the impact of wet etching with NaOH on aluminum alloy Al 6063, it was found that rhinovirus-16 (RV-16) was very susceptible to loss of viability over a 24 hour period, showing a 3- to 4-log reduction.[128] The same research revealed a lesser impact on the viability of respiratory syncytial virus 4 (RSV4), with the virus naturally showing reduction after 24 hours on Al 6063 alone, though significant decreases were recorded after just 2 hours when nanostructures were present.[128]

We recently developed a flexible omniphobic wrap featuring hierarchical structures (*i.e.* multiple length-scale structures) with repellent properties towards a multitude of fluids and

pathogenic bacteria, including *Staphylococcus aureus and Pseudomonas aeruginosa*, as well as inhibition of biofilm formation on the surface (Figure 2.6c).[2] To evaluate the repellency, a pathogen transfer analysis was demonstrated with GFP-expressing *E. coli* contaminating the repellent wrap and a commercial wrap through a simulated touch experiment (Figure 2.6c). The repellent wraps showed a significant reduction in the transferred bacteria between surfaces. In another work by Chauhan *et al.*,[129] cotton fabrics were modified with hexadecyltrimethoxysilane (HDTMS) to create a superhydrophobic and durable surface. To investigate antimicrobial effects, these surfaces were incubated with *E. coli* (1 x 10^5 CFU/mL) at 37 ºC for 24 hours and *E. coli* was unable to bind to the surface resulting in cell death and the formation of an inhibition zone around the treated substrates.[129]

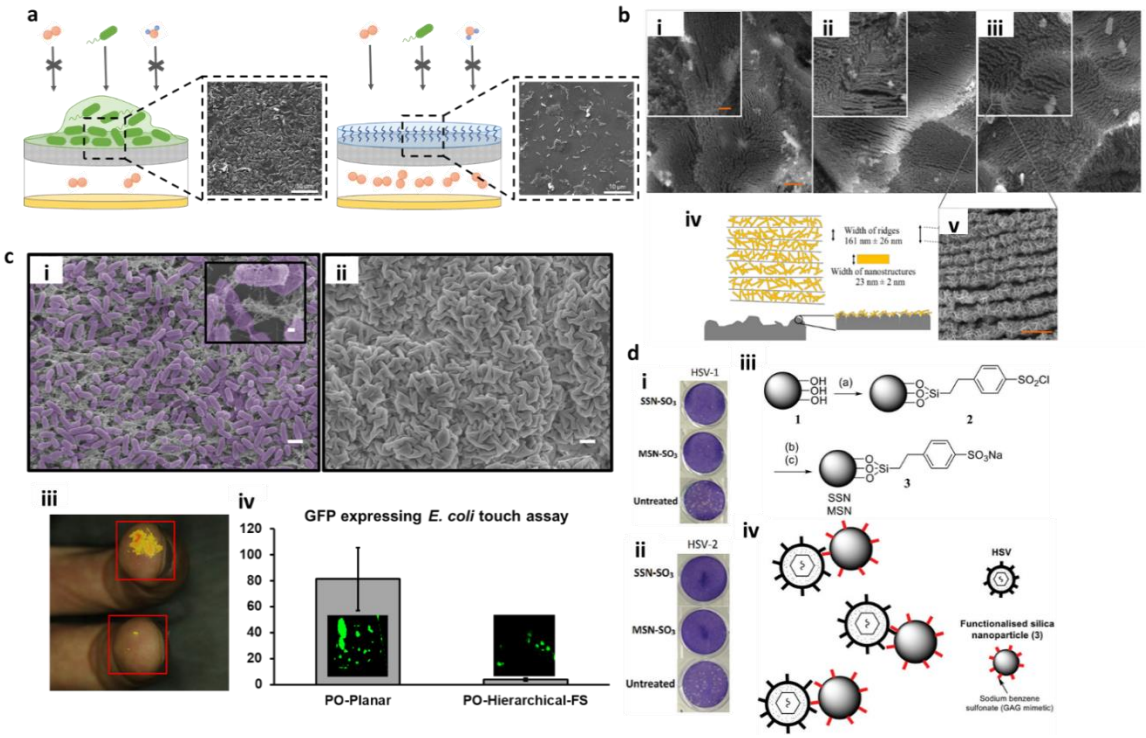

Figure 2.6 Emerging technologies with potential applications as antiviral coatings. *(a) Permeable membrane with fluorosilane based lubricant-infused coating (i, ii, iii) schematic of biofouling on membrane with and without the lubricant-infused layer, (iv) SEM of biofouling on untreated membrane and (v) SEM of biofouling on lubricant-infused membrane, after 21 days of incubation. Reproduced with permission from [125]. (b) The induced nanostructures on Aluminum 6063 are shown here via SEM, created by wet etching for (i) half hour, (ii) one hour and (iii) three hours (Scale bars = 2 µm, inset scale bars = 1 µm). (iv) Schematic representations of the etched samples at higher (top) and lower (bottom) magnification. (v) SEM of the three-hour etched surface at higher magnification revealing the presence of random nanostructures (Scale bar = 500 nm). Reproduced with permission from [129]. (c) An omniphobic hierarchical wrinkled structure that prevents the adhesion of bacteria and the growth of their biofilms. SEM of the fixed biofilm of P. aeruginosa on (i) planar polystyrene and (ii) hierarchically structured polystyrene surface. The scale bars on larger SEM are 1 µm and the inserted are 100 nm. (iii) analysis of bacterial transfer from an intermediate surface to human hands (iv) bacterial transfer from contaminated surface to planar plastic shrink film and hierarchically structured shrink film. Reproduced with permission from [2]. (d) GAG mimetic modified mesoporous silica nanoparticles (i, ii) plaque reduction assay of SSN-SO3 and for HSV1 and HSV2 respectively, (iii) synthesis of GAG mimetic silica nanoparticles, (iv) schematic of proposed mode of antiviral activity. Reproduced with permission from [130].*

Mannelli *et al.* demonstrated the effect of wetting properties on the stability of influenza A on glass surfaces treated with various hydro and fluoro-carbon chain lengths silanes. Three wetting condition combinations were considered; hydrophilic/oleophilic, hydrophobic/oleophilic, and hydrophobic/oleophobic.[131] They were able to demonstrate the degradation of the viral envelope in the latter two cases, with the hydrophobic/oleophilic surface showing the largest amount of viral inactivity, an 80% reduction in viral activity, while for glass there was little to no reduction in the virus activity.[131] These emerging natural pathogen repellent/inactivating technologies could potentially be used for preventing viral contamination of high-contact surfaces in various settings.

Other emerging materials that utilize micro and nanostructures to create antimicrobial effects are being investigated and developed using safe compounds while still displaying

promising antimicrobial properties. For example, solid and mesoporous silica nanoparticles (SSN and MSN, respectively) functionalised with glycosaminoglycan (GAGs) have been implemented to attract viral glycoproteins and eliminate virus entry to host cells in solution.[130] This method could provide a close proximity for virucidal agents to act on the virus, providing a dual functionality (*i.e.* capture and deactivation). The electrostatic and hydrophobic interaction between the GAGs and the virus (*e.g.* HSV-1 and -2), along with the facility of surface functionalization and biocompatibility of silica nanoparticles, make this system a promising method for eliminating infection in solution.[130] This effect can be seen with the plaque reduction assay run on both HSV-1 (Figure 2.6d i) and HSV-2 (Figure 2.6d ii) which both displayed significant antiviral activity compared to the control case. Micro-sized SiO_2 particles (SiO_2 MPs) were also used for antiviral studies in solutions where the surface of the SiO_2 MPs were treated with APTES to add C_{60} to their surface as a photosensitizer. Under blue LED light at a wavelength of 470 nm, these particles showed antiviral behaviour. These treated particles could potentially be coated on to existing surfaces to confer antiviral properties.[98]

Another class of materials based on pyridinium has been used to capture viruses in solution,[132] and air,[133] and could potentially be used as surface coatings. Cross-linked poly(N-benzyl-4-vinylpyridinium bromide) (BVP) and crosslinked poly(N-benzyl-4-vinylpyridinium chloride) have been used for removing pathogenic viruses and have been shown to remove more than 99.5% of viruses such as of enterovirus, HSV, poliovirus, and HIV.[132,133] The affinity of the viruses towards pyridinium was attributed to the combination of the positive charge of the resin and the negative charge on the surface of the viruses, as

well as the hydrophobic interactions. This affinity can potentially be exploited to incorporate antiviral agents within the matrix of the resin to attract and inactivate the viruses on site. Xue *et al.* showed more than 90% virucidal effect in solution with only 50 ppm of the synthesised polymers, which consisted of quaternary pyridinium-type polymers (*e.g.* Poly(4VP-co-NVP)), comprising of 4-Vinylpyridine (4VP) and N-vinyl pyrrolidone (NVP), quaternized with benzyl halides,[134] which can potentially be added as a coating to surfaces.

Quantum dots (QDs) are another category of optically active nanomaterials that have potential for use in antimicrobial coatings. More recently, research has been directed at fabricating antimicrobial coatings using QDs as an active agent. Ristic *et al.* evaluated the antibacterial effectiveness of graphene quantum dots (GQDs), which, unlike other types of semiconducting QDs, are biocompatible while retaining the ability to produce ROS.[135] They suspended MRSA and *E. coli* with varied concentrations of GQDs before irradiation with blue light (465-475 nm, 1W). They used propidium iodide (PI) staining to visualize membrane damage and found that approximately 90% of both cell species were not viable after 15 min of irradiation in a 200 µg/mL GQD suspension.[135] Similarly, Habiba *et al.* demonstrated antibacterial activity in Ag-NPs decorated with GQDs, which were further surface modified with PEG to promote biocompatibility. Minimum inhibitory concentrations of 50 µg/mL and 25 µg/mL were obtained for the nanoparticle suspensions against *P. aeruginosa* and *S. aureus*, respectively.[136] The non-toxicity of GQDs has been well-established. For example, Zhu *et al.* demonstrated that adding 400 µg of GQDs to 150µL of MG-63 cell culture medium resulted in no significant reduction to cell viability

in an MTT assay.[137] To the best of our knowledge, research has yet to test the antiviral potential of QDs on surfaces, however, based on the ROS mechanism seen with other antiviral agents this material shows promise for antiviral capabilities.

In an effort to develop technologies with antiviral properties, several companies have utilized antiviral strategies to manufacture products and coatings. EnvisionSQ has developed a product called GermStopSQ,[138] a coating that claims to adhere to any surface and is semi-permanent. The EnvisionSQ website states that their technology is 99.9999% effective in eliminating bacteria, fungi and viruses (both enveloped and non-enveloped). Covalon has recently introduced a product called CovaGuard,[139] which they assert is formulated to inactivate SARS-CoV-2 and other viruses, as well as bacteria, both immediate and sustained. They highlight the use of benzalkonium chloride (BAC) in their formulation, which can be applied (through spraying) on any surface and remains antimicrobial and antiviral for four days. Biogate is another company which has a product called MicroSilver BG™,[140] comprising of microporous silver additive. They have claimed that their product is not cytotoxic and can be incorporated into various materials. Bio-Fence has fabricated chlorine-binding polymer coatings that are antimicrobial and antiviral.[141] Once the surface is depleted, it can be coated again by spraying the Chlorine, according to their website. SurfaceWise^2 is another surface coating approved by United States Environmental Protection Agency (EPA) to have antiviral activity with a single application.[142] Caliwel™ BNA Coating, based on calcium hydroxide, has also been approved by EPA for its antiviral and antimicrobial behavior.[143,144] BioFriend™

BioMask™ is another company with FDA approval that produces masks that are able to trap pathogens including viruses and inactivate them.[145]

In the future, a combination of pathogen-repellent coatings with antiviral materials could create synergistic effects, through which the surface repels the majority of the viruses while the coated antiviral agents inactivate any attached viruses that have not been repelled, providing a double layer of protection against viruses. This could greatly reduce the number of pathogens transferred from fomites to person, and then from person to person. The improved biocompatibility and lower toxicity of structurally-engineered repellent materials would allow them to be used in a larger range of applications including the highly regulated food[146] and medical industries.[147]

Combining a spectrum of materials with different antimicrobial mechanisms is expected to lead to smart surfaces that attract, bind, and eliminate a multitude of pathogens.

Finally, integrating simple and real-time sensing capabilities to these antimicrobial surfaces, in addition to mitigating the risk of transmission, could help in identifying the pathogens present in the environment, and eventually aiding the public health authorities in managing infectious disease outbreaks.

Table 2.3 *Emerging technologies with potential to be used as antiviral coatings*

Material and Structure	Antimicrobial Testing		Promising Features	Challenges	Ref.
	Virus	Bacteria			
Micro/nano Structuring					
Nanostructured Aluminum	Respiratory syncytial virus (RSV) Rhinovirus (RV)	*Pseudomonas aeruginosa Staphylococcus aureus*	Dual action of antiviral and antibacterial 3-4 log reduction in viability counts of RV within 2 hours	Limited to aluminum surfaces Nanostructures are not controlled during fabrication	128

Material and Structure	Antimicrobial Testing		Promising Features	Challenges	Ref.
	Virus	Bacteria			
			More rapid reduction of RSV than control 92% inactivation of *P. aeruginosa* 87% inactivation of *S. aureus*, respectively within 3 hours. Mechanically durable, viable option for high-touch surfaces		
Nanostructured anatase-rutile-carbon (NsARC) coating	N/A	*Escherichia coli*	Photocatalytic activity was shown to present in UV light (4-log reduction in EOP, over 4 hours) and visible light (3-log reduction, and in the dark (2-log reduction). These results broaden the possible applications to everyday environments.	Did not investigate durability; currently only grown on stainless steel surfaces.	51
Hierarchical micro and nanostructure based on thin film wrinkling on plastic shrink wraps.	N/A	*Staphylococcus aureus Pseudomonas aeruginosa Escherichia coli*	Reduces biofouling for bacteria. Flexibility allows them to be used in both medical devices or as medical surfaces	Requires heating to temperatures of 145C to conform around an object/surface.	2

Material and Structure	Antimicrobial Testing		Promising Features	Challenges	Ref.
	Virus	Bacteria			
Hexadecyltrimethoxysilane (HDTMS) modified cotton fabric	N/A	*Escherichia coli*	Extremely durable, maintained its repellent properties after washing in solvents and hot water. Simple manufacturing method. Inactivation of *E. coli via* inhibition zone started showing after 12 hours and continued up to 24 hours	Does not investigate why the inhibition zone is created by the hydrophobicity, or how the chemical modification would work on other fabrics	129
Lubricant-infused surfaces					
Fluorosilane-based omniphobic lubricant-infused coating on permeable membrane	N/A	Planktonic bacteria	Significantly reduced the formation of biofilm growth and formation of a 21-day period	Did not investigate potential antibiofouling effects on pathogenic bacteria.	125
Tethered-liquid perfluorocarbon surface	N/A	*Pseudomonas aeruginosa Escherichia coli*	*Pseudomonas aeruginosa* was grown in coated PVC medical tubing for 6.5 weeks and showed an eight-fold reduction in the formation of the biofilm. The surfaces also reduced blood related biofouling	Reduction of biofilm *in vitro* only lasted 24 hours. Lubricant layer can evaporate over time resulting in the loss of performance.	5
PTFE membrane infused with perfluoropolyether	N/A	*Staphylococcus aureus Pseudomonas aeruginosa Escherichia coli*	The PTEF lubricant-infused substrates showed 99.6% decrease in biofilm formation in a 7-day incubation	Lubricant layer can evaporate over time resulting in a loss of performance.	119

Material and Structure	Antimicrobial Testing		Promising Features	Challenges	Ref.
	Virus	Bacteria			
			under flow, for *Staph. aureus*. While showing a 96-97.2% reduction for the other two pathogens in a 2-day period		
Liquid/particle-based material					
GAG mimetic functionalized solid and mesoporous silica nanoparticles (SSN-SO3 and MSN-SO3)	HSV-1 and HSV-2	N/A	The GAG mimetic MSN and SSN act as a viral binding inhibitor that inhibits HSV 1 and 2 from infecting cells within 1 hour	GAG modification is attractive towards viruses, so it should be combined with an antiviral modification	130
poly(N-benzyl-4-vinylpyridinium bromide (BVP) resin	enterovirus, HSV, poliovirus, and HIV coxsackievirus and echovirus human rotavirus, influenza virus, human adenovirus, and Japanese encephalitis virus	N/A	efficient removal of viruses from aqueous solutions based on pyridinium affinity for viruses. 64-fold reduction for HRV, 256 fold reduction for Influenza A, 32-fold reduction Ad-37 and 16 fold reduction in JEV after 30 min.	Toxicity was not discussed and means of use on various surfaces. This method is attractive towards viruses, so it should be combined with an antiviral modification	132
poly(N-benzyl-4-vinylpyridinium chloride)	Bacteriophage T4	N/A	efficient removal of viruses from air based on pyridinium affinity for viruses	A membrane was fabricated, addition of this material to existing membranes was not investigated. This method is attractive towards viruses, so it should be combined with	133

Material and Structure	Antimicrobial Testing		Promising Features	Challenges	Ref.
	Virus	Bacteria			
				an antiviral modification	
water-soluble pyridinium-type polyvinylpyrrolidones with different counter anions comprising of 4-Vinylpyridine (4VP) and N-vinyl pyrrolidone (NVP) (Poly(4VP-co-NVP), quaternized with benzyl halides	Influenza virus	*Staphylococcus aureus* and *Escherichia coli*	Adsorption of the polymer onto the virus envelope followed by penetration inactivates the virus at small titers (50 ppm). They also displayed the ability To inactivate *E. coli* within 3 min.	Only showed antiviral effect on enveloped viruses. Potential to add on surfaces was not explored	[134]
Graphene quantum dots (GQDs) suspension	N/A	*E. coli* and MRSA	90% of both cell species were not viable after 15 min of irradiation with blue light in a 200 µg/mL GQD suspension.	Performed in solution, not tested against virus titers	[135]
Silver nanoparticles (Ag-NPs) decorated with GQDs	N/A	*P. aeruginosa* and *S. aureus*	Minimum inhibitory concentrations of 50 µg/mL and 25 µg/mL were obtained for the nanoparticle suspensions against *P. aeruginosa* and *S. aureus*, respectively, after incubation with NPs for 24 h.	Performed in solution, not tested against virus titers	[136]

2.7 Conclusion

Modification of surfaces to confer antiviral capabilities is an area that is ripe for investigation. With the current SARS-CoV-2 pandemic, there has been a rapid surge in the

number of studies that focus on quantifying the survival of SARS-CoV-2 on various surfaces.[6,148,149] We anticipate that several of the technologies presented here could be used as surface coatings to reduce the spread of infectious diseases, including COVID-19, *via* surfaces. We petition researchers to apply a more systematic approach to their investigations in studying the antimicrobial properties of surfaces, rigorously testing each category of viruses – enveloped or non-enveloped, DNA-based or RNA-based – prior to making claims of effectiveness. Above all, it is imperative that research claiming antimicrobial capabilities becomes more accurate about effectiveness against viruses, only making these claims when viral studies have been executed. Surfaces capable of immediately repelling and/or inactivating pathogens are urgently needed, and it is now the responsibility of scientists, industry, and governments to work together towards this goal.

2.8 Author Information

Corresponding Authors

Tohid F. Didar – Department of Mechanical Engineering, School of Biomedical Engineering, and Michael G. DeGroote Institute of Infectious Disease Research, McMaster University, 1280 Main Street West, Hamilton, L8S 4L8, Canada
Leyla Soleymani – Department of Engineering Physics and School of Biomedical Engineering, McMaster University, 1280 Main Street West, Hamilton, L8S 4L8, Canada

Authors

Sara M. Imani – School of Biomedical Engineering, McMaster University, 1280 Main Street West, Hamilton, L8S 4L8, Canada
Liane Ladouceur – School of Biomedical Engineering, McMaster University, 1280 Main Street West, Hamilton, L8S 4L8, Canada
Terrel Marshall – Department of Engineering Physics, McMaster University, 1280 Main Street West, Hamilton, L8S 4L8, Canada
Roderick Maclachlan – Department of Engineering Physics, McMaster University, 1280 Main Street West, Hamilton, L8S 4L8, Canada

Author Contributions

T.F.D. and L.S. supervised and conceived the research. S.M.I. and L.L. designed and wrote the main manuscript text with help from T.F.D and L.S. T.M. and R.M. contributed to specific sections. All authors contributed to editing the manuscript.

The authors declare no competing financial interest.

2.9 Acknowledgements

TFD acknowledges the financial support provided by NSERC Discovery and CRD grants, Ontario Early Researcher Award grant and McMaster start-up funds to T.F.D.

2.10 Vocabulary

Plaque assay: A method of viral quantification relying on the formation of plaque-forming units of infected (lysed) cells *in vitro* after inoculation with a viral titer. Plaque-forming units are counted manually and given in units of PFU/mL. Alternatively, immunostaining targeting viral antibodies can be used to quantify viral activity, measured in units of focus forming units (FFU/mL). Reactive oxygen species (ROS): Oxygen-containing free radicals produced during photoactivity and a variety of metabolic processes. In excess quantities, cause oxidative damage to components of the cell, including lipid membranes and genetic material. **Bacteriophage:** A virus that specializes in infecting and replicating inside bacteria. **Photocatalysis:** A process in which chemical reactions are generated in the presence of light. In semiconductors, this can result in the development of electron/hole pairs and reactive oxygen species in the presence of oxygen-containing compounds. **Enveloped virus:** Virus whose outermost layer is an envelope derived from the host cell's plasma membrane and composed of phospholipids, lipoproteins, and glycoproteins. Non-enveloped viruses are instead protected mainly by a shell-like protein capsid. All viruses possess a capsid, but not all are enveloped. **Electrospinning/spraying:** Related fabrication processes by which polymer solutions in an electric field are forced through an opening when electrostatic repulsion between droplets exceeds surface tension. Electrospinning occurs when the droplets form a continuous stream; electrospraying occurs when the droplets separate. **Positive and negative-sense ssRNA:** Viruses that replicate using single stranded RNA may produce a strand complimentary or identical to the genetic material produced in the host cell. Positive-sense strands possess the same nucleotide sequence, and may be directly translated into proteins, while negative-sense strands possess the complimentary sequence.

2.11 References

(1) Llorens, A.; Lloret, E.; Picouet, P. A.; Trbojevich, R.; Fernandez, A. Metallic-Based Micro and Nanocomposites in Food Contact Materials and Active Food Packaging. *Trends in Food Sci. Technol.* **2012**, *pp 19–29*.
(2) Imani, S. M.; Maclachlan, R.; Rachwalski, K.; Chan, Y.; Lee, B.; McInnes, M.; Grandfield, K.; Brown, E. D.; Didar, T. F.; Soleymani, L. Flexible Hierarchical Wraps Repel Drug-Resistant Gram-Negative and Positive Bacteria. *ACS Nano* **2020**, *14*, 454–465.
(3) Nguyen, D. H. K.; Pham, V. T. H.; Truong, V. K.; Sbarski, I.; Wang, J.; Balčytis, A.; Juodkazis, S.; Mainwaring, D. E.; Crawford, R. J.; Ivanova, E. P. Role of Topological Scale in the Differential Fouling of: *Pseudomonas Aeruginosa* and *Staphylococcus Aureus* Bacterial Cells on Wrinkled Gold-Coated Polystyrene Surfaces. *Nanoscale* **2018**, *10*, 5089–5096.
(4) Crawford, R. J.; Webb, H. K.; Truong, V. K.; Hasan, J.; Ivanova, E. P. Surface Topographical Factors Influencing Bacterial Attachment. *Adv. Colloid Interface Sci.* **2012**, *172–182*, 142–149..
(5) Leslie, D. C.; Waterhouse, A.; Berthet, J. B.; Valentin, T. M.; Watters, A. L.; Jain, A.; Kim, P.; Hatton, B. D.; Nedder, A.; Donovan, K.; Super, E. H.; Howell, C.; Johnson, C. P.; Vu, T. L.; Bolgen, D. E.; Rifai, S.; Hansen, A. R.; Aizenberg, M.; Super, M.; Aizenberg, J. *et al.* A Bioinspired Omniphobic Surface Coating on Medical Devices Prevents Thrombosis and Biofouling. *Nat. Biotechnol.* **2014**, *32*, 1134–1140.
(6) Kampf, G.; Todt, D.; Pfaender, S.; Steinmann, E. Persistence of Coronaviruses on Inanimate Surfaces and Their Inactivation with Biocidal Agents. *J. Hosp. Infect.* **2020**, *104*, 246–251.
(7) Pirtle, E. C.; Beran, G. W. Virus Survival in the Environment. *Rev. Sci. Tech.* **1991**, *10* (3), 733–748.
(8) Recommendations for Prevention of HIV Transmission in Health-Care Settings https://www.cdc.gov/MMWR/preview/MMWRhtml/00023587.htm (accessed Jun 10, 2020).
(9) Otter, J. A.; Donskey, C.; Yezli, S.; Douthwaite, S.; Goldenberg, S. D.; Weber, D. J. Transmission of SARS and MERS Coronaviruses and Influenza Virus in Healthcare Settings: The Possible Role of Dry Surface Contamination. *J. Hosp. Infect.* , **2016**, *pp 235–250*.
(10) Weiss, C.; Carriere, M.; Fusco, L.; Fusco, L.; Capua, I.; Regla-Nava, J. A.; Pasquali, M.; Pasquali, M.; Pasquali, M.; Scott, J. A.; Vitale, F.; Vitale, F.; Unal, M. A.; Mattevi, C.; Bedognetti, D.; Merkoçi, A.; Merkoçi, A.; Tasciotti, E.; Tasciotti, E.; Yilmazer, A.; Yilmazer, A.; Gogotsi, Y.; Stellacci, F.; Stellacci, F.; Delogu, L. G. Toward Nanotechnology-Enabled Approaches Against the COVID-19 Pandemic. *ACS Nano* **2020**, *14*, 6383–6406.
(11) Sportelli, M. C.; Izzi, M.; Kukushkina, E. A.; Hossain, S. I.; Picca, R. A.; Ditaranto, N.; Cioff, N. Can Nanotechnology and Materials Science Help the Fight against Sars-Cov-2? *Nanomaterials* **2020**, *10*.
(12) Vincent, M.; Duval, R. E.; Hartemann, P.; Engels-Deutsch, M. Contact Killing and Antimicrobial Properties of Copper. *J. Appl. Microbiol.* **2017**, *124*, 1032–1046.

(13) Milanino, R. Copper in Medicine and Personal Care: A Historical Overview. In *Copper and the Skin*; 20006; pp 170–182. https://doi.org/10.1080/15376520490446365.
(14) Borkow, G. Using Copper to Fight Microorganisms. *Curr. Chem. Biol.* **2012**, *6*, 93–103..
(15) Nan, L.; Liu, Y.; Lü, M.; Yang, K. Study on Antibacterial Mechanism of Copper-Bearing Austenitic Antibacterial Stainless Steel by Atomic Force Microscopy. *J. Mater. Sci. Mater. Med.* **2008**, *19*, 3057–3062.
(16) Karlstrom, A. R.; Levine, R. L. Copper Inhibits the Protease from Human Immunodeficiency Virus 1 by Both Cysteine-Dependent and Cysteine-Independent Mechanisms. *Proc. Natl. Acad. Sci. U. S. A.* **1991**, *88*, 5552–5556.
(17) Sagripanti, J.; Goering, P. L.; Lamanna, A. *Interaction of Copper with DNA and Antagonism by Other Metals*; 1991; Vol. 110.
(18) Sunada, K.; Minoshima, M.; Hashimoto, K. Highly Efficient Antiviral and Antibacterial Activities of Solid-State Cuprous Compounds. *J. Hazard. Mater.* **2012**, *235–236*, 265–270.
(19) Warnes, S. L.; Summersgill, E. N.; Keevil, C. W. Inactivation of Murine Norovirus on a Range of Copper Alloy Surfaces Is Accompanied by Loss of Capsid Integrity. *Appl. Environ. Microbiol.* **2015**, *81*, 1085–1091.
(20) Warnes, S. L.; Keevil, C. W. Inactivation of Norovirus on Dry Copper Alloy Surfaces. *PLoS One* **2013**, *8*, 75017.
(21) Bleichert, P.; Santo, C. E.; Hanczaruk, M.; Meyer, H.; Grass, G. Inactivation of Bacterial and Viral Biothreat Agents on Metallic Copper Surfaces. *BioMetals* **2014**, *27*, 1179–1189.
(22) Noyce, J. O.; Michels, H.; Keevil, C. W. Inactivation of Influenza A Virus on Copper *versus* Stainless Steel Surfaces. *Appl. Environ. Microbiol.* **2007**, *73*, 2748–2750.
(23) Minoshima, M.; Lu, Y.; Kimura, T.; Nakano, R.; Ishiguro, H.; Kubota, Y.; Hashimoto, K.; Sunada, K. Comparison of the Antiviral Effect of Solid-State Copper and Silver Compounds. *J. Hazard. Mater.* **2016**, *312*, 1–7.
(24) Li, J.; Dennehy, J. J. Differential Bacteriophage Mortality on Exposure to Copper. *Appl. Environ. Microbiol.* **2011**, *77*, 6878–6883.
(25) Warnes, S. L.; Little, Z. R.; Keevil, C. W. Human Coronavirus 229E Remains Infectious on Common Touch Surface Materials. *MBio* **2015**, *6*.
(26) Borkow, G.; Gabbay, J. Putting Copper into Action: Copper-Impregnated Products with Potent Biocidal Activities. *FASEB J.* **2004**, *18*, 1728–1730. .
(27) Borkow, G.; Sidwell, R. W.; Smee, D. F.; Barnard, D. L.; Morrey, J. D.; Lara-Villegas, H. H.; Shemer-Avni, Y.; Gabbay, J. Neutralizing Viruses in Suspensions by Copper Oxide-Based Filters. *Antimicrob. Agents Chemother.* **2007**, *51*, 2605–2607.
(28) Borkow, G.; Zhou, S. S.; Page, T.; Gabbay, J. A Novel Anti-Influenza Copper Oxide Containing Respiratory Face Mask. *PLoS One* **2010**, *5*.
(29) Imai, K.; Ogawa, H.; Bui, V. N.; Inoue, H.; Fukuda, J.; Ohba, M.; Yamamoto, Y.; Nakamura, K. Inactivation of High and Low Pathogenic Avian Influenza Virus H5

Subtypes by Copper Ions Incorporated in Zeolite-Textile Materials. *Antiviral Res.* **2012**, *93*, 225–233.

(30) Ingle, A. P.; Duran, N.; Rai, M. Bioactivity, Mechanism of Action, and Cytotoxicity of Copper-Based Nanoparticles: A Review. *Applied Microbiology and Biotechnology*. 2014, pp 1001–1009.

(31) Li, Y.; Pi, Q. M.; You, H. H.; Li, J. Q.; Wang, P. C.; Yang, X.; Wu, Y. A Smart Multi-Functional Coating Based on Anti-Pathogen Micelles Tethered with Copper Nanoparticles: *Via* a Biosynthesis Method Using l-Vitamin C. *RSC Adv.* **2018**, *8*, 18272–18283..

(32) Dakal, T. C.; Kumar, A.; Majumdar, R. S.; Yadav, V. Mechanistic Basis of Antimicrobial Actions of Silver Nanoparticles. *Front. Microbiol.* **2016**, *7*, 1–17.

(33) Read, S. A.; Obeid, S.; Ahlenstiel, C.; Ahlenstiel, G. The Role of Zinc in Antiviral Immunity. *Advances in Nutrition*. 2019, pp 696–710.

(34) Halbus, A. F.; Horozov, T. S.; Paunov, V. N. Colloid Particle Formulations for Antimicrobial Applications. *Adv. Colloid Interface Sci.* **2017**, *249*, 134–148. .

(35) Champagne, V.; Sundberg, K.; Helfritch, D. Kinetically Deposited Copper Antimicrobial Surfaces. *Coatings* **2019**, *9*, 1–9.

(36) Rai, M.; Deshmukh, S. D.; Ingle, A. P.; Gupta, I. R.; Galdiero, M.; Galdiero, S. Metal Nanoparticles: The Protective Nanoshield against Virus Infection. *Crit. Rev. Microbiol.* **2016**, *42*, 46–56.

(37) Lara, H. H.; Ayala-Nuñez, N. V; Ixtepan-Turrent, L.; Rodriguez-Padilla, C. Mode of Antiviral Action of Silver Nanoparticles against HIV-1. *J. Nanobiotechnology* **2010**, *8*.

(38) Castro-Mayorga, J. L.; Randazzo, W.; Fabra, M. J.; Lagaron, J. M.; Aznar, R.; Sánchez, G. Antiviral Properties of Silver Nanoparticles against Norovirus Surrogates and Their Efficacy in Coated Polyhydroxyalkanoates Systems. *LWT - Food Sci. Technol.* **2017**, *79*, 503–510.

(39) Park, S. J.; Park, H. H.; Kim, S. Y.; Kim, S. J.; Woo, K.; Ko, G. P. Antiviral Properties of Silver Nanoparticles on a Magnetic Hybrid Colloid. *Appl. Environ. Microbiol.* **2014**, *80* , 2343–2350.

(40) Stohs, S. J.; Bagchi, D. Oxidative Mechanisms in the Toxicity of Metal Ions. *Free Radical Biology and Medicine*. 1995, pp 321–336.

(41) AshaRani, P. V; Mun, G. L. K.; Hande, M. P.; Valiyaveettil, S. Cytotoxicity and Genotoxicity of Silver Nanoparticles in Human Cells. *ACS Nano* **2009**, *3* (2), 279–290.

(42) Hodek, J.; Zajícová, V.; Lovetinská-Šlamborová, I.; Stibor, I.; Müllerová, J.; Weber, J. Protective Hybrid Coating Containing Silver, Copper and Zinc Cations Effective against Human Immunodeficiency Virus and Other Enveloped Viruses. *BMC Microbiol.* **2016**, *16* , 1–12.

(43) Nguyen, V. Q.; Ishihara, M.; Kinoda, J.; Hattori, H.; Nakamura, S.; Ono, T.; Miyahira, Y.; Matsui, T. Development of Antimicrobial Biomaterials Produced from Chitin-Nanofiber Sheet/Silver Nanoparticle Composites. *J. Nanobiotechnology* **2014**, *12*.

(44) Chen, Y. N.; Hsueh, Y. H.; Hsieh, C. Te; Tzou, D. Y.; Chang, P. L. Antiviral

Activity of Graphene–Silver Nanocomposites against Non-Enveloped and Enveloped Viruses. *Int. J. Environ. Res. Public Health* **2016**, *13*.

(45) Zodrow, K.; Brunet, L.; Mahendra, S.; Li, D.; Zhang, A.; Li, Q.; Alvarez, P. J. J. Polysulfone Ultrafiltration Membranes Impregnated with Silver Nanoparticles Show Improved Biofouling Resistance and Virus Removal. *Water Res.* **2009**, *43*, 715–723.

(46) De Gusseme, B.; Hennebel, T.; Christiaens, E.; Saveyn, H.; Verbeken, K.; Fitts, J. P.; Boon, N.; Verstraete, W. Virus Disinfection in Water by Biogenic Silver Immobilized in Polyvinylidene Fluoride Membranes. *Water Res.* **2011**, *45*, 1856–1864.

(47) Martínez-Abad, A.; Ocio, M. J.; Lagarón, J. M.; Sánchez, G. Evaluation of Silver-Infused Polylactide Films for Inactivation of Salmonella and Feline Calicivirus *in Vitro* and on Fresh-Cut Vegetables. *Int. J. Food Microbiol.* **2013**, *162*, 89–94.

(48) Joe, Y. H.; Park, D. H.; Hwang, J. Evaluation of Ag Nanoparticle Coated Air Filter against Aerosolized Virus: Anti-Viral Efficiency with Dust Loading. *J. Hazard. Mater.* **2016**, *301*, 547–553.

(49) Speshock, J. L.; Murdock, R. C.; Braydich-Stolle, L. K.; Schrand, A. M.; Hussain, S. M. Interaction of Silver Nanoparticles with Tacaribe Virus. *J. Nanobiotechnology* **2010**, *8*.

(50) Rogers, J. V; Parkinson, C. V.; Choi, Y. W.; Speshock, J. L.; Hussain, S. M. A Preliminary Assessment of Silver Nanoparticle Inhibition of Monkeypox Virus Plaque Formation. *Nanoscale Res. Lett.* **2008**, *3* 129–133.

(51) Krumdieck, S. P.; Boichot, R.; Gorthy, R.; Land, J. G.; Lay, S.; Gardecka, A. J.; Polson, M. I. J.; Wasa, A.; Aitken, J. E.; Heinemann, J. A.; Renou, G.; Berthomé, G.; Charlot, F.; Encinas, T.; Braccini, M.; Bishop, C. M. Nanostructured TiO 2 Anatase-Rutile-Carbon Solid Coating with Visible Light Antimicrobial Activity. *Sci. Rep.* **2019**, *9* 1–11.

(52) Ishiguro, H.; Nakano, R.; Yao, Y.; Kajioka, J.; Fujishima, A.; Sunada, K.; Minoshima, M.; Hashimoto, K.; Kubota, Y. Photocatalytic Inactivation of Bacteriophages by TiO2-Coated Glass Plates under Low-Intensity, Long-Wavelength UV Irradiation. *Photochem. Photobiol. Sci.* **2011**, *10*, 1825–1829.

(53) Korant, B. D.; Kauer, J. C.; Butterworth, B. E. Zinc Ions Inhibit Replication of Rhinoviruses. *Nature* **1974**, *248* , 588–590.

(54) Gupta, P.; Rapp, F. Effect of Zinc Ions on Synthesis of Herpes Simplex Virus Type 2-Induced Polypeptides (39417). *Proc. Soc. Exp. Biol. Med.* **1976**, *152*, 455–458.

(55) Fridlender, B.; Chejanovsky, N.; Becker, Y. Selective Inhibition of Herpes Simplex Virus Type 1 DNA Polymerase by Zinc Ions. *Virology* **1978**, *84*, 551–554..

(56) Arens, M.; Travis, S. Zinc Salts Inactivate Clinical Isolates of Herpes Simplex Virus *In Vitro*. *J. Clin. Microbiol.* **2000**, *38*, 1758–1762.

(57) Williams, M. C.; Gorelick, R. J.; Musier-Forsyth, K. Specific Zinc-Finger Architecture Required for HIV-1 Nucleocapsid Protein's Nucleic Acid Chaperone Function. *Proc. Natl. Acad. Sci. U. S. A.* **2002**, *99*, 8614–8619.

(58) Mishra, Y. K.; Adelung, R.; Röhl, C.; Shukla, D.; Spors, F.; Tiwari, V. Virostatic

Potential of Micro-Nano Filopodia-Like ZnO Structures against Herpes Simplex Virus-1. *Antiviral Res.* **2011**, *92*, 305–312.

(59) Qiu, M.; Chen, Y.; Chu, Y.; Song, S.; Yang, N.; Gao, J.; Wu, Z. Zinc Ionophores Pyrithione Inhibits Herpes Simplex Virus Replication through Interfering with Proteasome Function and NF-KB Activation. *Antiviral Res.* **2013**, *100*, 44–53.

(60) Park, G. W.; Cho, M.; Cates, E. L.; Lee, D.; Oh, B. T.; Vinjé, J.; Kim, J. H. Fluorinated TiO2as an Ambient Light-Activated Virucidal Surface Coating Material for the Control of Human Norovirus. *J. Photochem. Photobiol. B Biol.* **2014**, *140*, 315–320. h

(61) Sohm, B.; Immel, F.; Bauda, P.; Pagnout, C. Insight into the Primary Mode of Action of TiO2 Nanoparticles on *Escherichia Coli* in the Dark. *Proteomics* **2015**, *15* 98–113.

(62) Moongraksathum, B.; Chien, M.-Y.; Chen, Y.-W. Antiviral and Antibacterial Effects of Silver-Doped TiO 2 Prepared by the Peroxo Sol-Gel Method . *J. Nanosci. Nanotechnol.* **2019**, *19*

(63) Shakeri, A.; Yip, D.; Badv, M.; Imani, S.; Sanjari, M.; Didar, T. Self-Cleaning Ceramic Tiles Produced *via* Stable Coating of TiO2 Nanoparticles. *Materials (Basel).* **2018**, *11*, 1003..

(64) Akhtar, S.; Shahzad, K.; Mushtaq, S.; Ali, I.; Rafe, M. H.; Fazal-Ul-Karim, S. M. Antibacterial and Antiviral Potential of Colloidal Titanium Dioxide (TiO2) Nanoparticles Suitable for Biological Applications. *Mater. Res. Express* **2019**, *6*, 105409.

(65) Nakano, R.; Hara, M.; Ishiguro, H.; Yao, Y.; Ochiai, T.; Nakata, K.; Murakami, T.; Kajioka, J.; Sunada, K.; Hashimoto, K.; Fujishima, A.; Kubota, Y. Broad Spectrum Microbicidal Activity of Photocatalysis by TiO2. *Catalysts* **2013**, *3* 310–323.

(66) Khater, M. S.; Kulkarni, G. R.; Khater, S. S.; Gholap, H.; Patil, R. Study to Elucidate Effect of Titanium Dioxide Nanoparticles on Bacterial Membrane Potential and Membrane Permeability. *Mater. Res. Express* **2020**, *7*, 035005. .

(67) Rao, G.; Brastad, K. S.; Zhang, Q.; Robinson, R.; He, Z.; Li, Y. Enhanced Disinfection of *Escherichia Coli* and Bacteriophage MS2 in Water Using a Copper and Silver Loaded Titanium Dioxide Nanowire Membrane. *Front. Environ. Sci. Eng.* **2016**, *10*..

(68) Broglie, J. J.; Alston, B.; Yang, C.; Ma, L.; Adcock, A. F.; Chen, W.; Yang, L. Antiviral Activity of Gold/Copper Sulfide Core/Shell Nanoparticles against Human Norovirus Virus-Like Particles. *PLoS One* **2015**, *10*.

(69) Kim, J.; Yeom, M.; Lee, T.; Kim, H. O.; Na, W.; Kang, A.; Lim, J. W.; Park, G.; Park, C.; Song, D.; Haam, S. Porous Gold Nanoparticles for Attenuating Infectivity of Influenza A Virus. *J. Nanobiotechnology* **2020**, *18*, 1–11..

(70) Di Gianvincenzo, P.; Marradi, M.; Martínez-Ávila, O. M.; Bedoya, L. M.; Alcamí, J.; Penadés, S. Gold Nanoparticles Capped with Sulfate-Ended Ligands as Anti-HIV Agents. *Bioorganic Med. Chem. Lett.* **2010**, *20*, 2718–2721.

(71) Cagno, V.; Andreozzi, P.; D'Alicarnasso, M.; Silva, P. J.; Mueller, M.; Galloux, M.; Goffic, R. Le; Jones, S. T.; Vallino, M.; Hodek, J.; Weber, J.; Sen, S.; Janecek, E. R.; Bekdemir, A.; Sanavio, B.; Martinelli, C.; Donalisio, M.; Welti, M. A. R.;

Eleouet, J. F.; Han, Y.; *et al.* Broad-Spectrum Non-Toxic Antiviral Nanoparticles with a Virucidal Inhibition Mechanism. *Nat. Mater.* **2018**, *17*, 195–203.

(72) Choi, S. Y.; Cho, B. Extermination of Influenza Virus H1N1 by a New Visible-Light-Induced Photocatalyst under Fluorescent Light. *Virus Res.* **2018**, *248* (October 2017), 71–73.

(73) Botequim, D.; Maia, J.; Lino, M. M. F.; Lopes, L. M. F.; Simoes, P. N.; Ilharco, L. M.; Ferreira, L. Nanoparticles and Surfaces Presenting Antifungal, Antibacterial and Antiviral Properties. *Langmuir* **2012**, *28*, 7646–7656.

(74) Shi, Z.; Jayatissa, A. H. Perovskites-Based Solar Cells: A Review of Recent Progress, Materials and Processing Methods. *Materials*. 2018. https://doi.org/10.3390/ma11050729.

(75) Weng, D.; Lei, C.; Wu, T. T.; Sun, R.; Shen, M.; Lu, Y. Spontaneous and Continuous Anti-Virus Disinfection from Nonstoichiometric Perovskite-Type Lanthanum Manganese Oxide. *Prog. Nat. Sci. Mater. Int.* **2015**, *25*, 191–196.

(76) Manjunatha, C. R.; Nagabhushana, B. M.; Raghu, M. S.; Pratibha, S.; Dhananjaya, N.; Narayana, A. Perovskite Lanthanum Aluminate Nanoparticles Applications in Antimicrobial Activity, Adsorptive Removal of Direct Blue 53 Dye and Fluoride. *Mater. Sci. Eng. C* **2019**, *101*, 674–685.

(77) Ehi-Eromosele, C. O.; Olugbuyiro, J. A. O.; Adebisi, A. A.; Edobor-Osoh, A.; Ishola, I. M. The Effect of Silica Coatings on the Structural, Magnetic and Antimicrobial Properties of Silver Doped Manganite Magnetic Nanoparticles for Biomedical Applications. *J. Bionanoscience* **2017**, *11*, 548–553.

(78) Sinclair, T. R.; Patil, A.; Raza, B. G.; Reurink, D.; van den Hengel, S. K.; Rutjes, S. A.; de Roda Husman, A. M.; Roesink, H. D. W.; de Vos, W. M. Cationically Modified Membranes Using Covalent Layer-By-Layer Assembly for Antiviral Applications in Drinking Water. *J. Memb. Sci.* **2019**, *570*, 494–503.

(79) Hsu, B. B.; Wong, S. Y.; Hammond, P. T.; Chen, J.; Klibanov, A. M. Mechanism of Inactivation of Influenza Viruses by Immobilized Hydrophobic Polycations. *Proc. Natl. Acad. Sci.* **2011**, *108* 61–66.

(80) Klibanov, A. M. Permanently Microbicidal Materials Coatings. *J. Mater. Chem.* **2007**, *17* (24), 2479–2482.

(81) Larson, A. M.; Hsu, B. B.; Rautaray, D.; Haldar, J.; Chen, J.; Klibanov, A. M. Hydrophobic Polycationic Coatings Disinfect Poliovirus and Rotavirus Solutions. *Biotechnol. Bioeng.* **2011**, *108* 720–723.

(82) Gelman, F.; Lewis, K.; Klibanov, A. M. Drastically Lowering the Titer of Waterborne Bacteriophage PRD1 by Exposure to Immobilized Hydrophobic Polycations. *Biotechnol. Lett.* **2004**, *26* 1695–1700.

(83) Haldar, J.; An, D.; De Cienfuegos, L. Á.; Chen, J.; Klibanov, A. M. Polymeric Coatings That Inactivate Both Influenza Virus and Pathogenic Bacteria. *Proc. Natl. Acad. Sci. U. S. A.* **2006**, *103*, 17667–17671.

(84) Dang, H. T. T.; Tarabara, V. V. Virus Deposition onto Polyelectrolyte-Coated Surfaces: A Study with Bacteriophage MS2. *J. Colloid Interface Sci.* **2019**, *540*, 155–166.

(85) Klibanov, A. M. Permanently Microbicidal Materials Coatings. *J. Mater. Chem.*

2007, *17*, 2479–2482.
(86) Haldar, J.; Weight, A. K.; Klibanov, A. M. Preparation, Application and Testing of Permanent Antibacterial and Antiviral Coatings. *Nat. Protoc.* **2007**, *2*, 2412.
(87) Haldar, J.; Chen, J.; Tumpey, T. M.; Gubareva, L. V; Klibanov, A. M. Hydrophobic Polycationic Coatings Inactivate Wild-Type and Zanamivir-And/Or Oseltamivir-Resistant Human and Avian Influenza Viruses. *Biotechnol. Lett.* **2008**, *30*, 475–479.
(88) Park, D.; Larson, A. M.; Klibanov, A. M.; Wang, Y. Antiviral and Antibacterial Polyurethanes of Various Modalities. *Appl. Biochem. Biotechnol.* **2013**, *169*, 1134–1146.
(89) Liu, H.; Kim, Y.; Mello, K.; Lovaasen, J.; Shah, A.; Rice, N.; Yim, J. H.; Pappas, D.; Klibanov, A. M. Aerosol-Assisted Plasma Deposition of Hydrophobic Polycations Makes Surfaces Highly Antimicrobial. *Appl. Biochem. Biotechnol.* **2014**, *172* 1254–1264.
(90) Tuladhar, E.; de Koning, M. C.; Fundeanu, I.; Beumer, R.; Duizer, E. Different Virucidal Activities of Hyperbranched Quaternary Ammonium Coatings on Poliovirus and Influenza Virus. *Appl. Environ. Microbiol.* **2012**, *78*, 2456–2458.
(91) Liao, P.; Hu, J.; Wang, H.; Li, J.; Zhou, Z. Recent Advances in Surface-Functionalised Photosensitive Antibacterials with Synergistic Effects. *Biosurface and Biotribology*. Institution of Engineering and Technology December 1, 2019, pp 97–103..
(92) Aluigi, A.; Sotgiu, G.; Torreggiani, A.; Guerrini, A.; Orlandi, V. T.; Corticelli, F.; Varchi, G. Methylene Blue Doped Films of Wool Keratin with Antimicrobial Photodynamic Activity. *ACS Appl. Mater. Interfaces* **2015**, *7*, 17416–17424.
(93) Costa, L.; Faustino, M. A. F.; Neves, M. G. P. M. S.; Cunha, Â.; Almeida, A. Photodynamic Inactivation of Mammalian Viruses and Bacteriophages. *Viruses* **2012**, *4* , 1034–1074.
(94) Si, Y.; Zhang, Z.; Wu, W.; Fu, Q.; Huang, K.; Nitin, N.; Ding, B.; Sun, G. Daylight-Driven Rechargeable Antibacterial and Antiviral Nanofibrous Membranes for Bioprotective Applications. *Sci. Adv.* **2018**, *4*.
(95) Alvarado, D. R.; Argyropoulos, D. S.; Scholle, F.; Peddinti, B. S. T.; Ghiladi, R. A. A Facile Strategy for Photoactive Nanocellulose-Based Antimicrobial Materials. *Green Chem.* **2019**, *21*, 3424–3435.
(96) Carpenter, B. L.; Scholle, F.; Sadeghifar, H.; Francis, A. J.; Boltersdorf, J.; Weare, W. W.; Argyropoulos, D. S.; Maggard, P. A.; Ghiladi, R. A. Synthesis, Characterization, and Antimicrobial Efficacy of Photomicrobicidal Cellulose Paper. *Biomacromolecules* **2015**, *16*, 2482–2492.
(97) Verhaelen, K.; Bouwknegt, M.; Rutjes, S.; Maria, A.; Husman, R.; Duizer, E. Wipes Coated with a Singlet-Oxygen-Producing Photosensitizer Are Effective against Human Influenza Virus but Not against Norovirus. **2014**..
(98) Kim, J.; Lee, H.; Lee, J.-Y.; Park, K.-H.; Kim, W.; Lee, J. H.; Kang, H.-J.; Hong, S. W.; Park, H.-J.; Lee, S. Photosensitized Production of Singlet Oxygen *via* C60 Fullerene Covalently Attached to Functionalized Silica-Coated Stainless-Steel Mesh: Remote Bacterial and Viral Inactivation. *Appl. Catal. B Environ.* **2020**,

118862.
(99) Lhotáková, Y.; Plíštil, L.; Morávková, A.; Kubát, P.; Lang, K.; Forstová, J.; Mosinger, J. Virucidal Nanofiber Textiles Based on Photosensitized Production of Singlet Oxygen. *PLoS One* **2012**, *7*.
(100) Stanley, S. L.; Scholle, F.; Zhu, J.; Lu, Y.; Zhang, X.; Situ, X.; Ghiladi, R. A. Photosensitizer-Embedded Polyacrylonitrile Nanofibers as Antimicrobial Non-Woven Textile. *Nanomaterials* **2016**, *6*, 77.
(101) Iyigundogdu, Z. U.; Demir, O.; Asutay, A. B.; Sahin, F. Developing Novel Antimicrobial and Antiviral Textile Products. *Appl. Biochem. Biotechnol.* **2017**, *181*, 1155–1166.
(102) Nohynek, G. J.; Lademann, J.; Ribaud, C.; Roberts, M. S. Grey Goo on the Skin? Nanotechnology, Cosmetic and Sunscreen Safety. *Critical Reviews in Toxicology*. Taylor & Francis January 10, 2007, pp 251–277.
(103) Skocaj, M.; Filipic, M.; Petkovic, J.; Novak, S. Titanium Dioxide in Our Everyday Life; Is It Safe? *Radiology and Oncology*. Association of Radiology and Oncology December 1, 2011, pp 227–247.
(104) Zhang, X. Q.; Yin, L. H.; Tang, M.; Pu, Y. P. ZnO, TiO 2, SiO 2, and Al 2O 3 Nanoparticles-Induced Toxic Effects on Human Fetal Lung Fibroblasts. *Biomed. Environ. Sci.* **2011**, *24* (6), 661–669.
(105) de Lima, R.; Seabra, A. B.; Durán, N. Silver Nanoparticles: A Brief Review of Cytotoxicity and Genotoxicity of Chemically and Biogenically Synthesized Nanoparticles. *J. Appl. Toxicol.* **2012**, *32*, 867–879.
(106) Hackenberg, S.; Scherzed, A.; Kessler, M.; Hummel, S.; Technau, A.; Froelich, K.; Ginzkey, C.; Koehler, C.; Hagen, R.; Kleinsasser, N. Silver Nanoparticles: Evaluation of DNA Damage, Toxicity and Functional Impairment in Human Mesenchymal Stem Cells. *Toxicol. Lett.* **2011**, *201*, 27–33.
(107) Shi, Z.; Neoh, K. G.; Zhong, S. P.; Yung, L. Y. L.; Kang, E. T.; Wang, W. *In Vitro* Antibacterial and Cytotoxicity Assay of Multilayered Polyelectrolyte-Functionalized Stainless Steel. *J. Biomed. Mater. Res. - Part A* **2006**, *76*, 826–834.
(108) Buchman, J. T.; Hudson-Smith, N. V; Landy, K. M.; Haynes, C. L. Understanding Nanoparticle Toxicity Mechanisms to Inform Redesign Strategies to Reduce Environmental Impact. *Acc. Chem. Res.* **2019**, *52*, 1632–1642. .
(109) Umer, A.; Naveed, S.; Ramzan, N.; Rafique, M. S.; Imran, M. A Green Method for the Synthesis of Copper Nanoparticles Using L-Ascorbic Acid. *Rev. Mater.* **2014**, *19* (3), 197–203.
(110) El Badawy, A. M.; Silva, R. G.; Morris, B.; Scheckel, K. G.; Suidan, M. T.; Tolaymat, T. M. Surface Charge-Dependent Toxicity of Silver Nanoparticles. *Environ. Sci. Technol.* **2011**, *45*, 283–287.
(111) Wu, F.; Harper, B. J.; Harper, S. L. Differential Dissolution and Toxicity of Surface Functionalized Silver Nanoparticles in Small-Scale Microcosms: Impacts of Community Complexity. *Environ. Sci. Nano* **2017**, *4*, 359–372.
(112) Nie, Z.; Liu, J.; Zhong, C.-J.; Wang, L.-F.; Yang, Y.; Tian, Q.; Liu, Y. Enhanced Radical Scavenging Activity by Antioxidant-Functionalized Gold Nanoparticles: A Novel Inspiration for Development of New Artificial Antioxidants. **2007**.

(113) Jokinen, V.; Kankuri, E.; Hoshian, S.; Franssila, S.; Ras, R. H. A. Superhydrophobic Blood-Repellent Surfaces. *Adv. Mater.* **2018**, *30*, 1705104.
(114) Zhang, X.; Wang, L.; Levänen, E. Superhydrophobic Surfaces for the Reduction of Bacterial Adhesion. *RSC Advances*. Royal Society of Chemistry August 14, 2013, pp 12003–12020.
(115) Cheng, Y. T.; Rodak, D. E.; Wong, C. A.; Hayden, C. A. Effects of Micro- and Nano-Structures on the Self-Cleaning Behaviour of Lotus Leaves. *Nanotechnology* **2006**, *17*, 1359–1362.
(116) Hasan, J.; Roy, A.; Chatterjee, K.; Yarlagadda, P. K. D. V. Mimicking Insect Wings: The Roadmap to Bioinspiration. *ACS Biomaterials Science and Engineering*. 2019.
(117) Wong, T. S.; Kang, S. H.; Tang, S. K. Y.; Smythe, E. J.; Hatton, B. D.; Grinthal, A.; Aizenberg, J. Bioinspired Self-Repairing Slippery Surfaces with Pressure-Stable Omniphobicity. *Nature* **2011**, *477*, 443–447.
(118) Villegas, M.; Zhang, Y.; Abu Jarad, N.; Soleymani, L.; Didar, T. F. Liquid-Infused Surfaces: A Review of Theory, Design, and Applications. *ACS Nano* **2019**, *13*, 8517–8536.
(119) Epstein, A. K.; Wong, T. S.; Belisle, R. A.; Boggs, E. M.; Aizenberg, J. Liquid-Infused Structured Surfaces with Exceptional Anti-Biofouling Performance. *Proc. Natl. Acad. Sci. U. S. A.* **2012**, *109*, 13182–13187.
(120) Badv, M.; Jaffer, I. H.; Weitz, J. I.; Didar, T. F. An Omniphobic Lubricant-Infused Coating Produced by Chemical Vapor Deposition of Hydrophobic Organosilanes Attenuates Clotting on Catheter Surfaces. *Sci. Rep.* **2017**, *7*, 1–10.
(121) Badv, M.; Weitz, J. I.; Didar, T. F. Lubricant-Infused PET Grafts with Built-In Biofunctional Nanoprobes Attenuate Thrombin Generation and Promote Targeted Binding of Cells. *Small* **2019**, *15*, 1905562.
(122) Badv, M.; Alonso-Cantu, C.; Shakeri, A.; Hosseinidoust, Z.; Weitz, J. I.; Didar, T. F. Biofunctional Lubricant-Infused Vascular Grafts Functionalized with Silanized Bio-Inks Suppress Thrombin Generation and Promote Endothelialization. *ACS Biomater. Sci. Eng.* **2019**, *5*, 6485–6496.
(123) Imani, S. M.; Badv, M.; Shakeri, A.; Yousefi, H.; Yip, D.; Fine, C.; Didar, T. F. Micropatterned Biofunctional Lubricant-Infused Surfaces Promote Selective Localized Cell Adhesion and Patterning. *Lab Chip* **2019**, *19*, 3228–3237.
(124) Hosseini, A.; Villegas, M.; Yang, J.; Badv, M.; Weitz, J. I.; Soleymani, L.; Didar, T. F. Conductive Electrochemically Active Lubricant-Infused Nanostructured Surfaces Attenuate Coagulation and Enable Friction-Less Droplet Manipulation. *Adv. Mater. Interfaces* **2018**, *5*, 1800617.
(125) Osborne, M.; Aryasomayajula, A.; Shakeri, A.; Selvaganapathy, P. R.; Didar, T. F. Suppression of Biofouling on a Permeable Membrane for Dissolved Oxygen Sensing Using a Lubricant-Infused Coating. *ACS Sensors* **2019**, *4*, 687–693..
(126) Badv, M.; Imani, S. M.; Weitz, J. I.; Didar, T. F. Lubricant-Infused Surfaces with Built-In Functional Biomolecules Exhibit Simultaneous Repellency and Tunable Cell Adhesion. *ACS Nano* **2018**, *12*, 10890–10902.
(127) Wu, R.; Xing, S.; Badv, M.; Didar, T. F.; Lu, Y. Step-Wise Assessment and

Optimization of Sample Handling Recovery Yield for Nanoproteomic Analysis of 1000 Mammalian Cells. *Anal. Chem.* **2019**, *91*, 10395–10400.
(128) Hasan, J.; Xu, Y.; Yarlagadda, T.; Schuetz, M.; Spann, K.; Yarlagadda, P. K. Antiviral and Antibacterial Nanostructured Surfaces with Excellent Mechanical Properties for Hospital Applications. *ACS Biomater. Sci. Eng.* **2020**, *6*, 3608–3618.
(129) Chauhan, P.; Kumar, A.; Bhushan, B. Self-Cleaning, Stain-Resistant and Anti-Bacterial Superhydrophobic Cotton Fabric Prepared by Simple Immersion Technique. *J. Colloid Interface Sci.* **2019**, *535*, 66–74.
(130) Lee, E. C.; Davis-Poynter, N.; Nguyen, C. T. H.; Peters, A. A.; Monteith, G. R.; Strounina, E.; Popat, A.; Ross, B. P. GAG Mimetic Functionalised Solid and Mesoporous Silica Nanoparticles as Viral Entry Inhibitors of Herpes Simplex Type 1 and Type 2 Viruses. *Nanoscale* **2016**, *8*, 16192–16196.
(131) Mannelli, I.; Reigada, R.; Suárez, I.; Janner, D.; Carrilero, A.; Mazumder, P.; Sagués, F.; Pruneri, V.; Lakadamyali, M. Functionalized Surfaces with Tailored Wettability Determine Influenza A Infectivity. *ACS Appl. Mater. Interfaces* **2016**, *8*, 15058–15066.
(132) Kawabata, N.; Yamazaki, K.; Otake, T.; Oishi, I.; Minekawa, Y. Removal of Pathogenic Human Viruses by Insoluble Pyridinium-Type Resin. *Epidemiol. Infect.* **1990**, *105*, 633–642.
(133) Kawabata, N.; Ujino, I. Removal of Virus from Air by Filtration Using a Composite Microporous Membrane Made of Crosslinked Poly (N-Benzyl-4-Vinylpyridinium Chloride). *React. Funct. Polym.* **1998**, *37*, 213–218.
(134) Xue, Y.; Xiao, H. Antibacterial/Antiviral Property and Mechanism of Dual-Functional Quaternized Pyridinium-Type Copolymer. *Polymers (Basel).* **2015**, *7*, 2290–2303.
(135) Ristic, B. Z.; Milenkovic, M. M.; Dakic, I. R.; Todorovic-Markovic, B. M.; Milosavljevic, M. S.; Budimir, M. D.; Paunovic, V. G.; Dramicanin, M. D.; Markovic, Z. M.; Trajkovic, V. S. Photodynamic Antibacterial Effect of Graphene Quantum Dots. *Biomaterials* **2014**, *35*, 4428–4435.
(136) Habiba, K.; Bracho-Rincon, D. P.; Gonzalez-Feliciano, J. A.; Villalobos-Santos, J. C.; Makarov, V. I.; Ortiz, D.; Avalos, J. A.; Gonzalez, C. I.; Weiner, B. R.; Morell, G. Synergistic Antibacterial Activity of PEGylated Silver-Graphene Quantum Dots Nanocomposites. *Appl. Mater. Today* **2015**, *1*, 80–87.
(137) Zhu, S.; Zhang, J.; Qiao, C.; Tang, S.; Li, Y.; Yuan, W.; Li, B.; Tian, L.; Liu, F.; Hu, R.; Gao, H.; Wei, H.; Zhang, H.; Sun, H.; Yang, B. Strongly Green-Photoluminescent Graphene Quantum Dots for Bioimaging Applications. *Chem. Commun.* **2011**, *47*, 6858–6860.
(138) Technology: GermStopSQ – Envision SQ https://envisionsq.com/technology-germstop/ (accessed Aug 19, 2020).
(139) COVAGUARD^{TM} PLATFORM — Covalon Technologies Ltd. https://www.covalon.com/covaguard-platform (accessed Aug 19, 2020).
(140) Technologies - Bio-Gate AG https://www.bio-gate.de/en/technologies/ (accessed Aug 19, 2020).
(141) Bio-Fence – Antimicrobial, antiviral coatings https://www.bio-fence.com/

(accessed Aug 19, 2020).
(142) Homepage | Allied BioScience https://www.alliedbioscience.com/ (accessed Sep 1, 2020).
(143) Glynson, B. C. .; Yeterian, A. A.; Sigalos, J. L.; Mallow, W. A. Uses of Calcium Hydroxide, November 4, 2005.
(144) EPA-Approved Antimicrobial Surface Coating Represents Breakthrough In The Control And Spread Of Infectious Diseases https://www.prnewswire.com/news-releases/epa-approved-antimicrobial-surface-coating-represents-breakthrough-in-the-control-and-spread-of-infectious-diseases-301027074.html (accessed Sep 1, 2020).
(145) FDA Clears First Antiviral Surgical Mask https://www.medscape.com/viewarticle/745801 (accessed Sep 1, 2020).
(146) Møretrø, T.; Langsrud, S. Residential Bacteria on Surfaces in the Food Industry and Their Implications for Food Safety and Quality. *Compr. Rev. Food Sci. Food Saf.* **2017**, *16* (5), 1022–1041. https://doi.org/10.1111/1541-4337.12283.
(147) Chaoui, L.; Mhand, R.; Mellouki, F.; Rhallabi, N. Contamination of the Surfaces of a Health Care Environment by Multidrug-Resistant (MDR) Bacteria. **2019**. https://doi.org/10.1155/2019/3236526.
(148) Ong, S. W. X.; Tan, Y. K.; Chia, P. Y.; Lee, T. H.; Ng, O. T.; Wong, M. S. Y.; Marimuthu, K. Air, Surface Environmental, and Personal Protective Equipment Contamination by Severe Acute Respiratory Syndrome Coronavirus 2 (SARS-CoV-2) from a Symptomatic Patient. *JAMA - J. Am. Med. Assoc.* **2020**, *323*, 1610–1612.
(149) Kampf, G. Potential Role of Inanimate Surfaces for the Spread of Coronaviruses and Their Inactivation with Disinfectant Agents. *Infect. Prev. Pract.* **2020**, *2*, 100044.

3 Chapter 3: Flexible Hierarchical Wraps Repel Drug Resistant Gram Negative and Positive Bacteria

Sara M. Imani, Roderick Maclachlan, Kenneth Rachwalski, Yuting Chan, Bryan Lee, Mark McInnes, Kathryn Grandfield Eric D. Brown, Tohid F. Didar*, Leyla Soleymani*

ACS Nano 2020, 14, 1, 454–465, doi: 10.1021/acsnano.9b06287

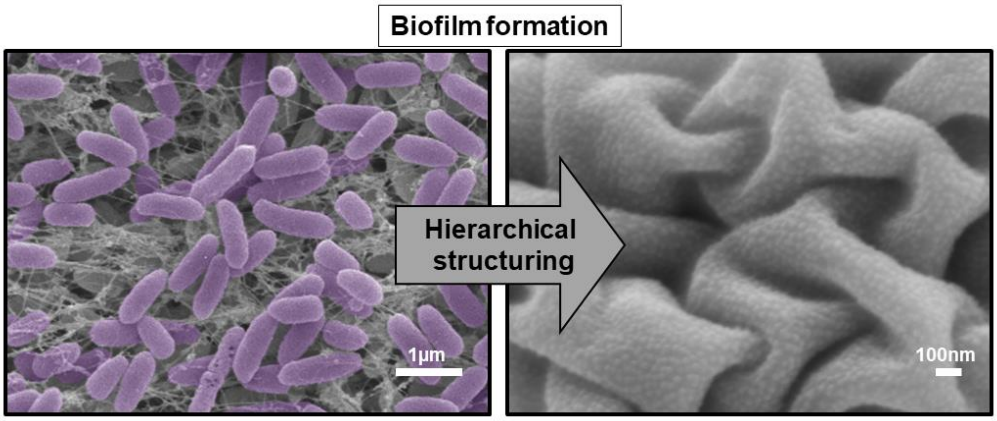

Preface

Objective A

In order to universally utilize repellent surfaces and take them from bench to real world, they need to be easily scalable, facile to produce, and effective in covering complex objects. This chapter focuses on developing an all solution-based flexible wrap, with built-in hierarchical structures which holds the potential of scaling-up while being able to conform onto various objects. The proposed fabrication method is amenable with the existing role-

to-role fabrication methods in companies in the field of plastic production and functional coatings, making it implementable in such setups. A detailed study on the importance of hierarchical structuring on repellency is conducted. Suppression of bacterial biofilms is studied on various surface textures, demonstrating the significance of hierarchical structuring in reducing biofilm formation. Transferring bacteria and contamination of intermediate surfaces is also studied to mimic real-life means of bacteria transfer which is shown to be suppressed by implementing hierarchical surfaces.

3.1 Abstract

Healthcare acquired infections are a major human health problem, and are becoming increasingly troublesome with the emergence of drug resistant bacteria. Engineered surfaces that reduce the adhesion, proliferation, and spread of bacteria have promise as a mean of preventing infections and reducing the use of antibiotics. To address this need, we created a flexible plastic wrap that combines a hierarchical wrinkled structure with chemical functionalization to reduce bacterial adhesion, biofilm formation, and the transfer of bacteria through an intermediate surface. These hierarchical wraps were effective for reducing biofilm formation of World Health Organization-designated priority pathogens Gram positive methicillin-resistant *Staphylococcus aureus* (MRSA) and Gram negative *Pseudomonas aeruginosa* by 87 and 84 %, respectively. In addition, these surfaces remain free of bacteria after being touched by a contaminated surface with Gram negative *E. coli*. We showed that these properties are the result of broad liquid repellency of the engineered surfaces and the presence of reduced anchor points for bacterial adhesion on the

hierarchical structure. Such wraps are fabricated using scalable bottom-up techniques and form an effective cover on a variety of complex objects, making them superior to top-down and substrate-specific surface modification methods.

Keywords: nanostructuring, microsturcturing, super hydrophobic, omniphobic, bacterial repellency, healthcare acquired infections.

3.2 Introduction

Bacterial contamination of hospital surfaces is a major cause of healthcare-acquired infections, resulting in mortality, prolonged hospital stays, increased use of antibiotic treatments, and a substantial cost to the healthcare system. [1–5] Multi-drug resistant pathogens including methicillin-resistant *Staphylococcus aureus* (MRSA) and *Pseudomonas aeruginosa* are identified by the World Health Organization (WHO) as priority pathogens for which urgent action is needed towards prevention and spread. [6] These pathogens have been detected on a number of hospital surfaces as sources of nosocomial infections even after cleaning with highly effective disinfecting solutions. [7] Hospital acquired infections caused by these pathogens are fatal, with reported 90-day mortality rates of 21% for MRSA and 19% for *P. aeruginosa* for patients in the United States. [8] Furthermore, this cause is the fourth leading origin of death in Canada which has increased in the past two decades as reported by Health Canada. [9] Surfaces that inhibit the adhesion and proliferation of bacteria are critical for minimizing the spread of multi-drug resistant bacteria in hospitals and high risk settings. [10] It is impractical and economically unfeasible

to replace everyday items with surfaces that are inherently repellent; however post-manufacturing treatments that can be easily and inexpensively applied to existing *high risk* surfaces provide a feasible solution for combating the spread of pathogens through surface contamination.

Flexible omniphobic surfaces having a high contact angle (>150°) and a low sliding angle (<5°) for water and low surface tension liquids are highly desirable for the abovementioned applications since they can be applied to a wide range of surfaces with various form factors for repelling liquid contaminants. The liquid repellency of omniphobic surfaces can be translated into anti-biofouling properties to reduce bacterial contamination and biofilm formation on high risk objects. [11–19] Lubricant-infused surfaces are a newly developed class of omniphobic surfaces, which demonstrate anti-biofouling properties and extremely low adhesion towards liquids with various surface tensions. [15,20–25] In spite of this, for such surfaces to sustain their repellency, their lubricant layer should remain intact throughout use, making them inapplicable to dry, open air, or *in operando* conditions involving fluidic flow, washing, or potential cycling where there is a potential for lubricant leaching. [26] A material with a bio-repellency profile in line with lubricant-infused surfaces that retains its properties in open air conditions is desired for protecting high risk surfaces from bacterial contamination, and has motivated this work.

To overcome the practical limitations of lubricant-infused surfaces, we sought to develop a new class of lubricant-free omniphobic flexible wraps that are applicable to a wide range of surfaces. Introduction of structures having features in the nano or microscale enables a robust omniphobicity without the use of lubricant due to the entrapment of air pockets

within the structures (Cassie state). [27–32] Additionally, hierarchically-organized structures with re-entrant textures have been used for creating high performance omniphobic surfaces with water and hexadecane contact angles as high as 173.1° and 174.4° respectively. [33–37] Several of the fabrication methods that are currently used for developing microstructures, nanostructures, or hierarchical omniphobic surfaces rely on photolithography, [38] emulsion templating, [39] electrospinning, [38] reactive ion etching, [36] and electrochemical etching/anodizing, [40,41] which are difficult to scale up for use in large area and high volume applications. [42] Alternatively, methods such as laser ablation [43] and microfluidic emulsion templating [39] are used to solve the scalability challenges that are involved in fabricating textured omniphobic surfaces. However, the physical and chemical processing steps involved in these methods are not compatible with flexible plastic wraps that can be universally applied to a wide range of surfaces. [42]

Wrinkling is a bottom up fabrication process that can be used to create tunable hierarchical structures with microscale and nanoscale features. [44–47]This method involves applying strain to a shape memory polymer substrate modified with a stiff layer. [44,48–51] Owing to their unique hierarchical structure, these surfaces can be created to be superhydrophobic (water contact angle of >163°) [49] and oleophobic (hexadecane contact angle> 101°) [52] with sliding angles below 5°, [49] which collectively reduce bacterial adhesion by detaching the liquid contaminants and reducing the contact area available for bacterial attachment. [11] Such surface have been previously used for studying the attachment of mammalian cells; [53–55]however, the challenge in applying these wrinkled surfaces as a universal omniphobic wrap is that, to date, the stiff layer needed for creating wrinkles has been deposited using

techniques such as sputtering, [56] spin coating, [48] and electrochemical deposition, [52,57] which are either too costly, not directly applicable to soft plastics, or not suitable for large area and high volume manufacturing. In this work, we sought to develop universal omniphobic flexible wraps, which are fabricated using scalable methods and can be applied to everyday surfaces to prevent bacterial contamination. To address this goal, we first investigated whether nanostructuring, microstructuring, or their combination into hierarchical architectures are important for creating repellent surfaces. Through this understanding, we implemented hierarchical structures combining "soft wrinkles" with fluorination and nanoparticles on the surface of commonly used plastic shrink wraps using a series of all-solution-processing techniques that are amenable to industry-scale batch processing. This allowed for the manufacturing of large plastic sheets, which can be wrapped and shrunk around a variety of objects, creating a scalable omniphobic coating for preventing bacterial adhesion and biofilm formation.

3.3 Results

3.3.1 Producing omniphobic flexible wraps

In order to create a flexible repellent wrap, we first investigated the role of microstructuring, nanostructuring, and hierarchical structuring on the surface properties of commonly-used polymer surfaces such as polystyrene (PS) and polyolefin (PO). Microstructuring was induced by Ultraviolet-Ozone (UVO) activation of a pre-strained heat shrinkable PS substrate, followed by thermal shrinking (Figure 3.1a, c). This processing results in the

creation of wrinkles on the PS substrate (PS-Micro) due to the stiffness difference between the surface layer and the bulk caused by the UVO treatment, and the degree of wrinkling can be tuned by varying the UVO exposure time (Supplementary Figure 3.5). [58] We also subjected the microstructured surfaces to fluorosilane (FS) treatment (PS-Micro-FS) to further lower their surface energy (Figure 3.1a, d). [59] Nanostructuring was induced by depositing colloidal silica nanoparticles (SiNPs) on (3-Aminopropyl)triethoxysilane (APTES)-modified PS substrates (Figure 3.1b, d), which were further modified by fluorosilane treatment (PS-Nano-FS). Finally, hierarchical structures (PS-Hierarchical-FS) were created by thermally shrinking the nanostructured samples (PS-Nano-FS) to combine shrinking-induced microscale wrinkling with the nanotexturing induced by nanoparticles (Figure 3.3.1b, d).

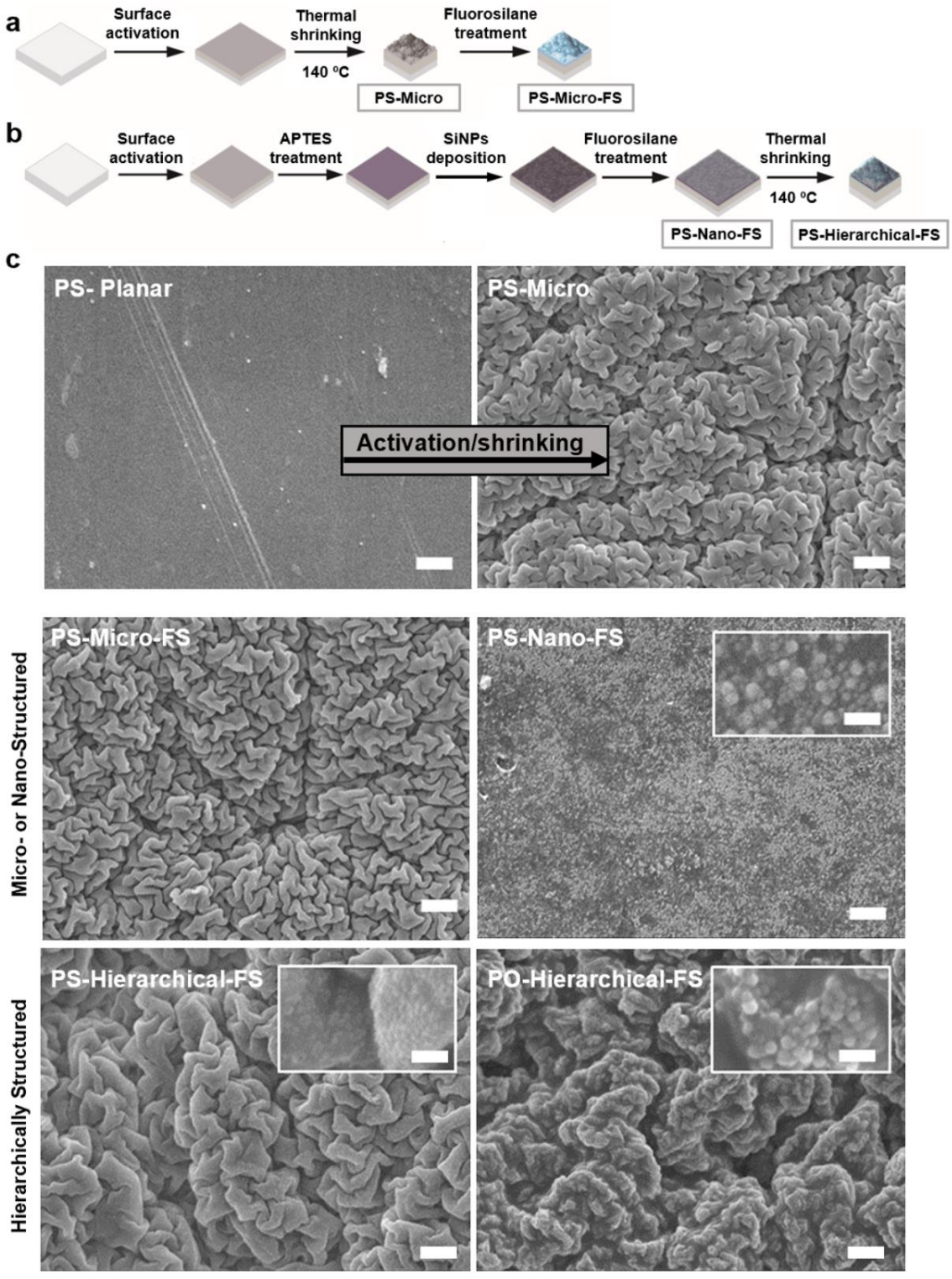

Figure 3.1 Schematic illustrating the process for fabricating omniphobic surfaces and wraps. *(a) Steps for creating microstructured surfaces (PS-Micro and PS-Micro-FS). (b)*

Steps for creating nanostructured surfaces (PS-Nano-FS) and hierarchical surfaces (PS-Hierarchical-FS). Similar process is done for producing PO-Hierarchical-FS. (c) Corresponding scanning electron microscopy (SEM) images to each processing step with high magnification insets showing the visible nanostructures (27 nm SiNPs). The scale bars on larger SEM images represent 1 µm and for the insets represent 100 nm. The insets provide high magnification representative images form the imaged substrates.

To investigate whether it would be possible to induce the same type of hierarchical structuring on a flexible material that could be universally applied to objects, we applied the same fabrication methods to pre-strained PO wraps that remain flexible after heat shrinking. The hierarchical structures created on PO (PO-Hierarchical-FS) demonstrated the same class of microscale wrinkles as observed with PS; however, the PO wrinkles contained a greater degree of fine secondary wrinkles (see Supplementary Figure 3.6 for marked secondary wrinkles). The observed difference in wrinkle sizes is attributed to the larger thermally-induced strain for PO (95%) [60] compared to PS (40%). [45] Although the chemical surface modification with fluorosilane was not visible in the SEM images, these were verified for the hierarchical surfaces using X-ray Photoelectron Spectroscopy (XPS) (Supplementary Figure 3.7). Incorporation of hierarchical structures within heat-shrinkable polymers presents a scalable approach towards tuning the surface properties of materials.

To evaluate the omniphobicity of the developed structures and compare the behavior of planar, microstructured, nanostructured, and hierarchical surfaces (schematics shown in Supplementary Figure 3.8), we measured the static contact angle of various test liquids such as milli-Q grade water (surface tension of 72.75 mJ/m^2 [61]), hexadecane (surface tension of 27.76 mJ/m^2 [61]), human whole blood (surface tension of approximately 55 mJ/m^2

[18]), and various ethanol/water concentrations (Figure 3.2 and Supplementary Figure 3.9). As expected, microstructuring made the PS surface more hydrophobic with PS-Micro having a water contact angle of 100±6° as compared to PS-Planar having a contact angle of 78.9±1.3°, which can be explained by the Cassie model (Supplementary Note 1). The contact angle further increased to 125±4° following the fluorosilane treatment (PS-Micro-FS) due to the decrease in the surface free energy leading to higher Young's contact angle and Cassie contact angle. The induction of nanotexturing (PS-Nano-FS) increased the water contact angle to 135±4°, which is beyond what was observed for the planar and microstructured surfaces. The hierarchical surfaces (PS-Hierarchical-FS) demonstrated superhydrophobicity with a water contact angle of 155°, which was not observed for the other surfaces. The increase in the number of length-scales elevates the contact angles by reducing the solid-liquid contact area and providing more trapped air in the underlying interface compared to having a single length-scale. [33] This can also be approximated by rewriting Cassie-Baxter relation recursively (Supplementary Note 1). [33,62] Additionally, hierarchical structures improve the stability of the solid-liquid-air interface, inhibiting filling of the air pockets within the structure. [30]

As a common measure for omniphobicity, we determined the oleophobicity of the surfaces by measuring the hexadecane contact angle. According to Young's relation, comparing hexadecane contact angle to water for the same surface, a smaller contact angle for hexadecane (lower surface tension) is predicted. Consequently, PS-Planar and PS-Micro demonstrated oleophilic behavior with contact angles too low to be accurately be measured. PS-Micro-FS demonstrated decreased oleophilicity (26±7°) due to the effect of

fluorosilanization on lowering the surface energy. PS-Nano-FS surfaces revealed a significantly higher hexadecane contact angle (55±3°) compared to the microstructured surfaces. Nanoparticles create a re-entrant texture and a more effective Cassie state for low surface tension liquids compared to the concave structure of the wrinkles (Supplementary Note 1). [30,33] The combination of both micro- and nano-structures observed in the PS-Hierarchical-FS surfaces led to an increase in oleophobicity as the contact angles reached 123±5°. This type of omniphobicity is also present with up to 70% ethanol (Supplementary Figure 3.9, Supplementary Note 2), which has an ultralow surface tension (25.48 mN/m [63]). In the hierarchical structures, the addition of nanoparticles distorts the concave texture of the wrinkles, allowing improved repellence of lower surface tension liquids compared to microstructures. Additionally, having wrinkles along with the nanoparticles provides a higher fraction of air beneath the droplet. The findings from water and hexadecane contact angle measurements indicate that hierarchical structuring enhances the water and hexadecane contact angles compared to micro- or nano-structured surfaces, resulting in improved omniphobicity.

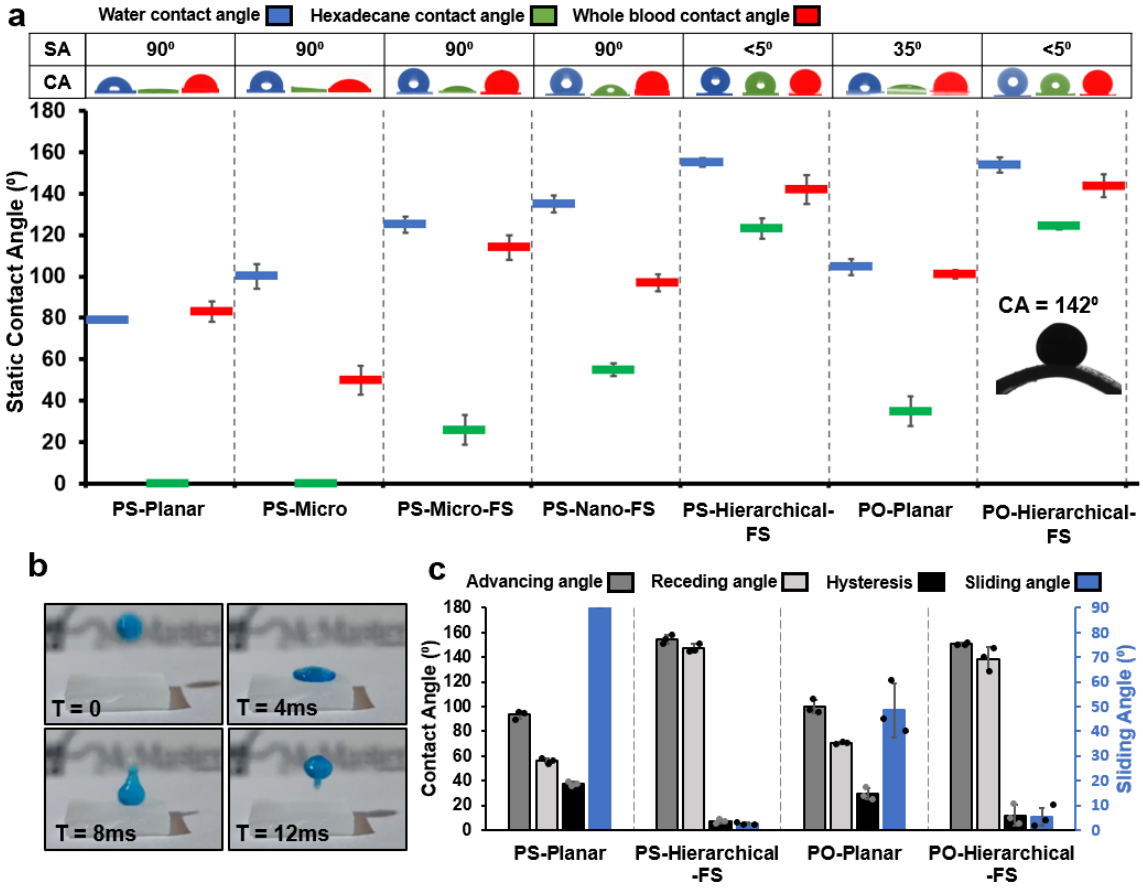

Figure 3.2 Surface repellency and assessment of omniphobicity. *(a) Graph showing the contact angle of different surfaces for water, hexadecane, and blood as test liquids. Table showing sliding angles for water on various surfaces (SA represents sliding angle) and representative color-coded images of the contact angles (CA represents contact angle). The inset shows the blood contact angle on a bent PO-Hierarchical-FS, showing the robustness of the surface upon bending. (b) Slow-motion snapshots of 10 μL droplet on PO-Hierarchical-FS at 4 ms intervals. (c) Advancing/receding contact angles, contact angle hysteresis, and calculated sliding angles. Error bars represent standard deviation from the mean for at least three samples. The "dots" represent the individual data points leading to the averages plotted as bars.*

To further validate the self-cleaning characteristics of our developed surfaces under biological conditions, the contact angle of whole human blood on each surface was examined. Blood is commonly used as an example for a complex liquid to test for

repellency of a surface. [64] PS-Hierarchical-FS surfaces maintained a high contact angle of 142±7° (Figure 3.2a). This hinted towards a self-cleaning and anti-biofouling behavior for the hierarchical structures.

We also measured the sliding angle of our surfaces, which is an essential measure for repellency and adhesiveness. Droplet sliding was *only* observed for the hierarchical structures, demonstrating their low adhesion and self-cleaning properties. The ability of the droplet to slide off the hierarchical surface with a low sliding angle (<5°) is due to the unevenness of the wrinkles as well as the presence of nanoparticles. As the surface is tilted, the droplet detaches itself sequentially from small areas due to the rough nature of the surface. [65] This results in a smaller adhesive force compared to the control groups, which have a larger surface area in contact with the water droplet.

The advancing/receding contact angles and the resultant contact angle hysteresis are also important metrics of omniphobicity and repellency since lowering the solid/liquid interfacial area results in a decrease in contact angle hysteresis. [33,66] The high advancing/receding contact angle (~140°) and low contact angle hysteresis (~10°) observed for the hierarchical surfaces (Figure 3.2c) allow for the low sliding angle (Figure 3.2c) and bouncing behavior of these surfaces (Figure 3.2b, Supplementary Figure 3.11a,c, and Supplementary Video 1-4). Low contact angle hysteresis and sliding angles as well as high advancing/receding contact angles, enables water to stay in a suspended Cassie state, [49] which is of key importance for achieving self-cleaning and anti-fouling properties (Supplementary Note 3,4).

Given the exceptional omniphobic performance of the hierarchical structures, we implemented these structures on flexible polyolefin wraps commonly used as packaging material (*e.g.* food industry). Similar to polystyrene, hierarchically-structured polyolefin wraps (PO-Hierarchical-FS) demonstrated super-hydrophobicity (water contact angle=154±4°), oleophobicity (hexadecane contact angle=124±2°), blood repellency (contact angles of 144±5°), and droplet sliding (sliding angles <5°). Furthermore, when *bent*, these surfaces showed a blood contact angle that is comparable to the unbent samples, demonstrating their omniphobic behavior under different form factors (Figure 3.2). Similar advancing/receding contact angle, contact angle hysteresis, and calculated sliding angle were recorded for PO samples as PS, resulting in a bouncing behavior for water droplets as shown in Supplementary Video 5-10, both on treated surfaces and also as a food packaging material (Supplementary Video 10). Furthermore, we have performed resiliency tests on the developed surfaces (Supplementary Table 3.1), subjecting them to vacuum (3 hours), sonication in ethanol (3 hours), and incubation in bleach (2 hours). In all cases, the surfaces remained repellent by maintaining their low sliding angle. These findings display omniphobic performance on a flexible surface with significance robustness and stability.

3.3.2 Assessment of bacterial attachment: biofilm formation and bacteria transfer to hierarchical wraps

We studied the effect of hierarchical structuring on the anti-biofouling behavior of our surfaces using various bacterial adhesion assays (Figure 3.3). We evaluated the biofilm formation of *P. aeruginosa* PA01, a Gram-negative bacterium, and *S. aureus* USA300

(MRSA), a Gram-positive bacterium, on various surfaces to investigate whether micro, nano, or hierarchical structuring has a significant effect on reducing biofilm attachment. *P. aeruginosa* and MRSA are clinically relevant pathogens that commonly form biofilms on medical devices and are found on various hospital surfaces. [7,67] To simulate the composition of a bacterial biofilm matrix, the adherence of alginate, a carbohydrate proxy for the extracellular polymeric substance (EPS) of a biofilm, was first tested, which showed a 10-fold reduction in adherence (Supplementary Figure 3.12). [68,69] This was followed by a biofilm assay that quantified the formation of *P. aeruginosa* and MRSA biofilms on various surfaces (Figure 3.3a, b). It is evident from the biofilm assay that the hierarchical structures effectively attenuate biofilm formation compared to the other control groups (reduced by ~85% compared to PS-Planar) for both MRSA and *P. aeruginosa*. Although PS-Micro-FS and PS-Nano-FS also reduced biofilm formation (66% and 78% for MRSA, 11% and 62% for *P. aeruginosa*), they did not achieve the same level of biofilm attenuation. This is explained by the occurrence of Cassie state in the hierarchical surfaces, [33] which makes the initial bacterial attachment to the surface unfavorable, thereby inhibiting the formation of mature biofilms. [11,14,15,70]

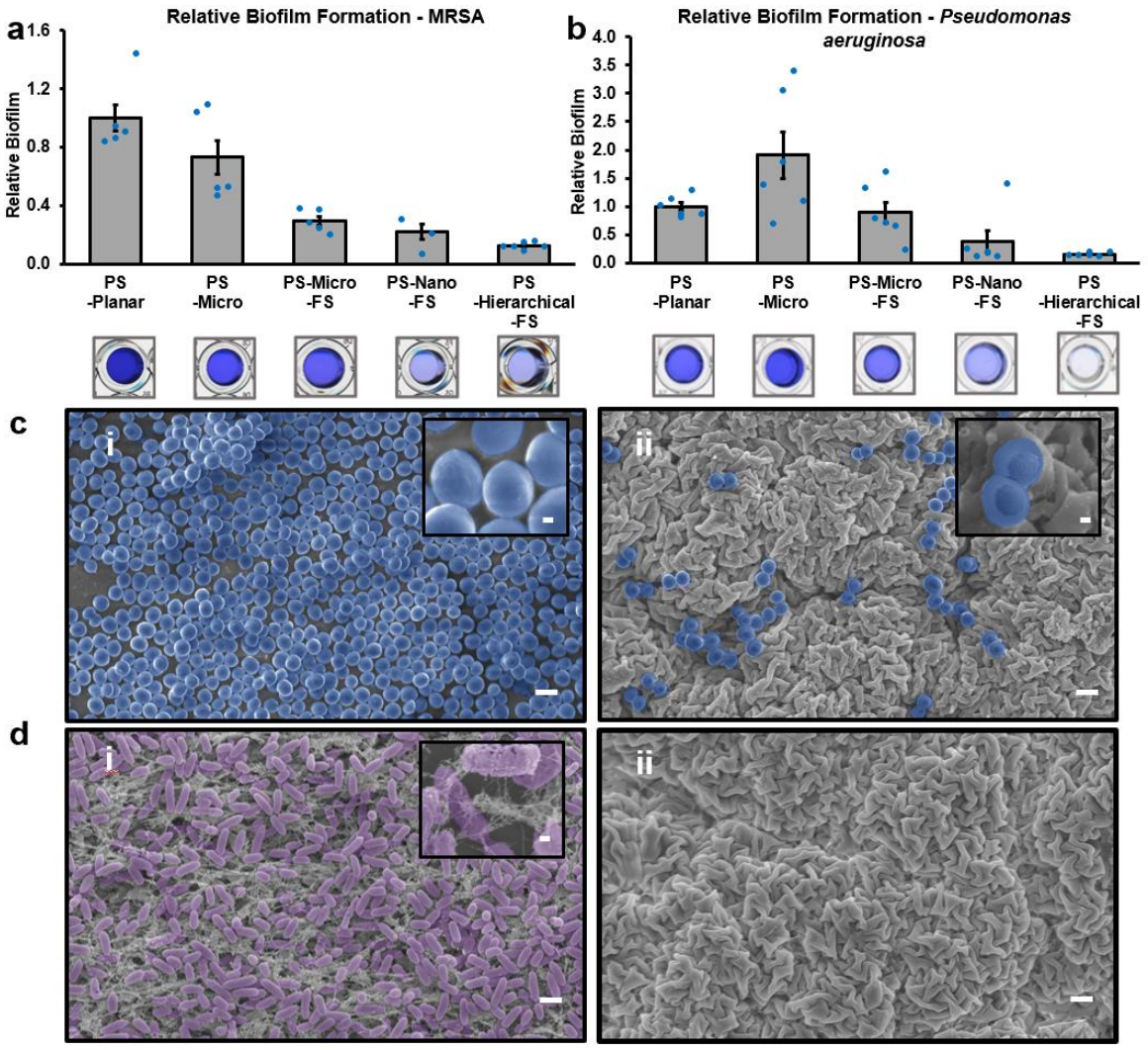

Figure 3.3 Biofilm assay on various polystyrene surfaces. *Crystal violet biofilm assay for MRSA (a) and P. aeruginosa (b) and representative images of the well containing the resuspended crystal violet as a measure of the extent of biofilm formation. The data is normalized to PS-Planar. (c) SEM of fixed biofilm of MRSA on PS-Planar (i) and on PS-Hierarchical-FS (ii). (d) SEM of fixed biofilm of P. aeruginosa on PS-Planar (i) and on PS-Hierarchical-FS (ii). The scale bars on larger SEM images are 1 µm and for the insets are 100 nm. Error bars represent standard deviation from the mean for at least three samples. The "dots" represent the individual data points leading to the averages plotted as bars.*

To visualize the interaction of the *P. aeruginosa* and MRSA biofilms with our hierarchical surfaces, we performed SEM on these surfaces and compared them to unmodified surfaces (Figure 3.3c, d)

under conditions where mature biofilm formation is possible. These images demonstrate the abundance and stacking of coccoid MRSA bacteria on the untreated polystyrene surface (PS-Planar), whereas adding the hierarchical texture significantly decreased the amount of adhered MRSA on PS-Hierarchical-FS (Figure 3.3c.i, ii). Deposition of MRSA cells within the ridges of the microstructure is observed, however the ability of these cells to form mature biofilms appears to be sterically hindered by the hierarchical surface structure. Similarly, the rod-shaped *P. aeruginosa* and the biofilm matrix joining adjacent cells (EPS) was clearly evident on the untreated surfaces (Figure 3.3d.i), but was almost completely abolished in the hierarchical (PS-Hierarchical-FS) sample (Figure 3.3d.ii). Unlike with MRSA, we do not see deposition of *P. aeruginosa* (Figure 3.3d.ii) within the ridges of the hierarchical structure, likely resulting from larger cell size and shape of *P. aeruginosa* cells.[11,18,71] These findings are well in agreement with the quantitative crystal violet assay and confirm the anti-biofouling behavior of the hierarchical samples. As expected, when the hierarchical structuring was implemented on the surface of the flexible PO wraps, the same type of anti-biofouling behavior was visualized through SEM of the biofilms (Figure 3.4a.i-iv).

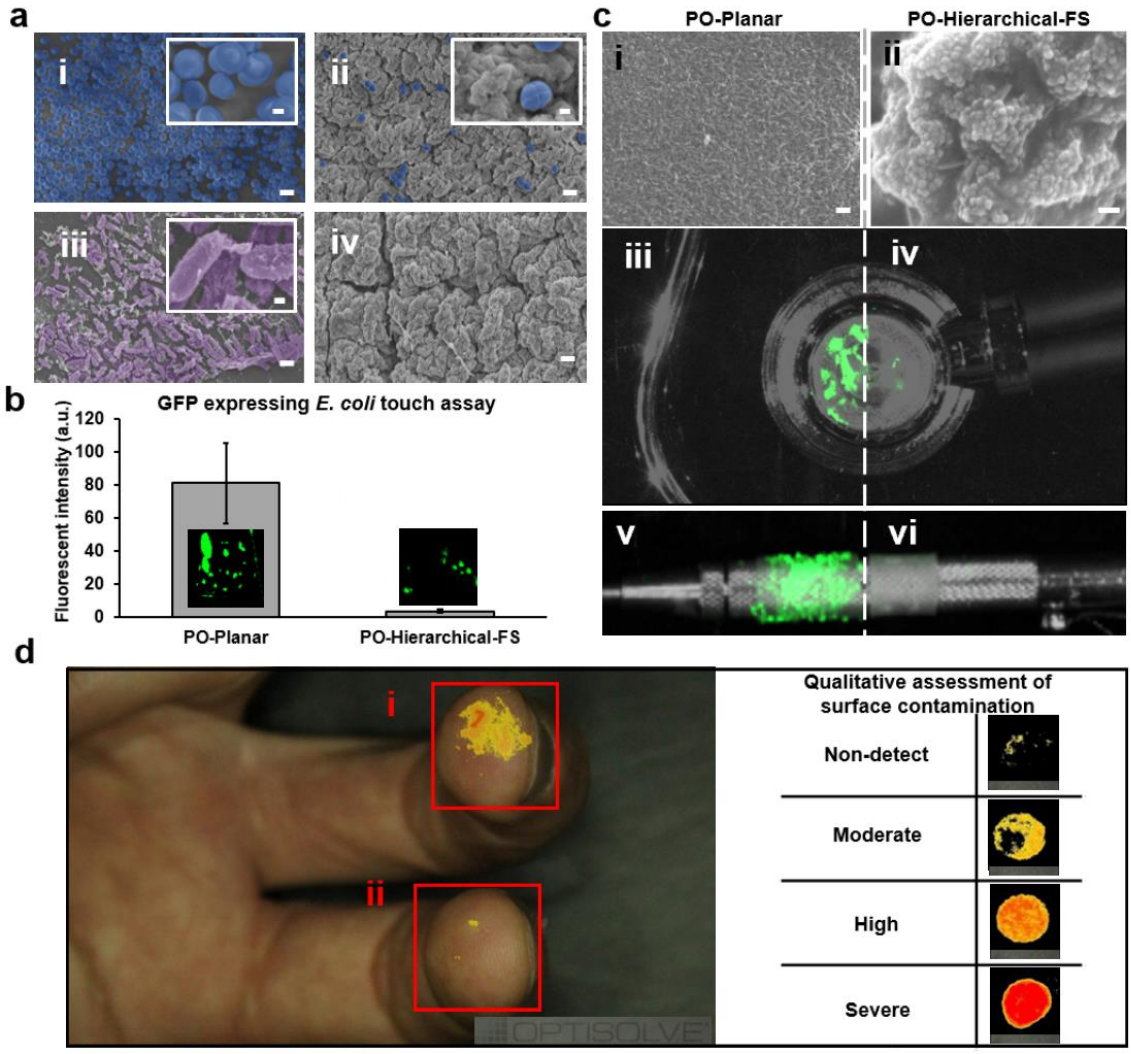

Figure 3.4 Biofilm and bacterial adherence on hierarchical wraps and touch assay. *(a) SEM of fixed biofilm of MRSA and P. aeruginosa on planar and hierarchical wraps. Figures i-iv show: (i) MRSA biofilm on PO-Planar (ii) MRSA biofilm on PO-Hierarchical-FS (iii) P. aeruginosa biofilm on PO-Planar (iv) P. aeruginosa biofilm on PO-Hierarchical-FS. Scale bars on larger SEM images are 1 µm and for the insets are 200 nm. (b) GFP expressing E. coli touch assay on planar and hierarchical polyolefin wraps, demonstrating repellency of the PO-Hierarchical-FS toward contact with a bacteria contaminated agar plug. Error bars represent means ± SD of at least three samples. (c) Touch assay performed on wrapped objects. Figures i-vi show: (i) SEM of PO-Planar (demonstrating surface texture, scale bar 1 µm) (ii) SEM of PO-Hierarchical-FS (demonstrating surface texture, scale bar 100 nm) (iii) E. coli transfer to PO-Planar wrapped around a stethoscope (iv) E. coli transfer to PO-Hierarchical-FS around a stethoscope (v) E. coli transfer to PO-Planar around a pen (vi) E. coli transfer to PO-Hierarchical-FS wrapped around a pen. (d) E. coli transfer from contaminated PO-Planar*

(i) and PO-Hierarchical-FS (ii) to human skin. Qualitative assessment legend for the amount of the available bacteria is also shown.

An important factor in the spread of infections is the transfer of bacteria to an intermediate surface, which would serve as a niche point for biofilm production or further bacterial transfer. [72] To evaluate the ability of our surfaces in reducing the spread of infection, we designed a touch-assay to quantify the transfer of bacteria from contaminated to clean surfaces. For the transfer of bacteria, agar plugs were used and were inoculated with GFP expressing *Escherichia coli* to mimic a contaminated object. Then both planar and hierarchical wraps were 'touched' with the inoculated agar plugs, and levels of fluorescence were measured to determine the magnitude of bacterial transfer (Figure 3.4b). PO-Hierarchical-FS films showed a 20-fold decrease in the fluorescent signal compared to PO-Planar, indicating that there is significantly less *E. coli* transferred to the hierarchical surfaces (Figure 3.4b). A similar experiment was performed on hierarchical polystyrene surfaces, showing a 15-fold decrease in the fluorescent signal on the treated surface compared to planar surfaces (Supplementary Figure 3.13). These results demonstrate the promise that these flexible hierarchical wraps hold for covering surfaces that pose a high risk for transferring infections. To demonstrate the applicability of the hierarchical wraps for reducing contamination on everyday objects, we covered a pen (Figure 3.4c), a stethoscope (Figure 3.4c), and a key (Supplementary Figure 3.14) as every objects or medical devices that are at high risks of bacterial contamination. [3,7] The same bacterial touch assay with GFP expressing *E. coli* was conducted and evaluated by a fluorescent scanner (Figure 3.4c). The objects covered with the hierarchical surfaces (Figure 3.4c.iv,vi) showed little or no measurable fluorescence signal after being 'touched' with the

contaminated agar plugs, whereas, objects covered with the control surface (Figure 3.4c.iii,v) showed large amounts of fluorescence. This demonstrates the ability of the hierarchical wraps to conform to the shape of different objects and reduce the transfer of a bacterial (*E. coli*) contaminant.

In addition, we investigated the performance of our surfaces in halting the transfer of bacterial contamination to a human hand. A hierarchical wrap and a control surface were "touched" with *E. coli* infused agar plugs, and then the contaminated surface was touched by a human hand. The transfer of the bacteria from hierarchical and control surfaces onto human skin was imaged using a surface imaging device (see methods section for details) designed to assess microbial contamination levels (Figure 3.4d). These images clearly demonstrate that building hierarchical structuring into our wraps significantly reduce the transfer of bacteria (*E. coli*) from a contaminated surface through an intermediate surface to the human skin. It is also interesting to note that the hierarchical wraps hold their repellent properties, under strain and while conforming to different form factors.

3.4 Conclusions

In this work, a comprehensive study was conducted to understand the role of micro, nano, or hierarchical structuring on the omniphobic and anti-bacterial properties of surfaces. We created three classes of structures through wrinkling (microstructured), self-assembly of nanoparticles (nanostructured), and their combination (hierarchically-structured). We found that hierarchical structuring provides superior hydrophobicity and oleophobicity with water contact angle of above 150°, blood contact angle of above 140, hexadecane

contact angle of above 110°, and sliding angles lower than 5°. All of the surfaces included a fluorosilane treatment for enhancing their hydrophobicity and oleophobicity; however, omniphobic behavior was not observed with microstructured or nanostructured surfaces even with the fluorosilane treatment. The omniphobicity originates from the stable Cassie state and the increased air pockets trapped beneath the liquids contacting the hierarchical surfaces for both low and high surface tension liquids. [33] When interfacing these hierarchical surfaces with bacterial contaminants, we observed that their omniphobicity can decrease biofouling by MRSA and *P. aeruginosa* (Figure 3.3). The latter are priority pathogens according to the World Health Organization, pose a substantial threat to morbidity and mortality worldwide, [6] and have an established role in healthcare-acquired infections. [67] Reducing the spread of bacteria is a key strategy for decreasing the incidence of life threatening bacterial infections. [19,67]

Similar to our rigid hierarchical surfaces, the flexible hierarchical wraps repel liquids with various surface tensions and prevent biofilm formation proving they retain the repellency characteristics observed with the rigid hierarchical surfaces. To understand if our surfaces were effective in reducing the spread of bacteria by serving as an intermediate transfer surface, we developed a "touch-assay". We showed that the application of this hierarchical omniphobic surface onto everyday items and medical devices reduced the transfer of *E. coli* onto these objects from a contaminated agar plug. As a result, less *E. coli* was transferred to human skin that came into contact with the contaminated hierarchical surfaces compared to contaminated control surfaces. Surfaces containing antibiotics, [73] lubricant-infused layers, [15,20] and micro/nanostrucutring [11] have been previously developed

to deliver antibacterial properties and bacterial repellency to various classes of medical devices. Surface coatings that contain antibiotics are expected to further exacerbate the emergence of antibiotic resistance, [7,74] lubricant-infused surfaces are difficult to use in open-air conditions due to lubricant evaporation, [26] and several of the previously-developed micro/nanostructure omniphobic materials are difficult to manufacture in the industrial scale, [36,40] posing a need for new strategies for developing scalable repellent coatings. Our hierarchical wraps could easily be applied onto various surfaces in hospitals that are commonly contaminated with bacterial pathogens such as, door knobs, bed tables, bed rails, and other high risk surfaces. [6] Additionally, since the hierarchical surfaces are fabricated through all-solution-processing, they would be amenable to large area applications and large volume manufacturing, being applicable to a wide range of surfaces that have a risk of being in contact with liquid-borne contaminants.

3.5 Methods

Reagents. (3-Aminopropyl)triethoxysilane (99%), 1H,1H,2H,2H-Perfluorodecyltriethoxysilane (97%), Ludox® TMA colloidal silica, and Alginic Acid sodium salt (sodium alginate), crystal violet were purchased from Sigma-Aldrich (Oakville, Onatrio). Ethanol (anhydrous) was purchased from Commercial Alchohols (Brampton, Ontario). Hydrochloric acid (36.5–38%) was purchased from Caledon (Georgetown, Ontario). Milli-Q grade water (18.2 MΩ) was used to prepare all solutions. LB Broth, Granulated Agar, Casamino Acids was purchased from Fisher Scientific (Canada). 20% Glucose Solution was purchased from TekNova (Canada). Glacial Acetic acid was purchased from Bioshop (Burlington, Ontario).

Wrinkled Surfaces Fabrication. Pre-strained polystyrene (Graphix Shrink Film, Graphix, Maple Heights, Ohio) and polyolefin (Cryovac D-955) was cut into desired substrate sizes using Robo Pro CE5000-40-CRP cutter (Graphtec America Inc., Irvine, California). The substrates were cleaned with ethanol, milli-Q water and dried with air. The PS was placed in a ramped up (4 minutes) UVO cleaner (UVOCS model T0606B, Montgomeryville, Pennsylvania) in order for the UV lamp to reach a stable intensity ensuring similar UVO treatment condition for all of the samples. PO was subject air-plasma in an Expanded Plasma Cleaner (Harrick Plasma) on HIGH RF power setting for 1 minute. To create the non-fluorinated microstructured sample, PS-Micro, the UVO treated PS was subject to thermal treatment by placing the substrates into an oven (ED56, Binder, Tuttlingen, Germany) pre-heated to 140°C for 5 minutes. To create the fluorinated microstructured sample, PS-Micro-FS, the activated substrates were submerged in a prepared fluorosilane solution for approximately 3 hours with agitation at room temperature in an incubating mini shaker (VWR International, Mississauga, Ontario) to covalently bond an FS layer onto the surface through hydrolysis and condensation reactions. [75] For the deposition of fluorosilane, a mixture of ethanol and milli-Q water with volume ratio of 3:1 was prepared. A catalytic amount of hydrochloric acid (0.1 wt%) was added into the solution with 0.5 wt% of fluorosilane. The solution was incubated at 40° for an hour before use. The fluorosilane deposition is similar with a protocol used to create omniphobic micro- and nano-structured fabrics. [76] Following deposition of coating, the substrates were sonicated in Milli-Q water and subsequent 10 min sonication in ethanol for 10 minutes and dried.

To create PS-Nano-FS and PS-Hierarchical-FS, the activated PS substrates (UVO treated) were submerged in 10% aqueous APTES (for creating the seed layer for nanoparticle solution for respected samples) for approximately 3 hours with agitation at room temperature in an incubating mini shaker. Following deposition of coating, the substrates were sonicated in Milli-Q water for 10 minutes and dried. SiNPs solution was created by vertexing 1 part Ludox TMA colloidal silica with 2 parts milli-Q water for 10 seconds and sonication for half an hour. The size of the SiNPs were measured using dynamic light scattering (DLS), and were found to be 27±0.6 nm (Supplementary Figure 3.15). For the deposition of SiNPs (after the APTES treatment), the substrates were fixed in petri dishes using double sided tape and submerged in the SiNPs solution overnight. The amine terminus on the aminosilane had electrostatic interactions with the negative surface charge of the SiNPs and allowed for the deposition of the nanoparticles on the surface. Following deposition, the substrates were sonicated in Milli-Q water for 10 minutes and dried. The SiNPs surface were placed in the prepared fluorosilane solution for approximately 3 hours with agitation (PS-Nano-FS). The substrates were then sonicated in milli-Q water for 10 minutes and dried. At this step, the Planar, nanoparticle treated samples are prepared (PS-Nano-FS). To add the microstructures to the nanoparticle treated surface, thermal treatment was performed by placing the substrates into an oven pre-heated to 140°C for 5 minutes (PS-Hierarchical-FS).

To create the PO treated wraps, the activated wrap was subject an overnight APTES treatment as described earlier followed by 10 minutes sonication in Milli-Q water. Subsequently, samples were immersed in SiNP solution (as described) for 3 hours followed

by 3 hours fluorosilane treatment (as described earlier). The treated surface was then further subject to heat shrinking either by a heat gun (Amtake HG6618) or by incubation in a pre-heated oven at 140°C for 5 minutes. To wrap the treated PO before the shrinking process, the object was wrapped and sealed with a sealer and further subject to the heat gun.

Surface physical characterization. SEM imaging was performed on a JEOL 7000F. Samples were coated with 3 nm of platinum prior to imaging. Contact angle measurement was made on a goniometer (OCA 20, Future Digital Scientific, Garden City, NY) with water droplets (5 µL) dispensed by automated syringe, and hexadecane (5 µL) and human whole blood (5 µL) by hand using a pipette. The sessile drop contact angle was provided *via* image processing software (Dataphysics SCA 20) through ellipse curve fit shape analysis of the droplets. Whole human blood was collected from healthy donors in BD heparinized tubes. All donors provided signed written consent and the procedures were approved by the McMaster University Research Ethics Board. Sliding angle measurements were made on a self-made tilting platform with angle controlled by an automated servo. Each value was averaged over at least three measurements.

Advancing and receding contact angle. Advancing and receding contact angle were evaluated using goniometer (OCA 20, Future Digital Scientific, Garden City, NY) *via* needle in sessile drop method. 5 µL of water was dispensed onto the surface and the contact angle was measured continuously in real time. The volume of the drop was then increase by 5 µL at a rate of 1 µL/s, then decreased by 5 µL at 1 µL/s. This cycle repeated 4 times for each sample in order to get an accurate reading of the two angles.

Surface chemical characterization. X-ray Photoelectron Spectroscopy (XPS) was used to assess the surface chemical composition of the hierarchical structures. Three samples were used for each condition, and means were determined. A Physical Electronics (PHI) Quantera II spectrometer equipped with an Al anode source for X-ray generation was used to record the XPS spectra (BioInterface Institute, McMaster University). XPS results were obtained at 45° take-off angles with a pass energy of 224 eV. The atomic percentages of carbon, oxygen, fluorine, nitrogen and silicon were calculated using the instrument's software.

Alginate assay for simulating fouling. A solution of 1% w/v sodium alginate in milli-Q water was made with constant stirring. The extent of alginate adhesion to different sample conditions was assessed by incubating each sample in the alginate solution for 30 seconds and subsequently weighing the sample without washing or drying. Samples were also weighed before being subject to alginate solution in order to calculate the amount of the adhered alginate.

Biofilm Adherence assays. *Pseudomonas aeruginosa* PAO1 and *Staphylococcus aureus* USA300 JE2 (MRSA) [77] were streaked from frozen onto LB agar and grown overnight at 37ºC. From this, overnight cultures in LB broth were diluted 1/100 in MOPS-minimal media supplemented with 0.4% glucose and 0.5% casamino acids (TekNova,United States) for *P. aeruginosa*, [78] or TSA media supplemented with 0.4% glucose and 3% NaCl for MRSA. [79] A 24-well polystyrene assay plate (Corning, United States) was prepared by inserting a single nanoparticle-treated or untreated device into each well, then subsequently

flooding each well with 2 mL of the 1/100 diluted bacterial suspension. The assay plates were then incubated without shaking at 37°C for 72 hours for *P. aeruginosa* and 24 hours for MRSA without any substitution of the media to allow biofilms to form. Post incubation, the devices were removed from each well using sterile forceps and rinsed gently with water by submersing them 4-5 times into a beaker of water to remove planktonic bacterial cells. Biofilms attached to the devices were stained with 0.1% crystal violet, washed with sterile water, then solubilized in 30% acetic acid. A 200 µL bacterial suspension and solubilized crystal violet were transferred to a 96-well microtiter plate (Corning, United States). The optical density (OD) of the bacterial suspension (bacterial culture following the period used for biofilm production) was read at 600 nm using a Tecan Infinite m1000 plate reader (Tecan, United States) to evaluate the culture density. The OD of the resuspended crystal violet was measured at 570 nm. Relative biofilm adherence was calculated by the ratio of biofilm adhered (OD570) to culture density (OD600) as shown in the equation below."

$$\boldsymbol{Relative\ Biofilm\ Formed} = \frac{\boldsymbol{Biofilm\ Formation\ (OD_{570})}}{\boldsymbol{Cell\ Density\ (OD_{600})}}$$

Scanning Electron Microscopy – Bacteria Biofilm Fixation. MRSA and *P. aeruginosa* biofilms were grown on polystyrene and polyolefin surfaces as described in the previous section. Samples were then placed in a 0.25% glutaraldehyde solution (in sodium cacodylate buffer) for fixation for a minimum of 24 hours. Samples were subsequently rinsed with buffer before being stained with 1% osmium tetraoxide in sodium cacodylate buffer (pH=7.4). Samples were then sequentially dehydrated with ethanol solutions from 25% (in Milli-Q water) to 100%. Finally, samples were critically point dried (Leica

Microsystems, Wetzlar, Germany) and sputter coated with 3 nm of platinum before examination under SEM. Samples were imaged using a JEOL 7000F (JEOL, Peabody, MA) at an accelerating voltage of 4 keV. Images were artificially coloured to improve recognition of bacteria using GIMP (GIMP 4.0).

Bacteria contact touch assay. An overnight culture of *Escherichia coli* MG1655 harboring pUA66-GadB, [80] which constitutively expresses high levels of GFP, was grown in LB with 50 µg/ml kanamycin then pelleted. Cells were then re-suspended in 1/50 of the original volume of the culture to create a concentrated cell suspension. Agar plugs were made from 3% agar by dissolving 3 grams of agar in 100 mL water with a magnetic stirrer at room temperature. The temperature was then raised to 95 ºC while stirring for 20 minutes, then the solution was poured into petri dishes and cooled in room temperature. Once solidified, agar plugs were harvested from the cooled agar plated by poking tubes with approximately 15 mm diameter in it. 20 µL of 50x concentrated *E. coli* overnight culture was added to each agar plug, under a laminar air flow in a biosafety cabinet, and allowed the excess media to absorb within the agar, creating a layer of the bacteria on top of the agar. Subsequently, the bacteria infused agar plugs were contacted with PS-Planar, PS-Hierarchical-FS, PO-Planar, PO-Hierarchical-FS surfaces for 10 seconds, allowing the *E. coli* to transfer and stick to the them. The surfaces were then analyzed using a Chemidoc imaging system (BioInterface Institute, McMaster University) by fluorescein channel.

Bacterial transfer to human skin. In a similar method described in bacteria contact touch assay section, the contaminated PS-Planar, PS-Hierarchical-FS, PO-Planar, PO-Hierarchical-FS surfaces were touched with human skin and the extent of bacteria transfer

were analyzed. This was done through a handheld surface imaging technology provided by OptiSolve®, enabling imaging various surfaces and assessing their extent of contamination in real time.

3.6 Associated Content

Supporting information

The Supporting Information is available free of charge on the ACS Publications website. Assessing the chemical composition of the surface, discussion of the measured contact angles, schematic of the structures and their local geometric angle, discussion of the ethanol CA measurements, various ethanol/water concentration contact angle measurements, advancing/receding angles, contact angle hysteresis, calculated sliding angles, Pinning and bouncing of droplets, relative alginate adherence, GFP expressing *E. coli* touch assay on polystyrene, *E. coli* transfer to a wrapped key (PDF).

Video showing 10 µl of Water dropped onto PS-Planar from one inch at 480fps.

Video showing 10 µl of Hexadecane dropped onto PS-Planar from one inch at 480fps.

Video showing 10 µl of Water dropped onto PS-Hierarchical-FS from one inch at 480fps.

Video showing 10 µl of Hexadecane dropped onto PS-Hierarchical-FS from one inch at 480fps. Video showing 10 µl of Water dropped onto PO-Planar from one inch at 480fps.

Video showing 10 µl of Hexadecane dropped onto PO-Planar from one inch at 480fps.

Video showing 10 µl of Water dropped onto PO-Hierarchical-FS from one inch at 480fps.

Video showing 10 µl of Hexadecane dropped onto PO-Hierarchical-FS from one inch at 480fps. Video showing slow motion water droplets continuously running from a water

bottle on top of a PO-Hierarchical-FS surface, demonstrating bouncing and rolling off of the water droplets.

Video showing implementing the developed surface for food packaging, showing wrapped meat with polyolefin (PO-Planar and PO-Hierarchical-FS). The water droplets bounce off the treated surface and get stuck on the untreated PO.

The authors declare no competing financial interest.

3.7 Author information

Corresponding author

*Address correspondence to soleyml@mcmaster.ca, didar@mcmaster.ca

Author contributions

T.F.D and L.S designed and conceived the research. The experiments were designed by all authors and performed by S.M.I, R.M., K.R, Y.C, and B.L. Fluorescence imaging using the handheld surface imager was performed by M.M..All authors contributed to the writing of the manuscript.

3.8 Acknowledgments

The authors acknowledge and thank Professor Zeinab Hosseinidoust for help in designing bacterial adhesion experiments and Dr. Shawn French of McMaster University for helpful discussions. This work was supported by a Canadian Institutes of Health Research

Foundation grant (FDN-143215) to E.D.B., NSERC and Ontario Early Researcher Award grant to L.S., by a salary award to E.D.B. and L.S. from the Canada Research Chairs Program, NSERC Discovery Grant to K.G. and T.F.D., Ontario Early Researcher Award Grant to T.F.D., and McMaster start-up funds to T.F.D. The electron microscopy was carried out at the Canadian Centre for Electron Microscopy (CCEM), a national facility supported by the NSERC and McMaster University. B.L was the recipient of the Ontario Graduate Scholarship.

3.9 References

(1) Khan, H. A.; Baig, F. K.; Mehboob, R. Nosocomial Infections: Epidemiology, Prevention, Control and Surveillance. *Asian Pac. J. Trop. Biomed.* **2017**, *7*, 478–482.

(2) Lenz, R.; Leal, J. R.; Church, D. L.; Gregson, D. B.; Ross, T.; Laupland, K. B. The Distinct Category of Healthcare Associated Bloodstream Infections. *BMC Infect. Dis.* **2012**, *12*, 85.

(3) Lax, S.; Gilbert, J. A. Hospital-Associated Microbiota and Implications for Nosocomial Infections. *Trends Mol. Med.* **2015**, *21*, 427–432.

(4) Al-Tawfiq, J. A.; Tambyah, P. A. Healthcare Associated Infections (HAI) Perspectives. *J. Infect. Public Health* **2014**, *7*, 339–344.

(5) Knobben, B. A. S.; van der Mei, H. C.; van Horn, J. R.; Busscher, H. J. Transfer of Bacteria between Biomaterials Surfaces in the Operating Room—an Experimental Study. *J. Biomed. Mater. Res. Part A* **2007**, *80*, 790–799.

(6) Tacconelli, E.; Carrara, E.; Savoldi, A.; Harbarth, S.; Mendelson, M.; Monnet, D. L.; Pulcini, C.; Kahlmeter, G.; Kluytmans, J.; Carmeli, Y. Discovery, Research, and Development of New Antibiotics: The WHO Priority List of Antibiotic-Resistant Bacteria and Tuberculosis. *Lancet Infect. Dis.* **2018**, *18* , 318–327.

(7) Russotto, V.; Cortegiani, A.; Raineri, S. M.; Giarratano, A. Bacterial Contamination of Inanimate Surfaces and Equipment in the Intensive Care Unit. *J. Intensive Care* **2015**, *3*, 54.

(8) Nelson, R. E.; Slayton, R. B.; Stevens, V. W.; Jones, M. M.; Khader, K.; Rubin, M. A.; Jernigan, J. A.; Samore, M. H. Attributable Mortality of Healthcare-Associated Infections Due to Multidrug-Resistant Gram-Negative Bacteria and Methicillin-Resistant Staphylococcus Aureus. *Infect. Control Hosp. Epidemiol.* **2017**, *38* , 848–856.

(9) Evaluation of Healthcare-Associated Infection Activities at the Public Health Agency of Canada 2012-13 to 2016-17 - Canada.ca https://www.canada.ca/en/public-health/corporate/transparency/corporate-management-reporting/evaluation/healthcare-associated-infection-activities-2012-2017.html (accessed Jun 5, 2019).

(10) Percival, S. L.; Suleman, L.; Vuotto, C.; Donelli, G.; Percival, S. L. Healthcare-Associated Infections , Medical Devices and Biofilms : Risk , Tolerance and Control. *J. Med. Microbiol.* **2019**, No. May, 323–334.

(11) Nguyen, D. H. K.; Pham, V. T. H.; Truong, V. K.; Sbarski, I.; Wang, J.; Balčytis, A.; Juodkazis, S.; Mainwaring, D. E.; Crawford, R. J.; Ivanova, E. P. Role of

Topological Scale in the Differential Fouling of *Pseudomonas Aeruginosa* and *Staphylococcus Aureus* Bacterial Cells on Wrinkled Gold-Coated Polystyrene Surfaces. *Nanoscale* **2018**, *10* , 5089–5096.

(12) Fürstner, R.; Barthlott, W.; Neinhuis, C.; Walzel, P. Wetting and Self-Cleaning Properties of Artificial Superhydrophobic Surfaces. *Langmuir* **2005**, *21* , 956–961.

(13) Parkin, I. P.; Palgrave, R. G. Self-Cleaning Coatings. *J. Mater. Chem.* **2005**, *15* , 1689–1695.

(14) Vogel, N.; Belisle, R. A.; Hatton, B.; Wong, T.-S.; Aizenberg, J. Transparency and Damage Tolerance of Patternable Omniphobic Lubricated Surfaces Based on Inverse Colloidal Monolayers. *Nat. Commun.* **2013**, *4*, 2176.

(15) MacCallum, N.; Howell, C.; Kim, P.; Sun, D.; Friedlander, R.; Ranisau, J.; Ahanotu, O.; Lin, J. J.; Vena, A.; Hatton, B. Liquid-Infused Silicone as a Biofouling-Free Medical Material. *ACS Biomater. Sci. Eng.* **2014**, *1* , 43–51.

(16) Puckett, S. D.; Taylor, E.; Raimondo, T.; Webster, T. J. The Relationship between the Nanostructure of Titanium Surfaces and Bacterial Attachment. *Biomaterials* **2010**, *31* , 706–713.

(17) Colon, G.; Ward, B. C.; Webster, T. J. Increased Osteoblast and Decreased *Staphylococcus Epidermidis* Functions on Nanophase ZnO and TiO2. *J. Biomed. Mater. Res. - Part A* **2006**, *78* , 595–604.

(18) Crawford, R. J.; Webb, H. K.; Truong, V. K.; Hasan, J.; Ivanova, E. P. Surface Topographical Factors Influencing Bacterial Attachment. *Adv. Colloid Interface Sci.* **2012**, *179–182*, 142–149.

(19) Darmanin, T.; Guittard, F. Recent Advances in the Potential Applications of Bioinspired Superhydrophobic Materials. *J. Mater. Chem. A* **2014**, *2* , 16319–16359.

(20) Leslie, D. C.; Waterhouse, A.; Berthet, J. B.; Valentin, T. M.; Watters, A. L.; Jain, A.; Kim, P.; Hatton, B. D.; Nedder, A.; Donovan, K. A Bioinspired Omniphobic Surface Coating on Medical Devices Prevents Thrombosis and Biofouling. *Nat. Biotechnol.* **2014**, *32* , 1134.

(21) Badv, M.; Imani, S. M.; Weitz, J. I.; Didar, T. F. Lubricant-Infused Surfaces with Built-In Functional Biomolecules Exhibit Simultaneous Repellency and Tunable Cell Adhesion. *ACS Nano* **2018**, *12* , 10890–10902.

(22) Hosseini, A.; Villegas, M.; Yang, J.; Badv, M.; Weitz, J. I.; Soleymani, L.; Didar, T. F. Conductive Electrochemically Active Lubricant-Infused Nanostructured Surfaces Attenuate Coagulation and Enable Friction-Less Droplet Manipulation. *Adv. Mater. Interfaces* **2018**, *5*, 1800617.

(23) Osborne, M.; Aryasomayajula, A.; Shakeri, A.; Selvaganapathy, P. R.; Didar, T. F. Suppression of Biofouling on a Permeable Membrane for Dissolved Oxygen Sensing Using a Lubricant-Infused Coating. *ACS Sensors* **2019**, *4* , 687–693.

(24) Badv, M.; Jaffer, I. H.; Weitz, J. I.; Didar, T. F. An Omniphobic Lubricant-Infused Coating Produced by Chemical Vapor Deposition of Hydrophobic Organosilanes Attenuates Clotting on Catheter Surfaces. *Sci. Rep.* **2017**, *7* , 11639.

(25) Villegas, M.; Zhang, Y.; Abu Jarad, N.; Soleymani, L.; Didar, T. F. Liquid-Infused Surfaces: A Review of Theory, Design, and Applications. *ACS Nano* **2019**, *13* ,

8517–8536.

(26) Kim, P.; Kreder, M. J.; Alvarenga, J.; Aizenberg, J. Hierarchical or Not? Effect of the Length Scale and Hierarchy of the Surface Roughness on Omniphobicity of Lubricant-Infused Substrates. *Nano Lett.* **2013**, *13* (4), 1793–1799.

(27) Lafuma, A.; Quéré, D. Superhydrophobic States. *Nat. Mater.* **2003**, *2* , 457–460.

(28) Wenzel, R. N. Resistance of Solid Surfaces to Wetting by Water. *Ind. Eng. Chem.* **1936**, *28* , 988–994.

(29) Cassie, A. B. D.; Baxter, S. Wettability of Porous Surfaces. *Trans. Faraday Soc.* **1944**, *40*, 546.

(30) Nosonovsky, M. Multiscale Roughness and Stability of Superhydrophobic Biomimetic Interfaces. *Langmuir* **2007**, *23* , 3157–3161.

(31) Shirtcliffe, N. J.; McHale, G.; Newton, M. I.; Chabrol, G.; Perry, C. C. Dual-Scale Roughness Produces Unusually Water-Repellent Surfaces. *Adv. Mater.* **2004**, *16* , 1929–1932.

(32) Lin, P. C.; Yang, S. Mechanically Switchable Wetting on Wrinkled Elastomers with Dual-Scale Roughness. *Soft Matter* **2009**, *5*, 1011–1018.

(33) Kota, A. K.; Kwon, G.; Tuteja, A. The Design and Applications of Superomniphobic Surfaces. *Npg Asia Mater.* **2014**, *6*, e109.

(34) Hensel, R.; Neinhuis, C.; Werner, C. The Springtail Cuticle as a Blueprint for Omniphobic Surfaces. *Chem. Soc. Rev.* **2016**, *45* , 323–341.

(35) Zhang, J.; Seeger, S. Superoleophobic Coatings with Ultralow Sliding Angles Based on Silicone Nanofilaments. *Angew. Chemie Int. Ed.* **2011**, *50* , 6652–6656.

(36) Mazumder, P.; Jiang, Y.; Baker, D.; Carrilero, A.; Tulli, D.; Infante, D.; Hunt, A. T.; Pruneri, V. Superomniphobic, Transparent, and Antireflection Surfaces Based on Hierarchical Nanostructures. *Nano Lett.* **2014**, *14* , 4677–4681.

(37) Deng, X.; Mammen, L.; Butt, H.-J.; Vollmer, D. Candle Soot as a Template for a Transparent Robust Superamphiphobic Coating. *Science (80-.).* **2012**, *335*, 67–70.

(38) Tuteja, A.; Choi, W.; Mabry, J. M.; McKinley, G. H.; Cohen, R. E. Robust Omniphobic Surfaces. *Proc. Natl. Acad. Sci. U. S. A.* **2008**, *105*, 18200–18205.

(39) Zhu, P.; Kong, T.; Tang, X.; Wang, L. Well-Defined Porous Membranes for Robust Omniphobic Surfaces *via* Microfluidic Emulsion Templating. *Nat. Commun.* **2017**, *8*, 15823.

(40) Wu, W.; Wang, X.; Wang, D.; Chen, M.; Zhou, F.; Liu, W.; Xue, Q. Alumina Nanowire Forests *via* Unconventional Anodization and Super-Repellency plus Low Adhesion to Diverse Liquids. *Chem. Commun.* **2009**, No. 9, 1043–1045.

(41) Hizal, F.; Rungraeng, N.; Lee, J.; Jun, S.; Busscher, H. J.; Van Der Mei, H. C.; Choi, C.-H. Nanoengineered Superhydrophobic Surfaces of Aluminum with Extremely Low Bacterial Adhesivity. *ACS Appl. Mater. Interfaces* **2017**, *9*, 12118–12129.

(42) Chu, Z.; Seeger, S. Superamphiphobic Surfaces. *Chem. Soc. Rev.* **2014**, *43*, 2784–2798.

(43) Pendurthi, A.; Movafaghi, S.; Wang, W.; Shadman, S.; Yalin, A. P.; Kota, A. K. Fabrication of Nanostructured Omniphobic and Superomniphobic Surfaces with Inexpensive CO2 Laser Engraver. *ACS Appl. Mater. Interfaces* **2017**, *9*, 25656–

25661.

(44) Gabardo, C. M.; Yang, J.; Smith, N. J.; Adams-McGavin, R. C.; Soleymani, L. Programmable Wrinkling of Self-Assembled Nanoparticle Films on Shape Memory Polymers. *ACS Nano* **2016**, *10*, 8829–8836.

(45) Gabardo, C. M.; Zhu, Y.; Soleymani, L.; Moran-Mirabal, J. M. Bench-Top Fabrication of Hierarchically Structured High-Surface-Area Electrodes. *Adv. Funct. Mater.* **2013**, *23*, 3030–3039.

(46) Lin, S.; Lee, E. K.; Nguyen, N.; Khine, M. Thermally-Induced Miniaturization for Micro- and Nanofabrication: Progress and Updates. *Lab Chip* **2014**, *14*, 3475–3488.

(47) Adams-McGavin, R. C.; Chan, Y.; Gabardo, C. M.; Yang, J.; Skreta, M.; Fung, B. C.; Soleymani, L. Nanoporous and Wrinkled Electrodes Enhance the Sensitivity of Glucose Biosensors. *Electrochim. Acta* **2017**, *242*, 1–9.

(48) Ware, C. S.; Smith-Palmer, T.; Peppou-Chapman, S.; Scarratt, L. R. J.; Humphries, E. M.; Balzer, D.; Neto, C. Marine Antifouling Behavior of Lubricant-Infused Nanowrinkled Polymeric Surfaces. *ACS Appl. Mater. Interfaces* **2018**, *10*, 4173–4182.

(49) Scarratt, L. R. J.; Hoatson, B. S.; Wood, E. S.; Hawkett, B. S.; Neto, C. Durable Superhydrophobic Surfaces *via* Spontaneous Wrinkling of Teflon AF. *ACS Appl. Mater. Interfaces* **2016**, *8*, 6743–6750.

(50) Schauer, S.; Worgull, M.; Hölscher, H. Bio-Inspired Hierarchical Micro- and Nano-Wrinkles Obtained *via* Mechanically Directed Self-Assembly on Shape-

Memory Polymers. *Soft Matter* **2017**, *13*, 4328–4334.

(51) Efimenko, K.; Rackaitis, M.; Manias, E.; Vaziri, A.; Mahadevan, L.; Genzer, J. Nested Self-Similar Wrinkling Patterns in Skins. *Nat. Mater.* **2005**, *4*, 293–297.

(52) Dramé, A.; Darmanin, T.; Dieng, S. Y.; Taffin de Givenchy, E.; Guittard, F. Superhydrophobic and Oleophobic Surfaces Containing Wrinkles and Nanoparticles of PEDOT with Two Short Fluorinated Chains. *RSC Adv.* **2014**, *4*, 10935–10943.

(53) Zhou, Q.; Kühn, P. T.; Huisman, T.; Nieboer, E.; Van Zwol, C.; Van Kooten, T. G.; Van Rijn, P. Directional Nanotopographic Gradients: A High-Throughput Screening Platform for Cell Contact Guidance. *Sci. Rep.* **2015**, *5*, 16240.

(54) Liguori, G. R.; Zhou, Q.; Liguori, T. T. A.; Barros, G. G.; Kühn, P. T.; Moreira, L. F. P.; van Rijn, P.; Harmsen, M. C. Directional Topography Influences Adipose Mesenchymal Stromal Cell Plasticity: Prospects for Tissue Engineering and Fibrosis. *Stem Cells Int.* **2019**, *2019*.

(55) Abagnale, G.; Sechi, A.; Steger, M.; Zhou, Q.; Kuo, C.-C.; Aydin, G.; Schalla, C.; Müller-Newen, G.; Zenke, M.; Costa, I. G. Surface Topography Guides Morphology and Spatial Patterning of Induced Pluripotent Stem Cell Colonies. *Stem cell reports* **2017**, *9*, 654–666.

(56) Gabardo, C. M.; Kwong, A. M.; Soleymani, L. Rapidly Prototyped Multi-Scale Electrodes to Minimize the Voltage Requirements for Bacterial Cell Lysis. *Analyst* **2015**, *140*, 1599–1608.

(57) Gabardo, C. M.; Adams-McGavin, R. C.; Fung, B. C.; Mahoney, E. J.; Fang, Q.;

Soleymani, L. Rapid Prototyping of All-Solution-Processed Multi-Lengthscale Electrodes Using Polymer-Induced Thin Film Wrinkling. *Sci. Rep.* **2017**, *7*, 42543.

(58) Saha, S.; Chan, Y.; Soleymani, L. Enhancing the Photoelectrochemical Response of DNA Biosensors Using Wrinkled Interfaces. *ACS Appl. Mater. Interfaces* **2018**, *10*, 31178–31185.

(59) Erasmus, E.; Barkhuysen, F. A. Superhydrophobic Cotton by Fluorosilane Modification. *Indian J. Fibre Text. Res.* **2009**, *34*, 377–379.

(60) Pegan, J. D.; Ho, A. Y.; Bachman, M.; Khine, M. Flexible Shrink-Induced High Surface Area Electrodes for Electrochemiluminescent Sensing. *Lab Chip* **2013**, *13*, 4205–4209.

(61) Li, D.; Neumann, A. Contact Angles on Hydrophobic Solid-Surfaces and Their Interpretation. *J. Colloid Interface Sci.* **1992**, *148*, 190–200.

(62) Herminghaus, S. Roughness-Induced Non-Wetting. *Eur. Lett.* **2000**, *52*, 165–170.

(63) Vazquez, G.; Alvarez, E.; Navaza, J. M. Surface Tension of Alcohol Water + Water from 20 to 50 .Degree.C. *J. Chem. Eng. Data* **1995**, *40*, 611–614.

(64) Tesler, A. B.; Kim, P.; Kolle, S.; Howell, C.; Ahanotu, O.; Aizenberg, J. Extremely Durable Biofouling-Resistant Metallic Surfaces Based on Electrodeposited Nanoporous Tungstite Films on Steel. *Nat. Commun.* **2015**, *6*, 8649.

(65) Ensikat, H. J.; Ditsche-Kuru, P.; Neinhuis, C.; Barthlott, W. Superhydrophobicity in Perfection: The Outstanding Properties of the Lotus Leaf. *Beilstein J. Nanotechnol.* **2011**, *2*, 152–161.

(66) Wooh, S.; Vollmer, D. Silicone Brushes: Omniphobic Surfaces with Low Sliding

Angles. *Angew. Chemie Int. Ed.* **2016**, *55*, 6822–6824.

(67) Percival, S. L.; Suleman, L.; Vuotto, C.; Donelli, G. Healthcare-Associated Infections, Medical Devices and Biofilms: Risk, Tolerance and Control. *J. Med. Microbiol.* **2015**, *64*, 323–334.

(68) Boyd, A.; Chakrabarty, A. M. Pseudomonas Aeruginosa Biofilms: Role of the Alginate Exopolysaccharide. *J. Ind. Microbiol.* **1995**, *15*, 162–168.

(69) Hall-Stoodley, L.; Costerton, J. W.; Stoodley, P. Bacterial Biofilms: From the Natural Environment to Infectious Diseases. *Nat. Rev. Microbiol.* **2004**, *2*, 95.

(70) Yuan, Y.; Hays, M. P.; Hardwidge, P. R.; Kim, J. Surface Characteristics Influencing Bacterial Adhesion to Polymeric Substrates. *RSC Adv.* **2017**, *7*, 14254–14261.

(71) Fadeeva, E.; Truong, V. K.; Stiesch, M.; Chichkov, B. N.; Crawford, R. J.; Wang, J.; Ivanova, E. P. Bacterial Retention on Superhydrophobic Titanium Surfaces Fabricated by Femtosecond Laser Ablation. *Langmuir* **2011**, *27*, 3012–3019.

(72) Hizal, F.; Choi, C.-H.; Sjollema, J.; Nuryastuti, T.; Rustema-Abbing, M.; Rozenbaum, R. T.; van der Mei, H. C.; Busscher, H. J.; Wessel, S. W. Transmission of Monospecies and Dual-Species Biofilms from Smooth to Nanopillared Surfaces. *Appl. Environ. Microbiol.* **2018**, *84*, e01035-18.

(73) Vasilev, K.; Cook, J.; Griesser, H. J. Antibacterial Surfaces for Biomedical Devices. *Expert Rev. Med. Devices* **2009**, *6*, 553–567.

(74) Fux, C. A.; Costerton, J. W.; Stewart, P. S.; Stoodley, P. Survival Strategies of Infectious Biofilms. *Trends Microbiol.* **2005**, *13*, 34–40.

(75) Howarter, J. A.; Youngblood, J. P. Optimization of Silica Silanization by 3-Aminopropyltriethoxysilane. *Langmuir* **2006**, *22*, 11142–11147.

(76) Shillingford, C.; MacCallum, N.; Wong, T.-S.; Kim, P.; Aizenberg, J. Fabrics Coated with Lubricated Nanostructures Display Robust Omniphobicity. *Nanotechnology* **2013**, *25*, 14019.

(77) Fey, P. D.; Endres, J. L.; Yajjala, V. K.; Widhelm, T. J.; Boissy, R. J.; Bose, J. L.; Bayles, K. W. A Genetic Resource for Rapid and Comprehensive Phenotype Screening of Nonessential *Staphylococcus Aureus* Genes. *MBio* **2013**, *4*, e00537-12.

(78) AU - O'Toole, G. A. Microtiter Dish Biofilm Formation Assay. *JoVE* **2011**, 47, e2437.

(79) Mootz, J. M.; Benson, M. A.; Heim, C. E.; Crosby, H. A.; Kavanaugh, J. S.; Dunman, P. M.; Kielian, T.; Torres, V. J.; Horswill, A. R. Rot Is a Key Regulator of *Staphylococcus Aureus* Biofilm Formation. *Mol. Microbiol.* **2015**, *96*, 388–404.

(80) Zaslaver, A.; Bren, A.; Ronen, M.; Itzkovitz, S.; Kikoin, I.; Shavit, S.; Liebermeister, W.; Surette, M. G.; Alon, U. A Comprehensive Library of Fluorescent Transcriptional Reporters for *Escherichia Coli*. *Nat. Methods* **2006**, *3*, 623.

3.10 Supplementary Information for Flexible Hierarchical Wraps Repel Drug Resistant Gram Negative and Positive Bacteria

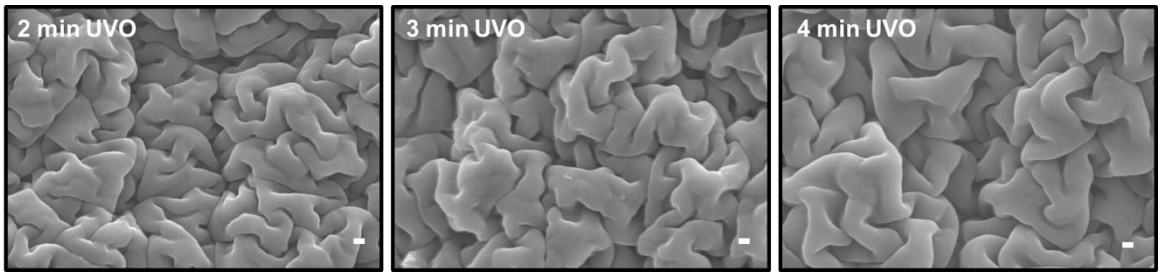

Supplementary Figure 3.5 *UVO treatment performed for 1, 2, 3, and 4 minutes on PS followed by thermal shrinkage, demonstrating control over the degree of wrinkles. Scale bars are present 100 nm.*

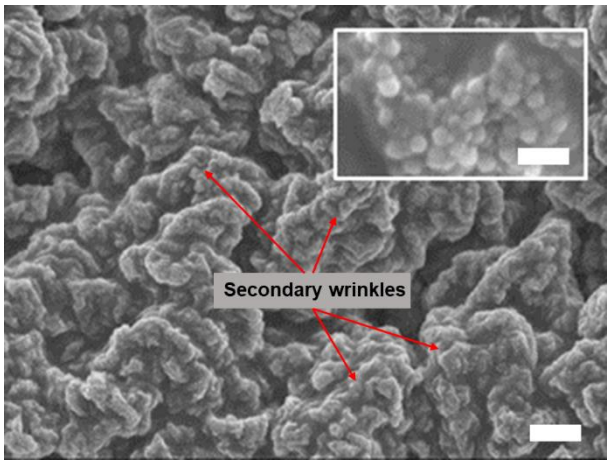

Supplementary Figure 3.6 *Secondary wrinkles shown on PO-Hierarchical-FS. The scale bars represent 1 µm and 100 nm on the image and inset respectively.*

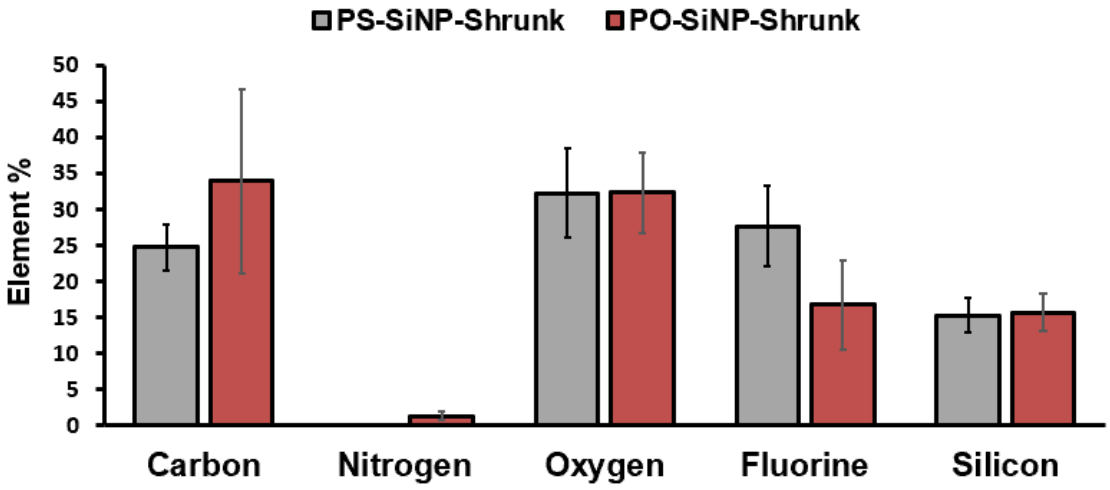

Supplementary Figure 3.7 *Assessing the chemical composition of the surface. To quantitatively assess the chemical composition of the hierarchical surfaces and confirm the success of the performed modifications, we performed X-ray photoelectron spectroscopy (XPS) on the PS-Hierarchical-FS and PO-Hierarchical-FS and compared them to the planar samples. Both pristine surfaces (PS-Planar and PO-Planar) were mainly composed of carbon (more than 95%) and oxygen (less than 5%). However, when subject to the treatments and inducing the hierarchical structures, the fluorine element appeared in the elemental analysis for PS-Hierarchical-FS and PO-Hierarchical-FS (27.7 % and 16.8%) which is indicative of successful FS treatment. Furthermore, presence of silicon element indicates the availability of SiNPs. The decrease in carbon comparing to the planar samples can be explained by the addition of other elements to the surface. The increase in the oxygen element (~32%) can be attributed to the surface activation and introduction of hydroxyl groups in the course of the modification steps. The performed XPS was a survey scan, therefore enabled us to do an elemental analysis rather than bond analysis (requires high resolution XPS). In spite of this, previous studies have used similar methodology for their treatments (APTES treatment, FS treatment) and have demonstrated successful modifications.* [1–6]

Supplementary Note 1 - discussion of the measured contact angles**:**

Static contact angle measurements were made for 5 µL droplets of milli-Q grade water (surface tension of 72.75 mJ/m^2 [7]) deposited onto the surfaces (Figure 3.2). The polystyrene surfaces showed hydrophilic characteristics as they had contact angles of 78.9±1.3° for PS-Planar. Based on the Wenzel model, [8] for a fully wetted state between the droplet and surface, the apparent contact angle can be estimated by, [8]

$$\cos\theta_w = r\cos\theta \quad (1)$$

where r is the ratio of the actual surface area in contact with the droplet to the projected surface area of the droplet and θ is the contact angle based on Young's relation. This equation indicates that a rough surface, with fully wetted state, would result in a lower Wenzel contact angle for θ<90°, and higher Wenzel contact angle for θ>90°. PS-Planar is hydrophilic (θ<90°), therefore by Wenzel model, it is assumed that the wrinkled non-fluorinated surface would be hydrophilic, however, based on the results for the PS-Micro surfaces, they were hydrophobic showing a contact angle higher than 90° (100±6°). To better describe the phenomenon happening, Cassie model should be implemented, [9] The contact angle for the droplet, θ_c, can be estimated as, [9–11]

$$\cos\theta_C = f_{SL}\cos\theta + f_{LV}\cos\pi = f_{SL}\cos\theta - f_{LV} \quad (2)$$

where f_{SL} is the ratio of the total area of solid-liquid interface to the projected area of the drop and f_{LV} is the ratio of the liquid-air interface to the projected area of the drop. This enables prediction of a higher Cassie contact angle due to fraction of liquid-air interface beneath the droplet regardless of the starting Young's contact angle. The fluorinated wrinkled surfaces (PS-Micro-FS) had higher contact angle (125±4°) compared to the PS-Micro surfaces. This is explained by the decrease in the surface free energy, which results in a higher Young's contact angle and leads to a higher Cassie contact angle.

The combination of both micro- and nano-structures on the surfaces achieved hydrophobicity of more than 150°. For hierarchical structures, the contact angle can be approximated theoretically by rewriting Cassie relation recursively, [12]

$$\cos\theta_{c,n} = \left(1 - f_{LV,n}\right)\cos\theta_{c,n-1} - f_{LV,n} \quad (3)$$

where $n = 1,2,3,\cdots$ correspond to the number of length scales present in the textured surface, with larger index corresponding to larger length scale. This means that the contact angle is expected to increase as the number of length scale increases. [10] It had also been shown in previous studies that multiscale roughness assists to improve the stability of solid-liquid-air interface. [13] Here, we demonstrated that having a combination of both nanoscale and microscale structures improved the hydrophobicity by approximately 20°.

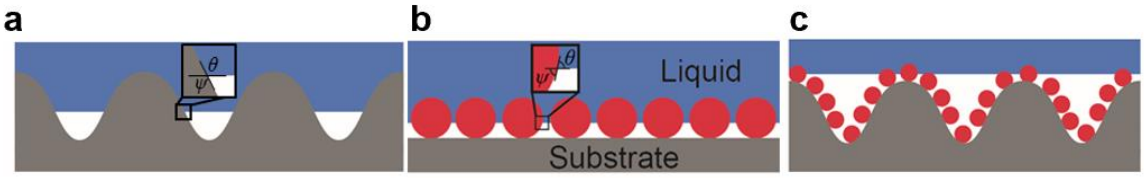

Supplementary Figure 3.8 *Schematic of the structures and their local geometric angle.*

The oleophobicity was tested with 5 µL droplets of hexadecane (surface tension of 27.76 mJ/m^2 [7]) deposited onto the surfaces and their static contact angles measured (Figure 3.2a). The non-fluorinated surfaces were oleophilic, with contact angles that were too low to accurately be measured. This was as expected since the Young's relation predicts a smaller contact angle for lower surface tension liquids. The inclusion of non-fluorinated wrinkles on surfaces (PS-Micro), also does not assist in making the surface less oleophilic. However, PS-Micro-FS samples, made the surface less oleophilic (26±7°) due to the effect of fluorosilanization on lowering the surface energy.

PS-Nano-FS surfaces revealed a significantly higher contact angles (55±3°) compared to the wrinkled surfaces (both PS-Micro and PS-Micro-FS) for improving the contact angle for hexadecane than water. This could be explained by the re-entrant texture of

nanoparticles compared to that of wrinkles (ψ <90° Supplementary Figure 3.8b). The wrinkles alone were not effective for keeping lower surface tension liquid in the Cassie state. In a Cassie state, when pockets of air are trapped beneath the droplet, the liquid forms a three-phase contact line at the local structure (Supplementary Figure 3.8), where the local geometric angle, ψ, becomes equal to the equilibrium contact angle, θ, based on Young's relation. [10] The structure of a wrinkle is similar with that of a concave texture where the local geometric angle has a high value, ψ >90° (Supplementary Figure 3.8a). Previous studies had concluded that concave structure does not support a stable Cassie state. [10,14] For a stable Cassie state, the Young's contact angle must be higher than the local geometric angle [10] and Young's relation equilibrium contact angle decreases for lower surface tension liquid. When the angle decreases to below the local geometric angle, the net traction on the liquid-air interface is downwards due to capillary forces, [10,15] which will lead to a fully wetted Wenzel state. For local geometric angles of high values, such as for wrinkles, the surface tension of the liquid needs to be high for a stable Cassie state.

The combination of both micro- and nano-structures in the PS-Hierarchical-FS samples, led to achieving oleophobicity as the contact angles reached to 123±5°. The addition of nanoparticles decreased the limitation of the concave texture of the wrinkles, allowing better repellence of lower surface tension liquid (Supplementary Figure 3.8c). In the meantime, having wrinkles also provided for a higher fraction of air beneath the droplet. The results showed that the surfaces created are omniphobic, with oleophobicity (>110°) and superhydrophobicity (>150°).

Supplementary Note 2 - discussion of the ethanol CA measurements**:**

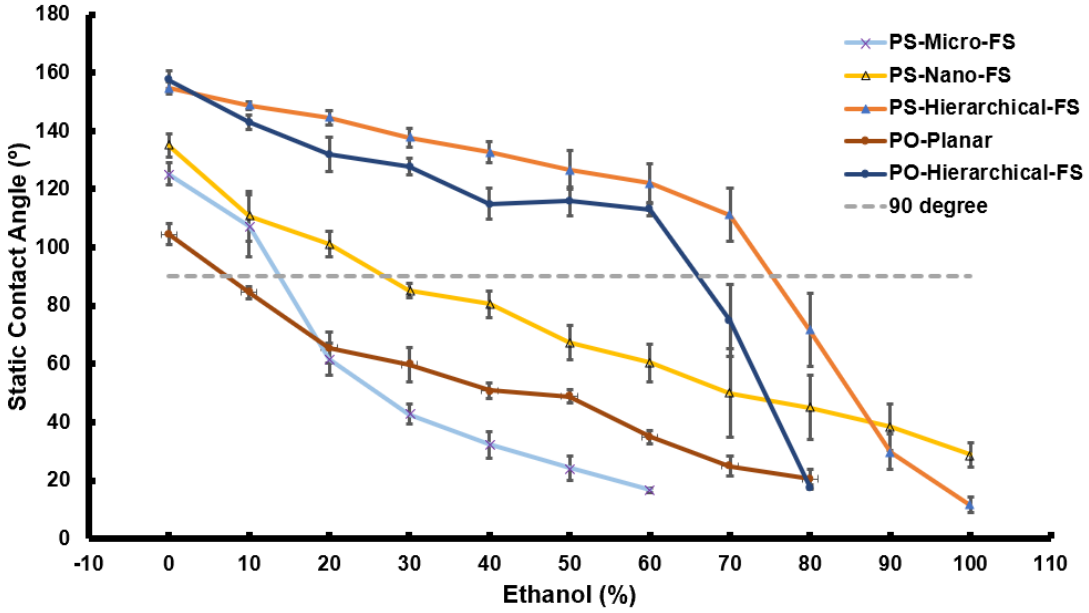

Supplementary Figure 3.9 *Measurement of contact angle at various ethanol/water concentrations.*

To further validate the omniphobic behavior of the developed hierarchical surfaces, we performed contact angle measurements using different ethanol and water contents ranging from 0% to 100%. This gives the advantage of tuning the liquid surface tension and validating the omniphobicity of the surface. Work by Epstein *et al*, showed multiscale roughness and the chemistry of the biofilm of bacteria such as B. subtilis, had previously revealed a contact angle plateau of ~135° for 0 % to 80% ethanol and this is in contrast with artificial replicas which have a drastic decrease in contact angle. [16] Our developed hierarchical surface, PS-Hierarchical-FS, showed a contact angle of above 100° from 0% to 70% ethanol content. The PO-Hierarchical-FS, however maintained the above 90° contact angle until 60% solution. PS-Nano-FS maintained a contact angle of above 100° with 20% ethanol (102°), while PS-Micro-FS was the least effective (61° contact angle at

20% ethanol), agreeing with earlier hexadecane contact angle results. We see that the addition of the hierarchical structures results in a repellency plateau, which greatly differs from the pseudo linear curve seen in PS-Nano-FS.

Supplementary Note 3 - Advancing Receding Angles and Contact Angle Hysteresis

The dynamic water droplet properties of treated and untreated polyolefin and polystyrene are evaluated. The contact angle hysteresis ($\Delta\theta_H$) of a given substrate is determined from the difference between the advancing and receding contact angle:

$$\Delta\theta_H = \theta_A - \theta_R \qquad (S1)$$

Where θ_A and θ_R are the advancing and receding contact angles. The contact angle hysteresis of a surface is an indication of the activation energy needed to move a droplet across a surface [17] in such a way that surfaces with a lower contact angle hysteresis would require less energy for a droplet to detach itself from the surface with less pinning, thus repelling water. [18] This leads to sliding or bouncing of the droplets on the surfaces. Low $\Delta\theta_H$ values are a sign that the wetting on the surface is in a Cassie state, [18] which is of key importance for super hydrophobic and oleophobic self-cleaning surfaces. On micro and nanostructured surfaces, contact angle hysteresis can be expected to be very low. The Sliding angle of a given droplet on a surface can be calculated *via* the advancing and receding contact angles:

$$\sin(\alpha) = k\gamma L / \rho V g \,(\cos(\theta_R) - \cos(\theta_A)) \quad (S2)$$

Where α is the sliding angle, k is a dimensionless factor, γ is the surface tension of water, L is the diameter of the contact, ρ is the density of water, V is the volume of water and g is the gravitational coeffect. [19] The coefficient k represents the shape and the elongation of

the droplet on a surface and is the percent difference between the contact length of the droplet on the surface (L) and the original diameter of the droplet (D) and can be calculated with the following formula: $k = (D-L)/D$. [20] Droplets on superhydrophobic surfaces can be assumed to be spherical, L will approach a value of 0, with this we assumed that k would have a value of 1. The calculated sliding angle for PS-Planar was evaluated to not exist ($k\gamma L/\rho Vg\ (\cos(\theta_R) - \cos(\theta_A))>1$), which indicates that the equation is not satisfied for no angle and water does not slide on PS-Planar (allocated sliding angle of 90^o for graphing). For both PS and PO, the reduction in the contact angle hysteresis (less than 5^o for PS-Hierarchal-FS and around 5^o for PO-Hierarchical-FS) and simultaneous increase in the advancing and receding contact angle, resulted in a large reduction in the sliding angle and overall adhesion of the water droplets to the surface. These findings agree with the measured results for the sliding angles seen in Figure 3.2a.

Supplementary Note 4 - Pinning and bouncing of droplets

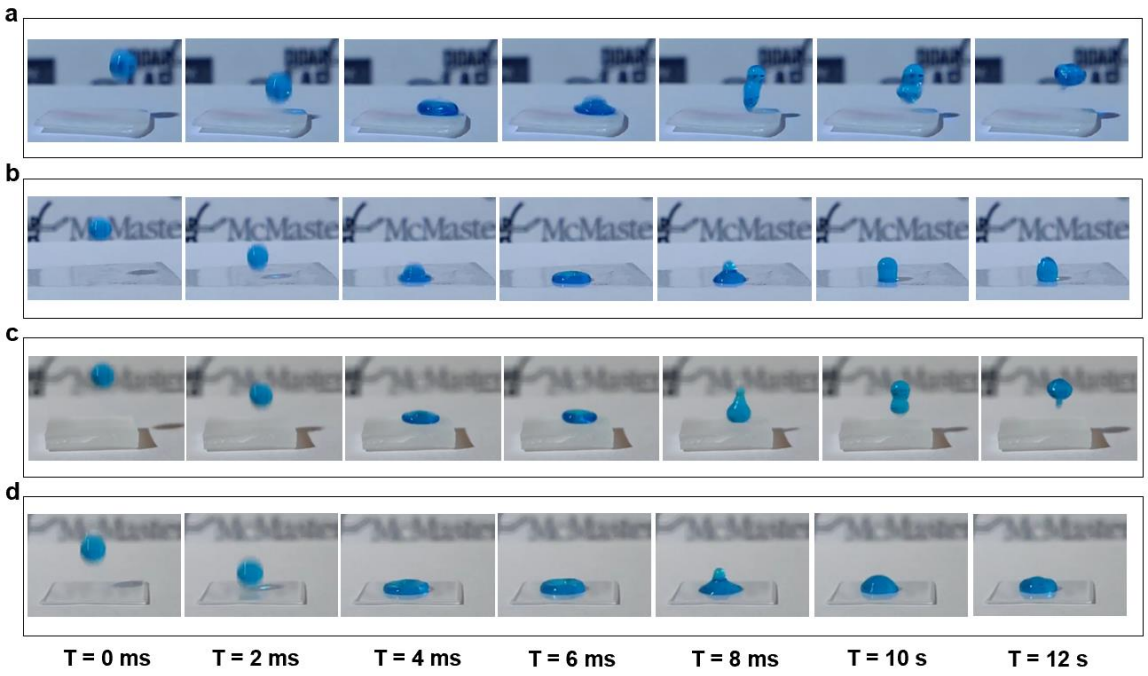

Supplementary Figure 3.10 *Images of Pinning and bouncing of droplets*

Slow-motion snapshots of the dynamic interaction of different surfaces with a 10 µL water droplet. Snap shots are taken at 2 ms intervals over 12ms. a) PO-Hierarchical-FS. b) PO-Planar. c) PS-Hierarchical-FS. d) PS-Planar. Full video of each sample can be seen in Supplementary Video 1-8. As discussed in Supplementary Note 3, the decrease in the contact angle hysteresis for the PS-Hierarchical-FS and PO-Hierarchical-FS corresponds to lower adhesion and thus a reduction in the amount of pinning of droplets on the surface. For the PO-Hierarchical-FS and PS-Hierarchical-FS, a complete release of the water droplet after contact with the surface is seen. For the PS-Planar and PO-Planar, complete pinning of the water droplet to the substrate occurs. Overall the introduction of both the micro and nano hierarchical structures on our flexible wraps had a large impact on the repulsion of liquids under different dynamic conditions. This dynamic repulsion and

release of water from surfaces is important when discussing self-cleaning properties as many of the interactions between liquids and surfaces do not occur under static conditions.

Resiliency test	Sliding angle post resiliency test
3 hours vacuum	<5°
3 hour sonication in ethanol	<5°
2 hour incubation in bleach	<5°

Supplementary Table 3.1 *Resiliency tests on hierarchical surfaces. Demonstrating repellency by maintaining their low sliding angle.*

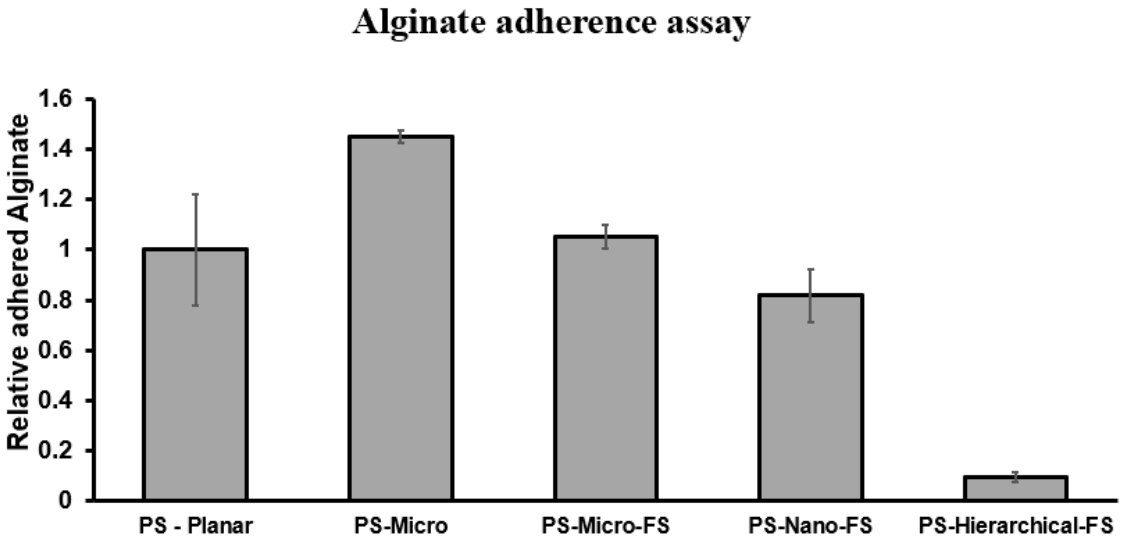

Supplementary Figure 3.11 *Relative alginate adherence. Extracellular polymeric substance (EPS) of bacteria such as Pseudomonas aeruginosa, has shown to be rich in alginate, a polysaccharide which substantially contributes to antibiotic resistance, persistence, and attachment of the biofilm to solid surfaces [21,22]. Furthermore, effect of alginate has extensively been studied as a fouling substance in different applications, such as studying membrane efficacy and fouling in various conditions for application such as waste water treatments. [23–25] To investigate the developed hierarchical surfaces repellency towards alginate, each treated or untreated polystyrene sample was submerged in alginate solution and the amount of the adhered alginate was evaluated. PS-Hierarchical-FS*

surfaces, demonstrated a significantly lower amount of alginate adhered to them which is about 10 times decreased compared to the other control groups (PS-Planar, PS-Micro, PS-Micro-FS, and PS-Nano-FS).

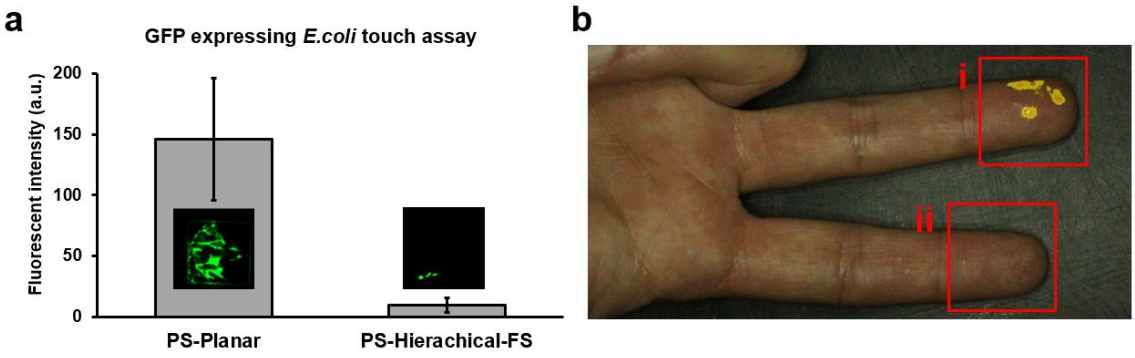

Supplementary Figure 3.12 *GFP expressing E.coli touch assay on polystyrene. (a) Touch assay on pristine and hierarchical polystyrene surfaces, demonstrating repellency of the PS-Hierarchical-FS toward bacteria's contact. Error bars represent means ± SD of at least three samples. (b) bacteria transfer from contaminated PS-planar (i) and PS-Hierarchical-FS (ii) to human skin.*

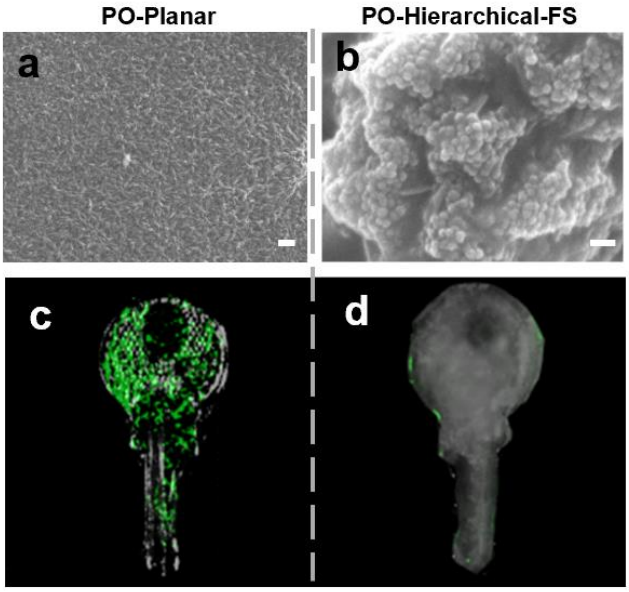

Supplementary Figure 3.13 *E. coli transfer to a wrapped key. (a) and (b) representative SEM images of PO surfaces. (c) and (d) GFP expressing E.coli touch assay on hierarchical and pristine polyolefin surfaces, demonstrating repellency of the PS-Hierarchical-FS toward bacteria's contact.*

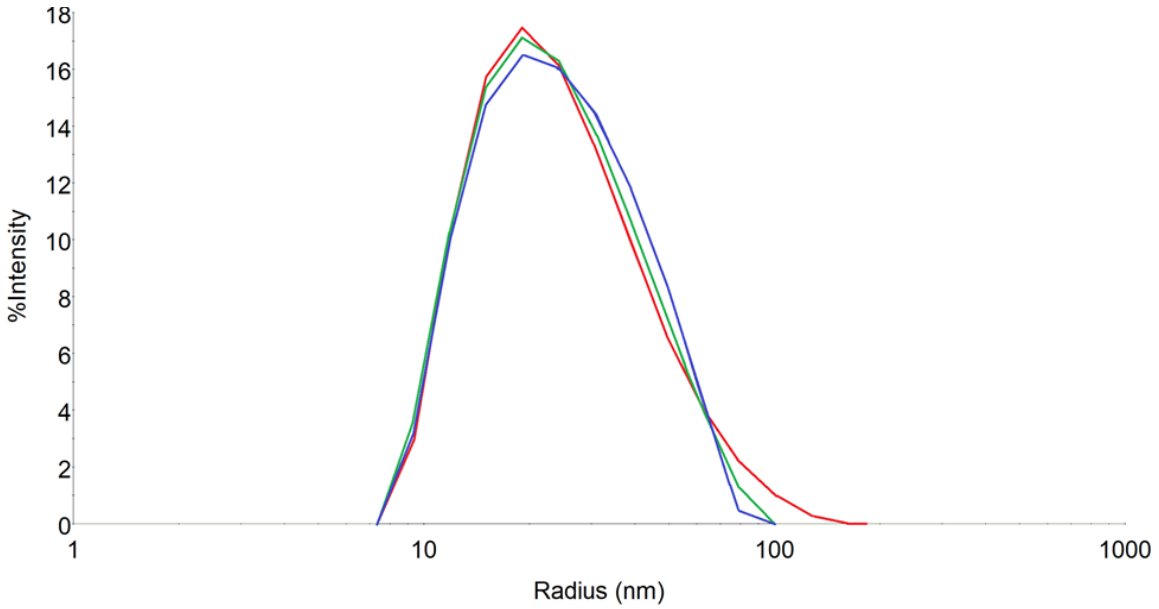

Supplementary Figure 3.14 *DLS measurements for SiNP. The peak of each measurement is the radius of the particles in the solution (3 different particle solutions were used). Solutions containing particles of different radii will have multiple peaks. Here, we have one distinct peak which is at 27±0.6 nm.*

Supplementary Videos:

Available at: ACS Nano

- File Name: Supplementary Video_1:
  - Description: 10 µl of Water dropped onto PS-Planar from one inch at 480 fps. As such, when the droplet meets the surface of the the PS-Planar it begins to spread out but is pulled back together by the surface tension of the water. This droplet remains pinned to the surface of the PS-Planar.
- File Name: Supplementary Video_2:
  - Description: 10 µl of Hexadecane dropped onto PS-Planar from one inch at 480 fps. Complete wetting of the surface from hexadecane is seen. As the droplets meets the surface the droplet begins to spread evenly across the surface until fully wetted and remains in this state.
- File Name: Supplementary Video_3:
  - Description: 10 µl of Water dropped onto PS-Hierarchical-FS from one inch at 480 fps. As the droplet meets the surface of the PS-Hierarchical-FS, it spreads out across the surface and is pulled back together by the surface tension of the water. Unlike hexadecane, the surface tension of water is much greater allowing the water droplet to return to a spherical shape and dislodge from the surface completely, resulting in the droplet bouncing off

the surface. Furthermore, the post-interactions of the droplet with the surface, even though having a lower velocity, results in the droplet bouncing off the surface with a lower amplitude.

- File Name: Supplementary Video_4:
  - Description: 10 µl of Hexadecane dropped onto PS-Hierarchical-FS from one inch at 480 fps. Unlike the PS-Planar, the addition the hierarchical structures on the surface prevents the full wetting of the hexadecane on the surface. As such, when the droplet meets the surface of the of the PS-Hierarchical-FS, it begins to spread out but is pulled back together by the surface tension of the hexadecane, due to the apparent reduction in the surface energy, thus returning the droplet to a spherical shape on the surface. This shows further oleophobic behaviors of the surfaces under dynamic conditions.
- File Name: Supplementary Video_5:
  - Description: 10 µl of Water dropped onto PO-Planar from one inch at 480 fps. As such, when the droplet meets with the surface of the PO-Planar it begins to spread out but is pulled back together by the surface tension of the water, because PO is slightly hydrophobic the water droplet returns to a semi-spherical shape on the surface. This droplet remains pinned to the surface of the PO-Planar and is not repelled from it.
- File Name: Supplementary Video_6:
  - Description: 10 µl of Hexadecane dropped onto PO-Planar from one inch at 480fps. Complete wetting of the surface from hexadecane is seen. As the droplets meet the surface, the droplet begins to spread evenly across the surface until fully wetted and remains in this state.
- File Name: Supplementary Video_7:
  - Description: 10 µl of Water dropped onto PO-Hierarchical-FS from one inch at 480 fps. As the droplet meets the surface of the PO-Hierarchical-FS the droplet spreads out across the surface and is pulled back together by the surface tension of the water. Unlike hexadecane, the surface tension of water is much greater allowing the water droplet to return to a spherical shape and dislodge from the surface completely, resulting the droplet bouncing off the surface. Furthermore, the post-interactions of the droplet with the surface, even though having a lower velocity, results in the droplet bouncing off the surface with a lower amplitude.
- File Name: Supplementary Video_8:
  - Description: 10 µl of Hexadecane dropped onto PO-Hierarchical-FS from one inch at 480 fps. Unlike the untreated pre-strained polyolefin, the

addition the hierarchical structures on the surface prevents the full wetting of the hexadecane on the surface. As such, when the droplet meets the surface of the of the PO-Hierarchical-FS it begins to spread out but is pulled back together by the surface tension of the hexadecane, due to the apparent reduction in the surface energy, thus returning the droplet to a spherical shape on the surface. This shows further oleophobic behaviors of the surfaces under dynamic conditions.

- File Name: Supplementary Video_9:
  - Description: Slow motion video of water continuously running from a water bottle on top of a PO-Hierarchical-FS surface, demonstrating bouncing and rolling off of the water droplets.
- File Name: Supplementary Video_10:
  - Description: Implementing the developed surface for food packaging, showing wrapped meat with polyolefin (PO-Planar and PO-Hierarchical-FS). The water droplets bounce off the treated surface and get stuck on the untreated PO.

3.10.1 References for Supplementary Information for Flexible Hierarchical Wraps Repel Drug Resistant Gram Negative and Positive Bacteria

(1) Lin, S.; Lee, E. K.; Nguyen, N.; Khine, M. Thermally-Induced Miniaturization for Micro- and Nanofabrication: Progress and Updates. *Lab Chip* **2014**, *14*, 3475–3488.

(2) Chan, Y.; Skreta, M.; McPhee, H.; Saha, S.; Deus, R.; Soleymani, L. Solution-Processed Wrinkled Electrodes Enable the Development of Stretchable Electrochemical Biosensors. *Analyst* **2019**, *144*, 172–179.

(3) Teare, D. O. H.; Emmison, N.; Ton-That, C.; Bradley, R. H. Cellular Attachment to Ultraviolet Ozone Modified Polystyrene Surfaces. *Langmuir* **2000**, *16*, 2818–2824.

(4) Howarter, J. A.; Youngblood, J. P. Optimization of Silica Silanization by 3-Aminopropyltriethoxysilane. *Langmuir* **2006**, *22*, 11142–11147.

(5) Shillingford, C.; MacCallum, N.; Wong, T.-S.; Kim, P.; Aizenberg, J. Fabrics Coated with Lubricated Nanostructures Display Robust Omniphobicity. *Nanotechnology* **2013**, *25*, 14019.

(6) Gabardo, C. M.; Adams-McGavin, R. C.; Fung, B. C.; Mahoney, E. J.; Fang, Q.; Soleymani, L. Rapid Prototyping of All-Solution-Processed Multi-Lengthscale Electrodes Using Polymer-Induced Thin Film Wrinkling. *Sci. Rep.* **2017**, *7*, 42543.

(7) Li, D.; Neumann, A. Contact Angles on Hydrophobic Solid-Surfaces and Their Interpretation. *J. Colloid Interface Sci.* **1992**, *148*, 190–200.

(8) Wenzel, R. N. Resistance of Solid Surfaces to Wetting by Water. *Ind. Eng. Chem.* **1936**, *28*, 988–994.

(9) Cassie, A. B. D.; Baxter, S. Wettability of Porous Surfaces. *Trans. Faraday Soc.* **1944**, *40*, 546.

(10) Kota, A. K.; Kwon, G.; Tuteja, A. The Design and Applications of Superomniphobic Surfaces. *Npg Asia Mater.* **2014**, *6*, e109.

(11) Milne, A. J. B.; Amirfazli, A. The Cassie Equation: How It Is Meant to Be Used. *Adv. Colloid Interface Sci.* **2012**, *170*, 48–55.

(12) Herminghaus, S. Roughness-Induced Non-Wetting. *Eur. Lett.* **2000**, *52*, 165–170.

(13) Nosonovsky, M. Multiscale Roughness and Stability of Superhydrophobic Biomimetic Interfaces. *Langmuir* **2007**, *23*, 3157–3161.

(14) Marmur, A. From Hygrophilic to Superhygrophobic: Theoretical Conditions for Making High-Contact-Angle Surfaces from Low-Contact-Angle Materials. *Langmuir* **2008**, *24*, 7573–7579.

(15) Tuteja, A.; Choi, W.; Mabry, J. M.; McKinley, G. H.; Cohen, R. E. Robust Omniphobic Surfaces. *Proc. Natl. Acad. Sci. U. S. A.* **2008**, *105*, 18200–18205.

(16) Epstein, A. K.; Pokroy, B.; Seminara, A.; Aizenberg, J. Bacterial Biofilm Shows Persistent Resistance to Liquid Wetting and Gas Penetration. *Proc. Natl. Acad. Sci.* **2011**, *108*, 995 LP – 1000.

(17) Gao, L.; McCarthy, T. J. Contact Angle Hysteresis Explained. *Langmuir* **2006**, *22*, 6234–6237.

(18) Lafuma, A.; Quéré, D. Superhydrophobic States. *Nat. Mater.* **2003**, *2*, 457–460.

(19) Wooh, S.; Vollmer, D. Silicone Brushes: Omniphobic Surfaces with Low Sliding Angles. *Angew. Chemie Int. Ed.* **2016**, *55*, 6822–6824.

(20) Extrand, C. W.; Gent, A. N. Retention of Liquid Drops by Solid Surfaces. *J. Colloid Interface Sci.* **1990**, *138*, 431–442.

(21) Boyd, A.; Chakrabarty, A. M. *Pseudomonas Aeruginosa* Biofilms: Role of the Alginate Exopolysaccharide. *J. Ind. Microbiol.* **1995**, *15*, 162–168.

(22) Hall-Stoodley, L.; Costerton, J. W.; Stoodley, P. Bacterial Biofilms: From the Natural Environment to Infectious Diseases. *Nat. Rev. Microbiol.* **2004**, *2*, 95.

(23) Herzberg, M.; Kang, S.; Elimelech, M. Role of Extracellular Polymeric Substances (EPS) in Biofouling of Reverse Osmosis Membranes. *Environ. Sci. Technol.* **2009**, *43*, 4393–4398.

(24) Mi, B.; Elimelech, M. Organic Fouling of Forward Osmosis Membranes: Fouling Reversibility and Cleaning without Chemical Reagents. *J. Memb. Sci.* **2010**, *348*, 337–345.

(25) Hashino, M.; Katagiri, T.; Kubota, N.; Ohmukai, Y.; Maruyama, T.; Matsuyama, H. Effect of Membrane Surface Morphology on Membrane Fouling with Sodium Alginate. *J. Memb. Sci.* **2011**, *366*, 258–265.

4 Chapter 4: Hierarchical structures, with submillimeter patterns, micrometer wrinkles, and nanoscale decorations, suppress biofouling and enable rapid droplet digitization

Sara M. Imani, Roderick Maclachlan, Yuting Chan, Amid Shakeri, Leyla Soleymani*, Tohid F. Didar*

Small 2020, 16(50), 2004886, doi: 10.1002/smll.202004886

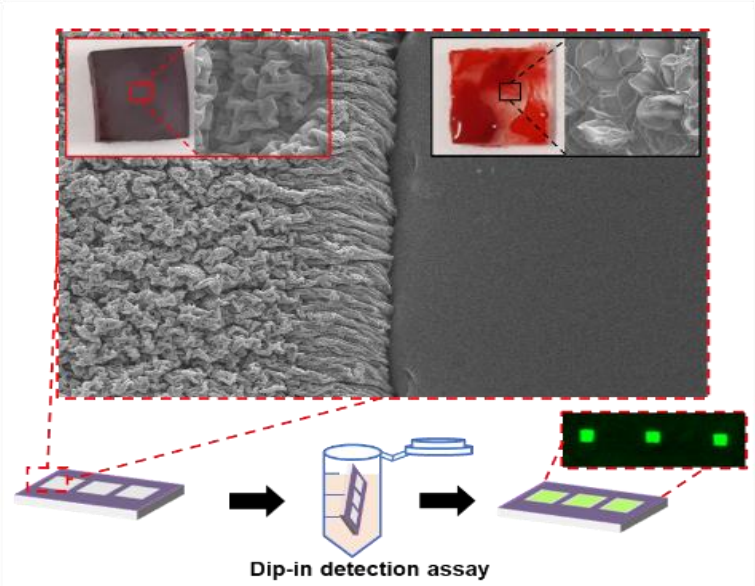

Preface

Objective B

In this chapter an all solution-based fabrication method is introduced to create hierarchical structures as a blood repelling material. In this study the importance of having hierarchical structures for blood repellency and inhibition of clot formation was explored. Furthermore, as the fabrication method is facile, patterning hydrophilic regions was integrated into the

hierarchical surface for droplet compartmentalization and a dip-based rapid biosensing platform.

4.1 Abstract

Liquid repellant surfaces have been shown to play a vital role for eliminating thrombosis on medical devices, minimizing blood contamination on common surfaces as well as preventing non-specific adhesion. Herein, we report an all solution-based, easily scalable method for producing liquid repellant flexible films, fabricated through nanoparticle deposition and heat-induced thin film wrinkling that suppress blood adhesion, and clot formation. Furthermore, we have combined superhydrophobic and hydrophilic surfaces onto the same substrate using a facile streamlined process. The patterned superhydrophobic/hydrophilic surfaces showed selective digitization of droplets from various solutions with a single solution dipping step, which provides a route for rapid compartmentalization of solutions into virtual wells needed for high-throughput assays. This rapid solution digitization approach was demonstrated for detection of Interleukin 6. The developed liquid repellant surfaces are expected to find a wide range of applications in high-throughput assays and blood contacting medical devices.

4.2 Introduction

Biofouling, coagulation and thrombosis are undesirable effects that occur when blood comes into contact with the surfaces of *in vitro*, *ex vivo*, and *in vivo* biomedical devices. [1]

These processes are initiated by the non-specific adsorption of blood proteins on surfaces and the formation of a complex protein layer. [2] To address this issue, surface modification strategies have focused on using bioinert polymers, [3–6] antithrombotic agents, [7–12] or changing the surface charge, wettability, chemical affinity and hydrophilicity. [13–17] Anticoagulants such as heparin have been widely used as coatings on biomedical devices to overcome these adverse effects. [18] Heparin-coated surfaces typically operate through either the release of heparin into the blood stream for inhibiting clotting in the vicinity of the device surface or reducing coagulation *via* immobilized heparin on the surface of the device. Anticoagulant coatings fail over time due to leaching and the loss of anticoagulant activity. Furthermore, administration of anticoagulants (*e.g.* heparin) both as a coating and a chronic medication, enters the bloodstream, elevating the risk of life-threatening heparin-induced thrombocytopenia (HIT), reported to occur in 1-5% of surgical patients. [19]

Recently, omniphobic coatings have been introduced on the surface of biomedical devices for reducing biofouling and the resultant blood coagulation, [20–29] while minimizing the administration of anticoagulants. [30] Liquid infused surfaces are one of the recent classes of omniphobic surfaces which have shown to significantly suppress biofouling and thrombosis with their performances surpassing previous anticoagulant based strategies in terms of longevity under blood flow, and anti-biofouling ability. [20–25,27–30] However, in order for these surfaces to sustain their omniphobic and repellent properties, the lubricant layer must be stable on the surfaces, making them difficult to use in open-air applications where the lubricant is susceptible to evaporation. [31] Another class of omniphobic surfaces are those with structural modifications wherein the micro- and nano-scale topography of

the surface provides omniphobic properties. Through the formation of micro, nano and hierarchical structures, air pockets are trapped within the features, leading to the formation of a Cassie wetting state, which reduces the apparent surface energy seen by liquids, [32] resulting in elevated contact angles and low sliding angles which lead to omniphobicity. [32] Additionally, the formation of the Cassie state reduces the effective surface area to which platelets and proteins in blood can bind to, and decreases shear stress at the surfaces reducing platelet adhesion. These two effects reduce the number of nucleation sights for thrombin generation. [33] Hydrophilic polymer surfaces have also shown significant antifouling properties and blood compatibility through the reduction of fibrinogen and platelet adhesion. As a result of the hydrophilicity of these surfaces, blood can still easily stain them, which can spread blood related pathogens between healthcare workers and patients. [34,35]

In spite of great performance demonstrated by several classes of hierarchically-structured omniphobic surfaces for reducing blood-related contamination (including sand-casting of SiO_2 and PDMS, [36] electrochemical anodization of titania, [37] and laser ablated stainless steel and titanium), [38] these high performance structures are fabricated using molds, electrodeposition or laser ablation, which are material dependent, difficult to scale and/or costly (due to material choice and equipment cost and upkeep). Hierarchical structures have recently been developed using a series of bottom up fabrication processes such as electrophoretic deposition, [39] emulsion templating, [40] electrospinning, [41] electrochemical techniques, [42] and reactive ion etching. [43] Among these, methods that allow for controlling the materials architecture over a range of length scales *and* can be

manufactured using easy-to-scale processes are highly desirable for creating application-specific omniphobic materials and translating these to real-life biomedical devices. In response, we sought to develop easy-to-scale hierarchical materials that combine tunable materials in the microscale, nanoscale, and molecular scale.

Nanoparticle-induced microscale wrinkling (NMW) is a process that uses the self-assembly of nanoparticles on pre-strained substrates followed by the application of strain to create microscale wrinkles with nanoscale features. [44] The nanoparticle size controls the nanoscale features and the size of the secondary microscale wrinkles, delivering tunability over multiple length scales. Such hierarchical structures, when combined with molecular layers, have demonstrated remarkable omniphobicity (water and hexadecane contact angles > 163° and 101° respectively, and sliding angles > 5°). [45,46] Additionally, this method is compatible with batch scale solution-processing, which is widely used for large volume manufacturing.

Herein, we focus on developing liquid repellant hierarchical materials based on NMW and applying these to surfaces for reducing blood adhesion and coagulation with potential for use in *in vivo* systems like catheters and *in vitro* devices such as biosensors. We further tested the developed technology in dynamic systems (*e.g.* microfluidic devices) to assess the extent of blood adhesion. These materials are patterned on surfaces to spatially modulate their repellency for creating biosensing arrays integrating hydrophilic and superhydrophobic regions. This approach led to a strategy for one-step and instrument-free droplet digitization and was used in a proof-of-concept dip-based Interleukin 6 (IL-6) detection chip, demonstrating the application of our approach for use in *in vitro* biomedical

devices. This opens up a platform to utilize such devices in in vitro biosensing assays in complex fluids where shorter amount of contact time is needed.

4.3 Results and discussion

4.3.1 Fabrication and characterization of hierarchical liquid repellant surfaces

In order to create hierarchically-structured surfaces using NMW, we designed a fabrication process (**Figure 4.1a**) in which gold nanoparticles (AuNPs) modified with a molecular fluorosilane (FS) layer for reducing surface energy were deposited on the surface of a pre-strained polymer substrate (Figure 4.1b,i) to create a stiff layer (Figure 4.1b,ii). Upon shrinking, this stiff layer transformed into a hierarchical surface combining nanoscale features with microscale wrinkles (Figure 4.1b,iii).

The fabrication process started with surface activation of pre-strained polystyrene (PS) using ultraviolet-Ozone (UVO) treatment to induce hydroxyl groups on PS (Figure 4.1a,ii) for subsequent surface functionalization with (3-Aminopropyl)triethoxysilane (APTES) (Figure 4.1a,iii). Following APTES deposition, 12 nm AuNPs were bound to the surface through the electrostatic interactions of the amine terminus of APTES and the citrate surfactants present on AuNPs (Figure 4.1a,iv). [47,48] A self-assembled monolayer (SAM) of fluorosilane (FS) was then covalently attached to the surface through hydrolysis and condensation reactions using APTES as an intermediate linker (see methods for more information, Figure. 1a,v), which generated a nanostructured surface using AuNPs as building blocks (PS-AuNP-Planar). The PS-AuNP-Planar substrate was then shrunk at 145^{o} C for 10 minutes to induce hierarchical structuring (PS-AuNP-Shrunk, Figure 4.1a,vi).

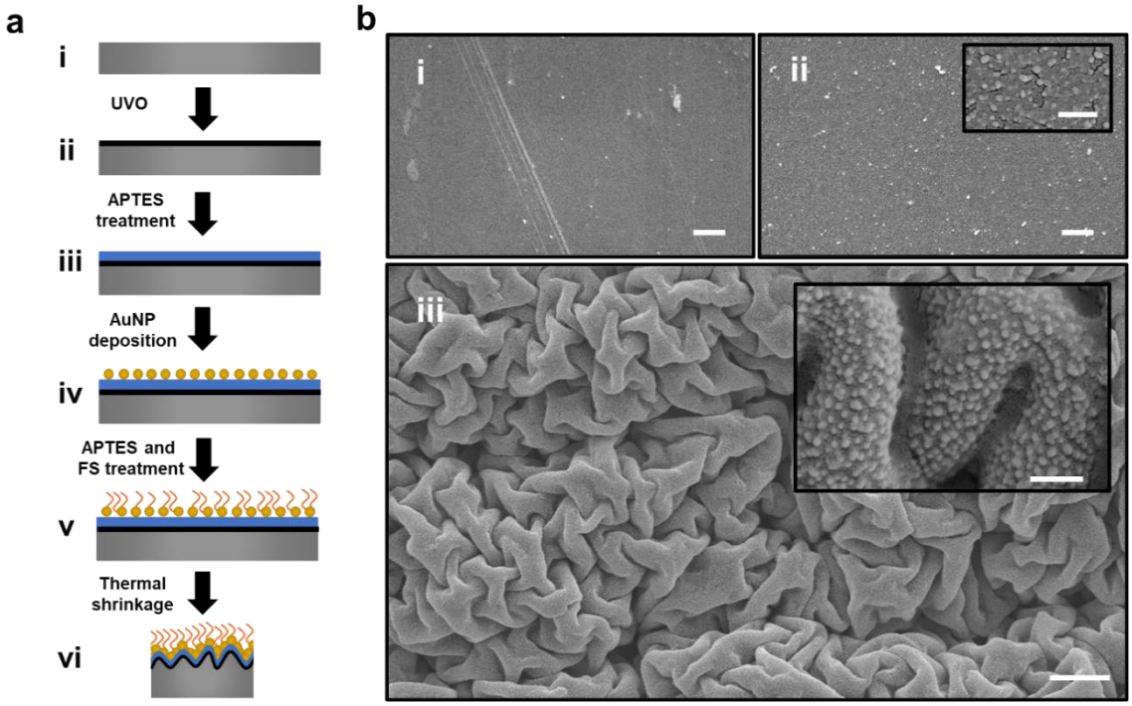

Figure 4.1 Schematic depicting the fabrication process of liquid repellant surfaces and corresponding SEM images. *a) Process steps for the formation of the AuNP decorated surface and the hierarchically structured surfaces. b) SEM images depicting the untreated PS (i), AuNP decorated PS (ii, PS-AuNP-Planar), and final hierarchically-structured PS (iii, PS-AuNP-Shrunk). The scale bars in the larger SEM images represent 1 μm and those in the insets represent 100 nm.*

The repellency of PS-AuNP-Planar and PS-AuNP-shrunk was evaluated alongside the untreated polystyrene (PS-planar), polystyrene substrate after shrinking (PS-shrunk), and polystyrene substrate after fluorosilinizaiton (PS-FS-Planar) by measuring contact angles (CA) using various test liquids, as well as sliding angles (SA) (**Figure 4.2a**). In order to understand the hydrophobic and oleophobic properties, the CA of the surfaces were assessed using the following test liquids: milli-Q grade water (surface tension of 72.75 mJ/m^2), [49] hexadecane (surface tension of 27.76 mJ/m^2), [49] human whole blood (surface tension of approximately 55 mJ/m^2) [50] and various ethanol/water concentrations (%v/v).

The hydrophobicity of the various surfaces created here was evaluated by measuring the water contact angle (Figure 4.2a) Both unmodified surfaces, PS-Planar and PS-Shrunk, showed a hydrophilic behavior (CA of 79±1.3° and 78±5.1° respectively). The successful FS treatment was verified by the observed elevation in the CA for the PS-FS-Planar (96±3.8°) compared to PS-Planar. Coating the substrate with nanoparticles (PS-AuNP-Planar) increased the surface roughness and introduced re-entrant texture. This surface roughness introduced an effective Cassie wetting state and increased the apparent CA (water CA of 127±9.4°). [51,52] The water CA and contact angle hysteresis was then further improved (149.5±4°, 10.7±4.3° with advancing and receding CA of 160.6±0.6 and 149.9±3.7 respectively)) through the formation of hierarchical structures (PS-AuNP-Shrunk). When these surfaces were transformed into a cylinder (radius of curvature o was 5.5 mm), they sustained their CA (154.23±0.55), as well as their slippery behavior (Supplementary Video 1) with a contact angle hysteresis of 9.45±2.7 (advancing and receding CA 148.6±3.93 and 139.2±1.3 respectively). The smallest radius of curvature that was manufacturable with the polystyrene substrates was 2.25 mm radius and the repellent behavior was maintained while showing no fractures on the surface of the bent surfaces.

The hexadecane contact angle was also evaluated to test for oleophobicity for all the different classes of surfaces. The PS-planar and PS-shrunk surfaces were both completely wetted by hexadecane; however, the introduction of fluorosilane (PS-FS-Planar) and nanoparticles to the surface (PS-AuNP-Planar) increased the CA to 62±2.4° and 69±6°, respectively. Through the introduction of hierarchical structures (PS-AuNP -Shrunk), the surfaces were brought into the oleophobic regime with a hexadecane CA of 116±3°.

The heparinized blood CA was also measured to gain insight into the interaction of our oleophobic surfaces with complex liquids. With the introduction of these structures an increase from 83±4.5° (PS-Planar) to 138±3.1°(PS-AuNP-Shrunk) was seen. Overall, the formation of hierarchical structures combined with chemical modification demonstrated liquid repellency due to the high CAs recorded for this class of surfaces with various test liquids. This effect can be explained by the higher amounts of trapped air within the hierarchical structure compared to the other control groups. [53]

In order to gain a greater understanding and indication of the functional range of repellency with regards to liquid surface tensions for each of the surface topographies, the CA was measured for different water/ethanol concentrations, ranging from the surface tension of water 72.86 mN/m to ethanol 22.39 mN/m (at room temperature). As seen in Figure 4.2b, the hierarchical surfaces were able to maintain contact angles greater than 90° for ethanol concentrations of 80% and lower indicating that the surfaces remain repellent towards liquids with surface tension of 24.32 mN/m (80% ethanol) [54] and above, unlike the PS-FS-Planar and the PS-AuNP-Planar substrates which demonstrated CAs below 90° after 0% and 30% ethanol, respectively. Additionally, for an ethanol/water mixture with similar surface tension to hexadecane (60% ethanol) we can observe a similar contact angle of ~120º for both liquids using the PS-AuNP-Shrunk surfaces and ~70º for the PS-AuNP-Planar. However, this was not the case for the PS-FS-Planar surfaces, indicating the significance of micro and nanostructures on the generation of oleophobicity.

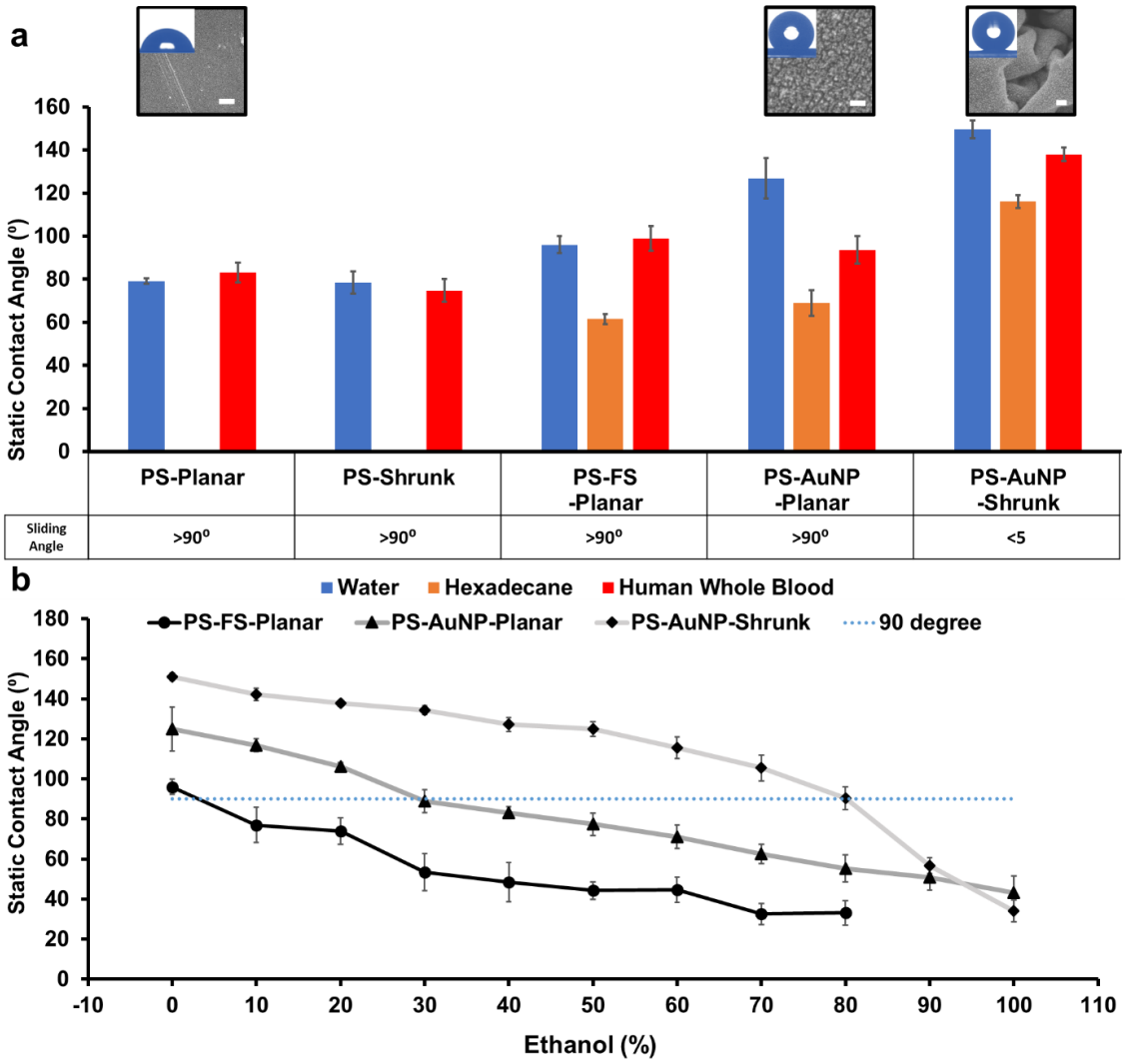

Figure 4.2 Surface Repellency. *a) Graph depicting the contact angle of different surfaces for water (blue), hexadecane (orange), and whole blood (red). Representative SEM images are also shown on the top with an image of the water droplet on the surface. The table shows the sliding angles of the different control groups. b) Graph showing the change in contact angle with varying ethanol concentrations in water. Dotted line at 90 degrees shows the point where surfaces enter the hydrophilic regime.*

The ability of the fabricated surfaces in repelling liquid droplets was further assessed by measuring the sliding angle, which is a key metric for classifying surfaces as repellant (Figure 4.2a). Among the investigated surfaces, only PS-AuNP-Shrunk demonstrated

droplets sliding off with sliding angles below 5°, which can be attributed to the roughness of the hierarchical surfaces (Figure 4.1b,iii) such that the formation of the Cassie state and the entrapment of air-pockets within the texture allow for the water droplets to only contact discrete sections of the surface. [55] These discrete contact patches decrease the adhesive forces experienced by the droplets, allowing the droplet to easily detach from the surface. To test the performance of the hierarchical surface for extended amounts of time in heparinized blood, the surfaces were incubated in heparinized blood for 48 hours and subsequently washed twice and dried. The surfaces were examined for their water contact angle following the blood incubation, demonstrating a water contact angle of 140.3±8.2 (compared to 149.5±4 before) which is in the hydrophobic region showing that their hydrophobic characteristic is resilient after a long incubation time in blood.

To assess the adhesion of the coating to the substrate and to test the resilience of the coating, we performed an adhesion test according to ASTM standard. In this method, two perpendicular cuts were made and subsequently brushed and taped over to clean the incision parts. Based on the smooth edges following the incision, we concluded that our surfaces demonstrated a 5B classification, which stands for the highest level of adhesion (Supplementary Figure 4.6)

4.3.2 Interaction of hierarchical surfaces with human whole blood (heparinized and citrated)

In order to understand the interaction of the various surfaces developed here with anticoagulated whole blood, we evaluated the repellant behavior of the surfaces under

conditions that are important for blood contacting medical devices and implants such as clot formation and blood adherence (blood stain). These *in vitro* assays might not completely mimic the complex environment in *in vivo* studies such as animal tests, but still has been proved to be important for assessing surfaces behavior. [56] The staining assay was designed to investigate the amount of blood that was sticking to each surface and see the extent by which the hierarchical surfaces attenuate staining (**Figure 4.3a**). In this assay, the surfaces were submerged in heparinized human whole blood (Supplementary Video 2) and were subsequently agitated in PBS to quantify the extent of blood adhesion using spectrophotometry (Figure 4.3a). The results revealed that the hierarchical surfaces (PS-AuNP-Shrunk) reduced blood adherence by over 90% compared to the untreated polystyrene surfaces (PS-Planar and PS-Shrunk). The PS-FS-Planar surface showed a 13% increase in blood adhesion which is due to the hydrophobic-hydrophobic interaction of these class of surfaces with proteins present in blood. [57] Furthermore, PS-AuNP-Planar surfaces reduced blood adhesion by 29% compared to the untreated samples. We also visually inspected these surfaces after incubating them in heparinized human whole blood for 30 minutes followed by rinsing them with water (Figure 4.3a). The blood repellency of the hierarchical surfaces (PS-AuNP-Shrunk) was visually evident. All surfaces remained stained after washing; however, the hierarchical surface did not contain a *visible* stain. It should be noted that the presence of AuNPs on the PS-AuNP-Planar and PS-AuNP-Shrunk surfaces resulted in the substrates having a grey hue, which made precise visual inspection difficult.

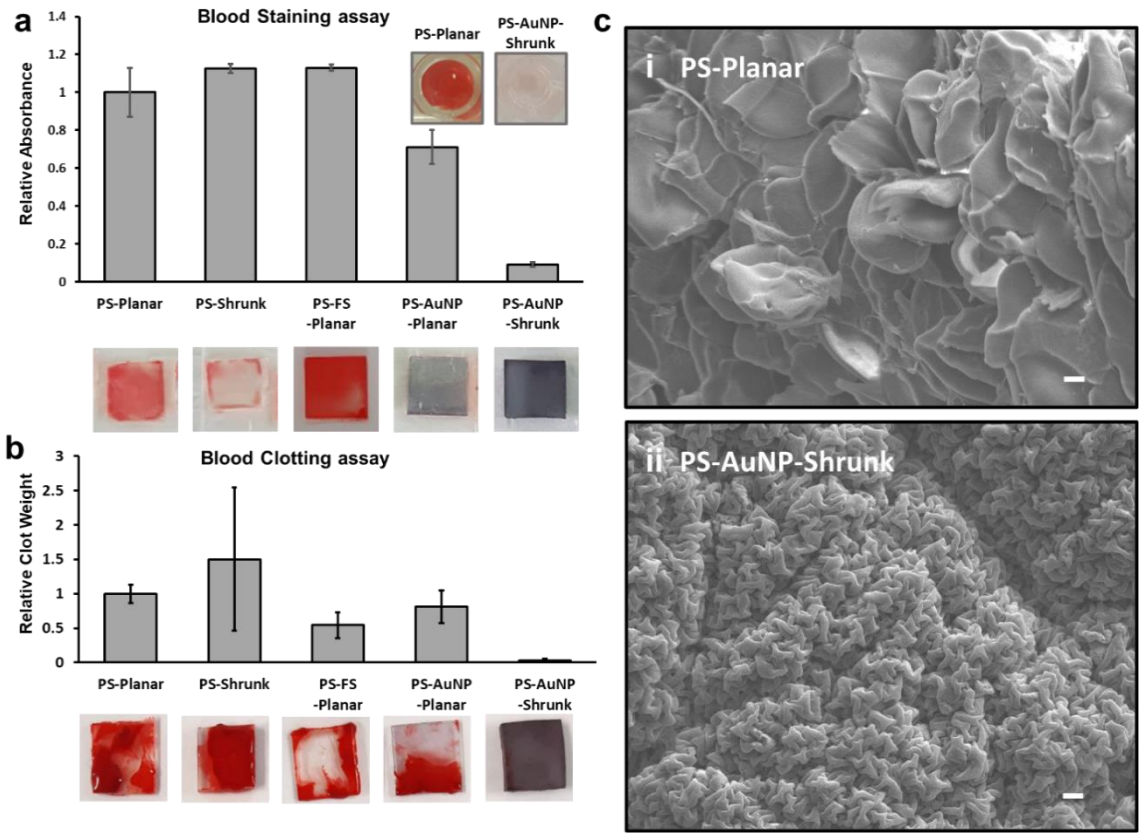

Figure 4.3 Study of blood repellency on the hierarchical surfaces. *a) All surfaces were incubated with blood for 30 minutes and after two washes, they were transferred to well plates containing water (transfer solution). The absorbance of the transfer solution was measured at 450 nm wavelength and normalized to the value obtained from PS-Planar. Representative images of the transfer wells corresponding to PS-Planar and PS-AuNP-Shrunk are shown at the top right of the figure. The representative images of the surfaces incubated in blood are shown at the bottom of the figure. b) Relative clot weight adhered to each surface is normalized to the adhered clot to the PS-Planar and compared to the other control groups. Representative images of samples are shown after being exposed to the clotting assay after a 2X PBS wash. Error bars represent standard deviation from the mean for the clot assay performed on at least three surfaces for each class. c) SEM images of the surfaces after the clotting assay and 2X PBS washes followed by fixation in 4% formaldehyde performed on the PS-Planar (i) and PS-AuNP-Shrunk (ii), demonstrating blood adherence to the planar surface. The scale bars represent 1 μm in (i) and (ii).*

In order to investigate the anticoagulant properties of the surface, they were subjected to citrated whole blood and the clotting was initiated by the introduction of calcium chloride

and two subsequent washes with phosphate buffered saline (PBS). The extent of adhered blood clots to each surface was verified by weighing the surfaces before and after the clotting assay. As shown in Figure 4.3b**,** the hierarchically-structured samples (PS-AuNP-Shrunk) significantly attenuated the adherence of blood clots compared to the PS-Planar and PS-AuNP-Planar surfaces. SEM imaging of the surfaces after the clotting assay demonstrated significantly lower blood cell accumulation and blood clot formation on hierarchically structured surfaces compared to the untreated surfaces (Figure 4.3cii**)**. These experiments demonstrate that the degree of liquid repellency determines the effectiveness of the surface in blood repellency, with PS-AuNP-Shrunk surfaces demonstrating superior performance in terms of superhydrophobicity, oleophobicity, and blood repellency compared to the other investigated surfaces. Furthermore, covalently coated self-assembled monolayers of FS, has been reported to be harmless [30,58] therefore, making our developed coating a promising candidate for real-life applications. However, long-term *in vivo* studies might be needed in the future to further confirm biocompatibility.

To investigate to behavior of the surfaces in dynamic conditions, we integrated the PS-AuNP-Shrunk surface in a microfluidic device and flowed heparinized blood through the channel. Subsequent to this, the channel was washed and imaged. As a control PS-Planar was also integrated into a microfluidic channel. The results showed significantly higher amount of blood cell adhesion within the channel on PS-Planar (23,200±2414 cell/mm2) than PS-AuNP-Shrunk (no cells were observed) (Figure 4.4a). This is also apparent in the acquired optical images (Figure 4.4a.i,ii) which a clear red stain is left in the PS-Planar channel. Furthermore, images obtained using optical microscopy indicate that blood cells

are visible in PS-Planar channel (Figure 4.4c,i), whereas in the PS-AuNP-Shrunk (Figure 4.4c,ii) the wrinkles are visible but there no blood cells found.

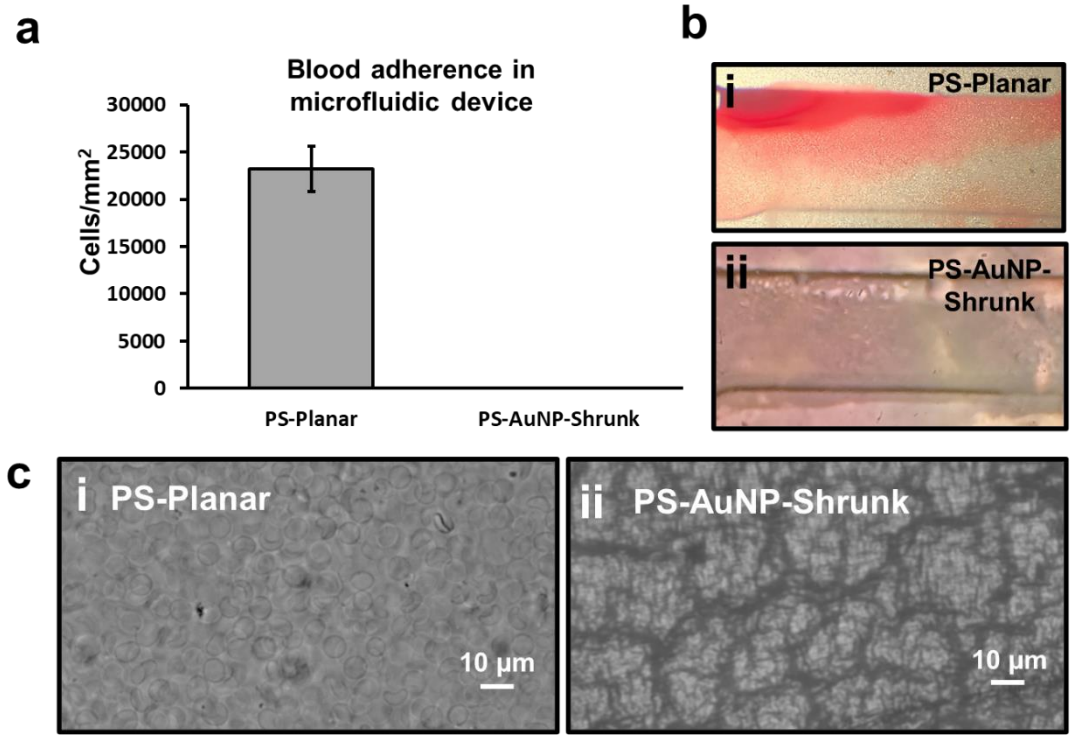

Figure 4.4 Dynamic conditions for blood adhesion tests. *a) number of blood cells per mm^2 in microfluidics channel subjected to heparinized blood flow and subsequent washing for both PS-Planar and PS-AuNP-Shrunk. b) Optical images showing blood adhesion in (i) PS-Planar and (ii) PS-AuNP-Shrunk. c) Bright-field microscope images comparing (i) PS-Planar (ii) PS-AuNP-Shrunk. Blood cells are visible in (i) and wrinkles are visible with no presence of blood cells in (ii).*

4.3.3 Patterned structures for digitizing droplets and dip-based bioassays

To further expand the application of the developed repellent surfaces, we introduced hydrophilic micro-patterns into the developed superhydrophobic surfaces through a benchtop masking method shown in the schematic in **Figure 4.5a.i-v**. Briefly, a vinyl mask

was patterned on the polystyrene surface using a craft cutter to protect the hydrophilic areas, while the substrate was modified with the nanoparticle and fluorosilane layers. The mask was then removed before heat shrinking the PS substrates. This method led to the development of hierarchical structures everywhere, except for the masked regions that retained their planar morphology upon shrinking because they did not possess a stiff surface layer. [59,60] The structural difference between the patterned area and the rest of the surface is clearly demonstrated in the SEM images in Figure 4.5b.

To demonstrate the capability of the patterned hydrophilic/superhydrophobic surfaces in digitizing water droplets they were dipped into aqueous solutions containing food colouring and fluorescent dyes (Figure 4.5c.ii-iii). We used this droplet digitization strategy to create a fluorescence biosensor for analyzing IL-6 (Supplementary Figure 4.7). To transform the patterned surfaces to biosensors, we first modified the hydrophilic areas with molecular linkers for antibody binding (APTES modification followed by 1-ethyl-3-(-3-dimethylaminopropyl) carbodiimide (EDC) and N-hydroxysuccinimide (NHS) bonding). [20,61] The hydrophilic areas were then functionalized with anti-IL6 capture antibodies. The assay was performed by dipping the biosensor into the target (IL-6) or control solutions (PBS), incubation for 60 minutes, washing the unreacted analyte, and dipping the biosensor into the solution of secondary antibodies modified with a Cy5 fluorescent label. In this assay, we observed a significant difference between the fluorescence intensity of the target and control solutions (Figure 4.5.e), demonstrating the potential of this materials-inspired digitization strategy for use in biosensing assays.

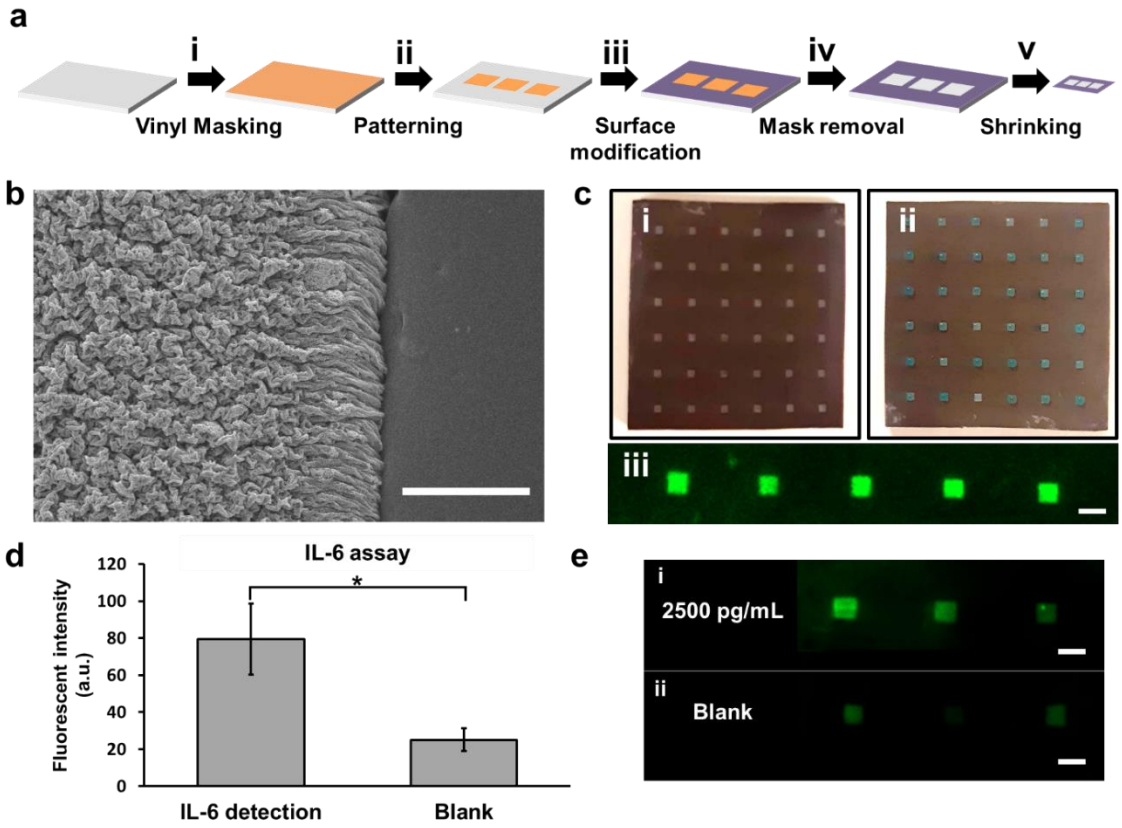

Figure 4.5 Digitization strategy enabled by patterning hydrophilic and liquid repellant areas *a) (i) the substrate is covered with a vinyl mask, (ii) the vinyl mask is patterned to create hydrophilic wells, (iii) the substrate is modified with nanoparticles and coated with fluorosilane, (iv) the mask is removed, (v) the substrate is shrunk. b) SEM images of the fabricated wells showing the planar (hydrophilic) and hierarchical liquid repellant regions (scale bar 1 µm). c) (i) shows patterned wells with planar (inside the squares) and modified regions. (ii) shows the patterned well after being dipped in blue dyed water, demonstrating digitization of water droplets (iii) digitizing Cy5-tagged anti IL-6 antibody on the patterned wells. d) IL-6 assay performed using 2500 pg/mL of target solution compared to control solutions by dipping the wells in solutions containing the assay components. Briefly, capture antibody was deposited on the wells through EDC-NHS chemistry, and then dipped in solution containing 2500 pg/mL IL-6. Subsequently, the sample was subjected in biotinylated IL-6 antibody and streptavidin dye. And for blank, all the steps were kept the same but for the IL-6 incubation. e) Representative fluorescent images of the assay used in (d).*

4.4 Conclusion

We have developed a scalable and low-cost method for producing patterned repellent surfaces. The repellency is created by introducing hierarchical structuring using nanoparticle-induced wrinkling designed to combine nanoscale features with microscale wrinkles. We demonstrated that hierarchical structuring results in superior performance in reducing blood coagulation and contamination compared to planar and nanostructured surfaces chemically-functionalized using fluorosilane. Furthermore, we introduced hydrophilic patterns into our substrate alongside the superhydrophobic areas, leading to virtual wells that can be used for the digitization of liquids in high throughput assays. The tunability of these surfaces allows for controlling the volume of the digitized drops as well as the localization of biomolecules. The facile fabrication method developed here can be applied to instances where both repellency and specificity are required for meeting functional requirements. This Cassie-based hierarchical surface (surface having hierarchical structures leading to Cassie state) opens up applications for *in vitro* assays in complex liquids, mainly for shorter periods of contact times (*e.g.* biosensing assays) for which Cassie state is satisfied.

4.5 Materials and Methods

Reagents. (3-Aminopropyl)triethoxysilane (99%) and 1H,1H,2H,2H-Perfluorodecyltriethoxysilane (97%), were purchased from Sigma-Aldrich (Oakville, Onatrio). Ethanol (anhydrous) was purchased from Commercial Alchohols (Brampton,

Ontario). Hydrochloric acid (36.5–38%) was purchased from Caledon (Georgetown, Ontario). Milli-Q grade water (18.2 MΩ) was used to prepare all solutions. Whole human blood was collected from healthy donors in BD heparinized tubes. All donors provided signed written consent and the procedures were approved by the McMaster University Research Ethics Board. Self-adhesive vinyl sheets (FDC 4304) were purchased from FDC graphic films (South Bend, Indiana). Streptavidin eFluor 660 was purchased from eBioscience (San Diego, CA). Recombinant human (*E. coli* derived) IL-6 was purchased from R&D systems (Minneapolis, MN). IL-6 monoclonal antibody (MQ2-13A5, capture antibody) and biotinylated IL-6 monoclonal antibody (MQ2-39C3, detector antibody) were purchased from ThermoFisher Scientific (ON, Canada).

Surface Fabrication. Using Robo Pro CE5000-40-CRP cutter (Graphtec America Inc., Irvine, California) pre-strained polystyrene (Graphix Shrink Film, Graphix, Maple Heights, Ohio) was cut into pieces. Polystyrene (PS) pieces then were cleaned with ethanol and milli-Q water and dried. In a pre-warmed UVO cleaner (UVOCS model T0606B, Montgomeryville, Pennsylvania), PS samples were placed and UVO treated for 4 mins. 12 nm gold nanoparticles (AuNPs) were synthesized as described elsewhere and were kept at 4°C until used. [44] Activated PS substrates were incubated on a shaker in 10% aqueous APTES (for creating the seed layer for nanoparticle solution for respected samples) for 3 hours at room temperature followed by sonication in water. To coat the AuNPs covered PS with fluorosilane, the substrates were first submerged in 10% aqueous APTES for 3 hours with agitation. The substrates were sonicated in milli-Q water for 10 minutes and dried. To

fluorosilanize the samples, a solution of ethanol and milli-Q water with volume ratio of 3:1 was prepared. A catalytic amount of hydrochloride acid (0.1 wt%) was added into the solution with 0.5 wt% of fluorosilane. The solution was incubated at 40° for an hour before use. [62] Following deposition of coating, the substrates were sonicated in Milli-Q water and subsequent 10 min sonication in ethanol for 10 minutes and dried (PS-AuNP-Planar). To add the microstructures to the nanoparticle treated surface, thermal treatment was performed by placing the substrates into an oven at 140°C for 5 minutes (PS-AuNP-Shrunk). As a control FS-treated planar surfaces, PS-Planar surfaces were FS treated in a similar method (PS-FS-Planar).

The patterned surfaces were fabricated in a similar way. Before the modification steps, a vinyl mask was placed on a clean (as described in the previous paragraph) PS sheet and cut in the desired pattern with the craft cutter. The vinyl was then removed from the regions where the treatment was required and the samples were subject to UVO treatment and the subsequent treatments while maintaining the vinyl mask on. After the final FS treatment, the vinyl mask was removed and the samples were subjected to heat treatment as described before. To enhance the hydrophilicity on the untreated regions, a 0.6 μL droplet of 12 M H_2SO_4 was deposited on the untreated regions, incubated for 10 minutes and subsequently washed 2 times with Milli-Q water.

Surface physical characterization. Scanning electron microscopy (SEM) imaging was performed in a JEOL 7000F. Samples were coated with 3 nm of platinum prior to imaging. For contact angle measurement a goniometer (OCA 20, Future Digital Scientific, Garden

City, NY) was used and water droplets were dispensed by automated syringe and other liquids by using A pipette. The sessile drop contact angle was provided via image processing software (Dataphysics SCA 20) through ellipse curve fit shape analysis of the droplets. Sliding angles were measured using a digital angle level (ROK, Exeter, UK). Each value was averaged over at least three measurements.

Whole human blood staining assay. Whole human blood was collected from healthy donors in BD heparinized tubes. All donors provided signed written consent and the procedures were approved by the McMaster University Research Ethics Board. Blood sessile drop contact angle was measured at room temperature using the goniometer. The extent of blood adherence was evaluated by dipping each sample in human whole blood and resuspending the adhered blood to each surface by transferring each substrate in a well and adding 700 µL of water. To ensure the adhered blood was transferred in solution, samples were placed on a shaker for 30 minutes. 200 µL of each well was transferred to a 96 well and the absorbance was measured at 450 nm wavelength on a SpectraMax plate reader. To ensure reproducibility, 6 samples per each condition was evaluated. Samples were also incubated in blood for 30 minutes and washed subsequently by dipping in water two times to evaluate the extent of stickiness of the surfaces.

Whole human blood clotting assay and scanning electron microscopy. In order to investigate the blood clot repellency properties, 500 µL of citrated human whole blood and 500 µL of 25 mM $CaCl_2$ in 1 M HEPES buffer were added to a 24 well containing the

treated samples and controls and incubated for 1 hour to allow for complete clot formation. Subsequently, samples were washed 2X with PBS. The quantification of the amount of the adhered clot was done by weighing the samples before and after the clotting assay. The weight difference was then reported in Figure 4.3b normalized to PS-Planar. The samples were fixed in 4% formaldehyde for 2 hours and coated with 3 nm Platinum. SEM was conducted to investigate blood clot formation and blood cell attachment.

Microfluidic channel and heparinized blood assay. Molds were created through vinyl (152.4 µm height) masking a PS surface and cutting the pattern for the channels with a craft cutter (2 mm width), then the molds were placed in a petri dish. PDMS (10:1) was poured on the created mold and cured over night at 60 degrees. The PDMS channels were then bonded to the PS-Planar or PS-AuNP-Shrunk through wet bonding. [63] This was done by creating a thin layer of PDMS (10:1) by depositing 400 µL PDMS in a petri dish and spin coating for 30 seconds at 7000 rpm. The PDMS channel was stamped on the spin coated layer then placed carefully on PS-Planar or PS-AuNP-Shrunk and cured overnight. For the heparinized blood assay, at 10 µL/min heparinized blood was flowed on PS-Planar or PS-AuNP-Shrunk for 30 minutes followed by a 10-minute wash. For evaluating the extent of blood adhesion, an optical image and bright field microscope image at 40X was acquired and the cells were counted.

Droplet digitization on patterned surfaces and volume measurement. The patterned surfaces were dipped in blue dyed water allowing the droplets to attach to the hydrophilic

patterns. The surfaces were also dipped in 8:1000 Cy5 tagged anti IL-6 antibody allowing the droplets to attach to the hydrophilic sites, this was confirmed by imaging the wells by a Chemidoc imaging system (BioInterface Institute, McMaster University) by Cy5 channel. The volumes were measured using image processing software (Dataphysics SCA 20) on Digital Scientific OCA20 goniometer (Garden City, NY, USA).

Detection of IL-6 on patterned oleophobic surfaces. The patterned hydrophilic wells were treated with 10% APTES solution for 3 hours, followed by 10 min sonication in DI water. This was then followed by treatment in EDC/NHS (2 mM EDC and 5 mM NHS in 0.1 M MES buffer) mixed with 1:100 ratio of capture antibody to initiate the carbodiimide cross-linking reaction and 1 µl of the solution was pipetted on to each well and was incubated overnight. Subsequently the wells were block by 2% BSA for an hour. The samples were then dipped into buffer containing 2500 pg mL^{-1} of IL-6 (in sample diluent composed of 1% BSA in phosphate-buffered saline), digitizing the solution on to the substrate. These droplets were let for 1 hour before washing in TBST and TBS. Surfaces were then dried with compressed air and dipped in biotinylated IL-6 monoclonal antibody (1:500 v:v diluted in the sample diluent buffer) for another hour. The samples were again washed using both wash buffers, and dried. Finally, the samples were dipped in the streptavidin dye (8:1000 v:v diluted in the reporter buffer) for 30 minutes in complete darkness, and subsequently washed with the wash buffers before the imaging. The binding of IL6 was confirmed and quantified by imaging the wells using a Chemidoc imaging

system (BioInterface Institute, McMaster University) by Cy5 channel. A schematic of the assay component can be found in Supplementary Figure 4.7.

Supporting Information

Supporting Information is available from the Wiley Online Library or from the author.

Acknowledgements

This work was supported by NSERC Discovery and CRD grants, Ontario Early Researcher Award grant and McMaster start-up funds to T.F.D.

Conflict of Interest

The authors declare no conflict of interest

4.6 References

[1] L.-C. Xu, J. W. Bauer, C. A. Siedlecki, *Colloids Surfaces B Biointerfaces* **2014**, *124*, 49.

[2] K. N. Sask, I. Zhitomirsky, L. R. Berry, A. K. C. Chan, J. L. Brash, *Acta Biomater.* **2010**, *6*, 2911.

[3] K. M. Hansson, S. Tosatti, J. Isaksson, J. Wetterö, M. Textor, T. L. Lindahl, P. Tengvall, *Biomaterials* **2005**, *26*, 861.

[4] D. E. Heath, S. L. Cooper, *J. Biomed. Mater. Res. Part A* **2010**, *94*, 1294.

[5] W.-B. Tsai, Y.-H. Chen, H.-W. Chien, *J. Biomater. Sci. Polym. Ed.* **2009**, *20*,

1611.

[6] K. Ishihara, *Langmuir* **2018**, *35*, 1778.

[7] P. H. Lin, C. Chen, R. L. Bush, Q. Yao, A. B. Lumsden, S. R. Hanson, *J. Vasc. Surg.* **2004**, *39*, 1322.

[8] J. M. M. Heyligers, H. J. M. Verhagen, J. I. Rotmans, C. Weeterings, P. G. de Groot, F. L. Moll, T. Lisman, *J. Vasc. Surg.* **2006**, *43*, 587.

[9] F. P. Seib, M. Herklotz, K. A. Burke, M. F. Maitz, C. Werner, D. L. Kaplan, *Biomaterials* **2014**, *35*, 83.

[10] J. Zhao, Y. Chen, S. Yang, S. Wu, R. Zeng, H. Wu, J. Zhang, Z. Zha, M. Tu, *Mater. Sci. Eng. C* **2016**, *58*, 133.

[11] Z. Yang, J. Wang, R. Luo, M. F. Maitz, F. Jing, H. Sun, N. Huang, *Biomaterials* **2010**, *31*, 2072.

[12] R. A. Hoshi, R. Van Lith, M. C. Jen, J. B. Allen, K. A. Lapidos, G. Ameer, *Biomaterials* **2013**, *34*, 30.

[13] M. A. Hiob, S. She, L. D. Muiznieks, A. S. Weiss, *ACS Biomater. Sci. Eng.* **2017**, *3*, 712.

[14] H. Oonishi, *Biomaterials* **1991**, *12*, 171.

[15] P. K. Chu, J. Y. Chen, L. P. Wang, N. Huang, *Mater. Sci. Eng. R Reports* **2002**, *36*, 143.

[16] K. Vallieres, É. Petitclerc, G. Laroche, *Macromol. Biosci.* **2007**, *7*, 738.

[17] M. Santos, M. M. M. Bilek, S. G. Wise, *Biosurface and Biotribology* **2015**, *1*, 146.

[18] A. I. De Agostini, S. C. Watkins, H. S. Slayter, H. Youssoufian, R. D. Rosenberg,

J. Cell Biol. **1990**, *111*, 1293.

[19] R. Biran, D. Pond, *Adv. Drug Deliv. Rev.* **2017**, *112*, 12.

[20] M. Badv, S. M. Imani, J. I. Weitz, T. F. Didar, *ACS Nano* **2018**, acsnano.8b03938.

[21] S. M. Imani, M. Badv, A. Shakeri, H. Yousefi, D. Yip, C. Fine, T. F. Didar, *Lab Chip* **2019**, *19*, 3228.

[22] M. Osborne, A. Aryasomayajula, A. Shakeri, P. R. Selvaganapathy, T. F. Didar, *ACS Sensors* **2019**, *4*, 687.

[23] M. Villegas, Y. Zhang, N. Abu Jarad, L. Soleymani, T. F. Didar, *ACS Nano* **2019**, *13*, 8517.

[24] M. Badv, C. Alonso-Cantu, A. Shakeri, Z. Hosseinidoust, J. I. Weitz, T. F. Didar, *ACS Biomater. Sci. Eng.* **2019**, *5*, 6485.

[25] M. Badv, J. I. Weitz, T. F. Didar, *Small* **2019**, *15*, 1905562.

[26] S. M. Imani, R. Maclachlan, K. Rachwalski, Y. Chan, B. Lee, M. McInnes, K. Grandfield, E. D. Brown, T. F. Didar, L. Soleymani, *ACS Nano* **2019**.

[27] A. Hosseini, M. Villegas, J. Yang, M. Badv, J. I. Weitz, L. Soleymani, T. F. Didar, *Adv. Mater. Interfaces* **2018**, *1800617*, 1.

[28] M. Villegas, Z. Cetinic, A. Shakeri, T. F. Didar, *Anal. Chim. Acta* **2018**, *1000*, 248.

[29] M. Badv, I. H. Jaffer, J. I. Weitz, T. F. Didar, *Sci. Rep.* **2017**, *7*, 11639.

[30] D. C. Leslie, A. Waterhouse, J. B. Berthet, T. M. Valentin, A. L. Watters, A. Jain, P. Kim, B. D. Hatton, A. Nedder, K. Donovan, E. H. Super, C. Howell, C. P. Johnson, T. L. Vu, D. E. Bolgen, S. Rifai, A. R. Hansen, M. Aizenberg, M. Super, J. Aizenberg, D. E. Ingber, *Nat. Biotechnol.* **2014**, *32*, 1134.

[31] P. Kim, M. J. Kreder, J. Alvarenga, J. Aizenberg, *Nano Lett.* **2013**, *13*, 1793.

[32] A. K. Kota, G. Kwon, A. Tuteja, *Npg Asia Mater.* **2014**, *6*, e109.

[33] V. Jokinen, E. Kankuri, S. Hoshian, S. Franssila, R. H. A. Ras, *Adv. Mater.* **2018**, *30*, DOI 10.1002/adma.201705104.

[34] H. Qin, C. Sun, C. He, D. Wang, C. Cheng, S. Nie, S. Sun, C. Zhao, *J. Memb. Sci.* **2014**, *468*, 172.

[35] L. Li, C. Cheng, T. Xiang, M. Tang, W. Zhao, S. Sun, C. Zhao, *J. Memb. Sci.* **2012**, *405*, 261.

[36] Z. Li, B. L. Nguyen, Y. C. Cheng, J. Xue, G. MacLaren, C. H. Yap, *J. Mater. Chem. B* **2018**, *6*, 6225.

[37] S. Movafaghi, V. Leszczak, W. Wang, J. A. Sorkin, L. P. Dasi, K. C. Popat, A. K. Kota, *Adv. Healthc. Mater.* **2017**, *6*, 1600717.

[38] S. Moradi, N. Hadjesfandiari, S. F. Toosi, J. N. Kizhakkedathu, S. G. Hatzikiriakos, *ACS Appl. Mater. Interfaces* **2016**, *8*, 17631.

[39] Y. S. Joung, C. R. Buie, *Langmuir* **2011**, *27*, 4156.

[40] P. Zhu, T. Kong, X. Tang, L. Wang, *Nat. Commun.* **2017**, *8*, DOI 10.1038/ncomms15823.

[41] A. Tuteja, W. Choi, J. M. Mabry, G. H. McKinley, R. E. Cohen, *Proc. Natl. Acad. Sci. U. S. A.* **2008**, *105*, 18200.

[42] W. Wu, X. Wang, D. Wang, M. Chen, F. Zhou, W. Liu, Q. Xue, *Chem. Commun.* **2009**, 1043.

[43] P. Mazumder, Y. Jiang, D. Baker, A. Carrilero, D. Tulli, D. Infante, A. T. Hunt, V.

Pruneri, *Nano Lett.* **2014**, *14*, 4677.

[44] C. M. Gabardo, J. Yang, N. J. Smith, R. C. Adams-McGavin, L. Soleymani, *ACS Nano* **2016**, *10*, 8829.

[45] C. S. Ware, T. Smith-Palmer, S. Peppou-Chapman, L. R. J. Scarratt, E. M. Humphries, D. Balzer, C. Neto, *ACS Appl. Mater. Interfaces* **2018**, *10*, 4173.

[46] A. Dramé, T. Darmanin, S. Y. Dieng, E. Taffin de Givenchy, F. Guittard, *RSC Adv.* **2014**, *4*, 10935.

[47] S. Saha, Y. Chan, L. Soleymani, *ACS Appl. Mater. Interfaces* **2018**, *10*, 31178.

[48] Z. Zhu, T. Zhu, Z. Liu, *Nanotechnology* **2004**, *15*, 357.

[49] D. Li, A. . Neumann, *J. Colloid Interface Sci.* **1992**, *148*, 190.

[50] R. J. Crawford, H. K. Webb, V. K. Truong, J. Hasan, E. P. Ivanova, *Adv. Colloid Interface Sci.* **2012**, *179–182*, 142.

[51] H. Nakae, R. Inui, Y. Hirata, H. Saito, *Acta Mater.* **1998**, *46*, 2313.

[52] L. Yan, K. Wang, J. Wu, L. Ye, *Colloids Surfaces A Physicochem. Eng. Asp.* **2007**, *296*, 123.

[53] M. Nosonovsky, *Langmuir* **2007**, *23*, 3157.

[54] G. Vazquez, E. Alvarez, J. M. Navaza, *J. Chem. Eng. Data* **1995**, *40*, 611.

[55] H. J. Ensikat, P. Ditsche-Kuru, C. Neinhuis, W. Barthlott, *Beilstein J. Nanotechnol.* **2011**, *2*, 152.

[56] W. van Oeveren, *Scientifica (Cairo).* **2013**, *2013*, 392584.

[57] P. Parhi, A. Golas, E. A. Vogler, *J. Adhes. Sci. Technol.* **2010**, *24*, 853.

[58] M. Badv, S. M. Imani, J. I. Weitz, T. F. Didar, *ACS Nano* **2018**, *12*, 10890.

[59] C. M. Gabardo, Y. Zhu, L. Soleymani, J. M. Moran-Mirabal, *Adv. Funct. Mater.* **2013**, *23*, 3030.

[60] C. M. Gabardo, A. M. Kwong, L. Soleymani, *Analyst* **2015**, *140*, 1599.

[61] A. Shakeri, S. M. Imani, E. Chen, H. Yousefi, R. Shabbir, T. F. Didar, *Lab Chip* **2019**, *19*, 3104.

[62] C. Shillingford, N. MacCallum, T.-S. Wong, P. Kim, J. Aizenberg, *Nanotechnology* **2013**, *25*, 14019.

[63] C. M. Gabardo, R. C. Adams-McGavin, O. M. Vanderfleet, L. Soleymani, *Analyst* **2015**, *140*, 5781.

4.7 Supplementary Information for Hierarchical structures, with submillimeter patterns, micrometer wrinkles, and nanoscale decorations, suppress biofouling and enable rapid droplet digitization

a

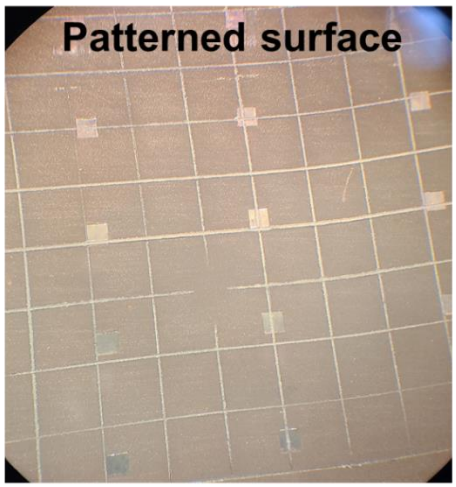

b

Example Appearance		Description	Classification	
Minimum Removal	Maximum Removal		ISO/JIS	ASTM
		The edges of the cuts are completely smooth; none of the squares of the lattice is detached.	0	5B
		Detachment of flakes of the coating at the intersections of the cuts. A cross cut area not greater than 5% is affected.	1	4B
		The coating has flaked along the edges and/or at the intersections of the cuts. A cross cut area greater than 5%, but not greater than 15% is affected.	2	3B
		The coating has flaked along the edges of the cuts partly or wholly in large ribbons, and/or it has flaked partly or wholly on different parts of the squares. A cross cut area greater than 15%, but not greater than 35%, is affected.	3	2B
		The coating has flaked along the edges of the cuts in large ribbons and/or some squares have detached partly or wholly. A cross cut area greater than 35%, but not greater than 65%, is affected.	4	1B
		Any degree of flaking that cannot be classified even by classification 4 or 1B	5	0B

Supplementary Figure 4.6 *a) Adhesion test on the patterned hierarchical surface, demonstrating the 5B class b) Classification table Adapted from* [1]

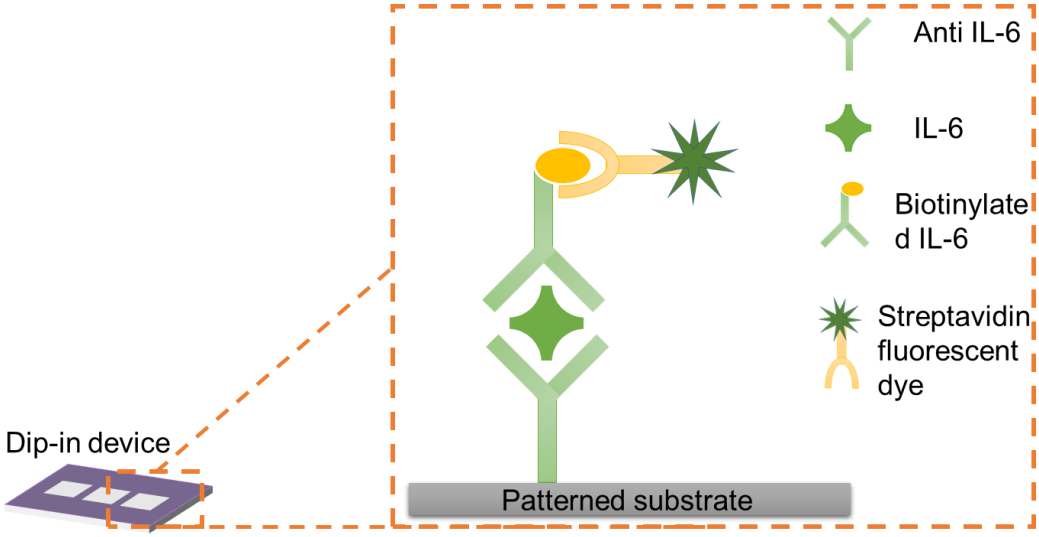

Supplementary Figure 4.7 *IL-6 assay components.*

4.7.1 References for Supplementary Information for Hierarchical structures, with submillimeter patterns, micrometer wrinkles, and nanoscale decorations, suppress biofouling and enable rapid droplet digitization

[1] "Elcometer 1542 Cross Hatch Adhesion Tester," can be found under https://www.elcometer.com/en/coating-inspection/adhesion-testers/cross-hatch-adhesion-testers/elcometer-1542-cross-hatch-adhesion-tester.html.

5 Chapter 5: Liquid Nano Electrodes enable One-pot Electrochemical Detection of Bacteria in Complex Matrices

Sara M. Imani, Enas Osman, Fatemeh Bakhshandeh, Shuwen Qian, Mark Gaskin, Deborah Yamamura, Yingfu Li, Tohid F. Didar*, Leyla Soleymani*

Will be submitted to Advanced Functional Materials

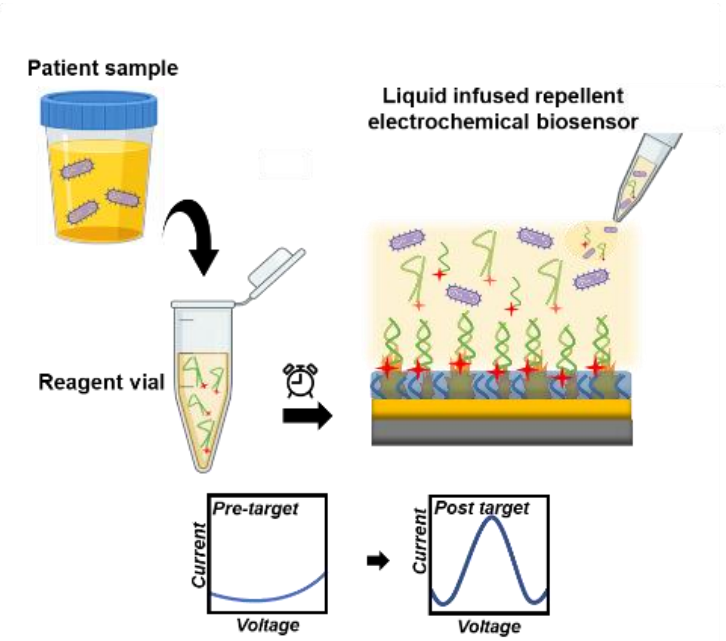

Preface:

Objective C

In this chapter, liquid infused coatings are integrated into an electrochemical biosensor to minimize the adverse effects of non-specific absorption on the sensing capabilities of the electrodes in complex biological liquids. Furthermore, in a one-pot rapid detection system (within an hour), a DNA barcode was released and captured by the designed electrodes to reduce the diagnosis time. For this study, clinical samples were tested with the developed

assay and electrodes, demonstrating rapid pathogen detection compared to non-treated electrodes.

5.1 Abstract

Non-specific absorption has posed a challenge in accurate target recognition in biosensing platforms, specifically when analyzing complex biological liquids where the target of interest (pathogens, biological analytes, *etc.*) often exists in. To address the need for reducing non-specific absorption, we integrated a repellent liquid infused coating within nanostructured gold electrodes (Liquid Nano Electrodes or LNEs) coated with biorecognition elements, in this case a double-stranded DNA probe specific to an *Escherichia coli* barcode. The LNEs promote selective target binding while repelling undesired species and generate an electrochemical signal upon contact with the released electroactive *E. coli* barcode in a one-pot assay where biological samples of interest are mixed with redox DNAzymes. The LNEs are effective in analyzing panels of clinical samples, distinguishing *E. coli* infected urine and blood culture samples from patient samples infected with other bacteria or non-infected. The assay was rapidly done within an hour with no sample dilutions, whereas nanostructured electrodes without the liquid infused coating were not able to detect infected complex biological samples nor buffer spiked samples (limit of detection of 10^2 CFU/ml for LNEs). The emergence of DNAzymes for identifying various bacteria, along with the developed on-pot assay and LNEs, rapid universal pathogen recognition can be realized.

5.2 Introduction

Electrochemical biosensors using nucleic acids as the biorecognition element have been developed for the detection and identification of bacteria. [1] These systems provide a rapid and point-of-care alternative to growth culture-based techniques for infectious disease diagnostics, and are envisioned to be less operationally-complex and expensive than standard methods for detecting bacterial nucleic acids *via* nucleic acid amplification. [1–3] Despite great promise, these electrochemical systems often lack simplicity due to the need for 1) sample processing when working with clinical specimens [2,3] and 2) step-wise addition of reagents inhibiting one-pot and one-step operation. [4–6] The underlying reason for the two abovementioned challenges is related to nonspecific binding. [7] Particularly, nonspecific binding of molecules in complex biological matrices reduces the signal generated on the biosensor surface, requiring sample processing steps such as target extraction and specimen dilution. Additionally, the presence of signal generating probes such as redox molecules before target introduction can generate large background signals due to non-specific interaction of these molecules with the sensor surface in the absence of the target. To overcome these limitations associated with non-specific binding, nucleic acid probes on the electrode surface are commonly mixed with low-fouling self assembled monolayers such as mercapto hexanol, hexane dithiol, dithiothreitol, and ethylene glycols. [8,9] These methods are generally effective but still require specimen dilution when working with complex matrices, which adds to the operational complexity of the assay and reduces the amount of target molecules available for analysis. [10–12]. Other blocking agents

commonly used in optical immunoassays such as bovine serum albumin are also used in electrochemical assays; [13] however, these result in the passivation of the electrode surface and the reduction of conductivity. Strategies for preserving electrode conductivity while reducing nonspecific binding have been developed by creating porous networks of antifouling reagents and conductive nanoparticles , [14] as well as developing anti-fouling conductive polymers. [15,16] Liquid infused surfaces provide an alternative for creating anti-biofouling electrochemical biosensors since they provide repellency against a broad range of background materials [17–19] while preserving electrochemical activity of surfaces. [20] These surfaces have shown strong repellency against complex media such as blood and plasma, [19,21,22] pathogenic contamination, [22] as well as proteins, [21,23] which has not been collectively achieved using other anti-biofouling strategies. [18,21] This makes liquid infused surfaces ideally-suited for one-pot biosensing in which a heterogeneous of mixture of known and unknown materials is present.

Herein, we sought to develop a one-pot bacterial sensor by combining liquid infused nanostructured electrodes (Liquid Nano Electrodes or LNEs) with redox DNAzymes for one-pot bacterial sensing. We determined whether it would be possible to mix clinical specimens with redox DNAzymes and use this one-pot solution on LNEs for one-pot sensing. We compared the ability of Liquid Nano electrodes with standard nanostructured electrodes in supressing the background signals generated by redox DNAzymes and reducing anti-biofouling in blood, plasma, and urine and benchmarked their limit-of-detection. We finally evaluated the ability of the one-pot assay in identifying *Escherichia coli* in specimens from patients with urinary and blood-stream infections.

5.3 Results and discussion

5.3.1 Fabricating Liquid Infused Electrochemical Biosensors

In order to fabricate LNEs, 100 nm of Au was sputtered on polystyrene surfaces, which were covered by a mask containing a star-shaped electrode design (**Figure 5.1**a). Subsequently, electrodes were fluorosilane (FS) treated through a 3-hour chemical vapour deposition method to lock down a fluorocarbon liquid layer for creating a repellent coating. After the chemical vapour deposition, nanostructures of gold were created by electroplating (FS-NanoAu) as shown in the scanning electron microscopy (SEM) images in Figure 5.1b i. The star-shaped design, having multiple sharp edges, leads to diffusion-limited growth and high-aspect-ratio electrodeposited architectures, providing a high surface area for thiolated DNA probes to bond to the electrode surface *via* thiol–gold chemistry (Figure 5.1b). [2,24] Gold electrodes where also electroplated without any prior FS treatments (NanoAu) to provide a control group against FS-NanoAu. Similar to FS-NanoAu surfaces, NanoAu electrodes demonstrated nanostructured features (Figure 5.1b.ii); however, the structures found on the latter are smaller. The larger features on FS-NanoAu electrodes can be attributed to the negatively charged FS covered surface, attracting more positively charged Au ions from the electroplating solution than the non FS treated surface (NanoAu), leading to electroplating larger structures per each growth-point. The electroactive surface area was also evaluated (**Supplementary Figure 5.6** a,b,c), showing similar characteristics

for FS-NanoAu and NanoAu electrodes, however, NanoAu showed 28% less electroactive surface area than FS-NanoAu.

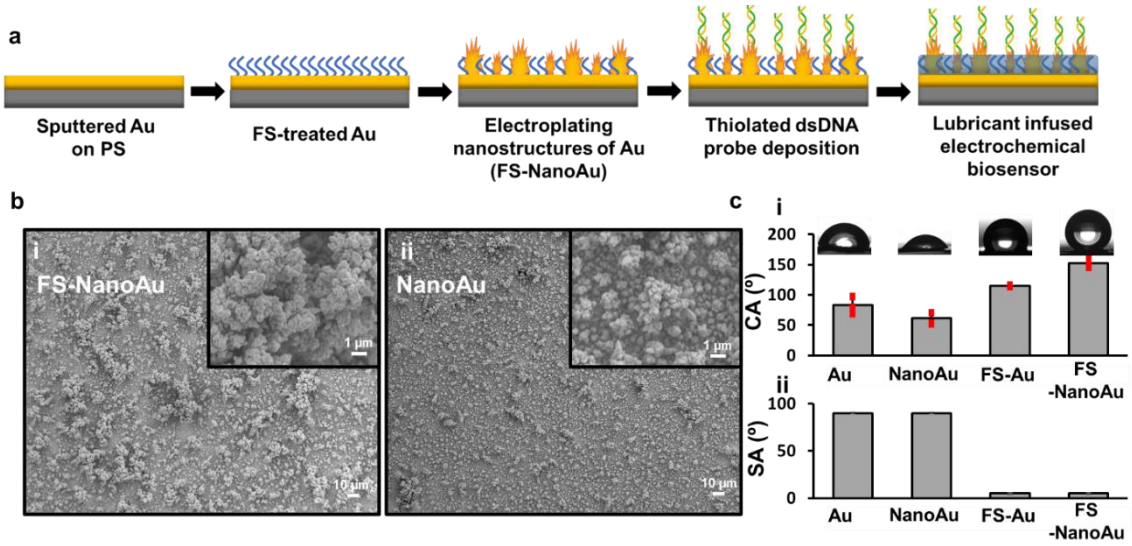

Figure 5.1 Fabrication and characterization of LNEs*. (a) Steps for creating LNEs. (b) Scanning electron microscopy images of (i) FS-NanoAu and (ii) NanoAu surfaces. The scale bars on larger SEM images represent 10 µm and for the insets represent 1 µm. (c) (i) Contact and (ii) sliding angle measurements of Au, NanoAu, FS-Au, and FS-NanoAu surfaces by deposition of 5 µL deionized water droplet. Representative images of the contact angle of water droplets are shown.*

Successful immobilization of the FS monolayer and repellent behaviour of the surfaces were evaluated by contact angle (CA) and sliding angle measurements (SA) shown (Figure 5.1c i,ii). Au and NanoAu surfaces showed a static water contact angle measurement of 83±12º and 61±9º which was then elevated to 115±1º and 152±5º for FS-Au and FS-NanoAu, respectively. This was due to the decrease in the surface free energy by the FS treatment, leading to higher Cassie-Baxter's contact angle, demonstrating successful FS immobilization. The increase in contact angles from FS-Au to FS-NanoAu, is due to the presence of multiple structural length scales in FS-NanoAu and having more stable Cassie-

Baxter states while having a low surface energy. [25,26] On the other hand, the further decrease in the contact angle from Au to NanoAu can be explained by the existence of the Wenzel state, in which the contact angle decreases if the surfaces are roughened for contact angles below 90º. [25,26] Furthermore, sliding angle measurements were performed post liquid infusion on both FS-treated and non FS-treated surfaces. The FS-treated surfaces showed sliding angles of below 5º as water droplets immediately started to move and slide off (shown as 5º on Figure 5.1c ii). On the non-treated surfaces, the drops got pinned and did not move (shown as 90º on Figure 5.1c ii). Therefore, FS-NanoAu electrodes provide a repellent platform that is expected to reduce interference by unwanted molecules on the surface of biosensors.

In order to create a one-pot electrochemical assay for detecting *Escherichia coli*, we used RNA-cleaving DNAzymes with an electroactive region tagged with methylene blue. The interaction between *E. coli* and the methylene blue-tagged DNAzyme, results in the release of a DNA barcode, which is captured by the probe immobilized on the electrode (Figure 5.1a and **Figure 5.2a**). [2,27] Similar to the commercially-available rapid tests, the assay involves two steps. First the specimen is added to the reagent vial (30 minutes), and then a drop of the reagent/specimen mixture is added to the biosensor (30 minutes), after which the electrochemical current is measured. The reagent vial contains DNAzymes, whereas the specimen consists of *E. coli* spiked in buffer or biological fluids, or clinical samples derived from individuals with an *E. coli* infection. The thiolated DNA probes used herein are designed as double-stranded, one strand is complementary to the released DNA barcode, while the other strand serves as a protector to reduce the probability of

hybridization between the thiolated probe and the unreacted DNAzyme. Our results indicate that the use of this double stranded probe is critical in ensuring a sufficient target-to-blank ratio (Supplementary Figure 5.7a). Immobilization of the double-stranded DNA probe was validated using cyclic voltammetry on both FS-NanoAu and NanoAu electrodes (Supplementary Figure 5.6 d,e), showing probe deposition on both classes of electrodes. The highly repellent behaviour of the liquid infused chips is expected to result in an enhanced detection system due to the reduction of non-specific binding between the components of the reagent vial and specimen and the surface of the electrode.

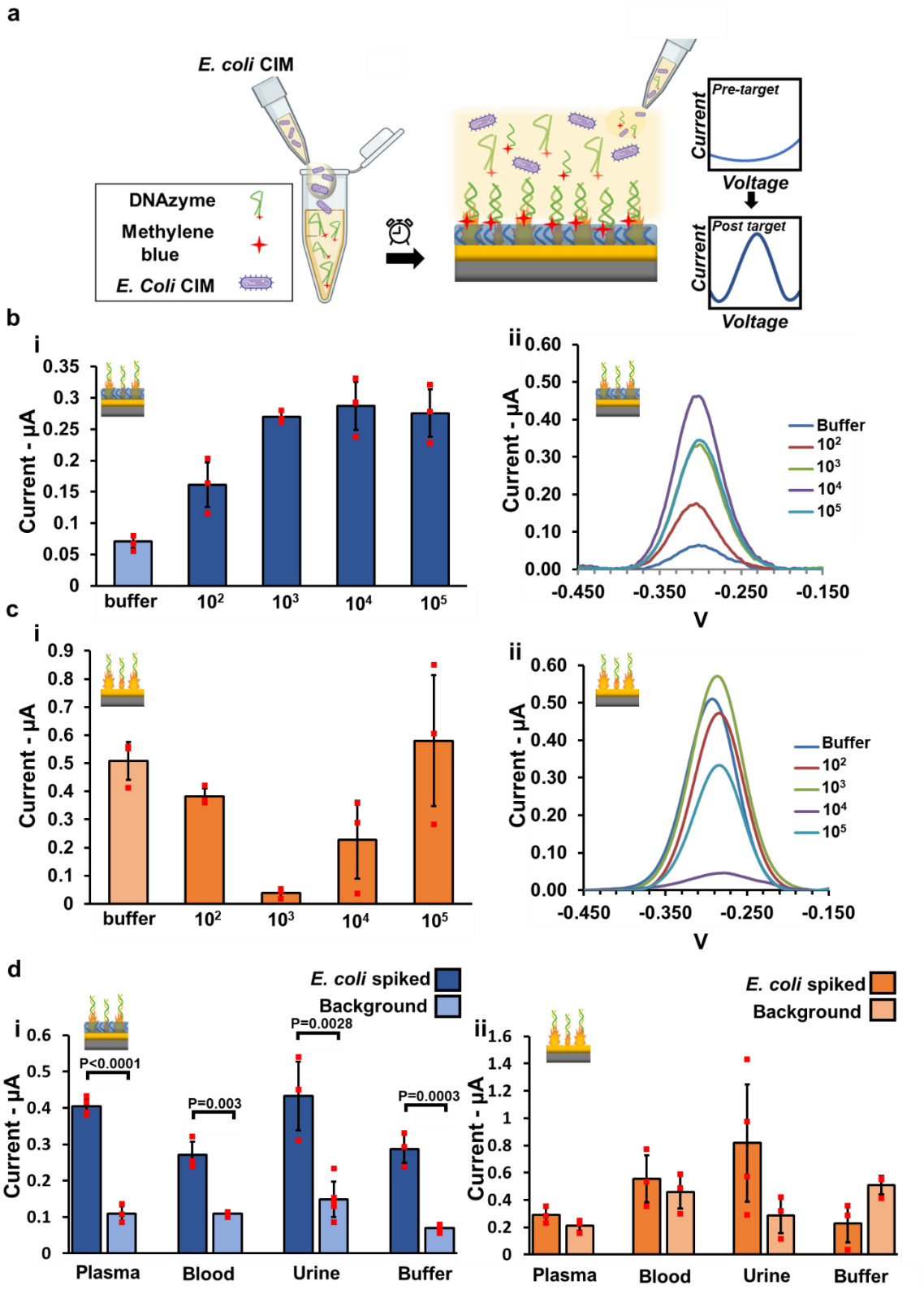
a
E. coli CIM
DNAzyme
Methylene blue
E. Coli CIM
Pre-target
Current
Voltage
Post target
Current
Voltage
b
i
Current - µA
buffer
10²
10³
10⁴
10⁵
ii
Current - µA
Buffer
10²
10³
10⁴
10⁵
V
c
i
Current - µA
buffer
10²
10³
10⁴
10⁵
ii
Current - µA
Buffer
10²
10³
10⁴
10⁵
V
d
E. coli spiked
Background
i
Current - µA
P<0.0001
P=0.003
P=0.0028
P=0.0003
Plasma
Blood
Urine
Buffer
E. coli spiked
Background
ii
Current - µA
Plasma
Blood
Urine
Buffer

Figure 5.2 E. coli detection using the LNEs*. (a) Schematic diagram of mixing DNAzymes with E. coli CIM for methylene blue barcode release, followed by incubation on LNEs for barcode detection from buffer or complex biological matrixes (e.g. urine) (b) Varying concentration of E. coli spiked in buffer to evaluate the response of the LNEs following incubation for 30 min at 37 °C with the vial mixture containing the released methylene blue barcode. (i) bar graph (ii) representative square wave scans. (c) Similar evaluation was done on NanoAu electrodes. Since the vial mixture contains buffer, CIM, redox DNAzymes, and released methylene blue barcode, can be considered complex. Therefore, the on NanoAu electrodes which do not have proper blocking, are showing large error and inconsistent data. (i) bar graph (ii) representative square wave scans. (d) Human whole plasma, whole blood, urine, and buffer were used as test liquids to assess E. coli detection on (i) LNEs and (ii) NanoAu electrodes. LNEs are showing significance difference in between E. coli spiked and the background signal of the respected test liquid. However, NanoAu electrodes are showing random and inconclusive data on E. coli detection in various test liquids.*

5.3.2 Electrochemical response of LNEs against *E. coli* for various test liquids

Detection and identification of *E. coli* in biological fluids such as urine or blood are critical for diagnosing urinary tract infections [28,29] or blood stream infections. [30] There is a need for rapid and simple assays for identifying bacterial pathogens such as *E. coli* that can be used at the point-of-care without the long turnaround times (24-48 hours) [31,32] associated with growth cultures.

To evaluate the performance of the liquid infused electrodes and compare them with nanostructured electrodes, the two classes of electrodes were used to analyze the crude intracellular matrix (CIM) of *E. coli* at varying concentrations (10^2 – 10^6 CFU/mL). Following the on-chip incubation of the bacteria, the solution was washed off and a negative pulse was applied to the electrodes to remove weakly bound or non-specifically adsorbed DNA strands. This practice showed an improvement in minimizing signal

variations for the same concentration by about 30% for the clinical data (Supplementary Figure 5.7b). The LNEs were able to detect *E. coli* at a concentration of 10^2 CFU/mL in buffer (Figure 5.2b i,ii); whereas, the NanoAu surfaces, showed indistinguishable data from the blank for all concentration, leaving the detection inconclusive (Figure 5.2c i,ii). This shows that the repellent coating on the LNEs enhances the limit-of-detection of the assay by lowering the blank signal.

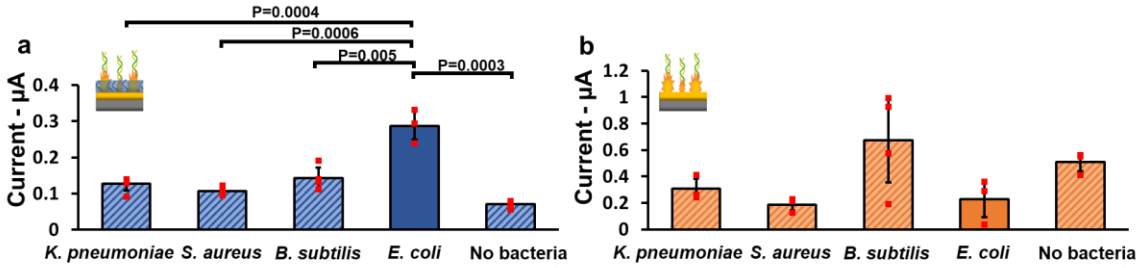

Figure 5.3 – E. coli specificity test. *Specificity test ran by mixing 10^4 CFU/mL of K. pneumoniae, S aureus, B. subtilis, E. coli, or buffer with the redox DNAzymes followed by incubation on (a) LNEs and (b) NanoAu electrodes. LNEs are showing a significant difference in between E. coli and the other control group whereas NanoAu electrodes are showing inconclusive data for E. coli detection along with considering bacteria and buffer. The error bars represent the standard deviation from the mean obtained using at least three separate electrodes per sample.*

The ability of the assay to detect *E. coli* in various complex biological liquids was also tested. Human plasma, whole blood, urine, and buffer were spiked with 10^4 CFU/mL of *E. coli* and tested using nanostructured and LNEs (Figure 5.2d i,ii). For all *E. coli* samples, the LNEs showed significantly higher signals compared to blanks. However, the NanoAu electrodes demonstrated indistinguishable signals when comparing spiked specimens and blanks. This is likely due to the finding that the blank specimens, still containing the redox

DNAzymes, showed lower amounts of background signal on LNEs (less than 150 nA) than that of the NanoAu ones, ranging from 211 nA to 508 nA. Based on these findings, we expected the LNEs to be suitable for one-pot analysis of clinical specimens.

To validate the specificity of the assay and its ability to identify *E. coli* amongst other bacteria, various Gram-negative and Gram-positive bacteria (*Klebsiella pneumoniae*, *Staph aureus*, *Bacillus subtilis*, and *E. coli* at 10^4 CFU/mL) were analyzed using LNEs and NanoAu chips (**Figure 5.3** a,b). The LNEs demonstrated stronger and statistically significant electrochemical signal for *E. coli*, therefore leading to specific and reliable detection of *E. coli* compared to other bacteria. Such characteristics was not observed in the case of NanoAu electrodes, as they did not allow for *E. coli* identification, showing higher signals for *B. subtilis* and buffer than *E. coli* (Figure 5.3 b). This data confirms that the LNEs highly promote less interferences from unwanted species and molecules in a complex detection liquid leading to specificity in detection and bacterium identification.

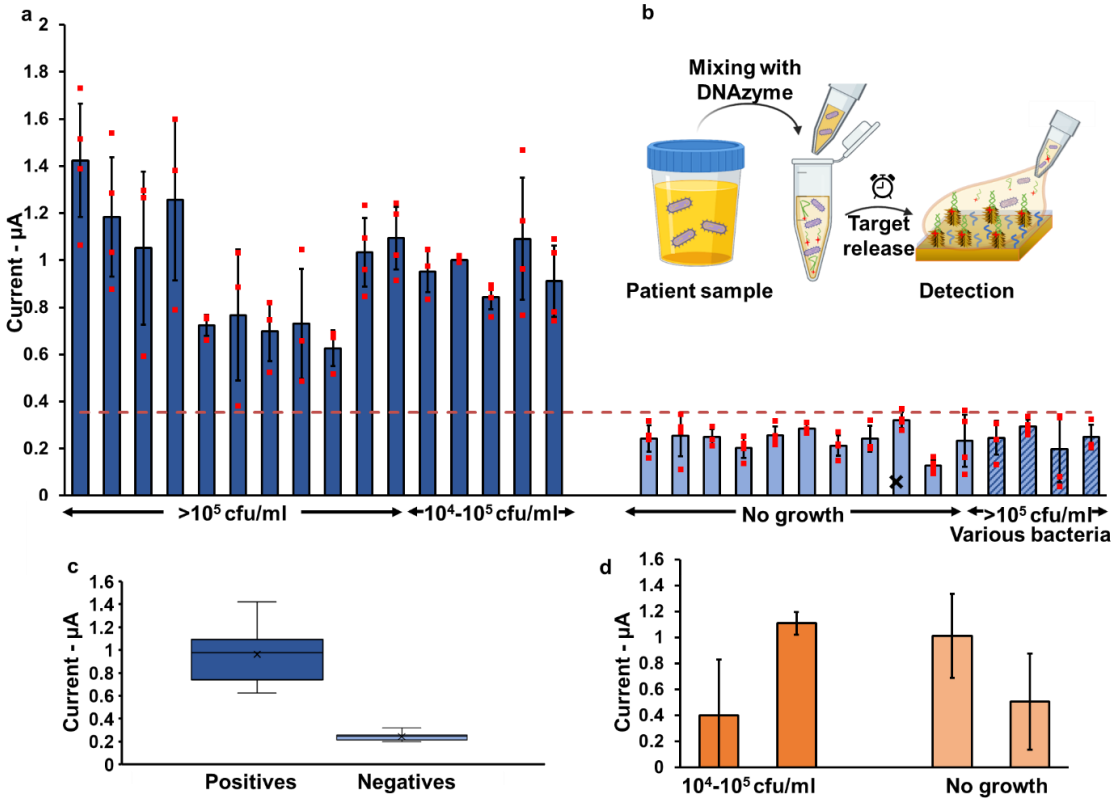

Figure 5.4 Clinical study on patient urine samples*. (a) The collected data comprises of 11x E. coli+/culture+ (>10^5), 5x E. coli+/culture+ (10^4-10^5), 11x E. coli-/culture-, 4x E. coli-/culture+ (>10^5 of Enterococcus, K. oxytoca, S. aureus, K. pneumoniae) tested on LNEs. The clinical study shows confident detection of above 10^4 on LNEs. All E. coli infected samples are statistically significant from the non infected ones. (b) Schematic illustration of E. coli detection steps in patient's urine samples. (c) Box and whisker plot demonstrating distribution of E. coli+ and E. coli- samples. (d) 2x E. coli+/culture+ (>10^5) and 2x E. coli-/culture- samples tested on NanoAu electrodes.*

5.3.3 Detecting clinical urinary tact infections (UTIs) caused by *E. coli*

Given the promising behaviour of LNEs in analyzing spiked samples, we sough to determine whether this assay can be used in analyzing specimens from patients having urinary tract infection symptoms. We collected 31 urine samples from such patients, which included 11 *E. coli*+/UTI+ (>10^5 CFU/mL), 5 *E. coli*+/UTI+ (10^4 -10^5 CFU/mL), 11 *E.*

coli-/UTI-, and 4 *E. coli*-/UTI+ (>10^5 CFU/mL of *Enterococcus*, *Klebsiella oxytoca*, *S. aureus*, *K. pneumoniae*) specimens (**Figure 5.4**a). These clinical specimens were added to the reagent vial and were tested on LNEs (Figure 5.4b).

To determine the clinical sensitivity and specificity of this assay a detection threshold of 370 nA was calculated based on a 95% confidence interval by Analyse-it for Microsoft Excel. This threshold led to the sensitivity of 100% and specificity of 98% (one data point on the X marked bar in Figure 5.4b was =>370 nA), enabling categorization of *E. coli*+ samples from the *E. coli*- ones (Figure 5.4c). This was in accordance with >10^4 CFU/mL threshold for UTI+ patients,. [2,33–35] To evaluate the diagnostic ability of the developed platform, A receiver operating characteristic (ROC) plot was constructed (**Supplementary Figure 5.8**). The area under the curve (AUC) was measured to be 1 for the ROC plot, which meets the standard criteria for evaluating diagnostic tests.

The NanoAu electrodes were also tested (Figure 5.4d) for a smaller subset of clinical samples (2 *E. coli*+/culture+ (>10^5 CFU/mL) and 2 *E. coli*-/culture-). As expected, based on the spiked study, there are no substantial differences detected for the no growth and positive samples.

5.3.4 Clinical study for detecting blood stream infection caused by *E. coli* and specificity assessment

To assess whether the developed detection system would be effective in the detection of *E. coli* in the blood of patients suspected of having blood-stream infections or bacteremia, we

used the LNEs to analyze specimens derived from such patients (**Figure 5.5**). Clinical blood cultures having *E. coli* (quantified in **Supplementary Figure 5.9**, **Supplementary Note 1**), *S. aureus*, or no bacteria were acquired from patients with symptoms of bacteremia or sepsis after the samples were analyzed using the liquid culture-based BacT/ALERT system [36] at the hospital. Upon receiving the samples, the blood cultures were incubated inside the reagent vial and subsequently incubated on LNEs (Figure 5.5b). Among these specimens, three were *E. coli*+, two were *E. coli*-/culture+ (*S. aureus*+), and four were culture-. The LNEs were able to specifically detect *E. coli* infected samples by demonstrating larger signal amplitudes than *S. aureus* infected and negative blood samples, differentiating *E. coli*+ samples from the other control groups (Figure 5.5a). Even though our analysis includes a limited number of clinical specimens, our ability in identifying the microorganism causing the blood-stream infection without the commonly used sub-cultures conducted following the use of the BacT/Alert system [36] shows the promise of our approach in rapid and culture-free bacterial identification. Rapid bacterial identification is critical in patients with bloodstream infections as it will guide physicians in prescribing precision and effective treatments more rapidly for a condition that is time sensitive has a high fatality rate. [31,37]

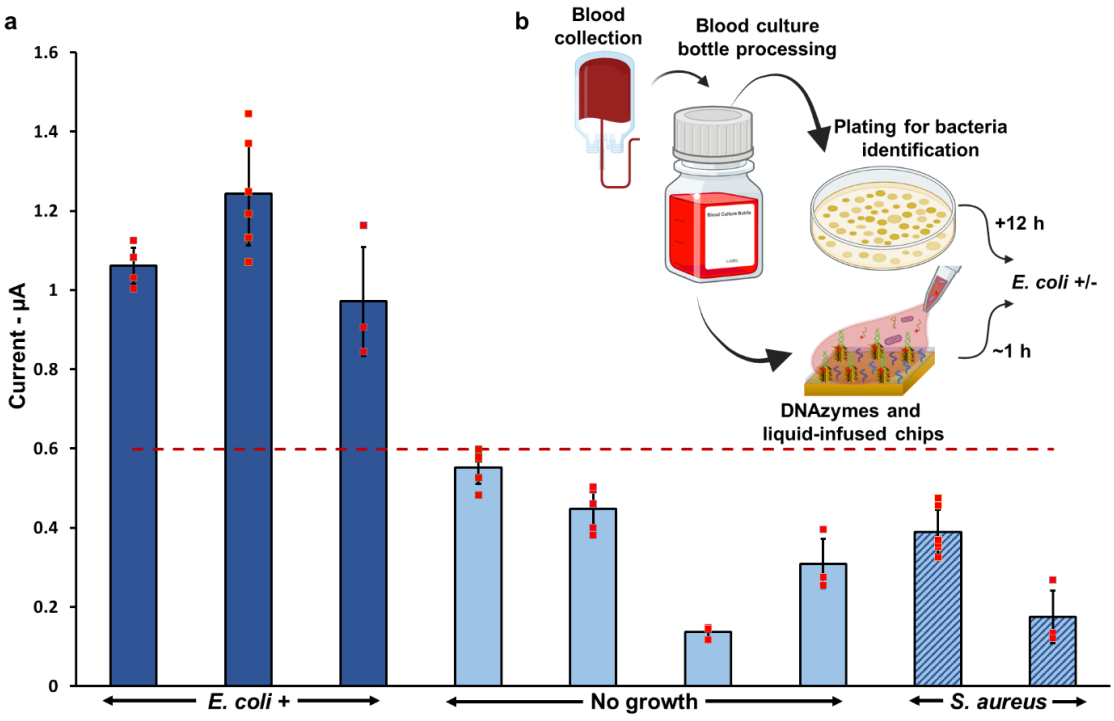

Figure 5.5 Clinical study on patient's blood culture samples*. (a) Symptomatic patient's blood culture samples being E. coli+, S. aureus+, or with no bacteria were tested on the LNEs. All E. coli infected samples are statistically significant from the non infected ones. (b) Schematic of collected patient blood culture samples and detection steps*

5.4 Conclusion

In response to the high demand for *E. coli* detection in clinical setups as a major pathogen in urinary tract and blood stream infections, rapid and point-of-care assays are sought for.[28,30] Testing pathogens in a range of complex and unprocessed clinical specimens using simple and one-pot assays has proven to be challenging due to interference of the sample matrix with the biosensor, as well as the interference of the signalling probes with the biosensor in the absence of the target analyte.

To develop a one-pot assay that is universally applicable to a range of specimen type, we created a new class of anti-biofouling electrodes and combined these with *E. coli*-specific redox DNAzymes that release a redox DNA barcode in response to the target. These released targets are detected on the anti-biofouling electrodes, which 1) reduce the interference of the unreacted redox DNAzymes with the electrode surface and as such reduce blank signals and 2) reduce the impact of the specimen type on the analytical performance of the assay.

In this work, we identified *E. coli* in buffer, unprocessed plasma, unprocessed whole blood, and unprocessed urine using the newly developed anti-biofouling electrodes created using a liquid infused surface modification, which was not possible using electrodes that lacked this surface processing step. Furthermore, without any sample processing, clinical specimens from symptomatic urinary tract infection patients were analyzed with a sensitivity of 100% and specificity of 98%. Additionally, specimens from patients with blood stream bacteria or sepsis was studied. LNEs were able to successfully identify the *E. coli* infected blood specimens. Reducing the sample-to-result time from days obtained with growth culture to an hour using the newly developed assay would be life saving for patients suffering from sepsis whose survival rates are ~80% for the first hour of antibiotic administration and this number is decreased for every hour of delay in treatment administration by ~8%. [37,38] The one-pot assay developed here, enabled by the anti-biofouling electrodes, can be easily applied to the detection of other pathogens and even non-pathogenic clinical biomarkers.

5.5 Materials and Methods

Materials

Trichloro(1H,1H,2H,2H-perfluorooctyl)silane (FS), perfluoroperhydrophenanthrene (PFPP), 6-mercapto-1-hexanol (MCH, 99%), tris(2-carboxyethyl)phosphine hydrochloride (TCEP), sodium chloride (NaCl, ≥99.0%), magnesium chloride (MgCl2, ≥99.0%), Phosphate buffer solution (1.0 M, pH 7.4), gold(III) chloride solution (HAuCl4, 99.99%), potassium hexacyanoferrate(II) trihydrate ([Fe(CN)6]4−, ≥99.95%) were purchased from Sigma-Aldrich. Hydrochloric acid (HCl; 37% w/w) was purchased from LabChem. Sulfuric acid (H2SO4, 98%) and 2-propanol (99.5%) were purchased from Caledon Laboratories. Methylene blue NHS ester was purchased from Glen research (Virginia, United states). Urea, and 40% 29:1 bis/acrylamide were from Bioshop (Ontario, Canada). The DNA oligonucleotides were purchased from Integrated DNA Technologies (IDT) and Yale. Sequence details can be found in **Supplementary Table 1**. The water used in all experiments was purified with a Milli-Q Synthesis A10 water-purification system and further autoclaved.

Electrode fabrication

Polystyrene sheets (Graphix Shrink Film, Graphix) were cleaned with IPA and water and air-dried. Subsequently, the sheet was covered with a vinyl mask (FDC 4304, FDC Graphic Films) and then cut to the working electrode pattern using a Robo Pro CE5000-40-CRP cutter (Graphtec America). The masked substrates were then gold sputtered to a final thickness of 100 nm with a direct current sputtering machine (MagSput, Torr International). The sputtered working electrodes were then cut and cleaned with IPA. For fabrication the

FS treated electrodes, they were placed in an air plasma cleaner (Harrick Plasma Cleaner, PDC-002, 230 V), and exposed to high-pressure air plasma for 3 min to be functionalized with hydroxyl groups. Then, they were transferred to a desiccator and 300 µL of FS was added in a container along with the electrodes in a separate container. The vacuum pump was then turned on so that the pressure of −0.08 MPa was reached to start the chemical vapour deposition process to create self-assembled monolayers or FS. The reaction was carried out for 3 hourse at room temperature. Subsequently, the electrodes were removed from the desiccator and placed in an oven at 60 °C for a minimum of 18 h. To ensure the removal of noncovalently attached FS molecules, the electrodes were sonicated for 5 minutes (VWR SympHony 97043-936 ultrasonic cleaner). Subsequently gold nanostructures were electrodeposited onto the electrodes by applying a static potential of −0.6 V for 600 s in a solution of 10 mM gold chloride (HAuCl4) and 5 mM HCl using a PalmSens4 (PalmSens) with Ag/AgCl as the reference and platinum wire as the counter electrode.

Methylene blue tagging and purification

The lyophilized 5'-Amino- modified *E. coli* DNAzyme is diluted in 0.1 M Carbonate/Bicarbonate buffer (pH 9) and mixed with Methylene Blue NHS Ester, then left to react for two hours at room temperature following the manufacturer instructions. To remove the excess methylene blue, the DNAzyme is then purified using 10% urea 40% 29:1 Bis/Acrylamide page gel (denaturing gel). An Ethanol precipitation step is performed by adding 0.1x Sodium acetate (pH=5.2), 2.5x 100% ethanol and left in -20ºC for 20+

minutes and centrifuged at 15,000 rpm, 4ºC. The precipitated sample is diluted in autoclaved water and loading dye, then loaded to the gel and run for 1 hour (36W). The DNAzyme bands are vitalized and cut using UV light (240 nm). Afterwards, the gel is crushed and eluted using an in-house elusion buffer (200 mM NaCl, 10 mM Tris pH=7.5, 1 mM EDTA). The crushed gel is eluted two more times on a vortex at setting 3 for 30 minutes. A final ethanol precipitation step is applied, the retrieved DNAzyme is then diluted in RNA/DNA free water and stored in -20ºC for future use.

CIM preparation steps

E. coli, S. aureus, K. pneumoniae, and *B. Subtilis* crude intracellular matrix was prepared by culturing a single colony in LB media overnight until optical density OD600 ~1.0 (~2 Å~ 109 cells/ml). After that, 1 mL of each bacterial culture is centrifuged at 10000g for 10 minutes and the clear supernatant is discarded. Cells are then suspended in 500 µL of 1X reaction buffer (HEPES 50 mM, NaCl 150 mM, $MgCl_2$ 15 mM, Tween 20 0.01%, pH 7.5). Subsequently, the cells suspension is lysed by heat (90 °C for 10 minutes). The Lysed cells are then centrifuged at 13000 g for 10 minutes and the clear supernatant is collected. Finally, the supernatant is passed through a 0.2 µm filter disc, aliquoted, and stored at −20 °C for future DNAzyme cleavage experiments. This CIM preparation protocol is adapted from. [39]

Surface physical characterization

Scanning electron microscopy imaging was performed on a JEOL 7000F. Contact angle measurements were done on a goniometer ((DSA30, Krüss Scientific, Hamburg, Germany)

with water droplets (5 μL) dispensed by automated syringe. The sessile drop contact angle was provided *via* image processing software ((Krüss ADVANCE). Sliding angle measurements were done using a digital angle level (ROK, Exeter, UK) and prior to each measurement electrode were infused with PFPP and a 5 μL water droplet was deposited. The angle which the droplet started to move was recorded as the sliding angle. Each value was averaged over at least three measurements.

Double-stranded probe immobilization

The electrodes were washed with IPA. Then they were electrochemically cleaned by applying cyclic voltammetry in 0.1 M H2SO4 (0–1.5 V, 100 mV s–1, 40 cycles). The electrodes were then incubated for 20 hours with 3 μL drop of 2 μM thiolated double-stranded probe solution which was reduced for 2 hours prior to deposition with 2 mM TCEP solution in the dark at room temperature. After probe deposition, the electrodes were back filled with 100 mM MCH for 15 minutes in the dark at room temperature. All of the electrochemical measurements were performed using a PalmSens4 (PalmSens).

Electrochemical characterization

The immobilization of the thiolated ssDNA probe was confirmed by using a cyclic voltammetry scan from 0 V to 0.5 V at a scan rate of 50 mV s^{-1} in 2 mM potassium hexacyanoferrate(II) solution. Electroactive surface area measurements were done by scanning electrodes in 0.1 M H_2SO_4 using cyclic voltammetry (0 V-1.5 V, 100 mV/s).

Detection of bacteria in buffer

The bacterial CIM samples were spiked in 25:25 buffer (100 mM $MgCl_2$, 0.001% Tween 20) and mixed with methylene blue tagged DNAzyme (0.5 µM) in a 1:1 ratio and incubated in the dark at room temperature for 30 minutes. The FS treated electrodes were infused with the lubricant (PFPP), then both FS treated and nano-structured electrodes were incubated with 3 µL of the *E. coli* CIM and methylene blue tagged DNAzyme mixture for 30 min at 37 °C. Healthy urine samples were also used instead of 25:25 buffer. 10^6 to 10^2 CFU/mL concentrations were evaluated in both matrixes. To assess the specificity, three control CIMs of other bacteria (*S. aureus, K. pneumoniae, B. Subtilis*) at 10^4 CFU/mL were measured and compared with the same concentration of *E. coli* and buffer. To assess the performance in complex matrixes whole blood, plasma, unfiltered urine samples were compared for 10^4 CFU/mL *E. coli* spiked *vs.* non-spiked. urine and whole human blood were collected from healthy donors. All donors provided signed written consent and the procedures were approved by the McMaster University Research Ethics.

Clinical study with patient urine samples and blood culture samples

Patient urine sample set (total 31) comprising of 11x *E. coli*+/culture+ (>10^5 CFU/mL), 5x *E. coli*+/culture+ (10^4 – 10^5 CFU/mL), 11x *E. coli*-/culture-, 4x *E. coli*-/culture+ (>10^5 CFU/mL of *Enterococcus*, *K. oxytoca*, *S. aureus*, or *K. pneumoniae*) were tested on LNEs. 2x *E. coli*+/culture+ (>10^5 CFU/mL) and 2x *E. coli*-/culture- samples were tested on

NanoAu electrodes. For the assessment, CIM extraction was done such that urine samples were heat treated at 55 ºC for 15 mins followed by centrifugation at 11K x g for 5 mins. The supernatant was then removed and mixed with methylene blue tagged DNAzyme in a 1:1 ratio and incubated in the dark at room temperature for 30 minutes. Subsequently, the mixture was incubated on the respected electrodes and electrochemical measurement were performed.

Patient blood samples comprised of 3 *E. coli*+, 2 *S. aureus*+, and 4 negative samples. To acquire the samples, blood specimens were collected from symptomatic patients and transferred to blood culture bottles. When flagged positive, blood cultures were further sub-cultured to verify the bacteria species. Vials of blood cultures (*E. coli*+, *S. aureus*+, and negatives) were transferred from Hamilton General Hospital to our lab. CIM was extracted and tested as mentioned in the previous paragraph.

Supporting information

Supporting Information is available from the Wiley Online Library

Acknowledgements

This work was supported by NSERC and Ontario Early Researcher Award grant to L.S., by a salary award to and L.S. from the Canada Research Chairs Program, NSERC Discovery Grant to T.F.D., Ontario Early Researcher Award Grant to T.F.D., and McMaster start-up funds to T.F.D.

Conflict of Interest

The authors declare no conflict of interest

5.6 References

[1] E. Cesewski, B. N. Johnson, *Biosens. Bioelectron.* **2020**, *159*, 112214.

[2] R. Pandey, D. Chang, M. Smieja, T. Hoare, Y. Li, L. Soleymani, *Nat. Chem.* **2021**, *13*, 895.

[3] L. Soleymani, Z. Fang, B. Lam, X. Bin, E. Vasilyeva, A. J. Ross, E. H. Sargent, S. O. Kelley, *ACS Nano* **2011**, *5*, 3360.

[4] M. R. Ali, M. S. Bacchu, M. A. A. Setu, S. Akter, M. N. Hasan, F. T. Chowdhury, M. M. Rahman, M. S. Ahommed, M. Z. H. Khan, *Biosens. Bioelectron.* **2021**, *188*, 113338.

[5] C. Luo, H. Tang, W. Cheng, L. Yan, D. Zhang, H. Ju, S. Ding, *Biosens. Bioelectron.* **2013**, *48*, 132.

[6] J. C. Liao, M. Mastali, V. Gau, M. A. Suchard, A. K. Møller, D. A. Bruckner, J. T. Babbitt, Y. Li, J. Gornbein, E. M. Landaw, *J. Clin. Microbiol.* **2006**, *44*, 561.

[7] A. Frutiger, A. Tanno, S. Hwu, R. F. Tiefenauer, J. Voros, N. Nakatsuka, *Chem. Rev.* **2021**, *121*, 8095.

[8] S. Campuzano, F. Kuralay, J. Wang, *Electroanalysis* **2012**, *24*, 483.

[9] B. L. Hanssen, S. Siraj, D. K. Y. Wong, *Rev. Anal. Chem.* **2016**, *35*, 1.

[10] Z. Zhang, R. Pandey, J. Li, J. Gu, D. White, H. D. Stacey, J. C. Ang, C. Steinberg, A. Capretta, C. D. M. Filipe, *Angew. Chemie Int. Ed.* **2021**, *60*, 24266.

[11] W. Li, G.-C. Fan, X. Fan, R. Zhang, L. Wang, W. Wang, X. Luo, *J. Mater. Chem. B* **2019**, *7*, 5842.

[12] G. Figueroa-Miranda, C. Wu, Y. Zhang, L. Nörbel, Y. Lo, J. A. Tanner, L. Elling, A. Offenhäusser, D. Mayer, *Bioelectrochemistry* **2020**, *136*, 107589.

[13] M. Bockaj, B. Fung, M. Tsoulis, W. G. Foster, L. Soleymani, *Anal. Chem.* **2018**, *90*, 8561.

[14] J. Sabaté del Río, O. Y. F. Henry, P. Jolly, D. E. Ingber, *Nat. Nanotechnol.* **2019**, *14*, 1143.

[15] L. Zhou, X. Li, B. Zhu, B. Su, *Electroanalysis* **2022**, *34*, 966.

[16] G. Wang, R. Han, X. Su, Y. Li, G. Xu, X. Luo, *Biosens. Bioelectron.* **2017**, *92*, 396.

[17] P. Kim, M. J. Kreder, J. Alvarenga, J. Aizenberg, *Nano Lett.* **2013**, *13*, 1793.

[18] M. Villegas, Y. Zhang, N. Abu Jarad, L. Soleymani, T. F. Didar, *ACS Nano* **2019**, *13*, 8517.

[19] T.-S. Wong, S. H. Kang, S. K. Y. Tang, E. J. Smythe, B. D. Hatton, A. Grinthal, J. Aizenberg, *Nature* **2011**, *477*, 443.

[20] A. Hosseini, M. Villegas, J. Yang, M. Badv, J. I. Weitz, L. Soleymani, T. F. Didar, *Adv. Mater. Interfaces* **2018**, *1800617*, 1.

[21] M. Badv, S. M. Imani, J. I. Weitz, T. F. Didar, *ACS Nano* **2018**, *12*, 10890.

[22] D. C. Leslie, A. Waterhouse, J. B. Berthet, T. M. Valentin, A. L. Watters, A. Jain, P. Kim, B. D. Hatton, A. Nedder, K. Donovan, E. H. Super, C. Howell, C. P. Johnson, T. L. Vu, D. E. Bolgen, S. Rifai, A. R. Hansen, M. Aizenberg, M. Super, J. Aizenberg, D. E. Ingber, *Nat. Biotechnol.* **2014**, *32*, 1134.

[23] S. M. Imani, M. Badv, A. Shakeri, H. Yousefi, D. Yip, C. Fine, T. F. Didar, *Lab Chip* **2019**, *19*, 3228.

[24] D. Weng, U. Landau, *J. Electrochem. Soc.* **1995**, *142*, 2598.

[25] A. K. Kota, G. Kwon, A. Tuteja, *NPG Asia Mater.* **2014**, *6*, e109.

[26] S. M. Imani, R. Maclachlan, K. Rachwalski, Y. Chan, B. Lee, M. McInnes, K. Grandfield, E. D. Brown, T. F. Didar, L. Soleymani, *ACS Nano* **2019**.

[27] R. Pandey, Y. Lu, E. Osman, S. Saxena, Z. Zhang, S. Qian, A. Pollinzi, M. Smieja, Y. Li, L. Soleymani, T. Hoare, *ACS Sensors* **2022**, *7*, 985.

[28] A. L. Flores-Mireles, J. N. Walker, M. Caparon, S. J. Hultgren, *Nat. Rev. Microbiol.* **2015**, *13*, 269.

[29] B. Foxman, *Infect. Dis. Clin.* **2014**, *28*, 1.

[30] P. J. Lillie, G. Johnson, M. Ivan, G. D. Barlow, P. J. Moss, *J. Hosp. Infect.* **2019**,

103, 128.

[31] P. R. Murray, H. Masur, *Crit. Care Med.* **2012**, *40*, 3277.

[32] S. Najeeb, T. Munir, S. Rehman, A. Hafiz, M. Gilani, M. Latif, *J Coll Physicians Surg Pak* **2015**, *25*, 108.

[33] M. G. Coulthard, *Pediatr. Nephrol.* **2019**, *34*, 1639.

[34] W. Primack, T. Bukowski, R. Sutherland, L. Gravens-Mueller, M. Carpenter, *J. Pediatr.* **2017**, *191*, 259.

[35] W. E. Stamm, *Infection* **1992**, *20*, S151.

[36] T. C. Thorpe, M. L. Wilson, J. E. Turner, J. L. DiGuiseppi, M. Willert, S. Mirrett, L. B. Reller, *J. Clin. Microbiol.* **1990**, *28*, 1608.

[37] A. Kumar, D. Roberts, K. E. Wood, B. Light, J. E. Parrillo, S. Sharma, R. Suppes, D. Feinstein, S. Zanotti, L. Taiberg, *Crit. Care Med.* **2006**, *34*, 1589.

[38] D. Nestor, H. Andersson, P. Kihlberg, S. Olson, I. Ziegler, G. Rasmussen, J. Källman, S. Cajander, P. Mölling, M. Sundqvist, *BMC Infect. Dis.* **2021**, *21*, 1.

[39] M. M. Ali, C. L. Brown, S. Jahanshahi-Anbuhi, B. Kannan, Y. Li, C. D. M. Filipe, J. D. Brennan, *Sci. Rep.* **2017**, *7*, 1.

5.7 Supplementary Information for Liquid Nano Electrodes enable One-pot Electrochemical Detection of Bacteria in Complex Matrices

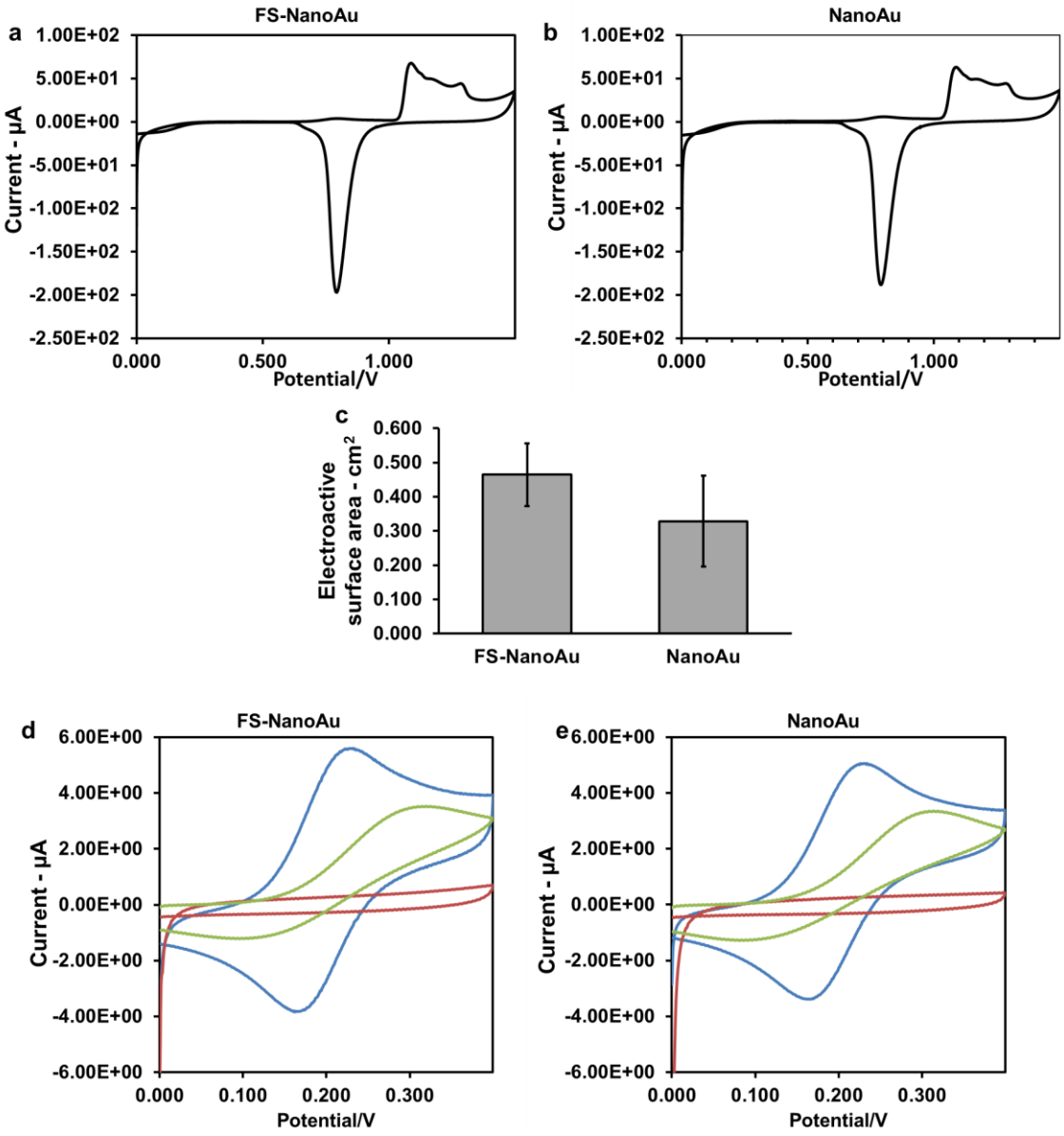

Supplementary Figure 5.6 *Surface area characterization of (a) FS-NanoAu and (b) NanoAu electrodes in 0.1 M H_2SO_4 using cyclic voltammetry (0 V-1.5 V, 100 mV/s). (c) Electroactive surface area comparison. Validation of probe deposition on in (d) FS-NanoAu and (e) NanoAu electrodes via cyclic voltammetry (0 V-0.5 V, 100 mV/s) in 2 mM*

potassium hexacyanoferrate (II) before probe deposition (post cleaning, blue), after probe deposition (red), and after backfilling with 6-mercapto hexanol (green)

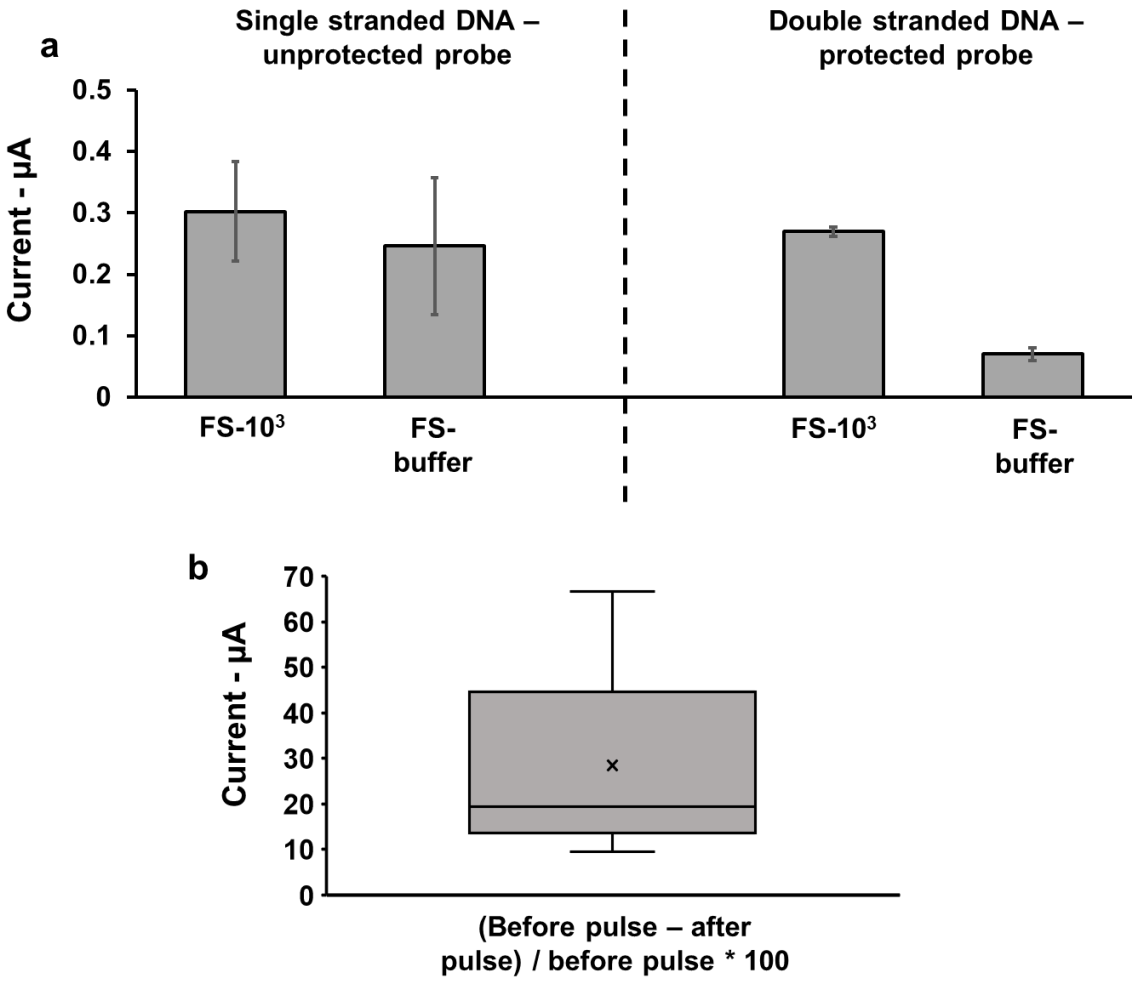

Supplementary Figure 5.7 *(a) Comparing single stranded DNA probe (unprotected probe) vs. double stranded DNA probe (protected probe) for 10^3 E. coli detection in buffer. The results indicate that the protected strand results in a sufficient target-to-blank ratio as well as more consistent data for each condition. (b) evaluating the percentage change in the error bars before and after the negative pulsing, demonstrating about 30% decrease in the error bars.*

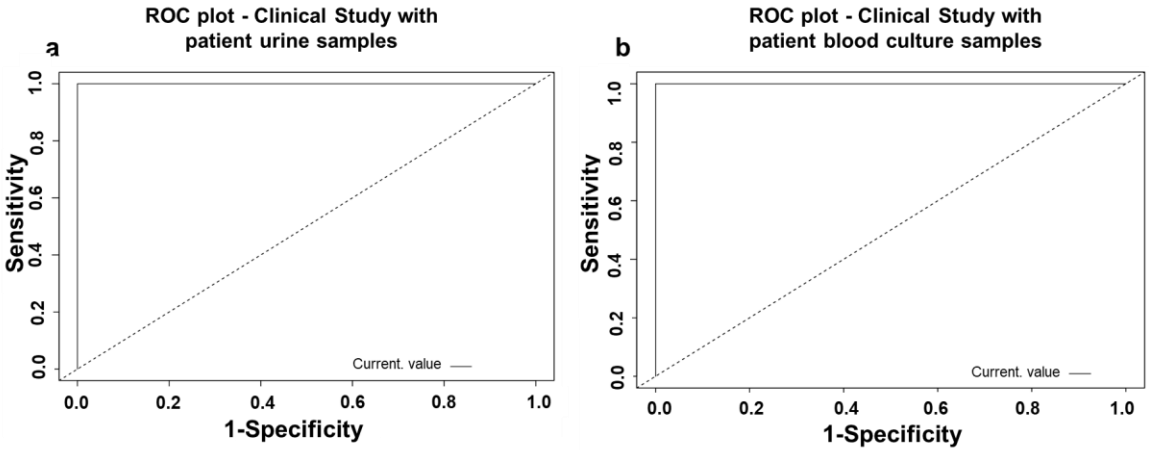

Supplementary Figure 5.8 *ROC plots. Sensitivity versus (1-Specificity) plot for the clinical data from (a) 31x patient urine samples (b) 9x patient blood culture samples.*

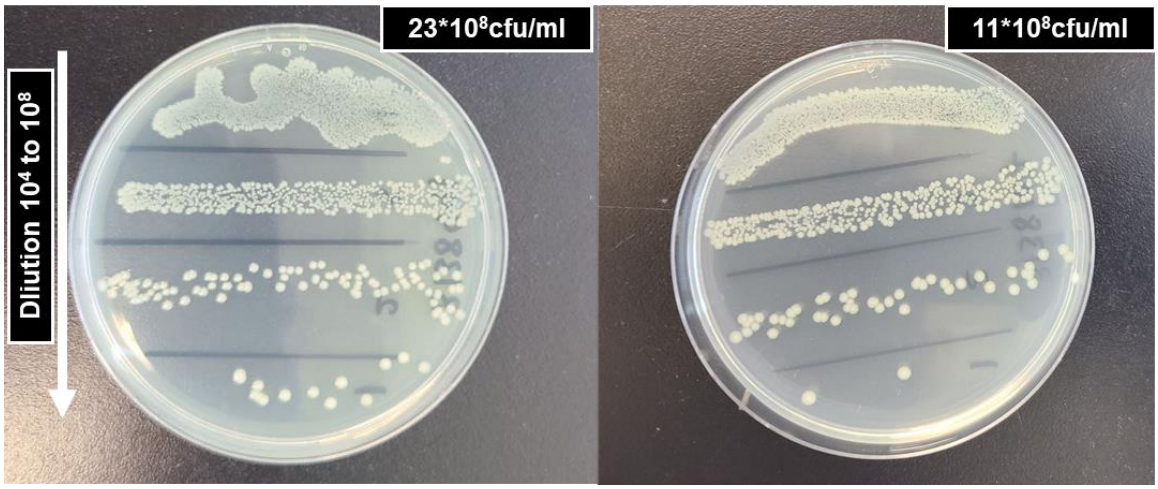

Supplementary Figure 5.9 *E. coli+ blood culture samples cultured on LB-Agar for quantification.*

Supplementary Note 1 - The *E. coli*+ blood culture samples were plated on LB-Agar for quantification. All samples showed 10^8 CFU/mL range. The range of blood stream bacteria can be 10-10^4 CFU/mL, [1] or even higher ranges of 10^8 CFU/mL. [2] Bacteria growth can occur from the time point that blood is collected from patients to the time point that blood cultures are positively flagged and transferred to our research lab.

Supplementary Table 5.1 *– Summary of the oligonucleotides used.*

Sequence	Note
5' TAG CTA GGA AGA GTC ACA CA-Thiol	Capture probe
3' – T CCT TCT CAG TGT GT – 5'	Protecting strand
5'- Amino - TTTTTTGTGTGACTCTTCCTAGCTrATGGTTCGATCAAGA GATGTGCGTCTTGATCGAGACCTGCGACCGTTTTTTTTTTT-biotin -3'	*E. coli* specific DNAzyme without MB tagging

5.7.1 References for Supplementary Information for Liquid Nano Electrodes enable One-pot Electrochemical Detection of Bacteria in Complex Matrices

[1] E. M. K. Kurundu Hewage, D. Spear, T. M. Umstead, S. Hu, M. Wang, P. K. Wong, Z. C. Chroneos, E. S. Halstead, N. J. Thomas, *SLAS Technol. Transl. Life Sci. Innov.* **2017**, *22*, 616.

[2] J. Gao, L. Jeffries, K. E. Mach, D. W. Craft, N. J. Thomas, V. Gau, J. C. Liao, P. K. Wong, *SLAS Technol. Transl. Life Sci. Innov.* **2017**, *22*, 466.

6 Chapter 6: Conclusions and Future Direction

6.1 Thesis summary

In this thesis robust methods for creating textured repellent surfaces with real-world applications were thoroughly discussed and introduced. Two different technologies were implemented, hierarchical structuring to create flexible repellent wraps and liquid infused electrodes for developing anti-biofouling selective electrochemical biosensors.

The developed hierarchical wraps have promising characteristics for setups that require anti-fouling, anti-microbial, anti-thrombogenic behavior by nanoparticle-induced wrinkling. Experiments were carefully designed to mimic real-life applications to investigate the potentials of the developed surfaces. With a theoretical perspective along with careful experimental design, the role of micro, nano, or hierarchical structuring on the omniphobic and antibacterial properties of surfaces were thoroughly studied. We demonstrated that a hierarchical structuring provides superior hydrophobicity and oleophobicity, leading to prominent bacterial repellency. Priority pathogens according to the World Health Organization were tested and potential role of intermediate surface for spread of infectious disease were tested with a developed a “touch-assay”. A potency of use of another class of the developed hierarchical surface for blood contacting setups were investigated by assessing blood repellency, contamination of surfaces by blood, and anti-thrombogenic behaviors, both in dynamic and static conditions. Furthermore, patterns of hydrophilic regions were integrated on these hierarchical repellent surfaces for droplet

digitization and means of a rapid dip-stick biosensing assay was assessed and introduced. In all these developed platforms, the main focus was that the fabrication methods will be easily scalable, will not require complicated machinery, and will be low cost.

To focus more on the enhancement of biosensing with proper blocking methods, as another application of repellent surfaces, we introduced electrochemical biosensing for the first time on liquid infused conductive surfaces. By implementing micro/nanostructures of gold grown on a fluorosilanized gold electrode, followed by DNA probe immobilization and lubricant infusion, a biofunctional repellent electrochemical biosensor for *E. coli* detection was fabricated. With a vision for real-life applications, clinical urine samples and blood samples from infected patients were tested and the developed chips were able to successfully perform and identify *E. coli* infected samples.

6.2 Thesis conclusions

1. A flexible repellent hierarchical surface featuring micro and nanostructures was created and tested among other textured surfaces for the evaluation of physical repellency, bacteria biofilm attachment, bacteria attachment, bacteria transfer *via* human touch. It was found that hierarchical surfaces outperformed micro and nanostructured surfaces in terms of physical characteristics (*e.g.* water CA>150º, SA<5º) and pathogen repellency. The hierarchical surfaces minimized biofilm formation by 85% and resulted in a 20-fold decrease in bacteria transfer. The

flexibility and ability to heat shrink, allowed for the developed wrap to be applied to various object while maintaining its repellency.

2. An all solution fabrication method for creating hierarchical surfaces with integrated patterns of hydrophilic regions was devised and blood repellency was explored on the hierarchical surface. We found that by comparing the hierarchical surface with other textured surfaces, there is a reduced blood adherence by over 90%. The patterned surfaces were also utilized for IL-6 detection.
3. By exploring the literature in antiviral materials and coatings, we found that this is a topic which can be further explored. Use of omniphobic or hierarchical repellent surfaces is an avenue which can be further researched for antiviral or virus repellent platforms.
4. A blocking method for reducing non-specific absorption in electrochemical biosensors was introduced by integrating liquid infused coatings within gold structured electrodes. A one-pot electroactive DNAzyme-based assay was designed to rapidly (within an hour) and specifically detect *E. coli* from samples, especially when detecting from clinical specimens (urine, whole blood). The limit of detection for buffer samples spiked with *E. coli* was 10^2 CFU/ml. In case of clinical urinary tract infection (UTI) samples, the developed electrodes demonstrated sensitivity of 100% and specificity of 98%, distinguishing positive samples from the negative ones with the $>10^4$ CFU/mL diagnosis threshold for UTI+ positive patients. For blood stream infections, we were able to specifically detect *E. coli* infected samples with no false positives or false negatives.

6.3 Contributions to the field

Flexible hierarchical wrap developed with facile fabrication methods for bacteria repellency

- A facile, streamlined, and all solution-based method for creating highly repellent flexible surfaces (hierarchical surfaces) was introduced for the first time. These surfaces can find applications for pathogen repellency, blood repellency, and biosensing.
- The flexible repellent wrap is capable of being wrapped and heat shrunk on various objects with different forms, solving the issue of applicability of repellent coatings to various surfaces.
- Systematic study of bacteria biofilm attachment for both Gram positive and negative bacteria (WHO priority pathogens) was performed to explore repellency on surfaces with various structures. This systematic and comprehensive study can be a benchmark when other researchers characterize repellent surfaces.
- A methodology for mimicking pathogen transfer from human hand to an intermediate contaminating surface was introduced, which can be utilized for studies on various pathogen when exploring repellent surfaces for real life applications.

Patterned hierarchical surfaces, with patterns of hydrophilic regions for biosensing and blood repellency

- Broad and systematic study of blood repellency on hierarchical repellent surface, both in static and dynamic conditions can be a benchmark when researchers design experiments for characterizing blood repellent surfaces.
- Hydrophilic regions were patterned into highly repellent hierarchical structures in a facile straightforward method.
- A patterned dip-based biosensor was introduced which opens up an avenue for rapid biosensing from complex liquids.

A comprehensive review on antiviral surfaces with directions for future research

- The need for more systematic research on antiviral surface was identified, allowing for a better understanding of virus interactions with surfaces, and development of more technologies to mitigate the spread of infection.
- To reduce the spread of viruses *via* contaminated surfaces, surface modification technologies with high potency were introduced (*e.g.* virus repellent surfaces).

Minimizing non-specific binding on electrochemical biosensors by implementing liquid infused coating

- Liquid infused coatings were implemented in an electrochemical biosensor for the first time to mitigate non-specific absorption for detection in complex biological liquids.
- Identification of *E. coli* from clinical samples was done rapidly, reducing the standard 24-48 hour diagnostic time to an hour for both urinary tract and blood stream infections.
- A one-pot electroactive DNAzyme-based assay was introduced for detecting *E. coli* for the first time form clinical samples.
- Broad clinical studies were performed with clinical specimens containing bacteria. Two diseases were covered, urinary tract infection and blood stream infection, caused by the same pathogen.
- The developed diagnosis system is able to identify pathogens without dilution, amplification steps, or complicated steps.

6.4 Future work

Materials and methods for repellent surface fabrication

In terms of the developed flexible hierarchical repellent surfaces, further studies on alternative chemicals can be performed such that more eco-friendly chemicals than fluorosilane or fluorine-free chemicals can be investigated such as natural waxes (soybean,

bee's wax, *etc*.). [1,2] FDA approved materials which lowers the surface energy can be further studied. Active nanoparticles with antimicrobial activity as well as repellency such as TiO_2, Ag, *etc.*, or naturally sourced particles can be used for the repellent wrap development. [3] Natural and biodegradable materials instead of the heat-shrinkable plastics can be studied to induce the similar concept of a heat-shrinkable wrap. Alternative means for integrating repellency on existing surfaces can be used, such as spraying methods. [4]

Universal pathogen studies for development of repellent surfaces

In the effort to create repellent surfaces and characterizing them, other pathogens such as viruses, fungi, and *etc.* can be further evaluated alongside bacteria studies. Studies have shown nosocomial fungal pathogen, *Candida albicans* lasting for up to four months on hospital surfaces. [5] Respiratory tract viruses such as coronaviruses and human influenza viruses can last for few days, gastrointestinal tract viruses such as human astrovirus and hepatitis A virus (HAV) can be detectable for two months on hospital surfaces. [5] Such findings suggests that more systematic research should be done for development of universally repellent surfaces to repel a wider range of pathogens.

Fundamental understanding of bacteria attachment to textured surfaces

In efforts to understand mechanisms and behavior of bacteria attachment or repellency on structured surfaces, more microscopical studies can be performed. Ideally, an online

imaging system where bacteria can be imaged while being incubated on the surfaces (*i.e.* liquid-phase electron microscopy). [6]

Blood contacting medical devices

The developed platform for blood repellency can be used to detect from complex biological liquids such as blood, as it has both repellent sites (hierarchical) and hydrophilic sites (biofunctional). More systematic studies can be performed to investigate limits of detection for the IL-6 system used in chapter 4. Furthermore, since the developed blood repellent surface is flexible and able to conform into different shapes, it can be applied to medical blood contacting devices.

Multiplexing liquid infused electrochemical electrodes and portability

The developed electrochemical biosensing platform can be further studied for other bacteria in urine such as *K. pneumoniae* and *Enterococcus*, or bacteria in blood such as *S. aureus* and *P. aeruginosa,* as it has shown promising behavior in complex liquids. [7–9] Rapid and selective detection in complex biological liquids, without dilutions or amplification steps has been a goal which has been long sought for in biosensing studies. With the developed highly repellent liquid infused electrodes, this goal has been realized. This opens the route for further investigations for other nucleic acid-based detections.

Large-scale clinical study on E. coli detection

The patient sample studies performed in chapter 5, are small-scale pre-clinical studies (31 urinary tract infections, 9 blood stream infections). Beyond the pilot scale ran in chapter 5, based on the disease prevalence and acceptable sensitivity and specificity, more populated samples sizes can be further tested. [10,11]

6.5 References

(1) Shen, T.; Fan, S.; Li, Y.; Xu, G.; Fan, W. Preparation of Edible Non-Wettable Coating with Soybean Wax for Repelling Liquid Foods with Little Residue. *Materials (Basel).* **2020**, *13* (15), 3308.

(2) Cirisano, F.; Ferrari, M. Sustainable Materials for Liquid Repellent Coatings. *Coatings* **2021**, *11* (12), 1508.

(3) Sánchez-López, E.; Gomes, D.; Esteruelas, G.; Bonilla, L.; Lopez-Machado, A. L.; Galindo, R.; Cano, A.; Espina, M.; Ettcheto, M.; Camins, A. Metal-Based Nanoparticles as Antimicrobial Agents: An Overview. *Nanomaterials* **2020**, *10* (2), 292.

(4) Li, X.; Shan, H.; Cao, M.; Li, B. Facile Fabrication of Omniphobic PVDF Composite Membrane via a Waterborne Coating for Anti-Wetting and Anti-

Fouling Membrane Distillation. *J. Memb. Sci.* **2019**, *589*, 117262.

(5) Kramer, A.; Schwebke, I.; Kampf, G. How Long Do Nosocomial Pathogens Persist on Inanimate Surfaces? A Systematic Review. *BMC Infect. Dis.* **2006**, *6* (1), 1–8.

(6) DiCecco, L.; D'Elia, A.; Miller, C.; Sask, K. N.; Soleymani, L.; Grandfield, K. Electron Microscopy Imaging Applications of Room Temperature Ionic Liquids in the Biological Field: A Review. *ChemBioChem* **2021**, *22* (15), 2488–2506.

(7) Lee, C.-W.; Chang, H.-Y.; Wu, J.-K.; Tseng, F.-G. Ultra-Sensitive Electrochemical Detection of Bacteremia Enabled by Redox-Active Gold Nanoparticles (RaGNPs) in a Nano-Sieving Microfluidic System (NS-MFS). *Biosens. Bioelectron.* **2019**, *133*, 215–222.

(8) Gao, J.; Jeffries, L.; Mach, K. E.; Craft, D. W.; Thomas, N. J.; Gau, V.; Liao, J. C.; Wong, P. K. A Multiplex Electrochemical Biosensor for Bloodstream Infection Diagnosis. *SLAS Technol.* **2017**, *22* (4), 466–474. https://doi.org/10.1177/2211068216651232.

(9) Flores-Mireles, A. L.; Walker, J. N.; Caparon, M.; Hultgren, S. J. Urinary Tract Infections: Epidemiology, Mechanisms of Infection and Treatment Options. *Nat. Rev. Microbiol.* **2015**, *13* (5), 269–284. https://doi.org/10.1038/nrmicro3432.

(10) Bujang, M. A.; Adnan, T. H. Requirements for Minimum Sample Size for Sensitivity and Specificity Analysis. *J. Clin. diagnostic Res. JCDR* **2016**, *10* (10), YE01.

(11) Flahault, A.; Cadilhac, M.; Thomas, G. Sample Size Calculation Should Be Performed for Design Accuracy in Diagnostic Test Studies. *J. Clin. Epidemiol.* **2005**, *58* (8), 859–862.